APPLICATIONS OF A LOW-REYNOLDS-NUMBER TURBULENCE MODEL AND WALL FUNCTIONS FOR STEADY AND UNSTEADY HEAT-TRANSFER COMPUTATIONS

by

Mohamed Abdel-Meguid Elhadidy

B.Sc. (Eng), M.Sc.

Thesis submitted for the degree of
Doctor of Philosophy
in the Faculty of Engineering
University of London
and
for the Diploma of Membership
of Imperial College.

Mechanical Engineering Department
Imperial College of Science and Technology
London SW7 2BX

BIBL.
LONDIN.
UNIV.

To:

My wife, Nebal
My parents, Mr and Mrs A. Elhadidy
and
My sister, Soad.

ABSTRACT

Two methods are described for computing turbulent flow and heat transfer close to walls, namely a "composite-model method" and a "wall-function method". In the composite model method, the Reynolds stress (-u'v') is calculated from the turbulent kinetic energy and a defined length scale of turbulence in the near-wall region. Outside this region, the Reynolds stresses are calculated from the kinetic energy of turbulence and its dissipation rate. The turbulent kinetic energy is determined from a differential transport equation which accounts for the low-Reynolds-number effect, while the turbulence dissipation rate is determined from a differential transport equation which is applicable only for high Reynolds numbers.

The wall-function method employs semi-analytical solutions, which are obtained from the solution of the basic equations governing the flow close to the wall with some guidance from experimental data, in the near-wall region, is also described. A new semi-analytical solution of the energy equation, which is applicable for the whole range of laminar-Prandtl-number fluids is developed. This analytical solution is obtained from the concept of dividing the flow domain in the near-wall region into two layers, namely the effective laminar sublayer and a turbulent layer, in which the variation of the effective thermal laminar sublayer thickness with the Reynolds number and with the laminar Prandtl number is considered.

Applications of the above-mentioned methods to the computations of steady hydrodynamic and steady and unsteady heat transfer are presented for the whole range of laminar Prandtl numbers in pipes.

A conjugate heat-transfer analysis, in which the solid wall is considered as a part of the computation domain, is considered. The effects of the stream-wise diffusion of heat inside the solid wall and in the flow field and the effects of the solid to fluid conductivity ratio are also presented.

In all the above situations, detailed comparisons with the available experimental data are provided. These comparisons show that the results obtained with the composite model were in better agreement with the experimental data than that obtained with the wall-function method; however, the results obtained with the wall function were in an acceptable agreement with the experimental data.

Finally, an experimental investigation is reported for an unsteady heat-transfer conjugate problem in which the unsteadiness is produced by a sudden increase in the temperature of the outer surface of the pipe wall. Measurements are made with thermocouples and the output signals are recorded on Ultra Violet Galvanometer Recorders. The obtained experimental data are used to provide more evidence on the validity of the composite model.

PREFACE

I have been a research student in the Heat Transfer Section of the Mechanical Engineering Department in the Imperial College of Science and Technology since September 1975. During my first year of research I was engaged in the development of a new model for the amplitude of temperature fluctuations (Elhadidy (1976)). By the end of the first year this work had to be terminated, owing to some financial problems. However, this work provided me with a basic understanding of turbulence modelling and finite-difference procedures.

The second year was devoted to the study of the unsteady heat-transfer problem associated with a steady, free-jet flow impinging on a solid body (Elhadidy (1977b) and (1977c)) and the steady heat transfer in the annular flow of a liquid metal (Elhadidy (1977a)).

During the last two years I have been involved in the development of an effective and efficient procedure to calculate the heat-transfer characteristics in turbulent wall flows for the whole range of laminar-Prandtl-number fluids. The results of this work comprise the material of this thesis and part of these results have been published by the author (Elhadidy (1979a) and (1979b)).

I would like to express my gratitude to all those who have contributed to my study at Imperial College.

First of all, I am most grateful to my supervisor,

Professor D B Spalding, for giving me the great opportunity of joining his research group, and for his guidance, interest and encouragement. The work I have done during my study was built upon his ideas and suggestions.

I am grateful to Dr G. Hulme of CHAM (Combustion Heat and Momentum Limited), Dr A.S.C. Ma and Dr M.M. Gibson for their help and interest in the present work.

The day-to-day exchange of ideas with other students and post-doctoral fellows has been most helpful. These include: Ahmed Abdelmeguid, Alaedin Awn, Amin Baghdadi, George Carroll, Ayodeji Demuren, Essam Khalil, Timothy Maxwell, Andrew Pollard, Vinoth Ramachandra, Amr Serag-El-Din, Dr Fabio Gori and Dr Kenjiro Suzuki.

I would like to thank Mr Bob King for his sincere help in conducting the experimental part of my work.

Thanks are due to Colleen King, Sue Farmiloe and Maggie Dean for their assistance in administrative matters. I would like also to thank Miss E.M. Archer and Mrs Sue Boot for providing very efficient library services.

I am grateful to Maggie Dean for her excellent typing of the thesis.

Finally, I wish to thank Combustion, Heat and Momentum Ltd and the Science Research Council for providing financial support during my study.

London
September 1979

Mohamed A Elhadidy

CONTENTS

	Page
Abstract	1
Preface	3
Contents	5
List of tables	9
List of figures	10
Nomenclature	16
CHAPTER 1: INTRODUCTION	
1.1 The problem considered	21
1.1.1 Problem specification	21
1.1.2 Nature of the flow	21
1.2 Practical relevance	22
1.3 Historical review	23
1.3.1 Turbulence modelling	24
1.3.2 Steady heat-transfer investigations	29
1.3.3 Unsteady heat-transfer investigations	45
1.4 Present study	49
1.4.1 Objective	49
1.4.2 Outline of present contribution	50
1.4.3 Layout of the thesis	52
CHAPTER 2: MATHEMATICAL ANALYSIS	
2.1 Introduction	56
2.2 Mean flow equations	56
2.3 Turbulence model	58
2.4 Governing differential equations in -x coordinates	60
2.5 Closure	63
CHAPTER 3: ANALYSIS OF THE NEAR-WALL REGION	
3.1 Introduction	64
3.2 Development of the wall functions	65

		Page
3.2.1	Momentum equation	66
3.2.2	Stagnation-enthalpy equation	68
3.2.3	Kinetic energy of turbulence and its dissipation rate	72
3.3	One-equation turbulence model	73
3.4	Closure	76
CHAPTER 4:	SOLUTION PROCEDURE	
4.1	Introduction	80
4.2	Finite-difference equations	81
4.2.1	Finite-differencing scheme	81
4.2.2	The unsteady stagnation-enthalpy equation	83
4.2.3	Steady-flow equations	85
4.3	Computational Algorithm	86
4.3.1	The steady parabolic equations	86
4.3.2	Steady and unsteady elliptic equations	88
4.3.3	Treatment of the conducting wall in the numerical procedure	89
4.4	Auxiliary information	90
4.4.1	Boundary and initial conditions	90
4.4.2	Choice of the thickness of the near-wall region	90
4.5	Closure	92
CHAPTER 5:	EXPERIMENTAL STUDY	
5.1	Introduction	94
5.2	Apparatus and procedure	95
5.2.1	Description of the apparatus	95
5.2.2	Recording equipment	99
5.2.3	Experimental procedure	100
5.3	Experimental conditions	102
5.4	Results	103
5.5	Accuracy of the experimental data	105
5.5.1	Discussion of errors in temperature measurements	106
5.5.2	Discussion of error in the resistance	109
5.5.3	Degree of reproducibility of the measurements	109
5.6	Concluding remarks	109

Page

CHAPTER 6: STEADY HYDRODYNAMIC AND HEAT-TRANSFER RESULTS

6.1 Introduction 126

6.2 Hydrodynamic results 126

6.2.1 Computational details 126
6.2.2 Mean-flow results 130
6.2.3 Turbulence results 132

6.3 Heat-transfer results 133

6.3.1 Computational details 133
6.3.2 Temperature profiles 134
6.3.3 Nusselt-number results 137

6.4 Conjugate problems 139

6.4.1 Problem specification 139
6.4.2 Computational details 140
6.4.3 Results and discussions 141

6.5 Concluding remarks 143

CHAPTER 7: UNSTEADY HEAT-TRANSFER RESULTS

7.1 Introduction 174

7.2 Comparison with previous experimental data 174

7.2.1 Problem specification 174
7.2.2 Computational details 175
7.2.3 Results and discussion 176

7.3 Comparison with the present experimental data 180

7.4 Parametric study 185

7.4.1 Reynolds-number effect 185
7.4.2 Laminar-Prandtl-number effect 185
7.4.3 Results of a step jump in the inlet-fluid temperature 186

7.5 Concluding remarks 188

CHAPTER 8: CONCLUDING REMARKS

8.1 Main results of the present study 212

8.2 Suggestions for future work 214

		Page
REFERENCES		215
APPENDIX A:	Transformation of the stagnation-enthalpy equation from (ψ-x) to (ω-x) coordinate system	233
APPENDIX B:	Finite-difference form of the stagnation-enthalpy equation	237

LIST OF TABLES

TABLE	TITLE	PAGE NO
1.1	Experimental investigations of liquid metal flows	32
2.1	Values of σ_ϕ and expression for d in equation (2.4.1)	62
3.1	Values of A_μ, A_D, C_D and C_μ	75
5.1	Galvanometer's resistance and sensitivity	101
6.1	Grid distribution	129
7.1	Experimental conditions of Stuart's data	176

LIST OF FIGURES

		Page no
Fig (1.1)	Comparison between the recommended equations for the turbulent Prandtl number and the experimental data for a liquid metal fluid with a laminar Prandtl number of .02.	5454
Fig (1.2)	Comparison between the recommended equations for the turbulent Prandtl number and the experimental data for a liquid metal fluid with a laminar Prandtl number of .007.	5555
Fig (3.1)	Variation of the P-function with the distance from the wall for different thickness of the effective laminar thermal sublayer.	7777
Fig (3.2)	Comparison between the analytically-developed temperature profiles and the experimental data of Fuchs et al (1973), Pr_ℓ=.007, Buhr et al (1968), Pr_ℓ=.021, Johnk et al (1961), Pr_ℓ=.7, and Gowen et al (1967) Pr =5.7 and 14.7.	7878
Fig (3.3)	Comparison between the present P-function and the previous recommended P-function for moderate and large laminar Prandtl numbers.	7979
Fig (4.1)	Grid arrangement.	9393
Fig (4.2)	The difference between the low and the high Reynolds number dissipation terms.	9393
Fig (5.1)	Schematic drowning of the experimental apparatus.	111
Fig (5.2)	Photograph of the experimental apparatus.	111
Fig (5.3)	Details of the test section.	112
Fig (5.4)	Photograph of the test section.	113
Fig (5.5)	Photograph of the fluid thermocouples probe.	113
Fig (5.6)	Details of the heating section.	114
Fig (5.7)	Photograph of the heating section.	114
Fig (5.8)	Heating boundary conditions.	116
Fig (5.9)	Fluid and wall temperature responses at x/D = 6.25.	119
Fig (5.10)	Fluid and wall temperature responses at x/D = 8.75.	122
Fig (5.11)	Fluid and wall temperature response at x/D = 13.75.	124
Fig (5.12)	Reproducibility of the fluid temperature response.	125

		Page no
Fig (6.1)	Effect of the number of grid points in the near-wall region on the centre line velocity.	146
Fig (6.2)	Effect of the number of grid points in the central region on the centreline velocity.	146
Fig (6.3)	Effect of the forward steps on the centreline velocity.	147
Fig (6.4)	Number of line-by-line iterations required at each forward step.	147
Fig (6.5)	Variation of the shear velocity with iterations at the first forward step.	148
Fig (6.6)	Variation of the shear velocity with iterations at the second forward step.	149
Fig (6.7)	Effect of the number of radial grid points on the centreline velocity.	150
Fig (6.8)	Effect of the forward steps on the centreline velocity.	150
Fig (6.9)	Comparison between the present predictions of the velocity variations in the entrance region and the experimental data of Barbin et al (1963).	151
Fig (6.10)	Comparison between the present predictions of the velocity variation in the entrance region and the experimental data of Walklate et al (1976).	151
Fig (6.11)	Comparison of the fully-developed velocity profile between the present predictions and the experimental data of Deissler et al (1952).	152
Fig (6.12)	Comparison between the predicted shear stress in the developing region and the experimental data of Barbin et al (1963).	153
Fig (6.13)	Comparison between the predicted fully-developed shear stress variations with the Reynolds number and the recommended equations of Blasius and Prandtl.	154
Fig (6.14)	Comparison between the predicted kinetic energy of turbulence and the experimental data in the near wall region ($Re = 5 \times 10^4$).	155
Fig (6.15)	Comparison between the predicted turbulence kinetic energy and the experimental data outside the near wall region ($Re = 5 \times 10^4$).	155
Fig (6.16)	Comparison between the predicted turbulent viscosity and the experimental data	156

Page no

Fig (6.17) Effect of the number of grid points in the near-wall region on the Nusselt number for large laminar Prandtl number fluid (Pr_ℓ = 14.3) 157

Fig (6.18) Comparison between the predicted temperature profiles and the experimental data of Hanratty and Johnk (1961), Pr_ℓ = .7 and Re = 3.5×10^4. 158

Fig (6.19) Comparison between the present prediction of the temperature profile in the near-wall region and the experimental data of Hanratty and Johnk (1961). 159

Fig (6.20) Comparison between the present prediction of the fully-developed temperature profiles and the experimental data of Gowen et al (1967) for large laminar Prandtl number fluids (Pr_ℓ = 5.7 and 14.3). 160

Fig (6.21) Comparison between the predicted temperature profiles and the experimental data of Buhr et al (1968) for laminar Prandtl number of .02. 161

Fig (6.22) Comparison between the predicted temperature profiles and the experimental data of Fuchs et al (1973) for laminar Prandtl number of .007. 161

Fig (6.23) Comparison of the predicted Nusselt number in the entrance region with the experimental data of Hanratty and Johnk (1961). 162

Fig (6.24) Comparison between the predicted Stanton number and the experimental data, Re = 2.5×10^4. 163

Fig (6.25) Comparison between the predicted Stanton number and the experimental data, Re = 5×10^4. 164

Fig (6.26) Comparison between the predicted Nusselt number and the experimental data for a liquid metal of Pr_ℓ = .02. 165

Fig (6.27) Comparison between the present prediction of Nusselt number and the experimental data for a liquid metal flow of Pr_ℓ = .005. 166

Fig (6.28) Computation domain in the conjugate problem. 167

Page no

Fig (6.29) Effect of the number of grid points in the solid wall on the inner and outer wall temperature. 167

Fig (6.30) Effect of the adial fluid conduction on the temperature profile at x/R = 0.5. 168

Fig (6.31) Effect of the axial fluid conduction on the temperature profile at x/R = 1.0. 168

Fig (6.32) Effect of the axial fluid conduction on the Nusselt number. 169

Fig (6.33) Effect of the conductivity ratio (λ_s/λ_f) on the temperature profile at x/R = 1. 169

Fig (6.34) Effect of the conductivity ratio (λ_s/λ_f) on the inner wall temperature. 170

Fig (6.35) Effect of the conductivity ratio (λ_s/λ_f) on the Nusselt number. 170

Fig (6.36) Temperature profiles inside the solid wall for different conductivity ratios; without axial conduction, Pe = 6 and δ/R = 0.2. 171

Fig (6.37) Effect of the pipe thickness on the temperature profile at x/R = 2. 172

Fig (6.38) Effect of the wall thickness on the inner wall temperature. 172

Fig (6.39) Developing temperature profiles, Pe = 6., λ_s/λ_f = 1.98 and δ_s/R = .2. 173

Fig (7.1) Effect of time step on the inner wall temperature. 184

Fig (7.2) Effect of time step on the mean bulk fluid temperature. 190

Fig (7.3) Comparison of the fully-developed (x/D=70) mean fluid temperature response with the experimental data of Stuart (1956), for water fluid with a Reynolds number of 6720. 191

Fig (7.4) Comparison of the fully-developed (x/D=70) mean fluid temperature with the experimental data of Stuart (1956) for water fluid with a Reynolds number of 11980 192

Fig (7.5) Mean fluid temperature responses at different downstream locations for water fluid with a Reynolds number of 6720. 193

		Page no
Fig (7.6)	Inner and outer wall temperature responses at different downstream locations for water fluid with a Reynolds number of 6720.	194
Fig (7.7)	Comparison of the predicted mean bulk fluid temperature and the experimental data of Kawamura (1977) for water fluid with a Reynolds number of 8740.	195
Fig (7.8)	Comparison of the predicted wall temperature response with the experimental data of Kawamura (1977).	195
Fig (7.9)	Comparison of the predicted heat-transfer coefficient with the experimental data of Kawamura (1977).	196
Fig (7.10)	Comparison of the predicted heat-transfer response with the experimental data of Kawamura (1977).	196
Fig (7.11)	Temperature profiles at x/D=5; Pr_ℓ=7.2 and Re=8740	197
Fig (7.12)	Temperature profiles at x/D=10; Pr_ℓ=7.2 and Re=8740.	198
Fig (7.13)	Temperature profiles at x/D=20; Pr_ℓ=7.2 and Re=8740.	199
Fig (7.14)	Comparison between the present predictions and the present measurements of the temperature responses at x/D=6.25.	202
Fig (7.15)	Comparison between the present predictions and the present measurements of the temperature responses at x/D=8.75.	205
Fig (7.16)	Comparison between the present predictions and the present measurements of the temperature responses at x/D=13.75.	207
Fig (7.17)	Mean fluid temperature response at different downstream locations for different Reynolds numbers.	208
Fig (7.18)	Heat transfer coefficient response at x/D=25 for different Reynolds numbers.	208
Fig (7.19)	Mean bulk temperature response in the developing region; $Re=2x10^4$ and Pr_ℓ=.026.	209

Page no

Fig (7.20) Mean bulk temperature response in the developing region; $Re=2x10^4$ and $Pr_\ell=.005$. 209

Fig (7.21) Time variations of the heat-transfer coefficient at x/D=20 for three laminar Prandtl numbers ($Pr_\ell=.005$, .026 and 7.2) 210

Fig (7.22) Fluid temperature response at different downstream locations to a step change in the inlet temperature; $Re=2x10^4$ and $Pr_\ell=7.2$. 211

Fig (7.23) Inner and outer wall temperature response at different downstream locations to a step change in the inlet temperature; $Re=2x10^4$ and $Pr_\ell=7.2$. 212

NOMENCLATURE

SYMBOL	MEANING AND UNITS	LOCATION OF FIRST APPEARANCE
a	Arbitrary function of x, m^{-1}	eqn. (2.4.1)
a_1 and a_2	Constants, dimensionless	eqn. (4.2.22)
a_3 and a_4	Constants, dimensionless	eqn. (4.2.23)
a_5 and a_6	Constants, dimensionless	eqn. (4.2.24)
a_7 and a_8	Constants, dimensionless	eqn. (4.2.25)
A_D	Constant, dimensionless	eqn. (3.3.4)
A_s	Constant, dimensionless	eqn. (1.3.6)
A_μ	Constant, dimensionless	eqn. (3.3.6)
$A_{I,J}$	Combined convection/diffusion coefficient, dimensionless	eqn. (4.2.1)
b	Arbitrary function of x, m^{-1}	eqn. (2.4.1)
b_D	Constant, dimensionless	eqn. (1.3.15)
B_s	Constant, dimensionless	eqn. (1.3.6)
$B_{I,J}$	Diffusion coefficient, m^2/s	eqn. (4.2.8)
$C_{I,J}$	Source term of ϕ	eqn. (4.2.1)
C_1 and C_2	Constants, dimensionless	eqn. (2.3.4)
C_3	Constant, dimensionless	eqn. (3.3.1)
C_4	Function of R_k, dimensionless	eqn. (3.3.2)
C_5	Function of R_k, dimensionless	eqn. (3.3.1)
C_D	Constant, dimensionless	eqn. (1.3.5)
C_p	Specific heat, ws/Kgk	eqn. (1.3.6)
C_μ	Constant, dimensionless	eqn. (2.3.2)
C	Arbitrary function of ϕ, dimensionless	eqn. (2.4.1)
d	Arbitrary function of ϕ, ϕ/m	eqn. (2.4.1)
D	Diameter of the pipe, m	page (21)

SYMBOL	MEANING AND UNITS	LOCATION OF FIRST APPEARANCE
DF	Damping factor, dimensionless	eqn. (6.2.3)
g	Gravitational acceleration, m/s^2	eqn. (1.3.10)
Gr	Grashof number, dimensionless	eqn. (1.3.10)
h	Heat-transfer coefficient ($h = \dot{q}''/(T_w - T_m)$), w/m^2K	eqn. (1.3.7)
$\bar{h}$	Static enthalpy ($\bar{h} = C_pT$), m^2/s^2	eqn. (2.2.6)
$\tilde{h}$	Stagnation enthalpy ($\tilde{h} = h+u^2/2$), m^2/s^2	eqn. (2.2.5)
k	Turbulent kinetic energy, m^2/s^2	page (21)
K	Von Karman's constant, dimensionless	eqn. (3.2.3)
ℓ	Turbulence length scale, m	page (21)
L	Mixing length, m	eqn. (1.3.3)
L_H	The length of the heated section, m	eqn. (1.3.9)
$\dot{m}'_g$	Mass flow rate per unit area at the surface of the control volume, Kg/sm^2	page (82)
Nu	Fully-developed Nusselt number ($Nu=hD/C_P\Gamma_{h,\ell}$)	eqn. (1.3.7)
Nu(x)	Nusselt number at a downstream distance x, dimensionless	eqn. (1.3.11)
P	Pressure, N/m^2	eqn. (2.2.2)
P	P-function, dimensionless	eqn. (3.2.15)
Pe	Peclet number ($Pe=Pr_\ell R_e$), dimensionless	eqn. (1.3.7)
Pe_g	Grid-Peclet number, dimensionless	page (82)
Pr	Prandtl number ($Pr=\mu/\Gamma_h$)	page (22)
$\dot{q}''$	Heat-transfer rate w/m^2	eqn. (1.3.2)
Q'	Heat-generated per unit time and volume w/m^3	eqn. (2.2.6)

SYMBOL	MEANING AND UNITS	LOCATION OF FIRST APPEARANCE
r	Radial coordinates measured from the axis of symmetry, m	eqn. (1.3.5)
R	Pipe radius, m	eqn. (1.3.22)
R^+	Dimensionless pipe radius ($R^+=\frac{Ru^*}{\nu}$), dimensionless	eqn. (1.3.22)
R_g	Gas constant, m^2/s^2K	eqn. (2.2.3)
R_h	Turbulent Reynolds number ($\frac{\ell\ v'}{\alpha}$), dimensionless	eqn. (1.3.14)
R_k	Turbulent Reynolds number ($k^{\frac{1}{2}}\ell\ /\nu$), dimensionless	eqn. (3.3.3)
R_m	Turbulent Reynolds number ($\ell\ v'/\nu$), dimensionless	eqn. (1.3.14)
R_e	Reynolds number (u_mD/ν), dimensionless	eqn. (1.3.7)
R_r	Dimensionless temperature, $\lambda_\ell(T_W-T)/\dot{q}"y$	eqn. (3.2.14)
$S_{I,J}$	Linearized source term, depends on ϕ	eqn. (4.2.18)
$S'_{I,J}$	Linearized source term, depends on ϕ	eqn. (4.2.18)
St	Stanton number, dimensionless	page (137)
t	Time, s	eqn. (2.4.8)
T	Temperature ^oK	eqn. (1.3.2)
T'	Temperature fluctuation, ^oK	eqn. (1.3.2)
T^+	Dimensionless temperature $\{(T_W-T)\rho C_p u^*/\dot{q}"\}$, dimensionless	eqn. (1.3.6)
T_m	Mean temperature ($2\int_o^R \rho urTdy/\rho r^2u_m$),K	eqn. (1.3.7)
u	Axial velocity, m/s	eqn. (1.3.1)
u'	Axial velocity fluctuation, m/s	Abstract
u*	Shear velocity ($\sqrt{\tau/\rho}$), m/s	eqn. (1.3.6)
u_m	Mean velocity, ($2\int_o^R \rho urdy/\rho r^2$), m/s	page (21)
u^+	Dimensionless velocity (u/u*)	eqn. (1.3.20)

SYMBOL	MEANING AND UNITS	LOCATION OF FIRST APPEARANCE
v	Radial velocity, m/s	eqn. (1.3.1)
v'	Radial velocity fluctuation, m/s	Abstract
x	Axial coordinate, m	eqn. (1.3.1)
y	Radial coordinate measured from the wall, m	eqn. (1.3.1)
y^+	Dimensionless distance (yu^*/ν)	eqn. (1.3.6)
$\tilde{y}$	Dimensionless distance ($K\ Pr_\ell y^+/Pr_t$)	eqn. (3.2.14)
z_B	A parameter to show the effect of free convection, dimensionless	eqn. (1.3.9)
z	Exponent	eqn. (3.2.18)

GREEK SYMBOLS

α	Kinametic thermal diffusivity of heat, m^2/s	eqn. (4.2.8)
β	Coefficient of thermal expension $1/^oK$	eqn. (1.3.10)
Γ_g	Diffusivity at the surface of the control volume	page (82)
Γ_h	Thermal diffusivity, kg/ms	page (22)
δx	Forward steps, m	eqn. (4.2.2)
$\delta\omega$	Normalized stream function steps	eqn. (4.2.4)
δx_g	Distance between two grid points	page (81)
ε	Turbulence dissipation rate m^2/s^3	page (27)
λ	Therman conductivity, w/m^ok	eqn. (3.2.9)
μ	Viscosity, kg/ms	page (21)
ν	Kinametic viscosity, m^2/s	eqn (4.4.1)
ρ	Density, kg/m^3	page (21)

GREEK SYMBOL	MEANING AND UNITS	LOCATION OF FIRST APPEARANCE
σ_k	Turbulent Prandtl number of k, dimensionless	eqn. (1.3.5)
σ_ε	Turbulent Prandtl number of ε, dimensionless	eqn. (2.3.4)
τ	Shear stress, N/m^2	eqn. (1.3.1)
ϕ	Dependent variable	eqn. (2.4.1)
ψ	Stream function, kg/s	eqn. (2.4.4)
ω	Dimensionless stream function	eqn. (2.4.3)

SUBSCRIPTS

eff	Effective	page (59)
f	Fluid	page (44)
H	At the edge of the thermal effective laminar sublayer	page (68)
ℓ	Laminar	page (21)
M	At the edge of the momentum effective laminar sublayer	eqn. (3.2.3)
s	Solid	page (44)
t	Turbulent	eqn. (1.3.1)
w	At the inner surface of the pipe wall	page (72)

CHAPTER 1

INTRODUCTION

1.1 The Problem Considered

1.1.1 Problem Specification

The problem considered in the present investigation is the computation of turbulent flow and heat transfer in straight pipes over a wide range of laminar Prandtl numbers. Both steady and unsteady heat transfer under steady-flow conditions have been investigated. In the steady and unsteady cases, the 'conjugate problem' has also been investigated in which the solid wall is considered as part of the computational domain.

1.1.2 Nature of the Flow

Turbulent pipe flow, like other wall flows, exhibits cross-stream variations in the Reynolds numbers of turbulence, defined as $(\rho k^{\frac{1}{2}} \ell/\mu_\ell)$ where k is the turbulent kinetic energy and ℓ is the turbulence length scale. This turbulence Reynolds number increases sharply from zero at the wall to a large value within a very thin layer adjacent to the wall; its thickness depends on the mean-flow Reynolds number $(\rho u_m D/\mu_\ell)$, where u_m is the mean flow velocity and D is the pipe diameter. Outside this thin layer, the molecular viscosity has almost no effect on the turbulent momentum transport; and the process of turbulent dissipation is almost isotropic. Consequently, the treatment of the turbulence in this region is rendered simpler than that in the near-wall region, where the effect of molecular viscosity is very important and the dissipation is not isotropic.

Similarly, the molecular diffusivity of heat ($\Gamma_{h,\ell}$) can be neglected in those regions where the turbulence Peclet number ($\rho k^{\frac{1}{2}} \ell / \Gamma_{h,\ell}$) is high. This Peclet number increases from zero at the wall more slowly than the turbulence Reynolds-number for small-Prandtl-number fluids, whereas the opposite is true for large Prandtl numbers. Therefore, for medium and large-laminar-Prandtl-number fluids ($Pr_{\ell} > 0.7$), the molecular diffusivity of heat has almost no effect on turbulent heat-transfer process in those regions in which the molecular viscosity has almost no effect on the turbulent momentum-transfer process. Consequently, the commonly-employed similarity between the turbulent heat and momentum transfer, which results in a turbulent exchange coefficient for heat that is proportional to that for momentum and independent of the flow Reynolds number and laminar Prandtl number, is valid in the regions of high turbulent Reynolds number. However, for small laminar-Prandtl-number fluids, where the turbulent heat-transport is affected in a complex way by the molecular thermal diffusivity over a considerable portion of the flow, the constant of proportionality between the turbulent exchange coefficients of heat and momentum depends on the laminar Prandtl number, the Reynolds number and the distance from the wall.

1.2 Practical Relevance

Computation of the steady turbulent heat-transfer characteristics for a wide variety of laminar-Prandtl-number-fluids is necessary for design purposes. In comparison with other fluids, liquid metals display a very high thermal conductivity. This property makes them very efficient heat-transfer media and leads to their employment

in industrial plants where high heat flux densities are present. Liquid sodium has the further advantage of a high boiling temperature, namely 900^{o}C at atmospheric pressure. Consequently, liquid sodium is now predominantly used as the coolant in Fast-Breeder Reactor designs.

The knowledge of the heat-transfer characteristics in turbulent flows under transient conditions is necessary for the reliable prediction of the unsteady operation of various heat-exchanger systems. This transient may be accidental or random; alternatively, it may be introduced on purpose, as in the case of a change in power level of an electric power station, or of the reaction rate in a chemical reactor.

Unsteady conjugate heat-transfer problems are of importance for accurate predictions of those experimental situations where the temperature transients are introduced either through the outer surface of the pipe walls or within the solid wall itself. A knowledge of the temperature response inside the solid wall is also essential for the calculation of the thermal fatigue stresses. These stresses constitute one of the major problems which arise in the sodium-cooled Fast Breeder Nuclear Reactor.

1.3 Historical Review

The previous work relevant to the problems considered in the present investigation can be classified under the following three categories:

(i) The turbulence modelling applicable to wall flows;

(ii) Steady-heat-transfer investigations;

(iii) Unsteady-heat-transfer investigations.

Brief reviews of the progress achieved in the above fields are presented in the following sections.

1.3.1 Turbulence Modelling

The majority of the proposed turbulence models are based on Boussinesq's idea (Launder and Spalding (1972)) of expressing the turbulent shear stress representing the cross-correlation of fluctuating velocities as a product of the "turbulent viscosity (μ_t)" and the local-mean-velocity gradient as follows:

$$\tau_t \equiv -\rho\overline{u'v'} = \mu_t \left(\frac{\partial u}{\partial y} + \frac{\partial v}{\partial x}\right) \quad , \quad (1.3.1)$$

where τ_t is the turbulent shear stress, u' and v' are the velocity fluctuations in x and y directions respectively.

Similarly, the turbulent heat transfer ($\dot{q}''_t$) is expressed as follows:

$$\dot{q}''_t \equiv -\rho\overline{v'T'} \doteq \Gamma_{h,t} \frac{\partial T}{\partial y} \quad , \quad (1.3.2)$$

where the turbulent diffusivity of heat ($\Gamma_{h,t}$) and the turbulent viscosity (μ_t) are considered to be functions of the flow field. Turbulence models based on Boussinesq's hypothesis differ from one another in the information they provide on the variation of the turbulent viscosity. Other turbulence models deal directly with the turbulent stresses. However the turbulence models are usually classified according to the numbers of differential equations used in each model.

(i.) Zero-equation models

In those models belonging to the zero-equation category, the turbulent viscosity is expressed by an algebraic formula containing only mean-flow quantitits. An example is that provided by Prandtl's mixing-length hypothesis (Launder and Spalding (1972)) as follows:

$$\mu_t = \rho L^2 \frac{\partial u}{\partial y} \quad , \quad (1.3.3)$$

where the mixing-length L depends on the geometry of the problem. For an account of the mixing length in different flow situations, see Launder and Spalding (1972) and Hinze (1975).

The mixing-length hypothesis is simple, requiring no additional differential equations to be solved; it can readily be modified to account for the low-Reynolds-number effects, (Van Driest (1956)), and yields satisfactory results for self-preserving flows. However, it suffers from the following drawbacks:

(a) The mixing length has to be prescribed as input.

(b) It does not take account of the convection and diffusion of turbulent energy.

(c) It implies zero turbulent viscosity in regions of zero velocity gradients.

(d) It has not been proven to be an effective tool in situations of recirculating flow.

(ii) <u>One-equation models</u>

A typical model in this category is that proposed by Prandtl. In this model, the turbulent viscosity is expressed in terms of the turbulent kinetic energy and length scale, as follows (Launder and Spalding (1972)):

$$\mu_t = \text{Constant } (\rho \ell \, k^{\frac{1}{2}}) \quad , \quad (1.3.4)$$

where ℓ is a length-scale of turbulence, which has to be prescribed beforehand and the kinetic energy of turbulence (k) is obtained from a transport equation. For two-dimensional,

steady and parabolic* flows, the equation for the conservation of turbulent kinetic energy in cylindrical coordinates is given by (Launder and Spalding (1972)):

$$\frac{\partial \rho uk}{\partial x} + \frac{1}{r}\frac{\partial \rho rvk}{\partial y} = \frac{1}{r}\frac{\partial}{\partial y}\left(\frac{\mu_t r}{\sigma_k}\frac{\partial k}{\partial y}\right) + \mu_t\left(\frac{\partial u}{\partial y}\right)^2 - C_D\frac{\rho k^{2/3}}{\ell} \quad , \quad (1.3.5)$$

where, σ_k and C_D are constants.

The above equation is derived from Navier-Stokes equations appropriate to turbulent flows through the following assumptions:

(a) The viscous transport of turbulent kinetic energy is neglected; this assumption is valid only for high-turbulent Reynolds-number-situations.

(b) The diffusive action of turbulence is presumed similar to molecular diffusion processes. Thus, the rate of transport of turbulence energy is taken as the product of the spatial gradient of k and the turbulent viscosity divided by the Prandtl number for the diffusion of turbulence energy, σ_k.

(c) The dissipation rate is assumed to be controlled by the processes which transfer energy from larger to successively smaller eddies and not by the dissipation motions themselves. This assumption can be applied only for high-turbulent-Reynolds-number flows where the small eddies are much smaller than the energy carrying eddies.

For low-turbulent-Reynolds-number flows, equation (1.3.5) requires the following modifications:

(a) The viscous diffusion of kinetic energy of turbulence must be included.

---

*i.e. those in which the downstream values of the dependent variables do not affect the upstream values.

(b) The length-scale appropriate to the viscous layer adjacent to the wall must be employed.

(c) The dissipation term must be re-modeled to account for the low-turbulent-Reynolds-number effect.

The above modifications can readily be introduced (Glushko (1965), Spalding (1967), Harlow and Nakayama (1967), Wolfshtein (1969), Norris and Reynolds (1975) and Hassid and Poreh (1975)), and consequently the one-equation (k) model of turbulence can handle both the low and high turbulent-Reynolds-number regions of the flow domain. However, the need to describe a length scale restricts the use of the one-equation model of turbulence to simple flow situations.

(iii) Two-equation models

For models in this category the turbulent viscosity is expressed in terms of a "turbulent velocity", which is again the square root of the turbulent kinetic energy, and a length scale or related variable which is usually in the form $k^m \ell^n$, where m and n are constants. The turbulent kinetic energy and the length scale (or related variable) are obtained from appropriate transport equations, a summary of these equations is given by Launder and Spalding (1972).

The most popular model in the category of two-equation models is that employing the kinetic energy of turbulence and its dissipation rate (ε), as proposed earlier by Chou (1945), Davidov (1961) and Harlow and Nakayama (1968) and modified by Jones and Launder (1972). In this model, known as the $k\text{-}\varepsilon$ model, the kinetic energy of turbulence is obtained from

its transport equation in which the same assumptions used in developing equation (1.3.5) are incorporated and an additional differential equation for the isotropic dissipation rate is formulated. This model, which is applicable only for high turbulent-Reynolds-numbers, has been well tested for a wide range of different flow situations, Launder et al (1972), Launder and Spalding (1973), Khalil, Spalding and Whitelaw (1975), Walklate et al (1976), Ramachandra (1979), as well as many others.

For low turbulent Reynolds-bumbers, the $k\sim\varepsilon$ model requires the following modifications:

(a) Re-modelling of the dissipation term of the turbulent kinetic energy equation.

(b) Re-modelling of the production and dissipation terms of the dissipation-rate equation.

(c) The viscous diffusion of kinetic energy of turbulence and its dissipation rate must be included.

With the present theoretical knowledge of turbulence and in the absence of the experimental data, ad hoc changes have been proposed to account for the low-Reynolds-number effect in the dissipation equation (Jones and Launder (1972 and 1973) and Hassid and Poreh (1975b)). These changes, as stated by the former authors, still require further adjustments and refinements and consequently this model is still in its early stages of development to be applicable to low Reynolds-number flow problems.

(iv) <u>Stress-equation models</u>

In these models, the turbulent stresses and heat fluxes are

calculated directly from their transport equations. Therefore these models are expected to perform more satisfactorily than those based on the eddy viscosity concept in situations such as corner flows where the turbulent viscosity is not a scalar quantity. However, these models are mathematically complex and require large computational times and storage; and the expectation has not yet been proved to be justified.

1.3.2 Steady Heat-Transfer Investigations

(a) Experimental studies

Experiments on steady-state turbulent heat-transfer in pipe flow have been extensively reported in the literature. Deissler and Eian (1952), Sleicher (1958), Abbrecht and Churchill (1960) and Johnk and Hanratty (1962) presented the temperature profiles and the Nusselt number results for air flows over a wide range of Reynolds numbers. The fully-developed temperature profiles for different laminar Prandtl numbers (Pr_ℓ = 0.7, 5.7 and 14.3) were reported for a wide range of Reynolds numbers by Gowen and Smith (1967). In this investigation the effect of the laminar Prandtl number on the temperature profile was also studied in the range $0.026 < Pr_\ell < 14.3$. This study showed that the experimental temperature results at different Pr_ℓ can be represented by the following emperical relation:

$$T^+ = A_s \ln y^+ + B_s \quad , \quad (1.3.6)$$

where T^+ is the dimensionless temperature defined by $(T_w - T)\rho C_p u^*/\dot{q}''$, u^* is the shear velocity ($\sqrt{\tau/\rho}$), and y^+ is the dimensionless distance from the wall and defined by

$\frac{yu^*\rho}{\mu_\ell}$. A_s was nearly constant while B_s was depending strongly on the laminar Prandtl number, for Pr_ℓ values of 0.026, 0.7, 5.7 and 14.3 the corresponding values of B_s were -7.25, 3., 34.5 and 76.3 respectively.

Johank and Hanratty (1961 and 1962b) and Abbrecht and Churchill (1960) presented the temperature profiles and the Nusselt number results in the developing region of a pipe flow with air over a wide range of Reynolds numbers.

The turbulent Prandtl number ($Pr_t = \frac{\mu_t}{\Gamma_{h,t}}$) results were presented by Sleicher (1958), Abbrecht and Churchill (1960) and Johnk and Hanratty (1961 and 1962) for air flows for several Reynolds numbers and for water flows by Smith, Gowen and Wasmund (1967). These results indicated that the turbulent Prandtl number was nearly constant over the pipe cross-section and was weakly dependent on the Reynolds number and the laminar Prandtl number.

Lubarsky and Kaufman (1955) and Watson (1956) provided comprehensive reviews of the earlier measurements of the heat-transfer characteristics of liquid metal flows. Most of these reported results were for the Nusselt number in fully developed pipe flows. The comparisons between these Nusselt number results presented by Lubarsky and Kaufman (1955) and Watson (1956) show wide scatter; this was attributed by Watson to the entrainment of gas or air in the liquid metal flow. In spite of this wide scatter, Lubarsky and Kaufman proposed the following empirical relation, which best represents most of the Nusselt number

results reviewed by them.

$$Nu = 0.625\ Pe^{0.4} \quad . \quad (1.3.7)$$

Pe is the Peclet number.

Among the experimental investigations reviewed by Lubarsky and Kaufman (1955) and Watson (1956), only two, namely those of Isakoff and Drew (1951) and Johanson, Hartnett and Clabaugh (1953), are significant for the present study. Isakoff and Drew (1951) reported the first complete study of the velocity, temperature profiles, the variation of Nusselt numbers and the turbulent Prandtl number. These results were presented for a wide range of Reynolds numbers (36700 - 370000) in a flow of mercury with a laminar Prandtl number of 0.0239. Johanson, Hartnett and Claybaugh (1953) presented the Nusselt number results in the developing and in the fully-developed regions for a flow of molten lead-bismuth eutectic. These results were reported in tabular form for a laminar Prandtl number range of 0.02 - 0.046 and a Reynolds number range of 7500 - 170000.

Experimental investigations reported after 1956 are presented in Table (1.1), where the particular liquid metal, its laminar Prandtl number, Reynolds number, heat-transfer boundary condition and the reported data are displayed. Brown, Amstead and Short (1957) reported one of the few measurements of the heat-transfer characteristics for high Reynolds numbers (Re = 250000 - 800000) with a laminar Prandtl number of 0.02. Unfortunately, the heat-transfer rate, which is required for the prediction of the reported temperature excess (T_w -T),

Table (1.1)

Experimental investigations of liquid-metal flows

Author	Fluid	Pr_ℓ	Re	Boundary condition	Reported data
Brown et al (1957)	Hg	.02	$2.5x10^5$: $8x10^5$	$\dot{q}$=constant	u, T, Pr_t and Nu
Subbotin et al (1961, 1962a, 1962b, and 1963)	Na and Hg	.005:.05	$2.69x10^4$: $2.28x10^5$	$\dot{q}$=constant	T, Pr_t and Nu
Baker et al (1962)	Nak	.0084:.0091	$4.8x10^4$:$2.71x10^5$	$\dot{q}$=constant	Nu
Buhr et al (1968)	Hg and Nak	.019:.029	$3.14x10^4$:$2.5x10^5$	$\dot{q}$=constant	T, Pr_t and Nu
Hochreiter (1971)	Hg	.024	$5x10^4$ and $8.9x10^4$	$\dot{q}$=constant	T, Pr_t and turbulence quantities
Flaherty (1974)					
Sleicher et al (1973)	Nak	.02:.0245	$2.6x10^4$:$3x10^5$	T=constant	T, Pr_t and Nu
Sheriff et al (1972 & 1973)	Na	.007	$4x10^4$:$1.25x10^5$	$\dot{q}$=constant	Pr_t
Fuchs (1973)	Na	.007	$7.14x10^3$ $1.428x10^5$	$\dot{q}$=constant	T and Pr_t
Fuchs et al (1973)	Na	.007	$7.14x10^3$: $1.428x10^5$	$\dot{q}$=constant	Pr_t

was not reported. However, the dimensionless temperature (T^+), the Nusselt number and the turbulent Prandtl number results are still of interest for comparison with the present results.

Subbotin et al (1961, 1962a, 1962b and 1963) reported the temperature profiles, the turbulent Prandtl number, the developing and the fully-developed Nusselt-number results for the flow of liquid metal with a laminar Prandtl number of 0.022 at two Reynolds numbers. In addition to that, Subbotin et al (1963) made reference to further temperature measurements with sodium flow at a laminar Prandtl number range of 0.0057 - 0.0075 and a Reynolds number range of 5850 - 178000, but, unfortunately, gave no details. The temperature profiles and the turbulent-Prandtl-number results reported by Subbotin were in poor agreement with the bulk of the measurements collected by Carr and Balzhiser (1967). The error in Subbotin's results was explained by Carr and Balzhiser as being due to the use of a temperature probe which was large enough to cause appreciable flow disturbance at the point of measurement. Regardless of this error in the temperature measurements, the use of the Nusselt-number results is very limited due to the manner in which the results have been correlated* (Nu vs Pe). Therefore Subbotin's results, except the Nusselt number, have not been employed in this study to test the accuracy of the present results.

Baker and Sesonske (1962) measured the average Nusselt number, over the whole pipe length, in a flow of sodium-

*The recent measurements, Buhr et al (1968) and Sleicher et al (1973) show that the Nusselt number depends on Pr_ℓ and Re separately and not on Pe.

potassium alloy of laminar Prandtl number .0085 and overa Reynolds number range of 58800 - 208000. The fully-developed Nusselt numbers were calculated from the average values given by Deissler's (1953) predictions and the following emperical relation was obtained:

$$Nu = 6.05 + 0.0074\ Pe^{.95} \qquad .(1.3.8)$$

Buhr, Carr and Balzhiser (1968) reported the first complete study on liquid-metal flows of mercury and sodium-potassium alloy in the laminar Prandtl-number range of .019 - 0.029 and a Reynolds number range of 31 400 - 251 000. The temperature profiles both with and without free convection, the Nusselt numbers and turbulent-Prandtl-number results, were presented in this study. Complete information regarding the inlet and outlet temperatures, the heat-transfer rate, the laminar Prandtl numbers and the Reynolds number for each run were also reported. The accuracy of the results presented were within acceptable limits. Buhr et al have also analysed several sets of temperature profile data in liquid metals. They found that the temperature profiles were affected by free convection when:

$$Z_B = \frac{Gr\ Pr_\ell}{Re}\ \frac{D}{L_H} > 20 \times 10^{-4} \qquad ,(1.3.9)$$

where Gr is the Grashof number defined as

$$Gr = \frac{D^4 \beta \rho^2 g (dT/dx)}{\mu_\ell^2} \qquad ,(1.3.10)$$

β is the coefficient of thermal expansion and g is the gravitational acceleration.

Hochreiter (1971) and Flaherty (1974) have performed measurements of temperature profiles, turbulent Prandtl

number and turbulence quantities (root-mean-square and energy spectrum of velocity and temperature). The results were presented for a flow of mercury with two different Reynolds numbers, Re = 50000 and 897000; for these flow situations the parameter defined by Buhr et al (equation (1.3.9)) were 67.7×10^{-4} and 42×10^{-4} respectively. Consequently Hochreiter and Flaherty's results would be slightly affected by a free convection.

Sleicher, Awad and Notter (1973) reported the heat-transfer characteristics (T, Nu and Pr_t) for a flow of sodium-potassium alloy at Reynolds number range of 26000 - 302000.

These results were given for constant wall temperature and the following emperical relations were also reported for the variations of Nusselt number

$$Nu(x) = Nu(\infty)\ \{1+2/(x/D)\} \qquad ,(1.3.11)$$

$$Nu(\infty) = 4.8 + 0.0156\ Pe^{.85}\ Pr_{\ell}^{.8} \quad \text{for constant wall temperature} \qquad ,(1.3.12)$$

$$Nu(\infty) = 6.3 + 0.0167\ Pe^{.85}\ Pr_{\ell}^{.8} \quad \text{for constant heat flux} \qquad .(1.3.13)$$

Where Nu(x) and Nu(∞) are the local and fully-developed Nusselt numbers respectively. The inlet temperature profiles for each run were not reported; this restricted the use of the reported temperature profiles to their normalized form only.

Finally, Sheriff and O'Kane (1973 and 1972) and Fuchs and Faesch (1973) reported the turbulent-Prandtl-number results for a sodium flow with laminar Prandtl number of 0.007. The fully-developed temperature profiles were also reported

by Fuchs (1973).

(b) Theoretical investigations

Theoretical studies of the heat-transfer characteristics in turbulent pipe flows are widely reported in the literature. Most of these investigations were based on zero-equation turbulence models. Deissler (1955), Sparrow, Hallmon and Siegal (1957), Mizushina, Orino, Oka and Fukuda (1971), and many others, presented the fully-developed heat-transfer results for large laminar-Prandtl-number flows. These analyses were based either on the concept of three sharply-defined fluid layers, laminar sublayer, buffer region and turbulent layer, or on the concept of the two layers, namely an effective laminar sublayer and a turbulent layer. The developing Nusselt number results were also reported for large laminar-Prandtl-number flows by Deissler (1955) and Sparrow et al (1957).

Results for the developing Nusselt number, fully-developed Nusselt number, and the temperature profiles for moderate laminar Prandtl number (Air) flows, were presented by Deissler (1953), Sparrow et al (1957), Stephenson, Massey and Oliver (1974) and Walklate, Heikal and Hatton (1976). Stephenson et al employed the mixing-length hypothesis while Walklate et al have employed the high-Reynolds number ($k\sim\varepsilon$) turbulence model with semi-analytical expressions (usually called wall functions, Launder and Spalding (1973)) in the layer adjacent to the wall.

The heat-transfer results for fully-developed flows of small laminar-Prandtl number fluids (liquid metals) were reported by Martinelli (1947), Lyon (1951), Kropholler

and Carr (1962), Leslie (1977) and many others. In these investigations a zero-equation turbulence model in which the flow domain is divided into distinct layers was employed, with a complete similarity between turbulent heat and momentum transfers (Pr_t = constant) being assumed. This complete similarity may be an acceptable assumption for moderate and large laminar-Prandtl number fluids where the turbulent heat-transfer process is influenced only by the flow motion; but for small laminar-Prandtl-number fluids, where the turbulent heat-transfer process is influenced by both fluid properties and the flow motion, the complete similarity between turbulent heat and momentum transfers is certainly not to be expected.

The effect of the fluid properties on the turbulent momentum and heat transfer processes was first introduced by Jenkins (1951). He modified Prandtl's mixing length hypothesis so as to account for the molecular momentum and heat transfer from eddies during their motion. The eddies were assumed to be spheres of a radius equal to the mixing length (ℓ) and were assumed to have a temperature (T_1) and velocity (u_1) equal to the flow temperature and velocity at the point of creation. The eddies than travelled a distance equal to the mixing length in a time equal to ℓ /v', where v' is the radial velocity fluctuation, to reach their final destination, having a temperature (T_2) and velocity (u_2) which are different to the flow temperature and velocity at the final destination point. During this motion, the surface temperature of the spheres were assumed to vary

linearly with time and the heat-transfer was allowed to take place by conduction. With these assumptions, the conduction equation was solved to obtain the heat-transfer from the spheres and parallel results were used to predict the momentum transfer from the eddies. The final form of the turbulent Prandtl number was then given as follows

$$Pr_t = Pr_\ell^{-1} \left[\frac{\frac{2}{15} - \frac{12}{\pi^2} R_m \sum_{n=1}^{\infty} \frac{1}{n^6} \{1-\exp(-n^2\pi^2/R_m)\}}{\frac{2}{15} - \frac{12}{\pi^2} R_h \sum_{n=1}^{\infty} \frac{1}{n^6} \{1-\exp(-n^2\pi^2/R_h)\}} \right] \quad ,(1.3.14)$$

where

$$R_m = \frac{\rho \ell \, v'}{\mu_\ell} \quad \text{and} \quad R_h = \frac{\rho \ell \, v'}{\Gamma_{h,\ell}}$$

Equation (1.3.14) was used by Jenkins together with the concept of dividing the flow domain into three layers to calculate the Nusselt number. These results were in better agreement with the experimental data than those obtained by Martinelli (1947), which were based on a complete similarity between turbulent heat and momentum transfer. However, the Nusselt number results obtained by Jenkins were still higher than the experimental data.

Deissler (1952) modified the mixing-length hypothesis in order to account for the heat transfer to or from the eddies during their flight. Deissler's analysis was different from Jenkins in the following two respects:

(i) The heat transfer between the eddies and the surrounding fluid was assumed to take place by laminar action instead of the assumed time temperature variation; and

(ii) The eddy dimensions were assumed to be proportional to the mixing length. Deissler also assumed the eddy Peclet

number ($\frac{v'\rho\delta}{\Gamma_{h,\ell}}$), where δ is the boundary layer thickness associated with the heat transfer from the eddy, to be proportional to the mean flow Peclet number ($\frac{\rho u_m D}{\Gamma_{h,\ell}}$). This analysis leads to the following relation for the turbulent Prandtl number:

$$Pr_t^{-1} = b_D \, Pe \, \{1 - \exp(-1/b_D Pe)\} \qquad ,(1.3.15)$$

where b_D is a constant which has been evaluated by Deissler from the turbulent Prandtl number measurements in air flow through pipe.

In the calculation of the Nusselt number, Deissler used a zero-equation turbulence model, in which the flow domain was divided into two layers with the turbulent Prandtl number obtained from (1.3.15). The Nusselt-number results were too small in comparison with the experimental data. This disagreement was mainly due to the turbulent Prandtl number values used in Deissler's investigation. These values of turbulent Prandtl numbers are compared with recent experimental data of Buhr et al (1968), Sleicher et al (1973), Brown et al (1957), Fuchs et al (1973) and Sheriffet al (1973) in figures (1.1 and 1.2) for fluids of laminar Prandtl number 0.02 and 0.007 respectively. These comparisons show that the turbulent Prandtl number values obtained from equation (1.3.15) are in poor agreement with the experimental data.

Aoki (1963) followed Deissler's analysis but with a heat-transfer coefficient between the eddies and the surrounding fluid which accounts for the small-scale turbulence mixing, obtaining the following relation for the turbulent Prandtl number;

$$Pr_t^{-1} = 0.014\ Re^{.45}\ Pr_\ell^{.2}\left[1-\exp\{-1/(0.014Re^{45}\ Pr_\ell^{.2})\}\right] \quad ,(1.3.16)$$

where the constant 0.014 was obtained from liquid-metal experimental data.

The turbulent-Prandtl-number results obtained from equation (1.3.16) are presented with the experimental data for fluids of laminar Prandtl number 0.02 and 0.007 in figures (1.1 and 1.2) respectively. Comparison between Aoki's results and the experimental data presented in these figures shows that Aoki's results are in an acceptable agreement with the experimental data.

Aoki also presented the Nusselt number results obtained from the Martinelli-Lyon correlation, Lyon (1951), which was given by;

$$Nu = 7 + 0.025\ (Pr_\ell / Pr_t)^{0.8} \quad . (1.3.17)$$

These Nusselt number results were in good agreement with the experimental data.

Azer and Chao (1960) modified Prandtl's mixing-length hypothesis in order to account for the momentum and heat transfer from the eddies during their flight. The eddies were assumed to be of a spherical shape with a radius equal to half the mixing length. In calculations of the momentum and heat transfer from the eddies, the heat-transfer coefficient and the coefficient of friction of a laminar flow over flat plate were employed. The turbulent quantities (v', u', and ℓ) were obtained from experimental data, instead of from the proportionality assumed between the eddies Reynolds number ($\frac{\rho v' \ell}{\mu}$) and the mean flow Reynolds number

$(\frac{\rho u_m D}{\mu})$ by Deissler (1952) and Aoki (1963). The turbulent Prandtl number obtained with the above analysis was complicated; but the following approximate relation was reported:

$$Pr_t^{-1} = \frac{1 + 135\ Re^{-.45} \exp\{-(2y/D)^{.25}\}}{1 + 380\ Pe^{-.58} \exp\{-(2y/D)^{.25}\}} \quad .(1.3.18)$$

The comparison of the turbulent Prandtl number calculated from equation (1.3.18) at $2y/D = 0.5$, where the turbulent Prandtl number is approximately equal to the mean value (Lawn (1977)), with the experimental data is shown in figures (1.1 and 1.2). This comparison shows that Azer and Chao's results for the turbulent Prandtl number are in poor agreement with the experimental data.

Kuns et al (1969) developed an empirical relation from the available experimental data for the turbulent Prandtl number; this relation was as follows:

$$Pr_t^{-1} = 1.5 \exp\{-.9\ (\frac{\mu_\ell}{\mu_t Pr_\ell})^{.64}\} \quad .(1.3.19)$$

The above equation is also compared with the experimental data in figures (1.1 and 1.2) for laminar Prandtl numbers of .02 and 0.007 respectively. It is seen that the results of Kuns et al are in poor agreement with the measurements.

The above review of the information regarding the heat-transfer computation of liquid-metal flows shows that the best available results for the turbulent Prandtl number are those obtained by Aoki (1963). These results are in good agreement with the available experimental data, figures (1.1 and 1.2); and the Nusselt number calculated

from the Martinelli-Lyon equation, with Aoki's results for the turbulent Prandtl number, are also in good agreement with the experimental data. As a consequence, Aoki's equation (1.3.16) has been used in the present investigations of the heat-transfer characteristics of liquid-metal flows.

The turbulent-heat-transfer investigations of liquid-metal flows reviewed above were all for flows with large Peclet number (Pe>100) and consequently the axial fluid conduction was neglected. However, the laminar Prandtl numbers of some liquid metal fluids may be as small as 3×10^{-3}. In such cases, even under turbulent flow conditions (Re$\approx$5000), the Peclet number becomes small and the axial fluid conduction cannot be neglected.

No previous studies of the effect of the axial fluid conduction on the heat-transfer characteristics in turbulent pipe flow have come to the author's attention, but the analogous investigation in a laminar flow has been reported by Schneider (1957). The results presented in this investigation indicate that the effect of the axial fluid conduction is important only for flows with a Peclet number less than one hundred and, moreover, the effect is restricted to the developing length which depends on the Peclet number; for a Peclet number of ten, the developing length was less than one tube diameter. A similar investigation, but for a slug flow, was also reported by Chu and Bankoff (1965). This investigation showed that the length over which the effect of the axial fluid

conduction is important, was less than that reported by Schneider for laminar flows.

In all the above investigations, the interface temperature or the heat flux between the fluid and the solid pipe wall was considered as given. This setting of the inner surface boundary conditions instead of its determination from the common solution of the heat conservation equations for a liquid and its surrounding solid wall is unsatisfactory; this is especially so for flows in short passages or those in which the ratio of the wall and fluid thermal conductivities is high or when the wall thickness is appreciably large.

The conjugate problem was first investigated by Perelman (1961) who considered the heat-transfer problem in a liquid flow with a constant velocity around a solid body, but no numerical results were given. Sell and Hudson (1966) followed Perelman (1961) and treated the problem of the heat transfer to a slug flow past a flat plate. They reported the effect of the plate thickness, the flow velocity and the thermal conductivity ratio of the solid wall to the fluid on the temperature at the solid-liquid interface.

Davis and Gill (1970) studied the conjugate heat transfer problem in a Poiseuille-Couette flow between two parallel plates. In this study, the parameters that determine the relative importance of the wall conductions were found to

be: the Peclet number, the thickness to the length ratio of the plates and the parameter $\beta = \frac{\lambda_w \delta_f}{\lambda_f L_H}$, where δ_f is the half distance between the two plates and L_H is the plate length. Increasing β and the thickness to length ratio increases the importance of the conduction in the solid wall, whereas increasing the Peclet number decreases it.

Luikov et al (1971 and 1974) investigated the conjugate problem in a Poiseuille-Couette flow over a flat plate and between two parallel plates. In their investigation the importance of the conduction in the solid wall was determined by a single parameter called the Brun number (Br) which was defined as follows:

$$Br = \frac{\lambda_f}{\lambda_s} \frac{\delta_s}{L_H} Pr_\ell^m Re^n$$

where m and n are the same exponents of the laminar Prandtl number and the Reynolds number respectively as in the relation which gives the Nusselt number ($Nu = \text{constant } Pr_\ell^m Re$) in the geometry under consideration when the conduction in the solid wall is neglected; δ_s is the plate thickness. Luikov (1974) found that an increase in the Brun number increased the importance of the conduction in the solid wall.

To the author's knowledge the only study of the conjugate-heat-transfer problem in turbulent flows has been reported by Sakakibara and Endoh (1977). They studied the effect of the Peclet number, thickness to length ratio and the wall to fluid conductivity ratio in the flow between two parallel plates. This study showed that any increase in the thickness to length ratio and the conductivity ratio

serves to increase the importance of the wall conduction, whereas increasing the Peclet number decreases it.

1.3.3 Unsteady Heat-Transfer Investigations

The unsteady heat-transfer phenomena in steady pipe flows has received a great deal of attention in recent years. Much of this attention was devoted to theoretical studies of both laminar and turbulent flows. The unsteady heat-transfer problems associated with laminar flow were theoretically investigated by Siegel et al (1959a, 1959b, 1961 and 1963), Sparrow et al (1968), Vilensky (1970) and Kuznetzov (1970). The theoretical and experimental investigations of the unsteady heat-transfer characteristics in turbulent flows will be discussed in detail in the following sections.

(a) Experimental studies

Treadwell (1955) and Stuart (1956) investigated the problem of the transient heat-transfer in steady pipe flow of water for a wide range of Reynolds number (6720 - 27000). The unsteadiness was initiated by a sudden heat input dissipated to a stainless-steel tube. Treadwell presented the centreline fluid temperature response at x/D = 48 and 66, while Stuart reported the mean flow temperature, which was measured at a distance of one third of the pipe radius from the wall at x/D = 70. The heat-balance computation over the heating section showed that a heat balance was not obtained for most of the runs. This indicated that one or more of the measurements of mass flow rate, temperature and power were in error. In addition to the reported data,

Treadwell (1955) and Stuart (1956) mentioned further temperature measurements in the solid wall, but unfortionately gave no results.

Koshkin et al (1970) examined the transient heat-transfer problem for air flow through pipes. The unsteadiness was introduced by either a sudden heat input dissipated to the pipe wall or a sudden change in the mass flow rate. The reported results consist of the temperature of the inner and outer wall surfaces and the heat-transfer coefficient at seven downstream locations (x/D = 17.1, 44, 71, 98, 126, 152 and 179). The mean flow temperature response was also reported, but only at the pipe exit. The inner wall temperature and the heat flux from the solid wall to the flow were determined from the solution of the conduction equation inside the solid wall with the measured temperature of the outer wall surface. The mean flow temperatures, over the cross-section, were determined from a heat balance over the pipe length from inlet to the cross-section under consideration. These reported results can be used only in their normalized form, due to the lack of any information regarding the heat generated inside the solid wall.

Finally, Kawamura (1977) investigated the transient heat-transfer problem produced by a sudden heat input dissipated through a solid tube. An experimental procedure, similar to that used by Koshkin (1970) was adopted, but for a water flow at two Reynolds numbers (3740 and 8740). In this procedure, the electric resistance of the solid wall and

the heat input over a test section of five diameters at the end of the thirty diameter heating section was measured. The mean wall temperature over that test section was determined from the measured resistance, and consequently the heat stored in the tube wall was calculated. From this and the measured heat input, the heat-transfer to the flow was determined. Then the mean flow temperature over the test section was deduced from the heat transfer to the flow and the measured mass flow rate. In this study, the unsteady heat-transfer results (heat-transfer coefficient, heat-transfer rate from the solid wall to the flow and the mean flow and wall temperatures), normalized with reference to the coresponding steady-state values, were reported; but, no information regarding the inlet temperature or the laminar Prandtl number of the water used was reported.

(b) Theoretical studies

Clark, Arpaci and Treadwell (1958a, 1958b and 1959) examined the conjugate transient turbulent heat-transfer problem in a pipe under steady-flow conditions. This problem was over-simplified through the following assumptions:

(i) The fluid temperature and velocity are constant over the flow cross-section.

(ii) The heat-transfer coefficient between the flow and the solid wall is evaluated from an empirical relation for steady and fully-developed flow through pipes.

(iii) The tube-wall temperature does not change with radius

(iv) The axial heat conduction is negligible in both fluid and tube walls.

On these above assumptions, the temperature variation with time following a sudden heat generation inside the solid wall

was presented and compared with experimental data.

Sparrow and Siegel (1960) investigated the transient heat-transfer problem initiated by a sudden increase in the wall temperature of a pipe under fully-developed flow conditions. In this investigation, the velocity profile and the thermal diffusivity were assumed to be given by the following formulae:

$$\frac{du^+}{dy^+} = \{1 + .015376\ u^+\ y^+\ [1-\exp\ (-.015376\ u^+\ y^+)]\}^{-1} \quad , 0<y^+<26 \qquad (1.3.20)$$

$$u^+ = 3.8 + 2.78\ell n(y^+) \quad , 26<y^+ \qquad (1.3.21)$$

$$(\Gamma_{h,\ell} + \Gamma_{h,t})/\mu_\ell = 1/Pr_\ell + .015376\ u^+y^+\ [1-\exp(-.015376\ u^+y^+)] \quad , 0<y^+<26 \qquad (1.3.22)$$

$$(\Gamma_{h,\ell} + \Gamma_{h,t})/\mu_\ell = 1/Pr_\ell + 3.6\ y^+(1-y^+/R^+)-1, \quad 26<y^+ \qquad (1.3.23)$$

With the above assumptions, the energy equation was solved analytically and the Nusselt number results were presented for a wide range of laminar Prandtl number (Pr_ℓ>.7). Comparison between these results and those obtained from a quasi-steady analysis* for the developing and fully-developed heat transfer coefficients was also presented in this study. These comparisons show large differences between these results especially at short times. This indicates that the quasi-steady assumption is unacceptable for unsteady heat-transfer computations.

---

* A steady-state heat transfer coefficient is employed.

Kakac (1973), 1975 and 1978) presented an exact solution for the unsteady parabolic energy equation for a fully-developed duct flow with a time-wise variation in the inlet temperature. Only the fully-developed temperature response at the midpoint of the duct to a sinusoldally varying inlet temperature was reported, but no information regarding the velocity profile and the thermal diffusivity employed in this investigation were given.

Finally, Kawamura (1977) presented the conjugate unsteady heat-transfer behaviour following a stepwise time variation in the heat input through the pipe wall. A zero equation turbulence model was employed, the flow was assumed to be fully-developed and steady, and the axial diffusion in the solid wall and the flow domain were neglected. The results for the mean fluid temperature, mean wall temperature, heat-transfer coefficient and the heat transfer to the fluid normalized with respect to the steady state values were reported for water flow with two Reynolds numbers (3740 and 8740).

1.4 Present Study

1.4.1 Objective

The overall objective of the present investigation is to develop and validate a computer prediction method for the hydrodynamic and heat-transfer problems in turbulent wall flows.

The specific aim is to predict the steady hydrodynamics and the steady and unsteady heat-transfer characteristics

in turbulent pipe flows for the whole range of laminar-Prandtl number fluids and to explore the effects of the streamwise diffusion of heat and the solid wall on the heat transfer results.

1.4.2 Outline of Present Contribution

The present approach is based on the numerical solution of the non-linear, partial and coupled differential equations governing the transport of mass, momentum, stagnation-enthalpy, kinetic energy of turbulence and turbulence dissipation rate. The equations governing the transport of the last two variables are those developed and tested for high turbulent Reynolds number in a large variety of flow situations as indicated before. The treatment of the low Reynolds number region adjacent to the wall presents the major subject of concern in the present study.

Owing to the lack of detailed experimental data in unsteady-heat-transfer problems, a brief experimental programme has also been undertaken. The following is a brief account of the contribution made in the above fields.

(a) The near-wall region

The near-wall region has been treated by two different methods. Firstly, the numerical computation in this region was avoided and instead semi-analytical relations, usually called the wall functions (Launder and Spalding (1973)), were employed. These relations are obtained from the analytical solution of the basic equations together with a zero-equation turbulence model and some guidance from experimental data.

The currently adopted wall function (Launder and Spalding (1973)) for the stagnation-enthalpy is restricted to the moderate and large laminar Prandtl number fluids ($Pr_\ell > 0.5$). A new wall function has been developed in the present study for application to the whole range of laminar Prandtl number fluids used in practice.

Secondly, a one-equation turbulence model which takes into account the low-Reynolds-number effects has been employed and the numerical computations extended to the wall itself. This approach, which will be called the composite model, enables the numerical procedure to be applied to flow siutations where the currently-used wall functions are invalid. These situations include unsteady heat-transfer problems, non-Newtonian fluids, flows with drag reduction etc. It is also expected that, the use of this composite model will yield better agreement with experimental data than does the wall-function approach.

(b) Numerical method

The present computations were performed with a computer code based on GENMIX (Spalding (1978)). The following modifications have been introduced to deal with the problem considered:

(i) The one-equation turbulence model was introduced in the near-wall region.

(ii) The "repeated line-by-line TDMA (Tri-Diagonal Matrix Algorithm)" was introduced so as to account for the fact that the procedure used was not fully implicit.

(iii) The hydrodynamic parameters were evaluated and stored after a marching integration in the downstream direction.

(iv) The axial conduction and the unsteady terms were introduced in the stagnation-enthalpy equation which was solved by the introduction of an iterating procedure in the space coordinates plan and a marching integration technique in the time domain.

(v) The computation domain was extended to include the solid pipe wall.

(c) Experimental study

The experimental programme was undertaken with a view to providing data for the validation of the composite-model approach, and to complement existing information on unsteady heat transfer. The quantities measured were the following

(i) The flow temperature profiles at three sections downstream of a sudden heat input.

(ii) The temperature on the outer surface of the wall at four stations downstream of the heat input.

(iii) The temperatures on the outer surface of the wall in the heating section.

1.4.3 Layout of the Thesis

The remainder of this thesis consists of seven chapters. Chapter (2) is concerned with the governing equations of mass, momentum, stagnation-enthalpy, kinetic energy of turbulence and turbulence dissipation rate. In Chapter (3) the wall functions and the low-Reynolds-number turbulence model are presented. The numerical solution procedure for the equations of chapter (2) and (3) is outlined in Chapter (4). The description of the experimental programme and the presentation of the experimental data are presented in Chapter (5), while Chapter (6) contains a comparison of the hydrodynamic and the steady heat-transfer results with available experimental data. The unsteady-

heat-transfer results are presented and compared with experimental data in Chapter (7). Finally, in Chapter (8) the conclusions of the present study are summarized, and recommendations for future work are proposed.

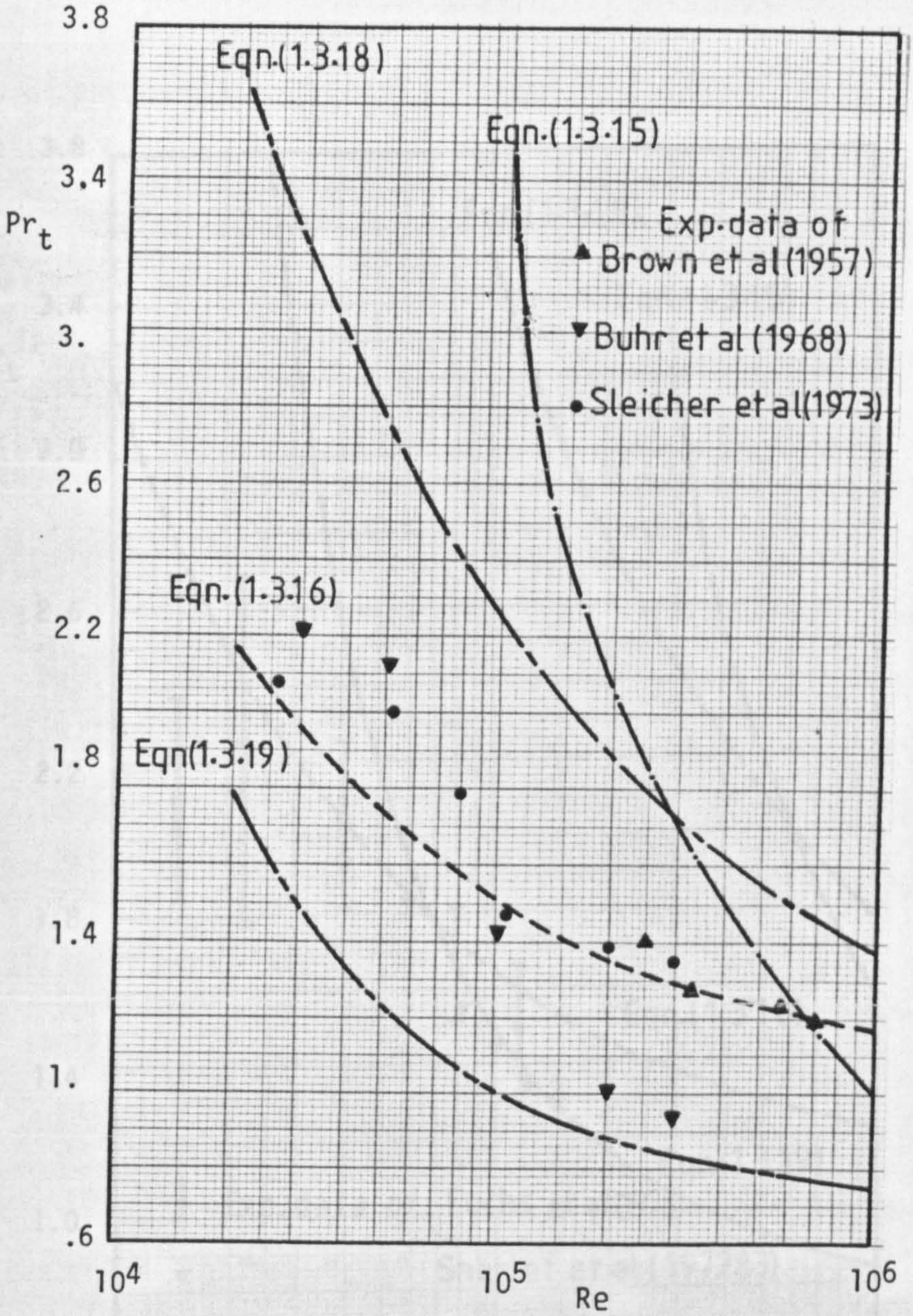


Fig (1.1) Comparison between the recommended equations for the turbulent Prandtl number and the experimental data for a liquid metal fluid with a laminar Prandtl number of .02.

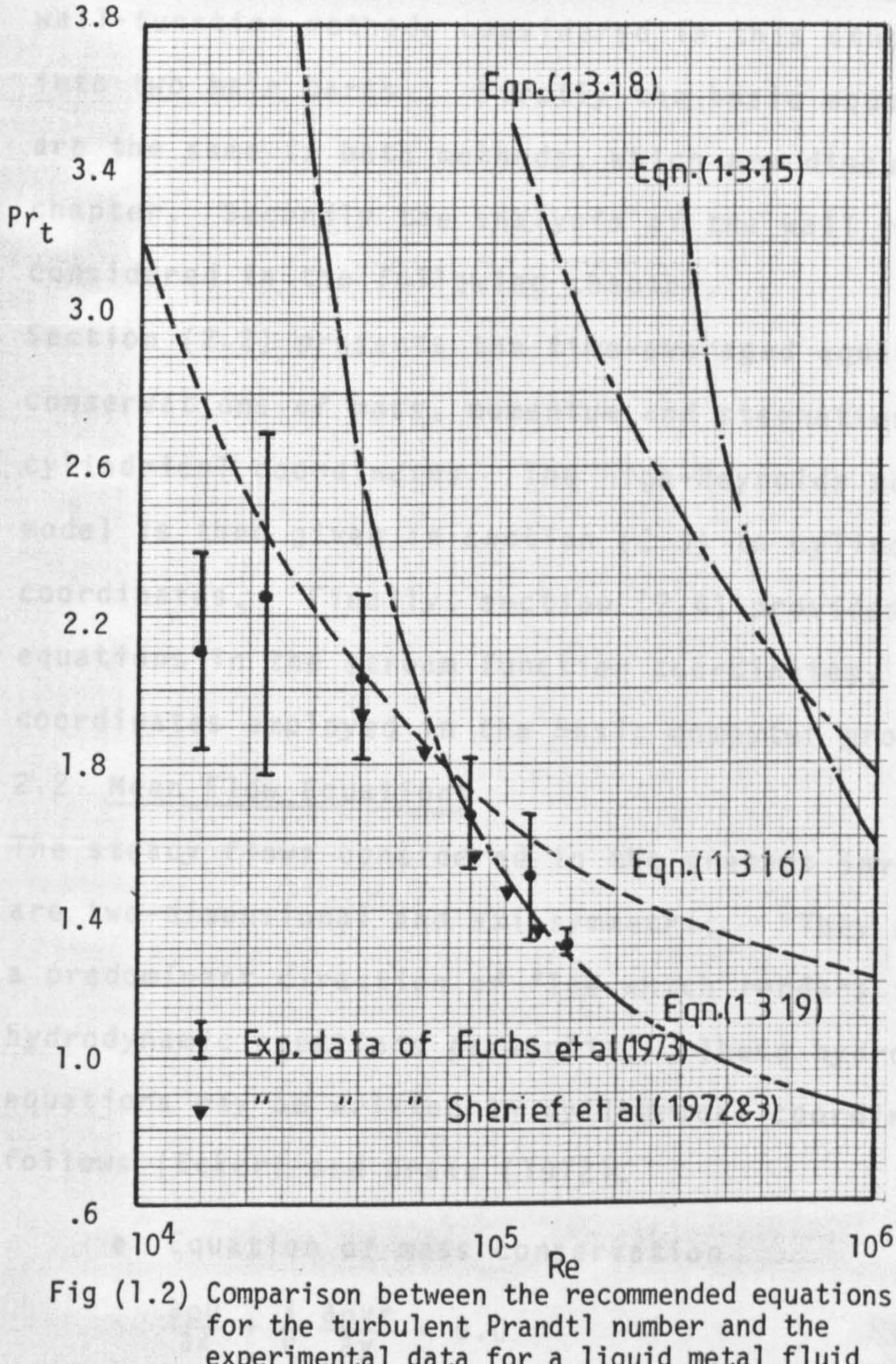


Fig (1.2) Comparison between the recommended equations for the turbulent Prandtl number and the experimental data for a liquid metal fluid with a laminar Prandtl number of .007.

CHAPTER 2

MATHEMATICAL ANALYSIS

2.1 Introduction

The mathematical analysis of the composite-model and the wall-function methods considered in this study is divided into two main parts. Firstly the basic equations which are the same in both methods, which are discussed in this chapter. Secondly the analysis of the wall region which is considered in the following chapter.

Section (2.2) presents the time-averaged equations of conservations of mass, momentum and stagnation-enthalpy in cylindrical coordinates. The high-Reynolds number turbulence model is then given in section (2.3) in cylindrical coordinates. Finally, section (2.4) provides the basic equations in the stream function coordinates, which are the coordinates employed in the basic computer program chosen.

2.2 Mean Flow Equations

The steady flows considered in the present investigation are two-dimensional and axi-symmetric. They also exhibit a predominant direction of flow which renders the governing hydrodynamic equations parabolic. These hydrodynamic equations may be written in cylindrical coordinates as follows (Eckert and Drake (1972)).

- Equation of mass conservation

$$\frac{\partial \rho u}{\partial x} + \frac{1}{r}\frac{\partial \rho v r}{\partial y} = 0.0 \quad , (2.2.1)$$

- Equation of momentum conservation

$$\frac{\partial \rho u u}{\partial x} + \frac{1}{r}\frac{\partial \rho u r v}{\partial y} = -\frac{dP}{dx} + \frac{1}{r}\frac{\partial}{\partial y}\{r(\mu_\ell \frac{\partial u}{\partial y} - \rho\overline{u'v'})\} \quad . (2.2.2)$$

Equations (2.2.1 and 2.2.2) contain four unknowns (u, v, $\frac{dP}{dx}$ and $\overline{u'v'}$) besides the density, which is either constant

(incompressible flows) or calculated from the equation of state (compressible flows). This latter equation is given by: $P = \rho R_g T$, (2.2.3)

where, R_g is the gas constant

The unknowns $\frac{dP}{dx}$ and $\overline{u'v'}$ must be specified before equations (2.2.1 and 2.2.2) can be solved. The pressure-gradient term, $\frac{dP}{dx}$, is calculated from the additional constraint on the mass-flow rate Spalding (1978). While the method of calculation of the Reynolds stress, $\overline{u'v'}$, will be discussed in the next section.

In the present analysis, the major attention is devoted to the study of the steady and unsteady heat-transfer problems in liquid-metal flows. Since liquid metals have very small laminar Prandtl numbers ($Pr_\ell \approx 10^{-3}$), even under turbulent-flow conditions at values of the Reynolds number up to 10^5, the Pecletnumber is relatively small. Thus the stagnation-enthalpy equation becomes elliptic in the stream-wise direction. For the unsteady, two-dimensional and axisymmetric flows under consideration, the stagnation-enthalpy equation in the cylindrical coordinates can be written as follows (Eckert and Drake (1972)):

$$\frac{\partial \rho \tilde{h}}{\partial t} + \frac{\partial \rho u \tilde{h}}{\partial x} + \frac{1}{r}\frac{\partial \rho r v \tilde{h}}{\partial y} = \frac{1}{r}\frac{\partial}{\partial y}\{r(\Gamma_\ell \frac{\partial \tilde{h}}{\partial y} - \rho C_p \overline{T'v'})\} + \frac{\partial}{\partial x}\{\Gamma_\ell \frac{\partial \tilde{h}}{\partial x} - \rho C_p \overline{T'u'}\}$$

$$+ \frac{1}{r}\frac{\partial}{\partial y}\{r(\mu_\ell - \frac{\rho u'v'}{\partial u/\partial y})\frac{\partial u^2/2}{\partial y}\} - \frac{1}{r}\frac{\partial}{\partial y}\{\Gamma_\ell r\frac{\partial u^2/2}{\partial y}\} \quad , (2.2.4)$$

where $\overline{u'T'}$ and $\overline{v'T'}$ are the turbulent heat fluxes which will be discussed in the next section and $\tilde{h}$ is the stagnation-enthalpy defined as:

$$\tilde{h} = C_p T + u^2/2 \quad , \qquad (2.2.5)$$

In the present investigation, the conjugate unsteady heat-transfer problems are also considered. In these problems, the heat-transfer boundary condition is imposed on the outer surface of the pipe wall and the solid wall is considered as a part of the computation domain. The enthalpy equation applicable to a cylindrical solid wall with unsteady heating conditions can be written as follows (Eckert and Drake (1972)):

$$\rho \frac{\partial \bar{h}}{\partial t} = \Gamma_{h,\ell} \{ (\frac{\partial^2 \bar{h}}{\partial x^2}) + \frac{1}{r} \frac{\partial}{\partial y} (r \frac{\partial \bar{h}}{\partial y}) \} + Q' \quad , \qquad (2.2.6)$$

where $\bar{h}$ is the static enthalpy, defined by $(C_p T)$ and Q' is the heat generated per unit time and volume.

2.3 Turbulence Model

In accordance with the discussion of the available turbulence models presented in section (1.3), the high-Reynolds-number two-equation ($k \sim \varepsilon$) turbulence model has been employed in the regions of high turbulent Reynolds numbers ($\rho k^{\frac{1}{2}} \ell / \mu_\ell$). This model (Launder and Spalding (1972)) is based on the eddy-viscosity concept in which the Reynolds stress ($\overline{u'v'}$) for parabolic flows is expressed as follows:

$$-\rho \overline{u'v'} = \mu_t \frac{\partial u}{\partial y} \quad , \qquad (2.3.1)$$

and the turbulent viscosity (μ_t) is expressed in terms of the turbulence kinetic energy and the turbulence dissipation rate as follows:

$$\mu_t = C_\mu C_D \rho k^2/\varepsilon \quad , \qquad (2.3.2)$$

where C_μ and C_D are constants of 0.5477 and 0.164 respectively (Spalding (1978)).

The exact transport equations for the turbulent kinetic energy and the turbulence dissipation rate are derived from the Navier-Stokes equations describing turbulent flows. These derivations have been presented by many researchers (e.g. Daly and Harlow (1970), Malhotra (1977), Samaraweera (1978) and El-Tahry (1979)), and therefore will not be presented in the present study. The final forms of equations for the turbulent kinetic energy and the turbulence dissipation rate for steady, two-dimensional parabolic flows in cylindrical coordinates is given by Launder and Spalding (1972)):

$$\frac{\partial \rho uk}{\partial x} + \frac{1}{r}\frac{\partial \rho rvk}{\partial y} = \frac{1}{r}\frac{\partial}{\partial y}\left(\frac{r\mu_{eff}}{\sigma_k}\frac{\partial k}{\partial y}\right) + \mu_t\left(\frac{\partial u}{\partial y}\right)^2 - \rho\varepsilon \quad ; (2.3.3)$$

$$\frac{\partial \rho u\varepsilon}{\partial x} + \frac{1}{r}\frac{\partial \rho rv\varepsilon}{\partial y} = \frac{1}{r}\frac{\partial}{\partial y}\left(\frac{r\mu_{eff}}{\sigma_\varepsilon}\frac{\partial \varepsilon}{\partial y}\right) + \mu_t\left(\frac{\partial u}{\partial y}\right)^2 C_1\frac{\varepsilon}{k} - \frac{C_2}{C_\mu C_D}\frac{\rho\varepsilon}{k}\varepsilon \quad ; (2.3.4)$$

where the constants σ_k, σ_ε, C_1 and C_2 were assigned values of 1., 1.3, 1.44 and 0.172, and μ_{eff} is the effective viscosity.

Following the eddy-viscosity concept, the turbulent heat transfers, $\overline{\rho v'T}$ and $\overline{\rho u'T'}$, can be expressed as follows:

$$-\overline{\rho u'T'} = \Gamma_{h,t}\frac{\partial T}{\partial y} \quad , \text{and} \quad , (2.3.5)$$

$$-\overline{\rho v'T'} \doteq \Gamma_{h,t}\frac{\partial T}{\partial x} \quad , (2.3.6)$$

where the turbulent diffusivity of heat ($\Gamma_{h,t}$) is related to the turbulent viscosity through the turbulent Prandtl number (Pr_t) as follows:

$$Pr_t = \frac{\mu_t}{\Gamma_{h,t}} \quad . (2.3.7)$$

2.4 Governing Differential Equations in ω-x Coordinates

The present calculations were performed with a computer code based on GENMIX (A General Computer Program for Two-Dimensional Parabolic Phenomena) by Spalding (1978). This program was specially devised for the solution of a system of simultaneous equations which arise in the theory of two-dimensional steady boundary layers, each having the general form:

$$\frac{\partial \phi}{\partial x} + (a+b\omega)\frac{\partial \phi}{\partial \omega} = \frac{\partial}{\partial \omega}\{c(\frac{\mu_{eff}}{\sigma_{\phi}})\frac{\partial \phi}{\partial \omega}\} + d \quad , \quad (2.4.1)$$

where:

a and b are arbitrary functions of the coordinates x

c and d may be arbitrary functions of any of the dependent variables,

ϕ stands for any one of a set of dependent variables, and

x and ω are the two independent variables which are related to stream function coordinates (ψ-x) according to:

$$x = x \quad , \quad (2.4.2)$$

$$\omega = \frac{\psi - \psi_I}{\psi_E - \psi_I} \quad , \quad (2.4.3)$$

where the subscripts I and E stand for the inner and outer boundaries of the flow domain and ψ is the stream function defined as:

$$\psi = \int_0^y \rho r u dy \quad . \quad (2.4.4)$$

In order to transform the governing differential equations (2.2.1, 2.2.2, 2.2.4, 2.3.3 and 2.3.4) from the cylindrical coordinates to the (ω-x) coordinates, these equations will

be first presented in the stream-function coordinates (Spalding (1978)) as follows:

- Momentum equation

$$\frac{\partial u}{\partial x} = \frac{\partial}{\partial \psi}\left(r^2 \rho u \mu_{eff} \frac{\partial u}{\partial \psi}\right) + \frac{1}{\rho u}\left(-\frac{dP}{dx}\right) \quad ; (2.4.5)$$

- Turbulent kinetic energy equation

$$\frac{\partial k}{\partial x} = \frac{\partial}{\partial \psi}\left(r^2 \rho u \frac{\mu_{eff}}{\sigma_k} \frac{\partial k}{\partial \psi}\right) + \frac{1}{\rho u}\{\mu_t \left(\frac{\partial u}{\partial y}\right)^2 - \rho \varepsilon\} \quad ; (2.4.6)$$

- Equation of turbulence dissipation rate

$$\frac{\partial \varepsilon}{\partial x} = \frac{\partial}{\partial \psi}\left(r^2 \rho u \frac{\mu_{eff}}{\sigma_\varepsilon} \frac{\partial \varepsilon}{\partial \psi}\right) + \frac{1}{\rho u}\{C_1 \mu_t \frac{\varepsilon}{k} \left(\frac{\partial u}{\partial y}\right)^2 - \frac{C_2}{C_\mu C_D} \rho \frac{\varepsilon}{k_\varepsilon} \varepsilon\} \quad . (2.4.7)$$

The enthalpy equation (2.2.4) which is elliptic in the stream-wise direction and unsteady can be re-written in (ψ-x) coordinates by the addition of the unsteady and the stream wise diffusion terms to the steady, parabolic equation presented by Spalding (1978). This yields;

$$\frac{1}{u}\frac{\partial \tilde{h}}{\partial t} + \frac{\partial \tilde{h}}{\partial x} = \frac{\partial}{\partial \psi}\{r^2 \rho u \Gamma_{h,eff} \frac{\partial \tilde{h}}{\partial \psi}\} + \frac{1}{\rho r u}\frac{\partial}{\partial x}\{\Gamma_{h,eff}\, r \frac{\partial \tilde{h}}{\partial x}\} +$$

$$\frac{\partial}{\partial \psi}\{(\mu_{eff} - \Gamma_{h,eff})\, r \frac{\partial u^2/2}{\partial y}\} \quad , (2.4.8)$$

$$\text{where, } \Gamma_{h,eff} = \mu_\ell / Pr_\ell + \mu_t / Pr_t \quad .(2.4.9)$$

The transformation of equation (2.4.8) to the (ω-x) coordinates is presented in Appendix A.

The final form is:

$$\frac{1}{u}\frac{\partial \tilde{h}}{\partial t} + (a+b\omega)\frac{\partial \tilde{h}}{\partial \omega} + \frac{\partial \tilde{h}}{\partial x} = \frac{\partial}{\partial \omega}\left(c\, \Gamma_{h,eff} \frac{\partial \tilde{h}}{\partial \omega}\right) + \frac{1}{\rho u r}\frac{\partial}{\partial x}\left(r\, \Gamma_{h,eff} \frac{\partial \tilde{h}}{\partial x}\right)$$

$$+ \frac{1}{\rho u r}\frac{\partial}{\partial \omega}\{(a+b\omega)^2 r \Gamma_{h,eff} \frac{\partial \tilde{h}}{\partial \omega}\} + \frac{(a+b\omega)}{\rho r u}\{\frac{\partial}{\partial x}(r \Gamma_{h,eff} \frac{\partial \tilde{h}}{\partial \omega}) + \frac{\partial}{\partial \omega}(r \Gamma_{h,eff} \frac{\partial \tilde{h}}{\partial x})\}$$

$$+ \frac{\partial}{\partial \omega}\left[\left(\frac{\mu_{eff} - \Gamma_{h,eff}}{(\psi_E - \psi_I)^2}\right) r^2 \rho u \frac{\partial u^2/2}{\partial \omega}\right] \quad , (2.4.10)$$

where a, b and c are defined as follows:

$$a \equiv \frac{-1}{(\psi_E - \psi_I)} \frac{d\psi_I}{dx} \qquad ,(2.4.11)$$

$$b \equiv \frac{-1}{(\psi_E - \psi_I)} \frac{d(\psi_E - \psi_I)}{dx} \qquad ,(2.4.12)$$

$$c \equiv \frac{r^2 \rho u}{(\psi_E - \psi_I)^2} \qquad .(2.4.13)$$

For the axisymmetric pipe flow without mass injection through the solid boundary, the stream functions at both the E and I boundaries are constants and consequently the a and b expressions, equations (2.4.11 and 2.4.12), are zero. Thus equation (2.4.10) was reduced to:

$$\frac{1}{u}\frac{\partial \tilde{h}}{\partial t} + \frac{\partial \tilde{h}}{\partial x} = \frac{\partial}{\partial \omega}\left(c\, \Gamma_{h,eff} \frac{\partial \tilde{h}}{\partial \omega}\right) + \frac{1}{\rho r u}\frac{\partial}{\partial x}\left(r\, \Gamma_{h,eff} \frac{\partial \tilde{h}}{\partial x}\right) +$$

$$\frac{\partial}{\partial \omega}\left\{\frac{(\mu_{eff} - \Gamma_{h,eff})}{(\psi_E - \psi_I)^2}\, r^2 \rho u \frac{\partial u^2/2}{\partial \omega}\right\} \qquad .(2.4.14)$$

Similarly, equations (2.4.5), (2.4.6) and (2.4.7) may be transformed to the (ω-x) coordinates obtaining the general form of (2.4.1), with the values of σ_ϕ and the expressions for d given in table (2.1).

Table (2.1)

Values of σ_ϕ and expression for d in equation (2.4.1)

Conservation of	σ_ϕ	d
Momentum, u	1.0	$-\frac{1}{\rho u}\frac{dP}{dx}$
Kinetic energy of turbulence, k	1.0	$\frac{1}{\rho u}\left\{\left(\frac{\partial u}{\partial y}\right)^2 \mu_t - \rho\varepsilon\right\}$
Turbulence dissipation rate, ε	1.3	$\frac{1}{\rho u}\left\{\mu_t C_1 \frac{\varepsilon}{k}\left(\frac{\partial u}{\partial y}\right)^2 - \frac{C_2}{C_\mu C_D}\frac{\rho\varepsilon}{k}\varepsilon\right\}$

2.5 Closure

The conservation equation of mass, momentum, stagnation-enthalpy, kinetic energy of turbulence and turbulence dissipation rate, which are employed in both the composite model and the wall-function methods, have been presented. The latter two equations were presented in the form which is valid for high-Reynolds numbers only.

In the following chapter, the wall function is presented together with the low-Reynolds-number-turbulence model. This will conclude the mathematical analysis of the present study.

CHAPTER 3

ANALYSIS OF THE NEAR-WALL REGION

3.1 Introduction

In the previous chapter, the conservation equations of mass, momentum and stagnation-enthalpy, together with the high-Reynolds number form of the transport equations for the turbulent kinetic energy and the turbulence dissipation rate were presented. In order to complete the mathematical representation of the problem, the low-Reynolds-number region adjacent to the wall is considered in the present chapter.

The review of the different turbulence models given in section (1.3)* indicated that only zero and one-equation models have been sufficiently tested for low-Reynolds number regions. The review also shows that the one-equation turbulence models are generally more accurate than the zero-equation models. However, the use of a one-equation model in the numerical computations of the flow adjacent to the wall, where the flow is characterised by a steep variation in the dependent variables, requires excessive computational time and storage. For example, Hassid and Poreh (1975) employed one hundred radial grid points, half of them in the near-wall region, with forward steps of 0.001 the pipe diameter in their pipe flow computations.

In many flow situations, e.g. steady, Newtonian flows and flows where the fluid physical properties (ρ, μ, C_p and $\Gamma_{h,\ell}$) are constant, it is possible to obtain a semi-analytical

---

* pages 24 - 29

solution for the basic equations in the near-wall region with the use of a zero-equation turbulence model and some guidence from experimental data. Consequently the numerical computation can be avoided in the layer adjacent to the wall and instead the semi-analytical solutions may be used to link the values of the dependent variables in the fully turbulent part of the flow with those at the wall. The use of these semi-analytical solutions, which are usually called "wall functions" (Launder and Spalding (1972)), is very attractive for engineering purposes. Therefore both the wall-function approach and the one-equation turbulence model of Hassid and Poreh (1975) were employed in the present study.

The semi-analytical solutions for the momentum and stagnation-enthalpy are developed in section (3.2), while the one-equation turbulence model which accounts for low-Reynolds-number effects is presented in section (3.3)

3.2 Development of the Wall Functions

Several formulations for the turbulent viscosity and the mixing length applicable to low-turbulent-Reynolds-number flows have been proposed in the literature; a summary of these may be found in Hinze (1975). Some of these proposals (e.g. Spalding (1961) and Van Driest (1956)) cover the flow in the near-wall region by a single equation. The use of these equations was not convenient in obtaining analytical solutions for the conservation equations of momentum and stagnation-enthalpy. The other proposals for the turbulent viscosity were based on the concept of division of the near-wall region into distinct layers as

follows:

(a) <u>The three-layer division</u> (Martinelli (1948))

(i) A laminar sublayer ($0<y^+<5$), where the turbulent transport of heat and momentum are neglected in comparison with the viscous transport:

(ii) A transitional layer ($5<y^+<30$), where both the molecular and turbulent transport are assumed to be of the same order; and

(iii) A turbulent layer ($y^+>30$), where the molecular transport of momentum is neglected in comparison with the turbulent transport, while the molecular transport of heat is neglected for moderate and large laminar Prandtl number fluids only.

(b) <u>The two-layer division</u> (Levich (1962))

(i) An effective laminar sublayer, the thickness of which will be discussed later, which is similar to the laminar sublayer in the three-layer analysis above, and

(ii) A turbulent layer, which covers the remainder of the flow domain.

Although the above methods of flow division introduced discontinuities in the dependent variables, the results in the turbulent layer were in acceptable agreement with experimental data. Moreover, these methods readily yield analytical solution for the present investigation. The concept was modified to account for the effect of the Reynolds number and the laminar-Prandtl-number, as will be shown in the following sections.

3.2.1 Momentum equation

Close to a wall, the convection terms in the momentum equation (2.2.2) can be neglected, and hence the latter reduces to

$$\frac{dP}{dx} = \frac{d\tau}{dy} = \frac{d}{dy}\{(\mu_\ell + \mu_t)\frac{du}{dy}\} \quad . \quad (3.2.1)$$

For flows without pressure gradient, the integration of the above equation leads to:

$$u^+ = \int_0^{y^+} \frac{dy^+}{1 + \mu_t/\mu_\ell} \quad . \quad (3.2.2)$$

The turbulent viscosity is defined in the effective laminar sublayer and in the turbulent layer as follows (Davies (1972)).

$$\begin{aligned} \mu_t/\mu_\ell &= 0.0 \quad ; \quad y^+ < y_M^+ \\ \mu_t/\mu_\ell &= Ky^+ \quad ; \quad y^+ > y_M^+ \end{aligned} \quad , \quad (3.2.3)$$

where the thickness of the effective momentum laminar sublayer (y_M^+) is to be determined from experimental data, and K is the Von Karman constant which is equal to 0.4. Combination of equations (3.2.2 and 3.2.3) gives

$$u^+ = y_M^+ - \frac{1}{K}\ell n\,(1 + Ky_M^+) + \frac{1}{K}\ell n\,(1 + Ky^+) \quad . \quad (3.2.4)$$

Comparison between equation (3.2.4) and the experimental velocity data presented by Hinze (1975), gives

$$y_M^+ = 11.635 \quad . \quad (3.2.5)$$

Substitution from (3.2.5) into (3.2.4) leads to:

$$u^+ = 7.79 + 2.5\,\ell n\,(1 + 0.4y^+) \quad . \quad (3.2.6)$$

The unity term in the logarithmic expression may be neglected and then equation (3.2.6) reduces to the well-known logarithmic velocity distribution

$$u^+ = 5.5 + 2.5\,\ell n\,y^+ \quad . \quad (3.2.7)$$

In order to account for the pressure-gradient effect on the velocity distribution, the shear stress used in defining y^+ and u^+ in equations (3.2.6 and 3.2.7) was replaced by an average shear stress which is given by Spalding (1978).

$$\tau = \tau_w + \tfrac{1}{2} y \frac{dP}{dx} \qquad (3.2.8)$$

3.2.2 The stagnation-enthalpy equation

With assumptions similar to those made for the momentum equation in the near-wall region, the stagnation-enthalpy equation (2.2.4) may be reduced to:

$$\frac{d\dot{q}''}{dy} = \frac{d}{dy}\left\{(\lambda_\ell + \lambda_t)\frac{dT}{dy}\right\} \qquad , \quad (3.2.9)$$

where $\dot{q}''$ is the heat transfer rate per unit area and λ is the thermal conductivity.

In order to define the turbulent thermal conductivity (λ_t), the near-wall region was divided conceptually into two layers about the point $y^+ = y_H^+$. The effective-thermal-sublayer thickness (y_H^+) was assumed to be equal to the momentum thickness (y_M^+) only when complete similarity between momentum and heat transport exists (i.e. $Pr_\ell \simeq Pr_t$). The temperature measurements of Kirillov (1962) and Gowen and Smith (1967) showed that the effective-thermal-laminar-sublayer thickness should be greater than the momentum one for small-laminar-Prandtl number fluids, whereas the opposite is true for large-laminar-Prandtl-number fluids. Thus the turbulent thermal conductivity in the thermal effective laminar sublayer ($0<y^+<y_H^+$) and in the turbulent layer ($y^+>y_H^+$) were prescribed similar to the prescribed turbulent viscosity (equation (3.2.3)) as follows:

$$\lambda_t/\lambda_\ell = 0.0 \quad ; \quad y^+ < y_H^+$$
$$\lambda_t/\lambda_\ell = \frac{Pr}{Pr_t} K y^+ \quad ; \quad y^+ > y_H^+ \qquad .(3.2.10)$$

The effective-thermal-laminar-sublayer thickness (y_H^+) was assumed by Levich (1962) and Davies (1972) to be given by:

$$y_H^+/y_M^+ = (Pr_t/Pr_\ell) \qquad ,(3.2.11)$$

and,

$$y_H^+/y_M^+ = (Pr_t/Pr_\ell)^{1/3} \qquad ,(3.2.12)$$

respectively. However, in the present study, the value of y_H^+ was determined from experimental measurements of the temperature profile.

Substitution from (3.2.10) into (3.2.9) gives, after integration;

$$T^+ \equiv \frac{(T_w - T)\rho C_p u^*}{q''} = y_H^+ Pr_\ell - \frac{Pr_t}{K} \ell n (1 + K\frac{Pr_\ell}{Pr_t} y_H^+) + \frac{Pr_t}{K} \ell n (1 + K\frac{Pr_\ell}{Pr_t} y^+) \; ;$$
$$.(3.2.13)$$

Or,

$$R_r = \{\tilde{y}_H - \ell n(1+\tilde{y}_H) + \ell n(1+\tilde{y})\}/\tilde{y} \qquad ,(3.2.14)$$

where $R_r \equiv \frac{\lambda_\ell (T_w - T)}{\dot{q}'' y}$ and $\tilde{y} = K \frac{Pr_\ell}{Pr_t} y^+$

In order to reveal the similarity between the temperature and velocity profiles, equations (3.2.4) and (3.2.13) may be re-arranged as follows:

$$T^+ = Pr_t (P + u^+) \qquad ,(3.2.15)$$

where P is the function that expresses the resistance of the laminar sublayer to heat transfer on account of the laminar Prandtl number being different from the turbulent one,

and is defined according to:

$$P = y_H^+ \frac{Pr_\ell}{Pr_t} - \frac{1}{K} \ell n\ (1+K \frac{Pr_\ell}{Pr_t} y_H^+) + \frac{1}{K} \ell n\ (1+K \frac{Pr_\ell}{Pr_t} y^+) -$$

$$\{y_M^+ - \frac{1}{K} \ell n\ (1+K\ y_M^+) + \frac{1}{K} \ell n(1+Ky^+)\} \quad \cdot\ (3.2.16)$$

For moderate and large laminar-Prandtl-number fluids ($Pr_\ell > 0.7$), equation (3.2.16) may be simplified, to give:

$$P \approx (y_H^+ \frac{Pr_\ell}{Pr_t} - y_M^+) + \frac{1}{K} \ell n\ (y_H^+/y_M^+) \quad \cdot\ (3.2.17)$$

Comparison between equations (3.2.16) and (3.2.17) shows that, the P-function depends on y_H^+ and Pr_ℓ/Pr_t for medium and large-laminar-Prandtl-number fluids, while it depends on y_H^+, Pr_ℓ/Pr_t and y^+ for small-laminar-Prandtl numbers. However, the experimental data for the P-function collected by Jayatillek (1969) for medium and large laminar-Prandtl-number fluids shows that, the P-function depends only on Pr_ℓ/Pr_t. This indicates that y_H^+ is a function of (Pr_ℓ/Pr_t), and this function was taken to be as follows:

$$y_H^+/y_M^+ = (Pr_t/Pr_\ell)^z \quad , \quad (3.2.18)$$

where z = 1.0 gives Levich's equation (3.2.11) and z = 1/3 gives Davies' equation (3.2.12). In the present study the z value will be obtained from experimental data.

In order to show the effect of the exponent z on the P-function (equation, 3.2.16), the P-function has been presented in figure (3.1) for three different values of z(z= 1/4 , 1/3 and 1/2) for a flow of Reynolds number of 5×10^4 over a wide range of laminar Prandtl numbers. The turbulent-Prandtl number was assumed equal to one for laminar Prandtl numbers greater than 0.5; for smaller laminar-Prandtl-

numbers, Aoki's equation (1.3.16) was employed. The results presented in figure (3.1) show that the larger the laminar-Prandtl-number the larger the ż-effect on the P-function. Consequently, the large-laminar-Prandtl-number temperature measurements were used to obtain accurate estimates of the z values.

A least-square-curve-fitting for the temperature measurements of Gowen and Smith (1967) in water flow showed that the thermal-effective-laminar-sublayer thickness is given by:

$$y_H^+ = y_M^+ \left(\frac{Pr_t}{Pr_\ell}\right)^{0.28} \qquad \cdot\cdot (3.2.19)$$

The dimensionless temperature results obtained from equation (3.2.14) with the y_H^+ value given by equation (3.2.19) are compared with the experimental data of Fuchs (1973), Buhr et al (1968), Johnk and Hanratty (1962) and Gowen and Smith (1967), for a wide range of laminar-Prandtl number (Pr_ℓ = .007 → 14.2) in figure (3.2). This comparison shows that the method of dividing the near-wall region into two layers, with equation (3.2.19) used to specify the thermal-effective-laminar-sublayer thickness, yields temperature profiles in good agreement with experimental data.

Substitution of (3.2.19) into (3.2.16) gives the following P-function, valid for the whole range of laminar-Prandtl numbers,

$$P = y_M^+ \left\{\left(\frac{Pr_\ell}{Pr_t}\right)^{0.72} - 1\right\} - \frac{1}{K} \ell n \left[\left\{1+Ky_M^+ \left(Pr_\ell/Pr_t\right)^{.72}\right\}/\left\{1+Ky_M^+\right\}\right]$$

$$+ \frac{1}{K} \ell n \left[\left\{1 + Ky^+ \frac{Pr_\ell}{Pr_t}\right\}/\left\{1 + Ky^+\right\}\right] \qquad \cdot (3.2.20)$$

The moderate and large-laminar-Prandtl-number version of the

P-function is deduced from equations (3.2.17) and (3.2.19) to be:

$$P = y_M^+ \{ (\frac{Pr_\ell}{Pr_t})^{.72} - 1 \} - \frac{1}{k} \ell n \, (Pr_\ell/Pr_t)^{0.28} \quad . \quad (3.2.21)$$

The P-functions given by equation (3.2.20) and those proposed by Jayatilleka(1967) and Launder and Spalding (1973) are compared in figure (3.3) for moderate and large-laminar-Prandtl-number fluids. The equation of Jayatilleka is:

$$P = 9.24 \{ (\frac{Pr_\ell}{Pr_t})^{.75} - 1.0 \} \{ 1 + 0.28 \exp(-.007 \frac{Pr_\ell}{Pr_t}) \} \quad , \quad (3.2.22)$$

while the formula of Launder and Spalding is:

$$P = 9.0 \, (\frac{Pr_\ell}{Pr_t} - 1) \, (\frac{Pr_\ell}{Pr_t})^{-.25} \quad . \quad (3.2.23)$$

Figure (3.3) shows that the P-function developed here is in good agreement with both Jayatillek's and Launder and Spalding's equations for the moderate and large-laminar-Prandtl-numbers. Consequently the present P-function, which has been tested for laminar Prandtl numbers between 0.007 and 1000, is recommended for use over the entire range of laminar Prandtl numbers.

3.2.3 Kinetic energy of turbulence and its dissipation rate.

Close to a wall, convection and diffusion of turbulent kinetic energy can be neglected and the production and dissipation of this quantity can be assumed to be in balance (Launder and Spalding (1972)). These lead to the following relation

$$k = \frac{\tau_w}{\rho (C_\mu C_D)^{.5}} \quad . \quad (3.2.24)$$

While the turbulence dissipation rate near to the wall can be obtained from equations (2.3.2, 3.2.3 and 3.2.24) as follows:

$$\varepsilon = \frac{(C_\mu C_D)^{\frac{3}{4}} k^{3/2}}{ky} \quad . \quad (3.2.25)$$

3.3 One-Equation Turbulence Model

In accordance with the discussion of section (1.3), the one-equation (k) turbulence model has been selected for the region of the low-turbulent-Reynolds-number adjacent to the wall. Many equations have been proposed for the turbulent kinetic energy, e.g. Glushko* (1965), Wolfshtein (1967), Norris and Reynolds (1975) and Hassid and Poreh (1975). These equations differ from the high-Reynolds-number form (equation (1.3.5)) mainly in the approximation of the dissipation term (ε) and in the relating of the turbulent viscosity to the turbulent-kinetic energy and the turbulent-length scale. All the proposed changes in these quantities (ε and μ_t) may be written in the following general forms:

$$\varepsilon = C_3 \nu \frac{k}{\ell^2} + C_4 C_D \frac{k^{3/2}}{\ell} \quad , \quad (3.3.1)$$

$$\mu_t = C_5 C_\mu \rho k^{\frac{1}{2}} \ell \quad , \quad (3.3.2)$$

where C_3 is a constant, C_4 and C_5 are functions expressed in terms of the turbulent-Reynolds number ($k^{\frac{1}{2}} \ell \rho/\mu$) and ℓ is the length scale equal to (0.4y) in the near-wall region.

The constant C_3 was assigned the values of .63, 0.0, 0.328 and 0.328

---

*As reported by Spalding (1975)

by Glushko, Wolfshtein, Norris and Reynolds, and Hassid and Poreh respectively. Very close to the wall, the viscous diffusion should be balanced by the dissipation term (Townsend (1954)), and the experimental measurements of Laufer (1954) and Clark (1968) indicate that the turbulent-kinetic energy of turbulence is proportional to the square of the distance from the wall. These conditions were only satisfied with the proposed values of the constant (C_3) by Norris and Reynolds, and Hassid and Poreh.

The following function (C_4) was recommended by Glushko (1968):

$$\left.\begin{aligned} C_4 &= .00909\ R_k && ;\quad .00909\ R_k < 0.75 \\ &= .00909\ R_k - (.00909\ R_k - .75)^2 && ;\quad .75 < .00909\ R_k < 1.25 \\ &= 1.0 && ;\quad .00909\ R_k > 1.25 \end{aligned}\right\} \quad (3.3.3)$$

While Wolfshtein (1967), most probably with the mixing length hypothesis in mind, 'damped' the length scale instead of damping the dissipation term ($k^{3/2}/\ell$); consequently his prescription for C_4 was given as follows:

$$C_4 = 1/\{1-\exp(-A_D R_k)\} \quad (3.3.4)$$

Norris and Reynolds (1975) considered C_4 as a constant equal unity. Hassid and Poreh (1975) employed a Van Driest damping function for the constant C_4 as follows:

$$C_4 = 1 - \exp(-A_D R_k) \quad (3.3.5)$$

The function C_5 was assumed by Wolfshtein (1967), Norris and Reynolds (1975) and Hassid and Poreh (1975) to be given by:

$$C_5 = 1 - \exp(-A_\mu R_k) \quad (3.3.6)$$

While Glushko (1965) used the same functional form of C_4 for C_5 but with R_k replaced by R_k/K.

The different values of the constant A_μ, A_D, C_D and C_μ suggested by Wolfshtein, Glushko, Norris and Reynolds, and Hassid and Poreh are presented in table (3.1).

Table (3.1)

Values of A_μ, A_D, C_D and C_μ

Author	A_μ	A_D	C_D	C_μ
Glushko	-	-	.125	.55
Wolfshtein	.04	.6575	.164	.55
Norris and Reynolds	.035	-	.11	.38
Hassid and Poreh	.03	.03	.164	.563

A survey of the different suggestions made regarding the constant C_3 and the functions C_4 and C_5 in equation (3.3.1) and (3.3.2) reveals that the value for C_3 proposed by Norris and Reynolds (1975) and Hassid and Poreh (1975) gives the best agreement with experimental evidence for the near-wall region. All the functional forms adopted for C_5 are identical, although the numerical values of the latter differ from author to author. The three proposals for C_4, namely, specify it to constant (Norris and Reynolds) or damping the length scale (Wolfshtein) or damping the dissipation term (Glushko, and Hassid and Poreh) were employed in turn in the present computation of turbulent pipe flow, as will be discussed in chapter 6. The best agreement between the

predicted profile of the kinetic energy of turbulence and the experimental data was obtained when the proposal of Hassid and Poreh was used. Consequently, their equation for the turbulent-kinetic energy was adopted in the present study. The final form of this equation is given below:

$$\frac{\partial \rho u k}{\partial x} + \frac{1}{r}\frac{\partial \rho v k r}{\partial y} = \frac{1}{r}\frac{\partial}{\partial y}\{r(\mu_\ell + \mu_t/\sigma_k)\frac{\partial k}{\partial y}\} +$$

$$\mu_t \left(\frac{\partial u}{\partial y}\right)^2 - \{\mu_\ell \frac{2kC_D}{\ell^2} + \frac{\rho C_D k^{3/2}}{\ell}\left[1-\exp(-A_\mu R_k)\right]\} \quad , \quad (3.3.7)$$

where

$$\mu_t = \rho C_\mu k^{\frac{1}{2}} \ell \{1-\exp(-A_\mu R_k)\} \quad , \quad (3.3.8)$$

and

$$\ell = y\{0.4-0.44\frac{2y}{D} + .24\left(\frac{2y}{D}\right)^2 - .06\left(\frac{2y}{D}\right)^3\} \quad . \quad (3.3.9)$$

3.4 Closure

The wall functions, which are employed in the near-wall region, have been developed for use with the wall-function method in this chapter. The development was based on the concept of dividing the near-wall region into two distinct layers; with the division taking place at $y_M^+ = 11.5$ for the momentum computation and at $y_H^+ = y_M^+ (Pr_t/Pr_\ell)^{.28}$ for the heat-transfer computation.

The low-Reynolds number one-equation (k) turbulence model proposed by Hassid and Poreh (1975) has been recommended for the application close to the wall in the composite model method.

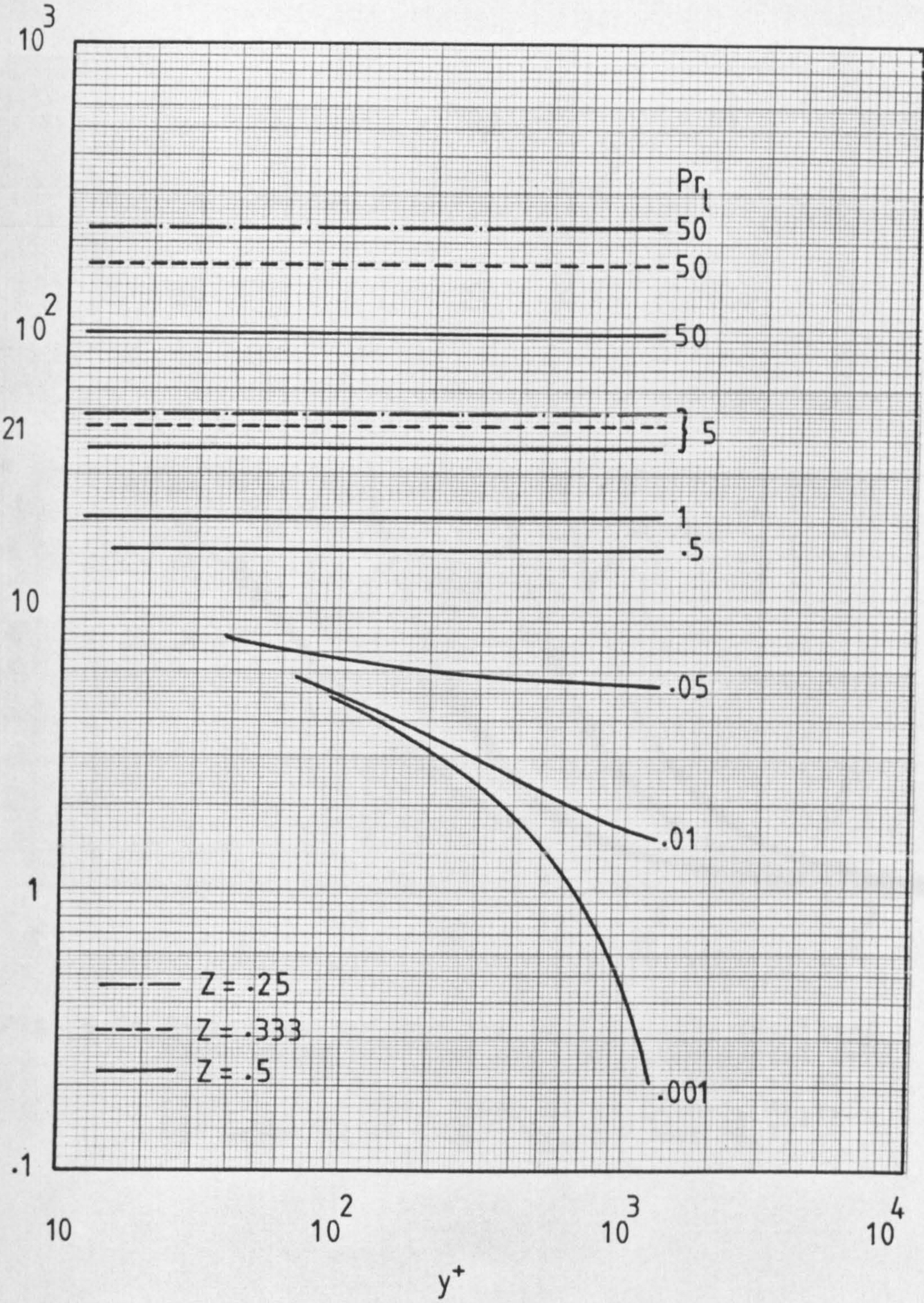


Fig (3.1) Variation of the P-function with the distance from the wall for different thickness of the effective laminar thermal sublayer.

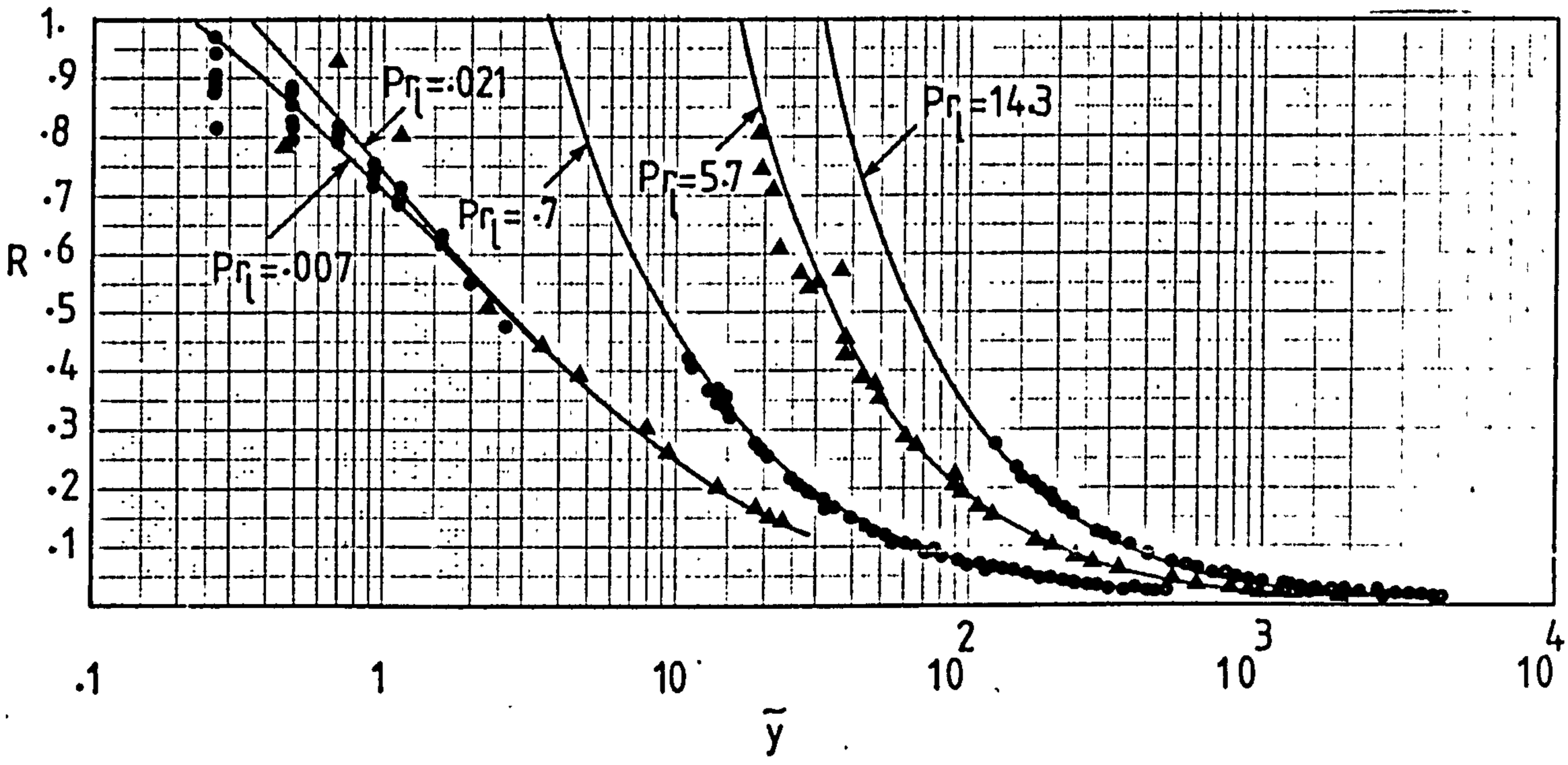


Fig (3.2) Comparison between the analytically-developed temperature profiles and the experimental data of Fuchs et al (1973), Pr_ℓ=.007, Buhr et al (1968), Pr_ℓ=.021, Johnk et al (1961), Pr_ℓ=.7, and Gowen et al (1967) Pr_ℓ=5.7 and 14.7.

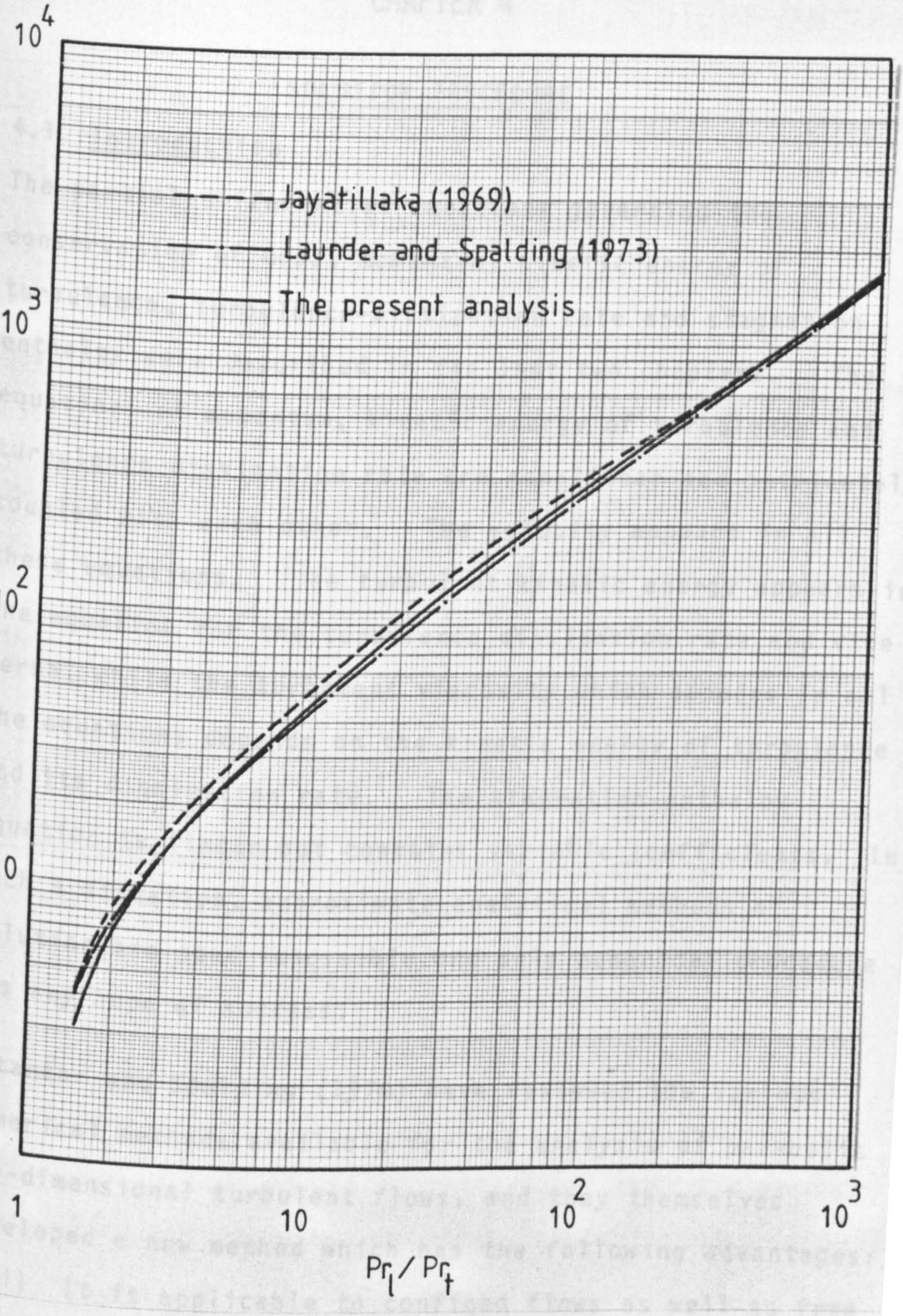


Fig (3.3) Comparison between the present P-function and the previous recommended P-function for moderate and large laminar Prandtl numbers.

CHAPTER 4

SOLUTION PROCEDURE

4.1 Introduction

The partial-differential equations governing the conservation of mass, momentum, kinetic energy of turbulence, turbulence-dissipation rate and stagnation enthalpy were described in the last two chapters. The equations of momentum, kinetic energy of turbulence and turbulence dissipation rate are non-linear and intricately coupled with each other. The velocity appears in all these equations. The turbulent kinetic energy appears in the equation for the turbulence dissipation rate and vice versa, while the turbulent viscosity which appears in all the equations depends on the kinetic energy of turbulence and its dissipation rate. The stagnation-enthalpy equation is linear but contains variable coefficients. In such a situation, approximate analytical methods of solution are near impossible and only numerical procedure has any hope of success.

Patankar and Spalding (1970) have reviewed the various numerical methods available for the analysis of parabolic two-dimensional turbulent flows, and they themselves developed a new method which has the following advantages:

(i) It is applicable to confined flows as well as free flows.

(ii) It is efficient in terms of computer time and storage so as to be a practical tool for both research and engineering purposes.

(iii) It has been very well tested for a large varity of two-dimensional flow situations; laminar, turbulent, supersonic, subsonic, cold and hot (with combustion) flows.

(iv) It can be easily extended to handle the unsteady, conjugate-heat-transfer problems under consideration in this thesis.

For the above reasons, Patankar and Spalding's method was employed in the present analysis.

The present chapter is divided in the following manner: the finite difference equations are presented in section (4.2); the computational algorithm is given in section (4.3), while all auxiliary information is contained in section (4.4).

4.2 Finite-Difference Equations

The finite-difference equations were obtained by integration of the partial-differential equations over small fictitious volumes called 'control volumes'. These control volumes were defined to surround the grid nodes in such a way that the boundaries of the control volume lie mid-way between adjacent grid nodes. This definition is modified somewhat for those grid nodes immediately adjacent to boundaries; in such cases surface of the control volume near the boundary actually coincides with the latter, as indicated in figure (4.1).

4.2.1 Finite-differencing scheme

In the formulation of the finite-difference equations, the values of the dependent variables are required at the surfaces of the control volumes. Two methods are usually employed for

this purpose (Spalding (1972)); the first is to assume that the variable in question varies linearly between the two nodes on either side of the surface under consideration, this procedure being referred to as 'central differencing'. The second is to employ a so-called 'up wind-differencing' scheme, in which it is assumed that the value of the variable at the surface of the control volume is equal to that at the 'upwind' node. Comparison between these finite-difference schemes for a one-dimensional convection-diffusion problem made by Spalding (1972) revealed that, when the absolute value of the grid-Peclet number* (Pe_g) was less than two, the central-difference scheme was more accurate. However for grid-Peclet number greater than two the upwind differencing was superior. Consequently, Spalding (1972) recommended the use of a 'hybrid' scheme whereby central differencing is adopted for $|Pe_g|<2$ and upwind differencing for $|Pe_g|>2$. It is this hybrid scheme that has been employed in the present study.

---

* The grid Peclet number was defined as:

$$Pe_g = \dot{m}'_g \, \delta x_y / \Gamma_y \quad ;$$

with m'_g denoting the mass flow rate per unit area at the surface in question, δx_y is the distance between the two grid nodes on both sides of the surface and Γ_y is the diffusivity at the surface

4.2.2 The unsteady stagnation-enthalpy equation

The finite-difference form of the unsteady stagnation-enthalpy equation (2.4.14) was obtained by integrating the latter over the control volume shown in figure (4.1). After introduction of the upwind-finite-difference scheme, the hybrid scheme which requires the grid Peclet number to be defined was introduced in the computer code, the following equation for the stagnation enthalpy at a point (I,J) in terms of the neighbouring stagnation enthalpies $\tilde{h}_{I+1,J}$, $\tilde{h}_{I-1,J}$ .....etc (full details of the derivation are given in appendix B) was obtained

$$A_{I,J}\,\tilde{h}_{I,J} = A_{I+1,J}\,\tilde{h}_{I+1,J} + A_{I-1,J}\,\tilde{h}_{I-1,J} + A_{I,J+1}\,\tilde{h}_{I,J+1} + A_{I,J-1}\,\tilde{h}_{I,J-1} + C_{I,J} \quad , \quad (4.2.1)$$

where the $A_{I,J}$, $A_{I+1,J}$, ... etc are combined convection/diffusion coefficients at the different boundaries and are given by:

$$A_{I+1,J} = \left[\frac{r\,\Gamma_{h,eff}}{(\psi_E - \psi_I)}\right]_{I+\frac{1}{2},J} \frac{\delta x}{h_{I+1,J} - y_{I,J}} \quad , \quad (4.2.2)$$

$$A_{I-1,J} = \left[\frac{r\,\Gamma_{h,eff}}{(\psi_E - \psi_I)}\right]_{I-\frac{1}{2},J} \frac{\delta x}{y_{I,J} - y_{I-1,J}} \quad , \quad (4.2.3)$$

$$A_{I,J+1} = \frac{(r\,\Gamma_{h,eff})_{I,J+\frac{1}{2}}}{(\rho u r)_{I,J}} \frac{\delta}{x_{I,J+1} - x_{I,J}} \quad , \quad (4.2.4)$$

$$A_{I,J-1} = \frac{(r\,\Gamma_{h,eff})_{I,J-\frac{1}{2}}}{(\rho u r)_{I,J}} \frac{\delta\omega}{x_{I,J} - x_{I,J-1}} \quad , \quad (4.2.5)$$

$$C_{I,J} = \left\{\left[\frac{(\mu_{eff} - \Gamma_{h,eff})r}{(\psi_E - \psi_I)}\right]_{I+\frac{1}{2},J} \frac{(u^2/2)_{I+1,J} - (u^2/2)_{I,J}}{y_{I+1,J} - y_{I,J}}\right.$$

$$-\left[\frac{(\mu_{eff} - \Gamma_{h,eff})r}{(\psi_E - \psi_I)}\right]_{I-\frac{1}{2},J} \left.\frac{(u^2/2)_{I,J}-(u^2/2)_{I-1,J}}{y_{I,J} - y_{I-1,J}}\right\} \delta x +$$

$$\tilde{h}_{I,J,t} \frac{\delta\omega\,\delta x}{u_{I,J}\delta t} \quad , \quad (4.2.6)$$

$$A_{I,J} = A_{I+1,J} + A_{I-1,J} + A_{I,J-1} + A_{I,J+1} + \frac{\delta\omega\delta x}{u_{I,J}\delta t} \quad , \quad (4.2.7)$$

Similarly, the finite difference form of the unsteady conduction equation (2.2.6) can be written as follows:

$$B_{I,J}\,\bar{h}_{I,J} = B_{I+1,J}\,\bar{h}_{I+1,J} + B_{I-1,J}\,\bar{h}_{I-1,J} + B_{I,J+1}\,\bar{h}_{I,J+1} + B_{I,J-1}\,\bar{h}_{I,J-1} + C_{I,J} \quad , \quad (4.2.8)$$

where

$$B_{I+1,J} = \left(\frac{\alpha\delta x}{y_{I+1,J}-y_{I,J}}\right) \frac{r_{I+\frac{1}{2},J}}{r_{I,J}} \quad ; \quad (4.2.9)$$

$$B_{I-1,J} = \left(\frac{\alpha\delta y}{y_{I,J}-y_{I-1,J}}\right) \frac{r_{I-\frac{1}{2},J}}{r_{I,J}} \quad , \quad (4.2.10)$$

$$B_{I,J+1} = \left(\frac{\alpha\delta y}{x_{I,J+1}-x_{I,J}}\right) \quad , \quad (4.2.11)$$

$$B_{I,J-1} = \left(\frac{\alpha\delta y}{x_{I,J}-x_{I,J-1}}\right) \quad , \quad (4.2.12)$$

$$C_{I,J} = \frac{\delta x\delta y}{\delta t}\, h_{I,J,t} + \left[\frac{Q'}{\rho}\right]_{I,J} \delta x\delta y \quad , \quad (4.2.13)$$

$$B_{I,J} = B_{I+1,J} + B_{I-1,J} + B_{I,J+1} + B_{I,J-1} + \frac{\delta x\delta y}{\delta t} \quad , \quad (4.2.14)$$

and α is thermal diffusivity (Γ_h/ρ).

4.2.3 Steady-flow equations

A procedure similar to that employed for the unsteady stagnation-enthalpy equation was applied to the general flow equation (2.4.1). The final equation for $\phi_{I,J}$ was obtained

$$A_{I,J}\ \phi_{I,J} = A_{I+1,J}\ \phi_{I+1,J} + A_{I-1,J}\ \phi_{I-1,J} + C_{I,J}\ , \qquad (4.2.15)$$

where $A_{I,J}$, $A_{I+1,J}$, $A_{I-1,J}$ and $C_{I,J}$ were defined as follows:

$$A_{I+1,J} = \left[\frac{r\ \Gamma_{\phi,eff}}{(\psi_E-\psi_I)}\right]_{I+\frac{1}{2},J}\ \frac{\delta x}{y_{I+1,J}-y_{I,J}}\ , \qquad (4.2.16)$$

$$A_{I-1,J} = \left[\frac{r\ \Gamma_{\phi,eff}}{(\psi_E-\psi_I)}\right]_{I-\frac{1}{2},J}\ \frac{\delta x}{y_{I,J}-y_{I-1,J}}\ , \qquad (4.2.17)$$

$$C_{I,J} = S_{I,J} + \phi_{I,J-1}\ \delta\omega\ , \qquad (4.2.18)$$

$$A_{I,J} = A_{I+1,J} + A_{I-1,J} + S'_{I,J} + \delta\omega\ ; \qquad (4.2.19)$$

where $S_{I,J}$ and $S'_{I,J}$ are the linearized source term, which for each of the dependent variables were given by the following

- For the u-equation

$$S_{I,J} = -\left(\frac{1}{\rho u}\right)_{I,J-1}\ \left|P_{I,J}-P_{I,J\ 1}\right|\ \delta\omega\ , \qquad (4.2.20)$$

$$S'_{I,J} = 0.0\ , \qquad (4.2.21)$$

- For the k-equation, Spalding (1977) recommended the following:

$$S_{I,J} = \left[\frac{1}{\rho u}\right]_{I,J}\ \{a_1\ \mu_t\ \left(\frac{\partial u}{\partial y}\right)^2 + a_2(\rho\varepsilon)\}_{I,J}\ \delta x\delta\omega\ , \qquad (4.2.22)$$

$$S'_{I,J} = \left[\frac{1}{\rho u}\right]_{I,J}\ \{a_3\ \mu_t\ \left(\frac{\partial u}{\partial y}\right)^2 + a_4(\rho\varepsilon)\}_{I,J}\ \frac{\delta x\delta\omega}{k_{I,J}}\ , \qquad (4.2.23)$$

where a_1, a_2, a_3 and a_4 had the values 1.5, $\frac{C_2}{C_\mu C_D}$ -1, and $\frac{C_2}{C_\mu C_D}$ respectively.

- For the ε-equation, Spalding (1977) recommended

$$S_{I,J} = \left[\frac{1}{\rho u}\right]_{I,J} \{a_5 \mu_t \left(\frac{\partial u}{\partial y}\right)^2 + a_6(\rho\varepsilon)\}_{I,J} \left(\frac{\varepsilon}{k}\right)_{I,J} \delta x \delta\omega \quad , \quad (4.2.24)$$

$$S'_{I,J} = \left[\frac{1}{\rho u}\right]_{I,J} \{a_7 \mu_t \left(\frac{\partial u}{\partial y}\right)^2 + a_8(\rho\varepsilon)\}_{I,J} \left(\frac{\varepsilon}{k}\right)_{I,J} \frac{\delta x \delta\omega}{\varepsilon_{I,J}} \quad , \quad (4.2.25)$$

where a_5, a_6, a_7 and a_8 had the values C_1, $\frac{C_2}{C_\mu C_D}$ -1, 0.0 and $\frac{2C_2}{C_\mu C_D}$ -1 respectively.

4.3 Computational Algorithm

4.3.1 The steady-parabolic equations

The finite-difference forms of the u, k and ε equations presented in section (4.2.3) were algebraic, non-linear and inter-linked, with the nodel values ϕ at a point (I,J) related to all neighbouring points with the exception of the downstream ones. In order to solve these equations the computational algorithm developed by Patankar and Spalding (1970) was employed. The linearized equations were uncoupled by the use of the known upstream values of the dependent variables in the calculation of the coefficients $A_{I,J}$, $A_{I+1,J}$, $A_{I-1,J}$ and $C_{I,J}$. These linear algebraic equations were solved by the application of TDMA (Tri-Diagonal Matrix Algorithm) traverses over the numerical grid. A marching-integration technique in the stream-wise direction was used to compute the variable field over the entire flow domain.

When the above computational algorithm was used with the composite model (where it was necessary to use a very fine radial grid spacing to correctly predict the large changes in the dependent variables) very small forward steps ($\delta X/D = .001$) were necessary for convergence. In order to increase these forward steps, a line-by-line iteration procedure was incorporated into the computational algorithm and the resulting solution procedure may be summarized as follows:

(i) The upstream values of the dependent variables, u, k and ε were stored; only one extra line of storage was required for each variable.

(ii) These upstream values were chosen as initial 'guesses' for the variables at the line under consideration.

(iii) The coefficients in the finite-difference equation for each variable were computed and solutions were obtained, u, k and ε were solved in that order. The old values in store were then replaced by the latest solutions.

(iv) The radial coordinates (y) of the grid points were calculated.

(v) The pressure, velocities and the radial coordinates of the grid points were adjusted to ensure the satisfaction of overall continuity.

(vi) The steps from (iii) to (v) were repeated. This process was terminated when satisfactory convergence was reached; the criteria for convergence was defined so that during two successive iterations the value of the shear velocity did not vary by more than one percent.

4.3.2 Steady and unsteady elliptic equations

The value of the stagnation enthalpy at a point (I,J) given by the finite-difference equation (4.2.1) is seen to be related to the four neighbouring space points and to the model value at the previous time step. In order to solve this set of equations it was necessary to introduce the iteration technique of Pun and Spalding (1977) at each time step and to keep in store the stagnation-enthalpy field of the previous time step. The computational procedure required in this case can be summarized as follows:

(i) The stagnation-enthalpy values at the previous time step were stored and used as initial 'guesses' for the time step under consideration.

(ii) The marching-integration technique was utilized in the stream-wise direction at the time step under consideration with the stored stagnation-enthalpy values for the downstream point (I,J+1).

(iii) The old values of the stagnation enthalpy were replaced by the new calculated field.

(iv) The last two steps above were repeated to convergence.

(v) The calculation proceeded to the next-time step and the cycle was repeated.

For the steady stagnation-enthalpy equation, the above procedure was employed with the exception that step (v) was deleted and (i) was replaced by the following step:

(i) A uniform stagnation enthalpy was assumed as an initial guess.

4.3.3 Treatment of the conducting wall in the numerical procedure

The inclusion of a wall of finite thickness and physical properties does not present any additional problems in the numerical procedure, because the finite-difference form of the conduction equation (4.2.8) is the same as the finite-difference form of the stagnation-enthalpy equation (4.2.1). The heat-transfer boundary condition in this case was applied at the outer surface of the pipe wall and the following relation was introduced at the interface between the flow and the solid wall.

$$\dot{q}''_s = \dot{q}''_f \quad , \quad (4.3.1)$$

where $\dot{q}''_s$ and $\dot{q}''_f$ are, respectively, the heat transfer rate per unit area from or to the solid wall and the heat transfer rate per unit area to or from the flow.

The relation for the heat flow (4.3.1) was incorporated into the numerical procedure in the following way, when either the wall-function method or the Reynolds number turbulence model (the composite model) is employed

$$A_{N,J}\, T_{N,J} = A_{N+1,J} + A_{N-1,J}\, T_{N-1,J} \quad ; \quad (4.3.2)$$

where,

$$A_{N+1,J} = \rho_s\, C_{p,s}\, \alpha_s/(y_{N+1,J}-y_{N,J}) \quad , \quad (4.3.3)$$

$$A_{N-1,J} = \rho_f\, C_{p,f}\, \alpha_f/(y_{N,J}-y_{N-1,J}) \quad , \quad (4.3.4)$$

$$A_{N,J} = A_{N+1,J} + A_{N-1,J} \quad , \quad (4.3.5)$$

and suffixes s and f, respectively refer to the solid and

the fluid and N is the grid point on the inner surface of the pipe wall.

4.4 Auxiliary Information

4.4.1 Boundary and initial conditions

The solution of the finite-difference forms of the governing differential equations require initial and boundary conditions. In the present study, different initial and boundary conditions for the stagnation-enthalpy equation were considered; these conditions will be presented later when the heat-transfer results are considered. The values of the other dependent variables (u, k and ε) were zero at the wall, while zero-gradient boundary conditions were assumed at the axis of symmetry.

The appropriate boundary condition for the turbulence dissipation rate at the edge of the near-wall region (when the low-turbulent-Reynolds number one-equation model of turbulence was employed there) was calculated as follows:

$$\varepsilon = \nu \frac{2kC_D}{\ell^2} + \frac{C_D k^{3/2}}{\ell} \{ 1 - \exp(-A_D R_k) \} \quad . (4.4.1)$$

The initial conditions for the dependent variables (u, k and ε) were assumed to be as follows:

$$u = u_{in} \quad , (4.4.2)$$

$$k_{in} = .0001\ u_m^2 \quad , (4.4.3)$$

$$\text{and } \varepsilon_{in} = C_D\ k^{3/2}/\ell \quad , (4.4.4)$$

where u_{in} is the inlet velocity which was assumed constant.

4.4.2 Choice of the thickness of the near-wall region

It was necessary to define the thickness of the near-wall

region in the case where the low-Reynolds-number one-equation model of turbulence was employed near the wall and the two-equation model of turbulence outside this region. This thickness was defined as the distance from the wall to that point in the flow above which the dissipation term in the low-Reynolds-number form of the k-equation (3.3.7) becomes identical to that in the high-Reynolds-number version. The dissipation term (ε) of the k-equation (3.3.7) was given as follows:

$$\varepsilon = \frac{\rho C_D k^{3/2}}{\ell} \left[1.0 - \exp(-A_D R_k) + \frac{2\mu_\ell}{\rho \ell k^{.5}} \right] \quad \cdot \quad (4.4.5)$$

In order to match the above dissipation term to the form valid for high Reynolds number, the last two terms of equation (4.4.5) must be zero or at least negligible in comparison with unity. To present the variation of these two terms with the dimensionless distance from the wall (y^+) in the near-wall region, it was necessary to relate the turbulent kinetic energy to the shear stress (τ). This relation was assumed as follows (Launder and Spalding ,(1972)):

$$\frac{\tau}{\rho k} = 0.3 \quad \cdot \quad (4.4.6)$$

The length scale (ℓ), equation (3.3.9), can be reduced in the near-wall region to

$$\ell = 0.4y \quad \cdot \quad (4.4.7)$$

Substitution from (4.4.6 and 4.4.7) into (4.4.5); yields

$$\varepsilon = \frac{\rho k^{3/2} C_D}{\ell} \{ 1. - \exp(-0.029y^+) + \frac{2.7}{y^+} \} \quad \cdot \quad (4.4.8)$$

The variation of the last two terms of equation (4.4.8) is presented in figure (4.2). The results reveal that the

difference between the low and high-Reynolds-number dissipation terms was less than three percent at $y^+ = 100$. Consequently this value was used as the dimensionless thickness of the near-wall region.

4.5 Closure

The finite-difference forms of the basic equations together with the required initial and boundary conditions have been presented in this chapter. The chapter also contains the computational algorithm which was used in obtaining the results presented in chapter 6 and 7.

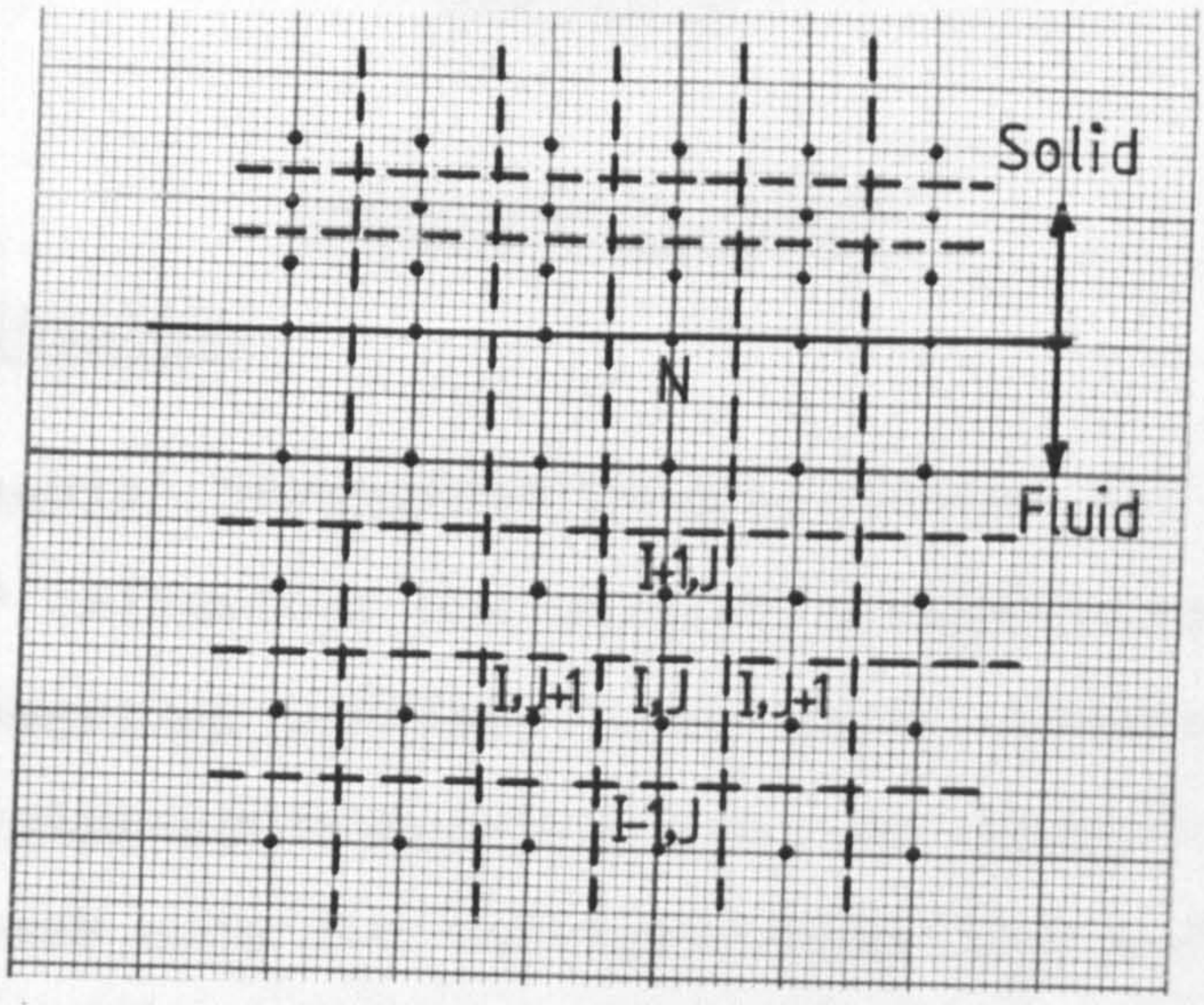


Fig (4.1) Grid arrangement.

Fig (4.2) The difference between the low and the high Reynolds number dissipation terms.

CHAPTER 5

EXPERIMENTAL STUDY

5.1 INTRODUCTION

An experimental investigation was carried out with the purpose of validating the present composite model of turbulence and complementing unsteady temperature measurements. The previous temperature measurements, as shown in section (1.3), were reported only for the fully-developed bulk mean temperature (Stuart (1956), Koshkin et al (1970) and Kawamura (1977)) and for the centre-line temperature (Treadwell (1955)).

The experiments were performed in a pipe with turbulent flow of water and the study included measurements of the flow temperature at different radial and axial locations and the wall temperatures downstream of a heating section. The temperatures were measured by thermocouple sensors and the outputs of these thermocouples were recorded with the aid of an Ultra Violet Galvanometer Recorder. Effects of changes in the Reynolds number on the temperature response were also investigated.

A description of the apparatus, recording equipment and the procedure employed is given in section (5.2). In section (5.3), the experimental conditions are described. Discussion of the accuracy of the experimental data are provided in section (5.4) and the results obtained are reported in section (5.5). Finally section (5.6) presents some concluding remarks.

5.2 Apparatus and Procedure

5.2.1 Description of the apparatus

A schematic drawing of the apparatus is shown in figure (5.1) and a photograph is presented in figure (5.2). The apparatus consisted of a settling chamber of 0.0508 metres inner diameter and 0.562 metres length with a contraction ratio of 2:1 over a length of 0.105 metres. This was followed by a copper tube of 0.0254 metres inner diameter, 0.0015875 metres thickness and 3 metres length. The hydrodynamic flow properties were developed in the first 47 diameters of the tube length. The heating took place in the next 40 diameters length and the remainder of the tube constituted the test-section for the study.

(i) Test section

The details of the test section are given in figure (5.3) and a photograph is presented in figure (5.4). The section consisted of a copper tube with 0.0254 metres inner diameter, .0015875 metres thickness and an effective length of 0.60325 metres. The whole test section was thermally insulated by a covering of 0.0254 metres thickness fibre glass.

The temperature of the outer surface of the tube was measured at four downstream locations (X/D = 6.25, 8.75, 13.75 and 23.75 measured from the start of the test section) by means of copper-constantan thermocouples of 101.6 micron* wire diameter. The copper-constantan wire material was chosen for its following properties.

- It has high resistance to corrosion from moisture

---

*1 micron = 10^{-6} metres

- Its rate of change of output with temperature is nearly linear
- It has a high sensitivity, $\frac{dE}{dT}$, where E is the output voltage and T is the temperature.
- Its accuracy is high in comparison with other materials at medium and low temperature ranges.
- It has a good transient response, depending on wire size.

The thermocouple junctions were made by a spot-welding technique and embedded to a depth of a wire diameter into the outer surface of the tube. In order to reduce the conduction error through the wires a length of 187.5 wire diameters was wrapped around the tube surface.

The flow-temperature response was measured at three different downstream sections from the start of the test section (X/D = 6.25, 8.75 and 13.75). At each section, the temperature response was measured at four radial locations (y/R = .1, .3, .6 and 1.) except at the last section where the temperature response was measured at $\frac{y}{R}$ = .1, .4 and .8 . Again the thermocouples were made from the copper-constantan wires used in the wall temperature measurements. The thermocouple wires used at each section had only one layer of insulation and were inserted in a stainless-steel tube of .001575 and 0.001067 metres outer and inner diameters respectively. Each tube, as shown in figure (5.5), has three circular holes, each of diameter 0.00095 metres, drilled by a high accuracy digital read-out surface mill, and the junctions were glued at the centre of these holes.

(ii) <u>Heating section</u>

The present experimental apparatus was designed for high-

Reynolds-number flows (Re $\tilde{\sim}$ 50,000); for this flow a rough estimate of the amount of thermal energy required to produce a 10^{o} temperature rise in the mean flow temperature was 40 kw. In order to obtain such a large amount of thermal energy, previous investigations* (Treadwell (1955), Stuart (1956), Koshkin et al (1970) and Kawamura (1977)) have shown that the pipe wall has to be used as a heater if the electric energy is to be used. In this case, it is very difficult to insert a large number of thermocouples into the flow field or to attach thermocouples to the solid wall. Even if such a heating section was designed successfully its life would be short; the MIT (Massachusetts Institute of Technology) experimental rig was burnt out before the experimental investigation was finished (Stuart (1956)).

In the present study, the electric heating was avoided and instead saturated steam was used as a heating medium in a counter-flow heat exchanger. The disadvantages of using steam were that the heat input to the flow was not uniformally changing with time over the heating length and the heating response was not as fast as that obtained by electric heating. However, these disadvantages presented no real problems since the temperatures of the outer surface of the inner tube which provided the heating-boundary conditions, were measured.

The heating section, as shown in figures (5.6) and (5.7) consisted of a double-tube heat-exchanger in which the inner tube was

---

* To obtain almost 10 kw

made of copper and the outer tube of .0635 metre inner diameter, was made from steel and insulated with a layer of fibre glass of 0.0254m thickness. To ensure symmetry in the heating conditions steam at constant atmospheric pressure was supplied from two inlets on both sides of the outer tube and left from two outlets to a condenser. In order to maintain atmospheric conditions in the steam, the heat exchanger was connected to an atmospheric drain through a bleeding valve. The effect of the spot heating at the steam inlet in the heat-exchanger was reduced by a local heat dissipator (an intermediate tube of .089 metre length between the outer and inner tubes). The heat exchanger also had two condensate drains on both ends to remove the steam condensate after each run.

The temperatures of the outer surface of the inner tube were measured at seven locations, figure (5.6), five of these locations were in the half of the heat exchanger near to the test section in order to obtain accurate heating boundary conditions in this part which affects the temperature in the test section more than does the other half. These temperatures were measured by a copper-constantan thermocouple which had junctions embedded into the outer surface of the inner tube. A neoprene rubber pad was inserted between each junction and the tube carrying the two wires, as shown in figure (5.6) to ensure complete contact between the junction and the surface and to prevent the contact between the steam and the junction. The rubber pad also allowed a length of 75 wire diameters, which had only one layer of insulation, between the junction and the tube carrying the wires to be kept in contact with the steam to reduce the conduction errors.

(iii) Water system

The water was supplied from the central-supply mains through a control valve to control the mass flow rate. The water flowed from the valve to a rotameter designed to measure the mass flow rate, and then through the settling chamber to the copper tube. From the tube the water flowed to an open drain.

(iv) Steam system

The steam was supplied from the College-main-boiler station through a control valve, from which the steam could either pass straight to the condenser through a by-pass pipe line controlled by a control valve or to the heat exchanger through a throw over steam supply valve, steam seperator and steam trap. The steam inside the heat exchanger was then circulated in the opposite direction to the water flow to the condenser and from there to an atmospheric drain.

5.2.2 Recording equipment

In the present study, the thermocouple output signals were recorded with the aid of an Ultra Violet Galvanometer Recorder (UVR). The UVR is a direct light beam writing oscillograph with a built-in photo flash unit which prints timing lines across the paper. Basically, the input voltage from the thermocouple causes a current to flow in a coil in the UVR. There is then a 'current-carrying' conductor in a magnetic field; thus the coil experiences an electromagnetic force which, since it has a lever arm, causes a torque. This torque tends to rotate the coil until it

is just balanced by the restoring torque of torsion springs. Consequently, this rotation is proportional to the current passing in the circuit and not to the voltage supply. Therefore it was essential to measure the resistence of each galvanometer circuit; these resistances, Table (5.1), were measured by a Solartron-digital voltmeter.

The recorder, in general, utilises a range of galvanometer covering frequency ranges from 0 - 8 KHz with a sensitivity range from .0008 - 25 mA/cm and has 24 channels. The linearity of the deflection on the recording paper produced by the galvanometer beam when compared with the deflecting current, is approximately $\pm$ 1 percent over 10 cms deflection from a centre position. The paper speeds vary from 1.25 to 2000 mm/s with an accuracy of $\pm$ 2 percent; however, a paper speed of 20 mm/s was used in the present study.

In the present investigation two types of galvanometers were used, A35 and B160, the former has a frequency response of 35 Hz and a response of approximately .0008 ma/cm and the latter has a frequency response of 160 Hz and a response of .005 ma/cm. The accurate sensitivity of each galvanometer is shown in Table (5.1) together with the equivalent sensitivities (mv/cm & ^{o}K/cm), while the location of the thermocouple junction corresponding to each galvanometer is shown in figures (5.3) and (5.6).

5.2.3 Experimental procedure

The experimental procedure consisted of recording the fluid-temperature responses, the wall-temperature responses, the

Table (5.1)

Galvanometer resistance and sensitivity

Channel number	Serial number	Sensitivity ma/cm	Resistance	Sensitivity mv/cm	Sensitivity ^{o}c/cm
1	29135	.00080	98.93	.079144	1.9232
2	29116	.00083	98.63	.079473	1.9893
3	29190	.00080	100.76	.083631	2.0322
4	29224	.00083	104.43	.086677	2.10625
5	29335	.00081	103.33	.083697	2.03384
6	29180	.00085	102.00	.0867	2.1068
7	29145	.00083	102.83	.085349	2.07398
8	29195	.00081	104.4	.08665	2.1056
10	29085	.00084	100.00	.084	2.0412
11	29205	.00081	104.33	.084507	2.05352
12	29196	.00082	103.75	.085075	2.06732
14	29339	.00082	108.6	.089052	2.163964
15	29239	.00078	107.01	.083468	2.02827
16	29415	.0008	111.36	.089088	2.16484
17	29221	.00081	109.55	.0887355	2.156273
18	Y2529	.00506	127.8	.646668	14.485
19	29414	.00080	616.1	.49288	11.0405
20	29295	.00080	605	.484	10.84
21	29146	.00083	618.83	.51363	11.505
22	29363	.00082	602.2	.4938	11.0612
23	29114	.00081	638.6	.517266	11.5868
24	29432	.00088	637.6	.561088	12.56837

heating-boundary conditions and the inlet flow temperature for different flow rate. A test at one mass flow rate was started by bleeding off the condensation from the steam pipe lines through a condensate valve at the lowest point in the steam-pipe line and from the heat exchanger. The water was then turned on and the mass flow rate was adjusted to obtain the required mass flow rate and the steam-bypass valve was turned on until steady-state conditions were almost reached in the water and steam-flow rates. This was followed by switching the UVR and the recording paper on, then the bypass valve was turned off and the throw over steam supply valve turned on until the steady state was reached.

5.3 Experimental Conditions

The inlet-hydrodynamic conditions at the start of the hydrodynamic-entrance length had a very small effect on the heat-transfer results either in the heating section or in the test section. However the settling chamber was used to ensure uniform conditions at the inlet.

For the heat-transfer conditions, the inlet flow temperature ahead of the heating section was $20^{o}C$, while the heating boundary conditions are given in figure (5.8). This figure shows the temperature response on the outer surface of the inner tube of the heat exchanger at the locations 18-24 for three Reynolds numbers (30000, 38000 and 49000).

The differences in the scales are due to the difference in the resistance of each galvanometer circuit

and in the sensitivity of each galvanometer.

A comparison between the temperature responses presented in figure (5.8) indicates that the temperature responses were neither the same for different Reynolds numbers (except at the location 18) nor uniform across the heating length. At the location 18 neither the response nor the steady state value was affecte by the change in Reynolds number; this indicates that the temperature response at this location was affected by the steam inlet and not by the water flow. At locations 19 - 24 the temperature responses were affected by the steam and the water flow. The larger the downstream distance from the steam inlet the slower the response and the larger the water-mass-flow rate the smaller the steady-state-heating temperature as being expected. Although the steady-state-wall temperatures downstream of the steam inlet (locations 19, 20, 21 and 22) decreased with the distance, the opposite was true for locations 23 and 24. This trend may be attributed to different factors, such as the variations of the heat-transfer coefficient between both the water and the steam and the solid wall, and the large changes in the steam-physical properties (ρ, μ, λ and C_p) and the velocity in the heat exchanger, which interact in a complex way to affect the wall temperature.

5.4 Results

The temperature response at X/D = 6.25 is presented in figure (5.9) for the three Reynolds numbers (30000, 38000, 49000). The fluid-temperature response at four radial locations (y/R = 1., .6, .3 and .1) were whown in figures (5.9a - 5.9d) while the temperature response at the outer surface of the pipe wall was plotted in figure (5.9e). The

difference in the vertical scale exhibited in these figures (5.9) was due to the difference in the galvanometer circuit resistance as mentioned in the last section.

Comparison between the temperature results presented at one location for different Reynolds number shows that the higher the Reynolds number, the faster the temperature response; this agreed with the experimental observation of Kowamura (1977). The comparison between the results at different locations but for the same Reynolds number indicated that the maximum temperature was close to the wall and the minimum was at the centreline. This trend was expected since this section was near to the heat exchanger where the maximum temperature was at the wall..

The temperature responses for further downstream sections (X/D = 8.75 and 13.75) are given in figures (5.10 and 5.11) respectively. In figure (5.10) the fluid temperature responses at four locations (y/R = 1., .6, .3 and .1) are plotted in figures (5.10a - 5.10d) and the wall temperature response is given in figure (5.10e). Figures (5.11a - 5.11c) show the fluid temperature response at three radial locations (y/R = .8, .4 and .1), while the wall temperature response is given in figure (5.11d). Again the results presented in figures (5.10 and 5.11) are for three Reynolds numbers (30000, 38000, and 49000).

Comparisons between figures (5.9d, 5.10d and 5.11c) indicate that the temperature close to the wall decreases with increasing downstream distance, while the temperature results

presented in figures (5.9a, 5.10a and 5.11a) reveal that the temperature near the centreline increases with increasing downstream distance. Again this trend is as expected since the pipe tube wall was insulated and the thermal energy was diffused from the wall region towards the centreline in the test section.

The comparison between the wall-temperature responses given in figures (5.9e, 5.10e and 5.11d) reveals that the steady-state-wall temperature decreases over the length from X/D = 6.25 to X/D = 8.75 and then increases. This observed trend over the length from X/D = 6.25 to X/D = 8.75 was as expected while the increase in the wall temperature was not to be expected. This unexpected trend could be due to the accuracy of the present measurements of the wall temperature. Thus the accuracy of the present experimental data will be discussed next.

5.5 Accuracy of the experimental data

The accuracy of the experimental data depends on both the accuracy of the recording device, which has been discussed (section (5.3)), and on the accuracy of the measured quantities (the galvanometer circuit resistance, and temperatures) which are discussed here.

5.5.1 Discussion of errors in temperature measurements

The output of a thermocouple immersed in a flow or attached to a solid wall represents an approximation to the actual temperature at the location, provided that the probe size does not disturb the flow field. In the present study the ratio of the projected area of the probe (probe length in the flow field times its diameter) to the cross-sectional area of the flow was 3.8 percent, which was within an acceptable limit; Treadwell (1955) and Stuart (1956) used an area ratio of 8 percent in a similar experiment.

The difference between the temperatures of the thermocouple junction, which is proportional to its output, and the point of interest is commonly called an "error". The main sources of error in the transient problem considered in the present investigation are usually caused by the heat conducted through the thermocouple wires to or from the junction ("conduction error") and by the thermocouple response lagging behind any changes in the temperature being measured ("response rate error"). Each of these errors is estimated herewith.

(i) Conduction error

In measuring the wall temperatures, as mentioned before in the last section, a wire length of 75 times its diameter was kept at almost isothermal conditions with the junction. In this case the conduction error is very small and can be neglected (Moffat (1962)). In measuring the fluid temperature, it was difficult to keep the junction and its adjacent wire

length at isothermal conditions without disturbing the flow conditions; consequently it was necessary to estimate the conduction error in this case.

The conduction error was studied by Sparrow (1968), who employed a one-dimensional analysis and arrived at the following equation:

$$\frac{E_c}{T_w - T_f} = \frac{1}{\cosh\{(kAr_r)^{-\frac{1}{2}} L_w\}} \quad , \quad (5.1)$$

where, E_c is the conduction error,

T_w is the wall temperature,

T_f is the fluid temperature,

k is the equivalent thermal conductivity of the thermocouple wires defined as $(k_{w1} + k_{w2})$,

k_{w1} and k_{w2} are the thermal conductivity of both wires,

A is the cross-sectional area of the wire,

R_r is the equivalent thermal resistance defined as:

$$R_r = \frac{1}{2\pi r_2 h} + \frac{\ell n(r_2/r_1)}{2\pi k_i} \quad , \quad (5.2)$$

r_1 is the equivalent wire radius $(\sqrt{2}\, r_w)$,

r_w is the wire radius

r_2 is the equivalent outer radius of the insulation $(L_1 + L_2)/4$,

L_1 and L_2 are the wire dimension with the insulation,

h is the heat-transfer coefficient between the probe and the flow,

L_w is the wire length from the junction to the wall.

The heat-transfer coefficient was calculated from the equation recommended by Moffat (1962) for wires normal to the flow, namely:

$$Nu \equiv \frac{2hr_2}{k_f} = 1.122\ (0.44 \pm 0.06)\ Re^{.5}\ Pr_{\ell}^{.31} \quad , (5.3)$$

where, k_f is the fluid conductivity.

For the Reynolds number of 3×10^4, the conduction error calculated from equation (5.1) was 1. and $0.18^{o}C$ at y/R = .1 and 1.0 respectively.

(ii) Response-rate error

The response-rate error of a thermocouple junction is usually presented in terms of a "characteristic time", which presents the time required for a thermocouple junction to complete 63.2 percent of its response to a step change in the flow temperature. The characteristic time (τ) of a uniform wire diameter without conduction or radiation losses and immersed in a free stream of uniform properties, was given by Moffat (1958)as follows:

$$\tau = \frac{3.5 \times 10^3\ \rho C_p\ (2r_w)^{1.25}\ G^{-15.8/\sqrt{T}}}{T} \quad , (5.4)$$

where,

τ is the characteristic time in seconds,

G is the mass velocity in lb/s ft^2,

T is the temperature in deg.R,

ρ is the average density for the two wires in lb/ft^3

C_p is the average specific heat for the two wires in Btu/lb $deg^{o}F$,

r_w is the wire radius in inches.

The characteristic time calculated from equation (5.4) was 0.006 seconds which is very small compared to the time of the transient changes in the present problem.

5.5.2 Discussion of the error in the resistance

The galvanometer circuit resistance was measured by a "Digital Voltmeter" solartron type 7075, which has a very high accuracy; the error is about $\pm$ .025 percent. However, in measuring the resistance it was necessary to introduce a large resistance in the circuit to decrease the effect of the current passing through the circuit on the thermocouple junction. With this large resistance in the circuit, the error in the galvanometer circuit resistance was $\pm$ 1 percent.

5.5.3 Degree of reproducibility of the measurements

Figure (5.12) shows the recorded displacements obtained on two different days for the same experimental conditions. The results are presented for four points at the first section; the degree of reproducibility obtained for other sections being typical of the reproducibility presented in figure (5.12). It is seen that the degree of reproducibility is generally good.

5.6 Concluding Remarks

An experimental program was conducted with the objective of providing suitable data for the validation of the composite turbulence model in the unsteady heat-transfer computations. The need for these measurements arose from the lack of suitable experimental data in the literature.

The measurements were made of the temperature response in the thermal developing region of a pipe flow and in its solid wall.

Although some of the present experimental results showed an unexpected trend at the wall, this was not expected to discredit the obtained experimental data. Wall temperature measurements is a difficult field and numerous errors are involved. The author has taken extra care to minimise the sources of error but does not claim their elimination. It is therefore concluded that the present measurements were satisfactory since the target was to obtain actual overall flow characteristics and general trends to validate the prediction results obtained with the composite model as will be shown in chapter (7).

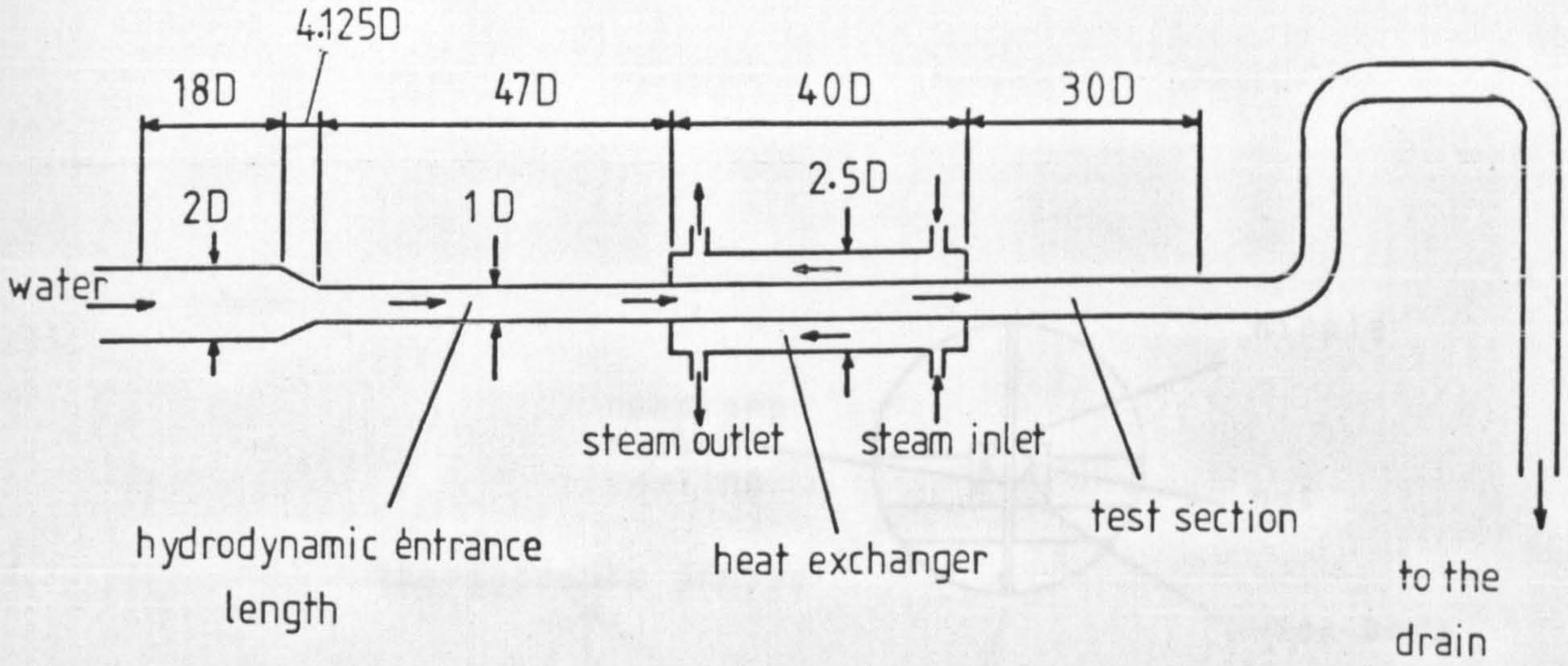


Fig (5.1) Schematic drawing of the experimental apparatus

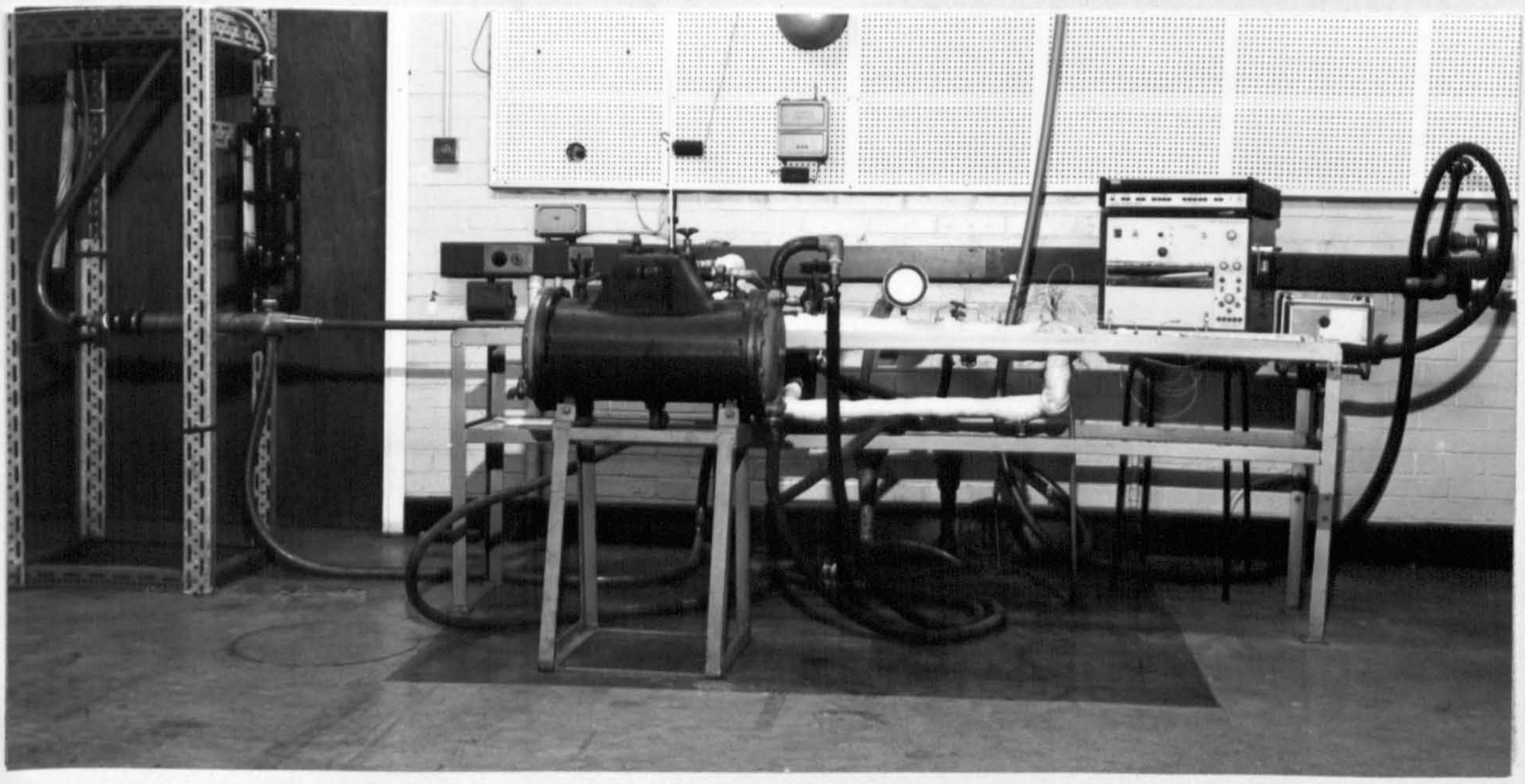


Fig (5.2) Photograph of the experimental apparatus

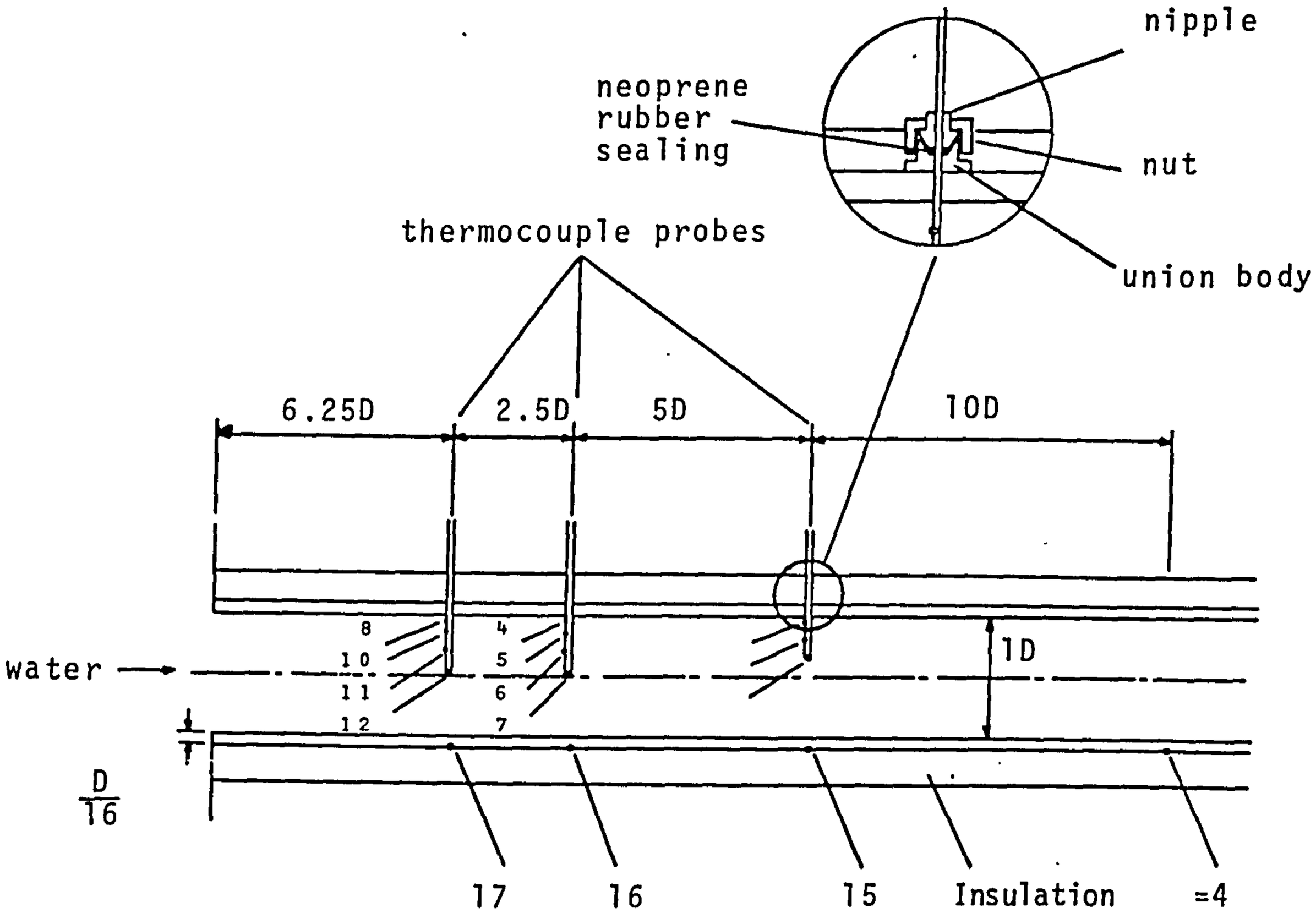


Fig (5.3) Details of the test section

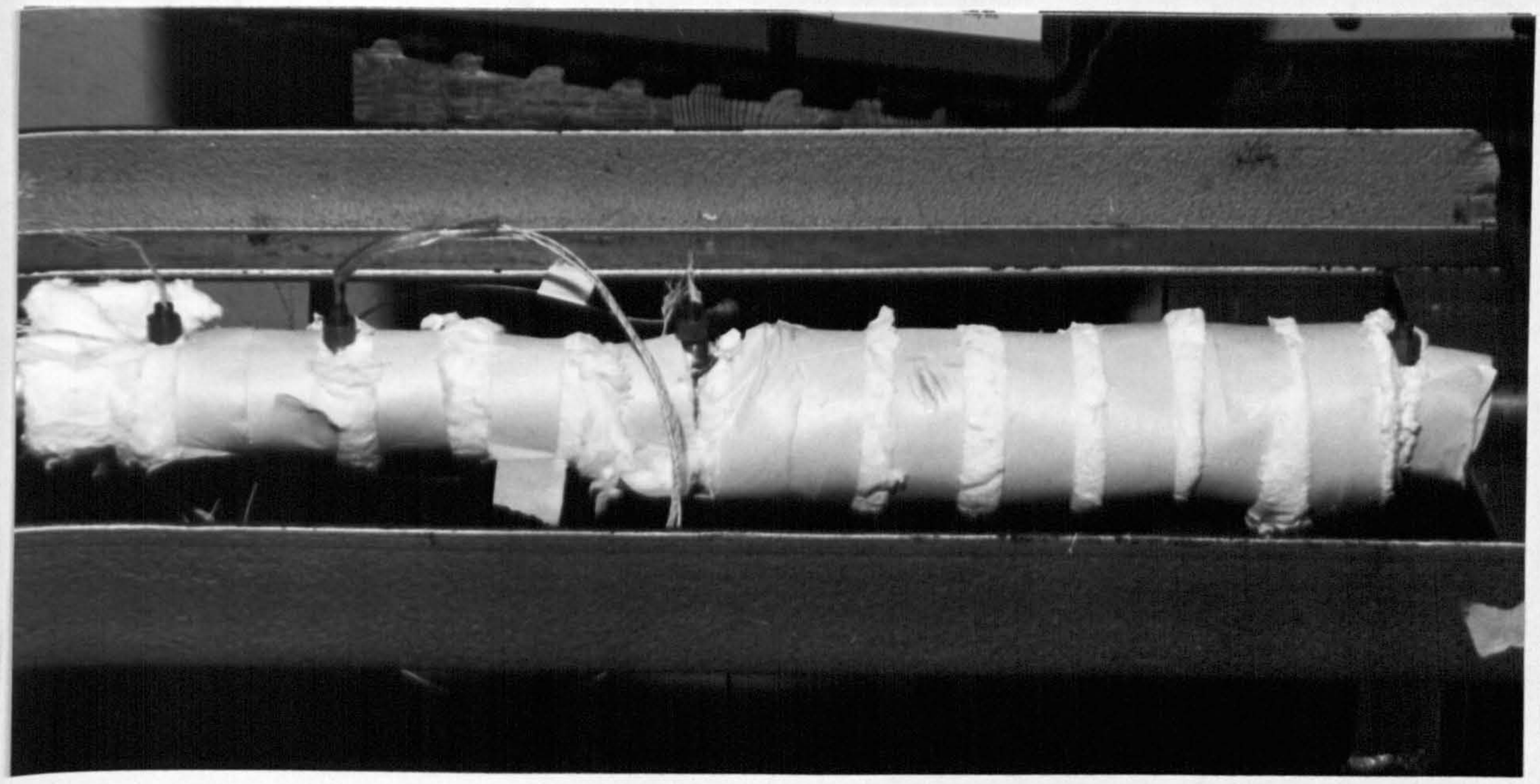


Fig (5.4) Photograph of the test section

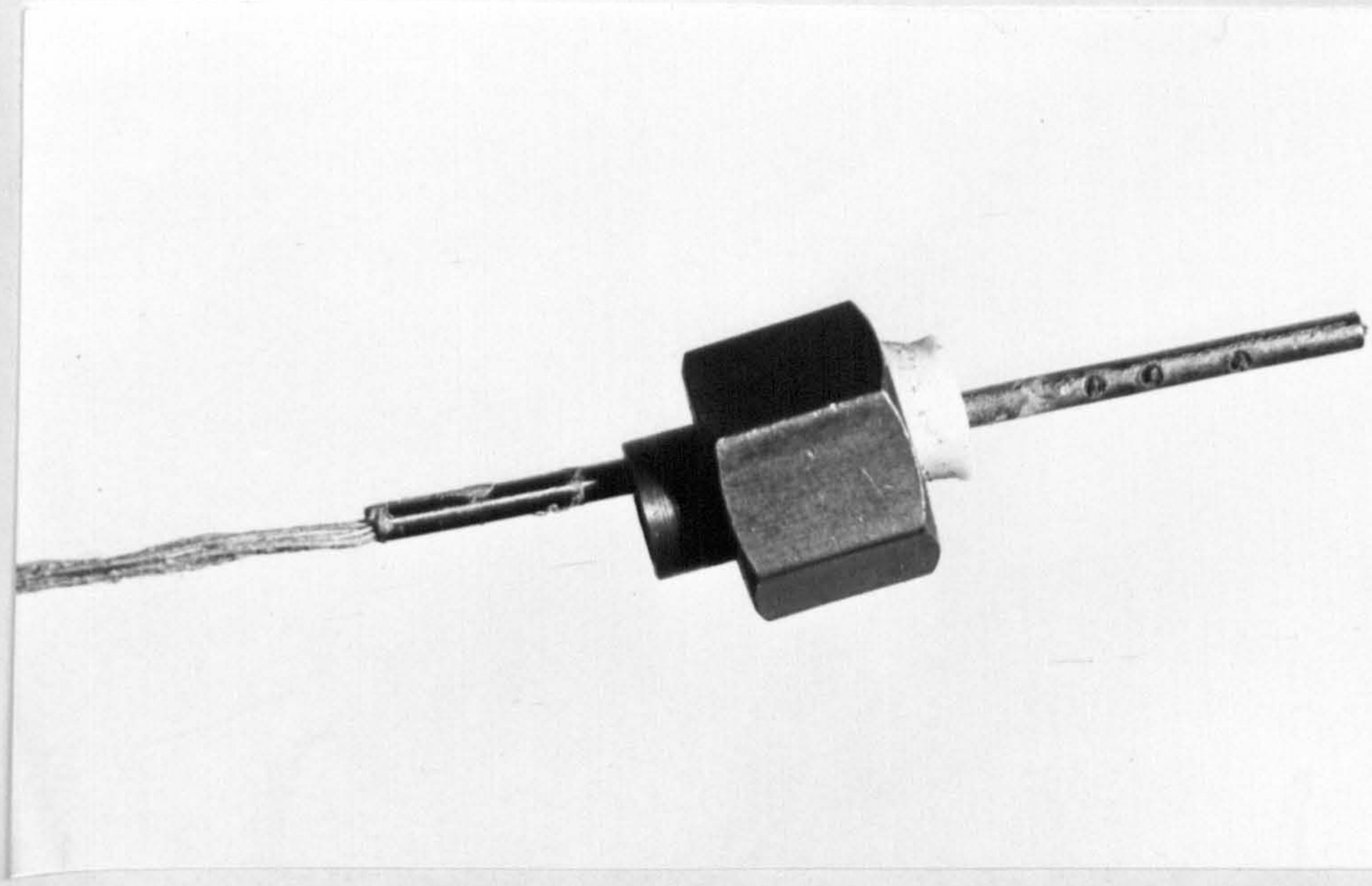


Fig (5.5) Photograph of the fluid thermocouples probe

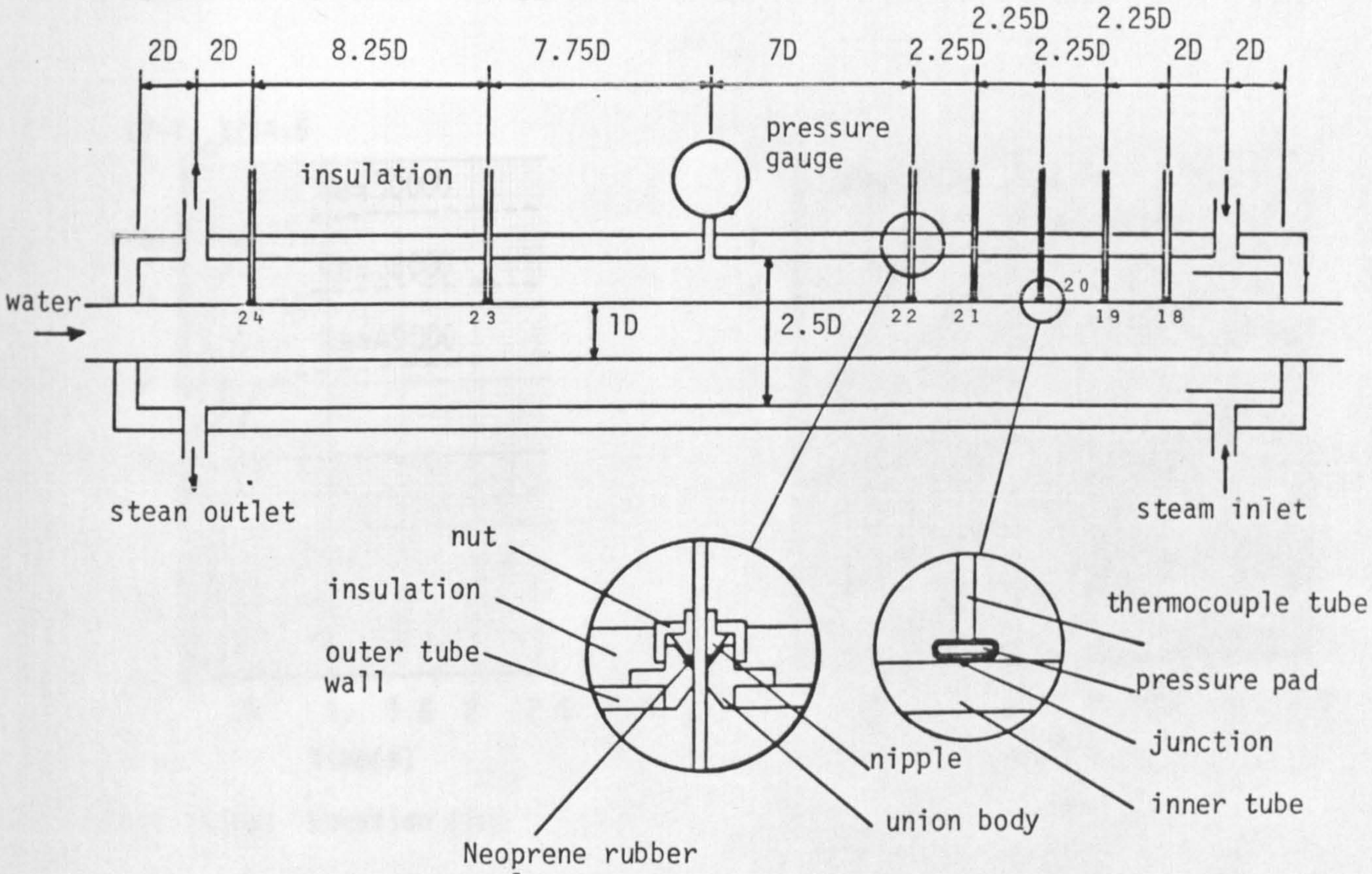


Fig (5.6) Details of the heating section

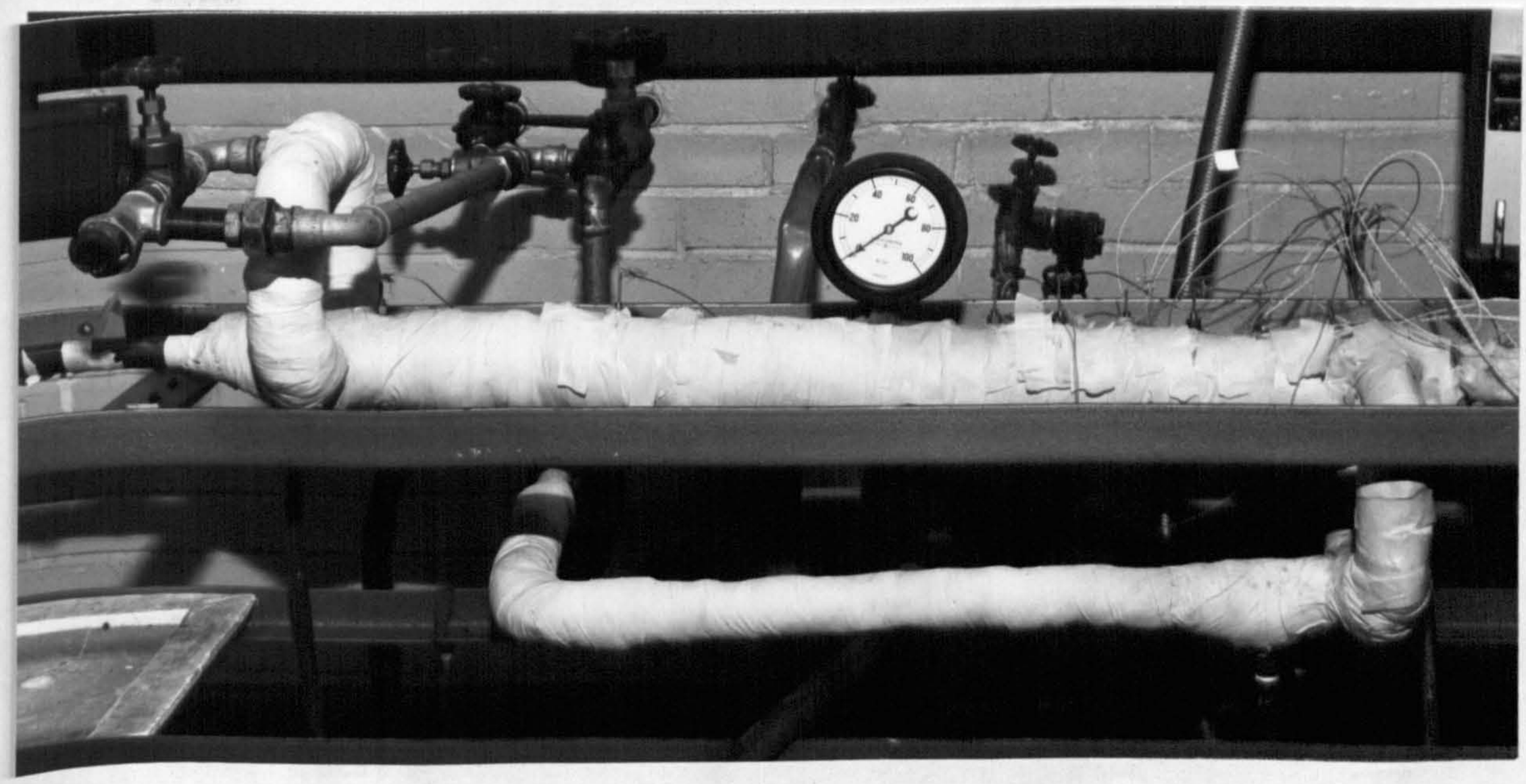


Fig (5.7) Photograph of the heating section

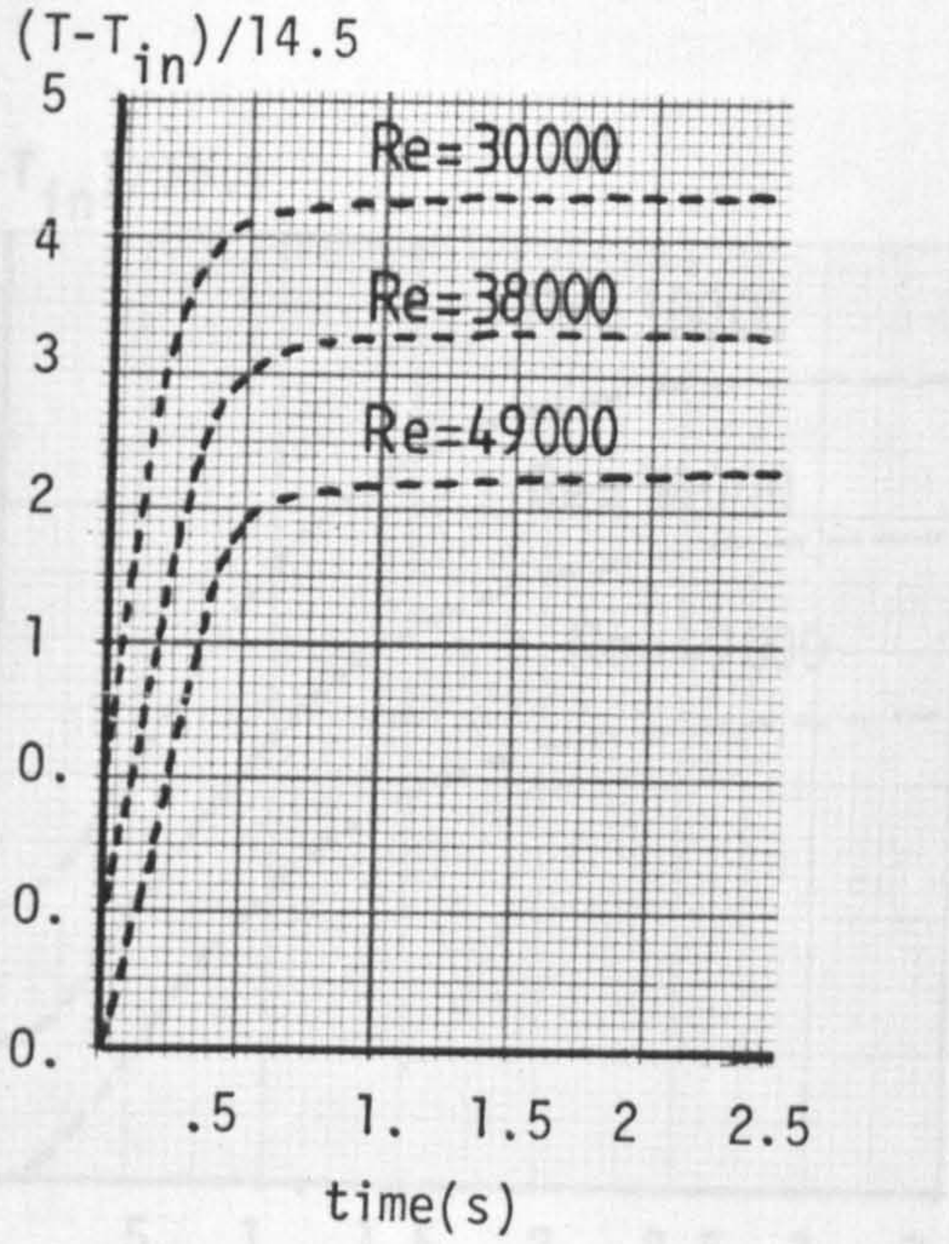


Fig. (5.8a) Location (18)

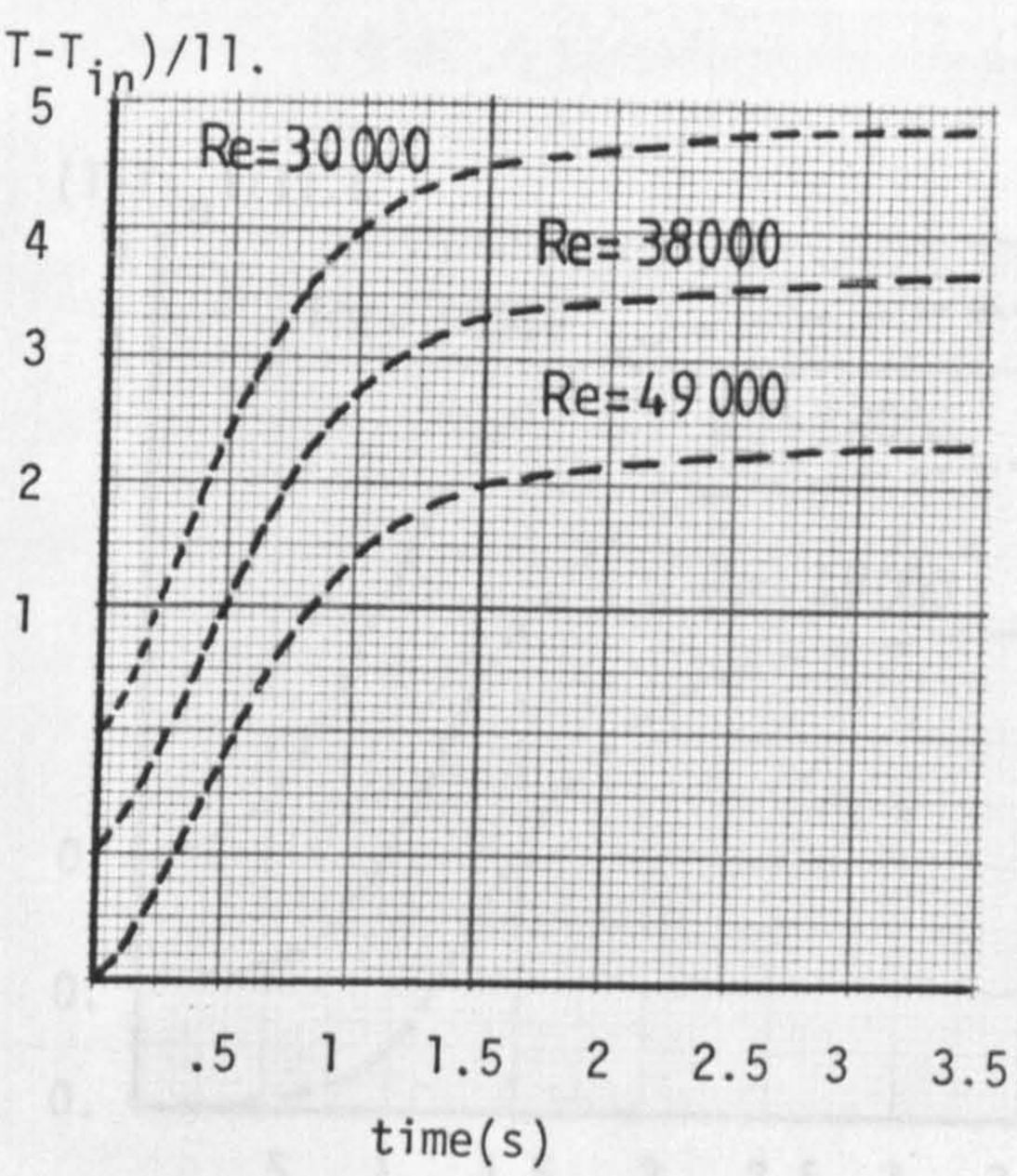


Fig (5.8b) Location (19)

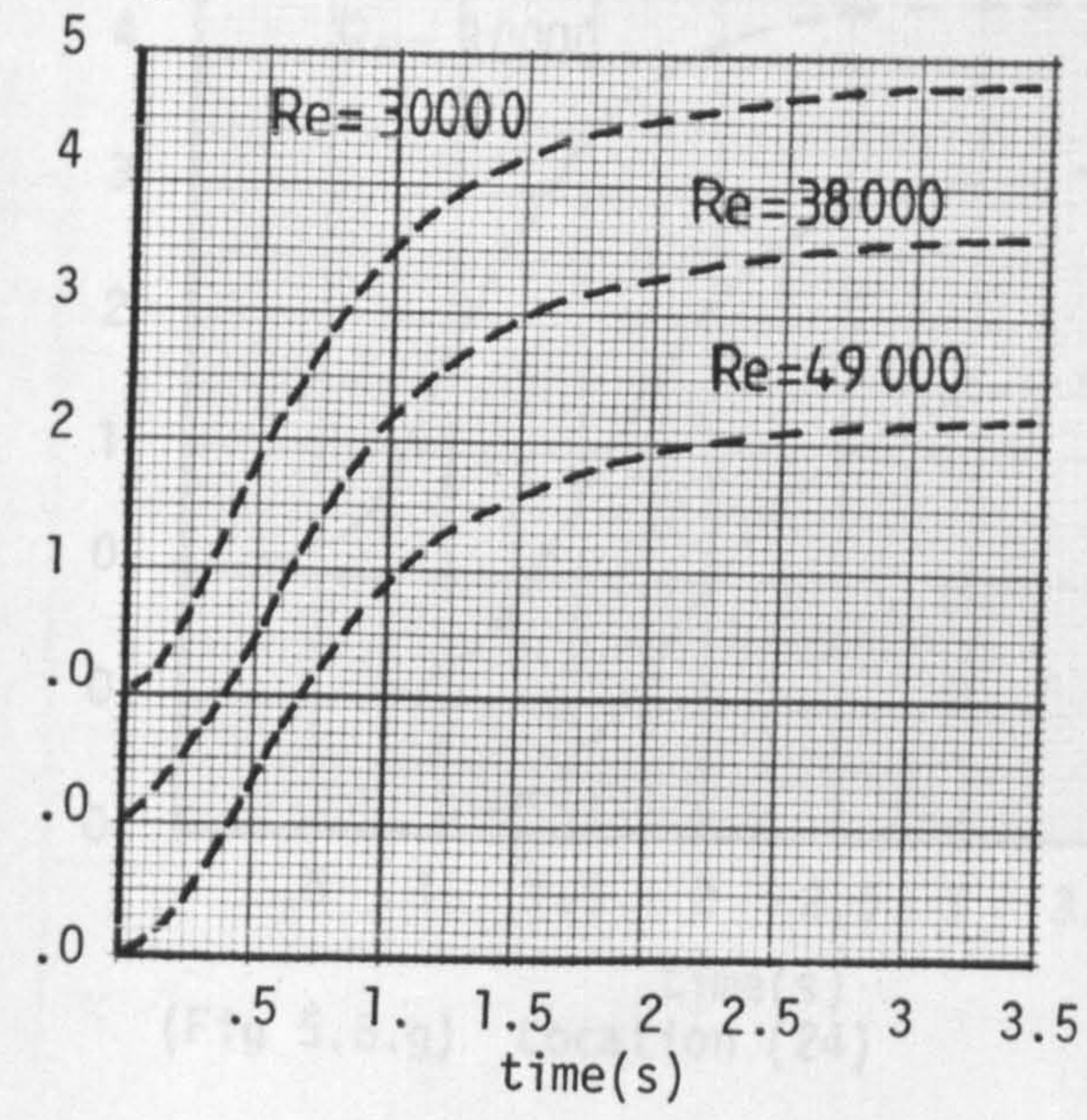


Fig (5.8c) Location (20)

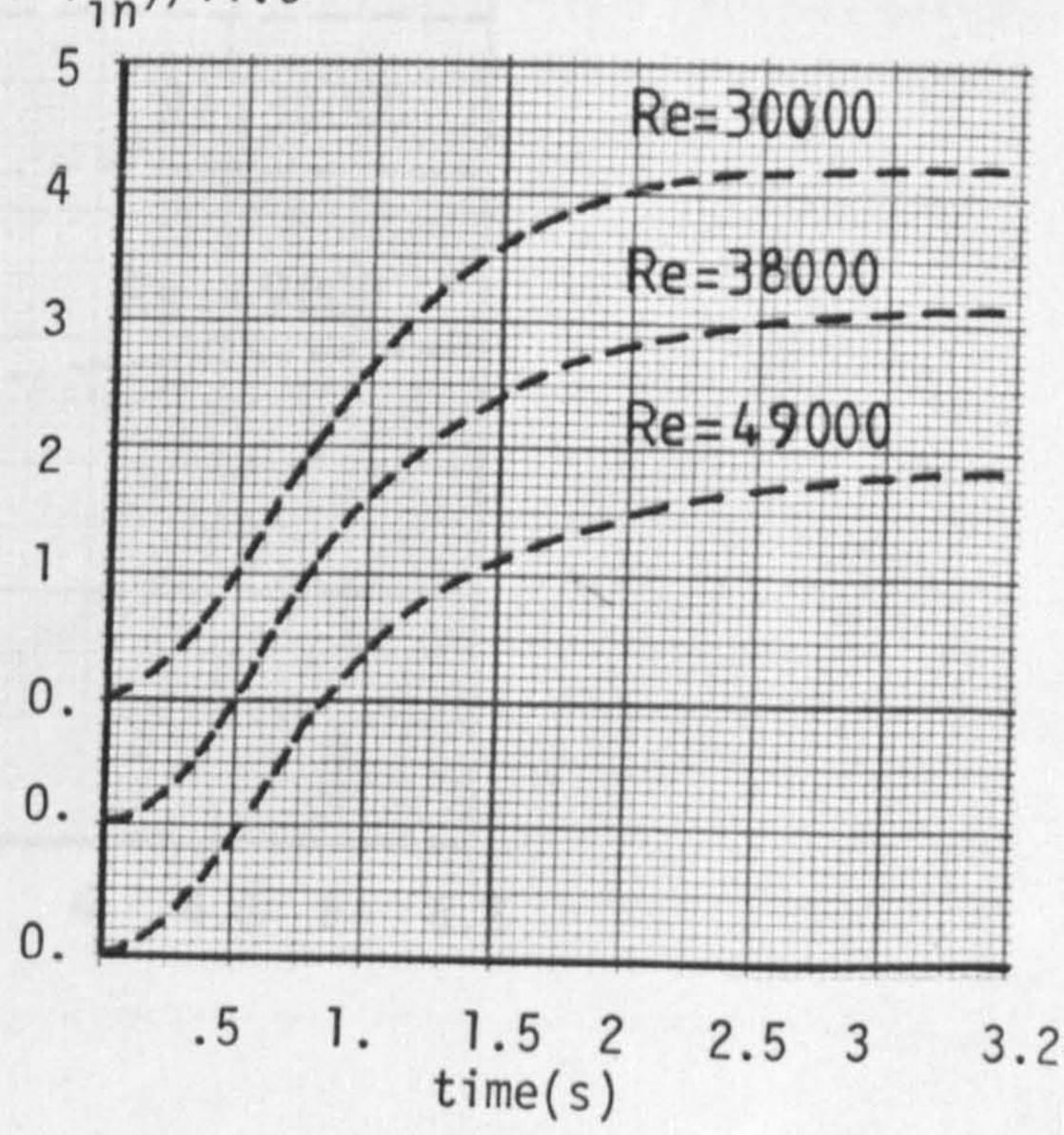


Fig (5.8d) Location (21)

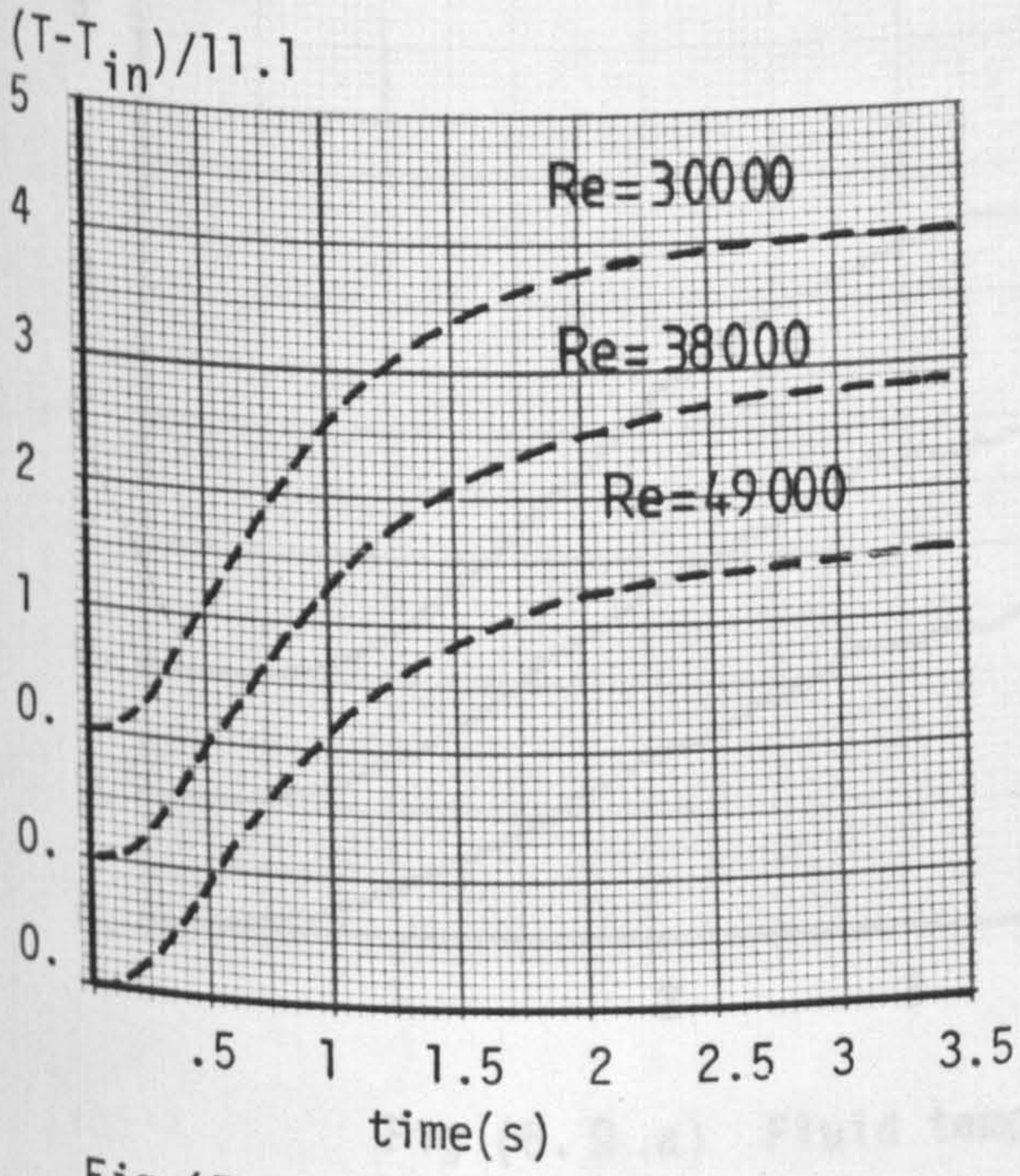


Fig (5.8e) Location (22)

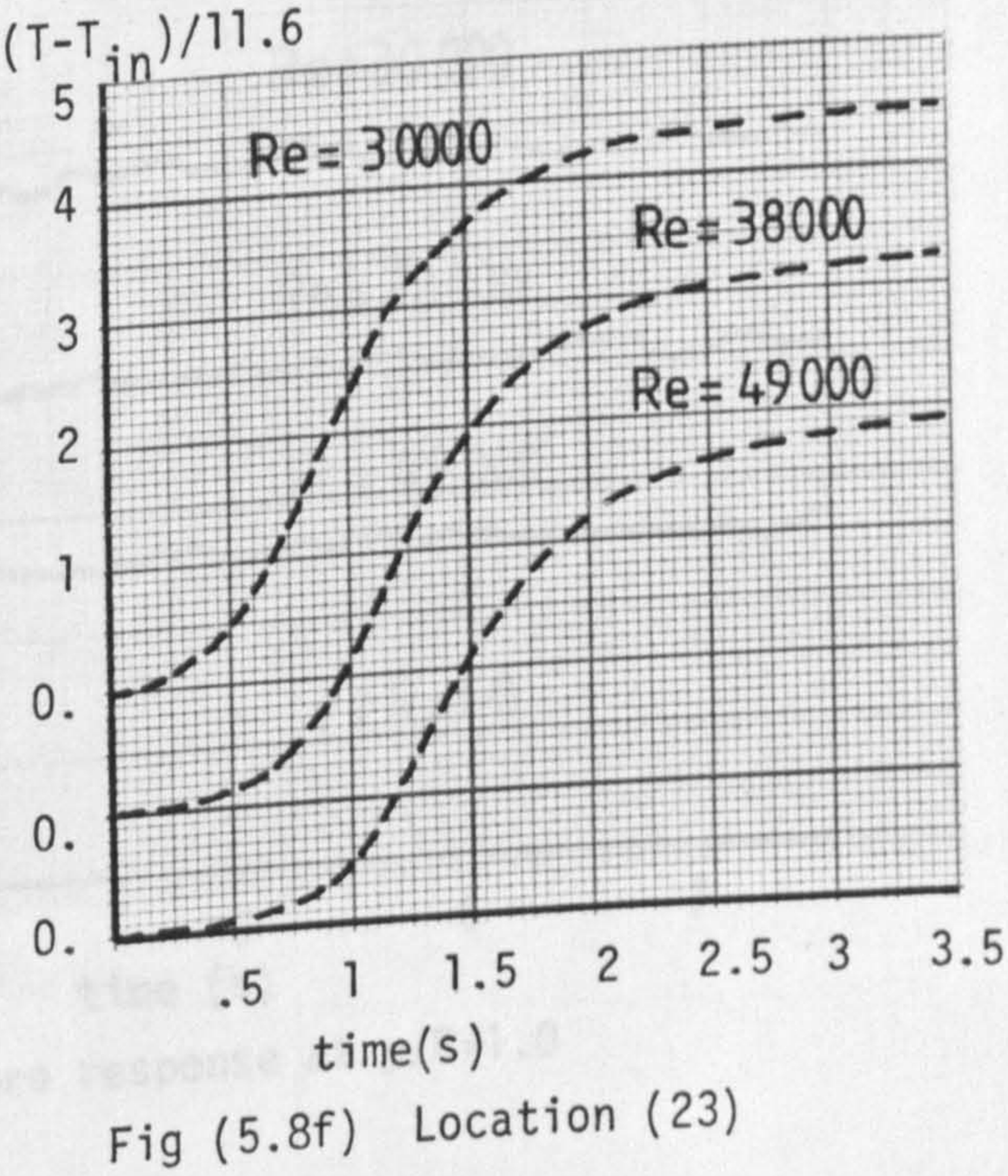
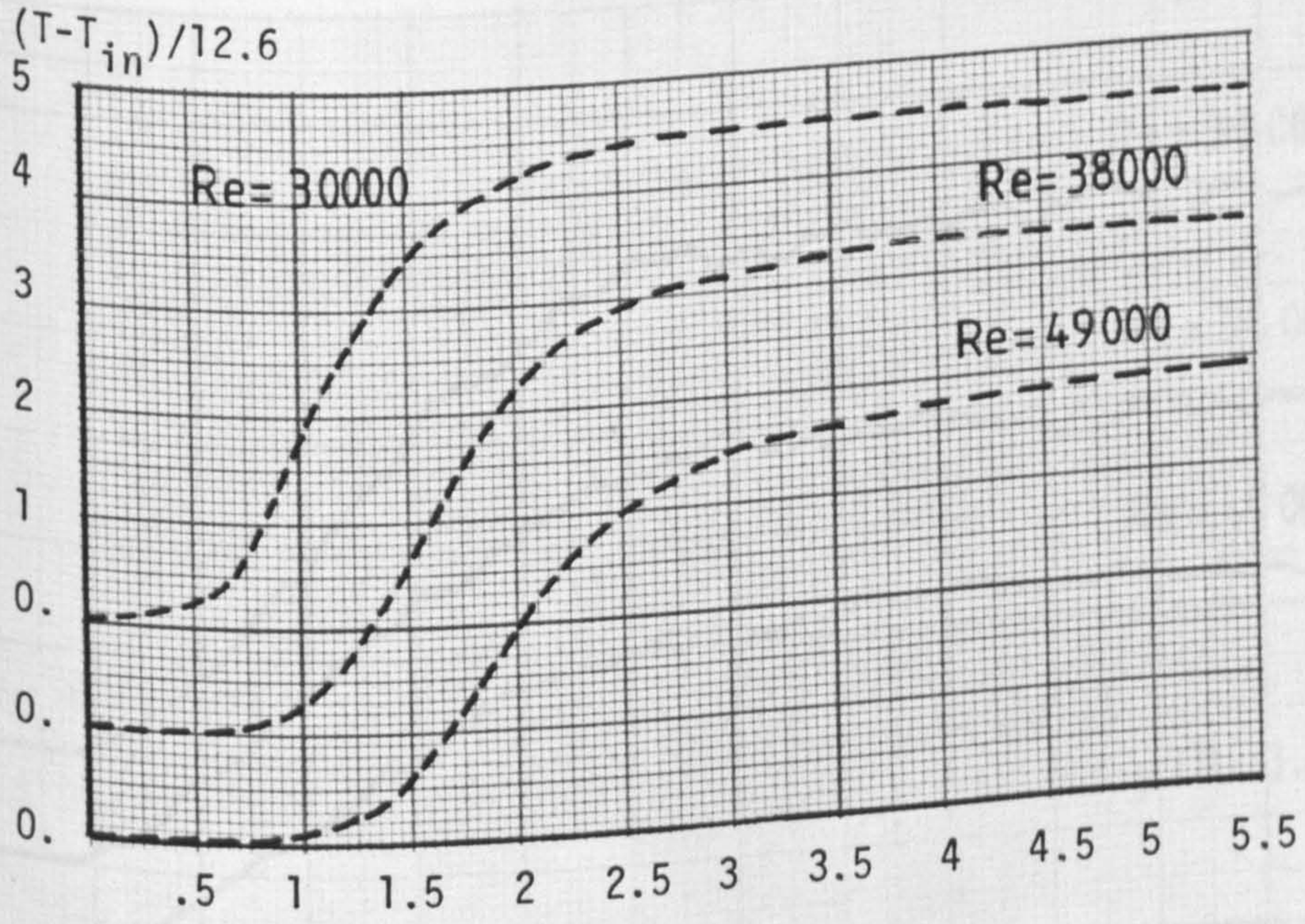


Fig (5.8f) Location (23)



(Fig 5.8.g) Location (24)

Fig (5.8) Heating boundary conditions

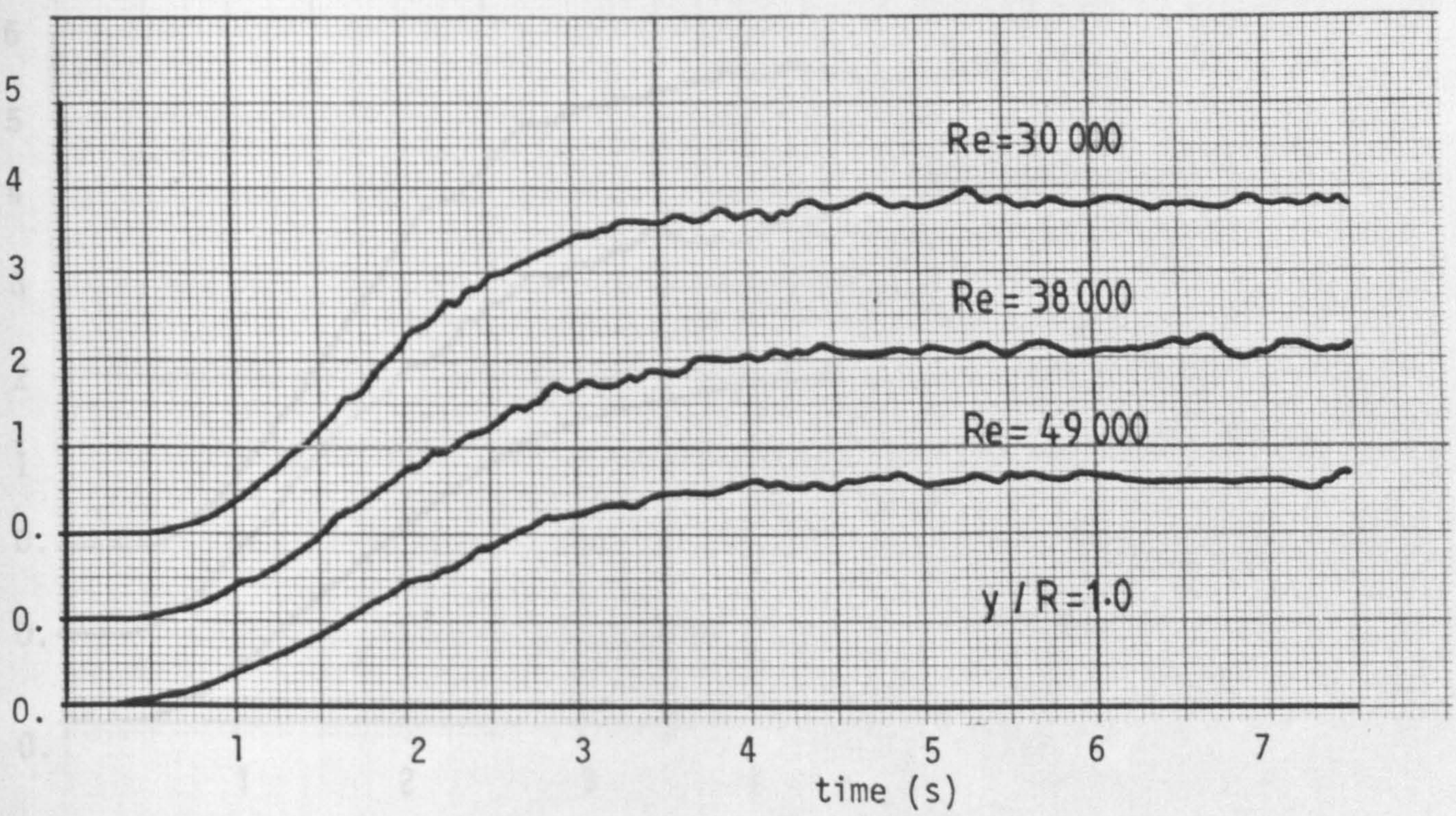


Fig (5.**9**.a) Fluid temperature response at y/R=1.0

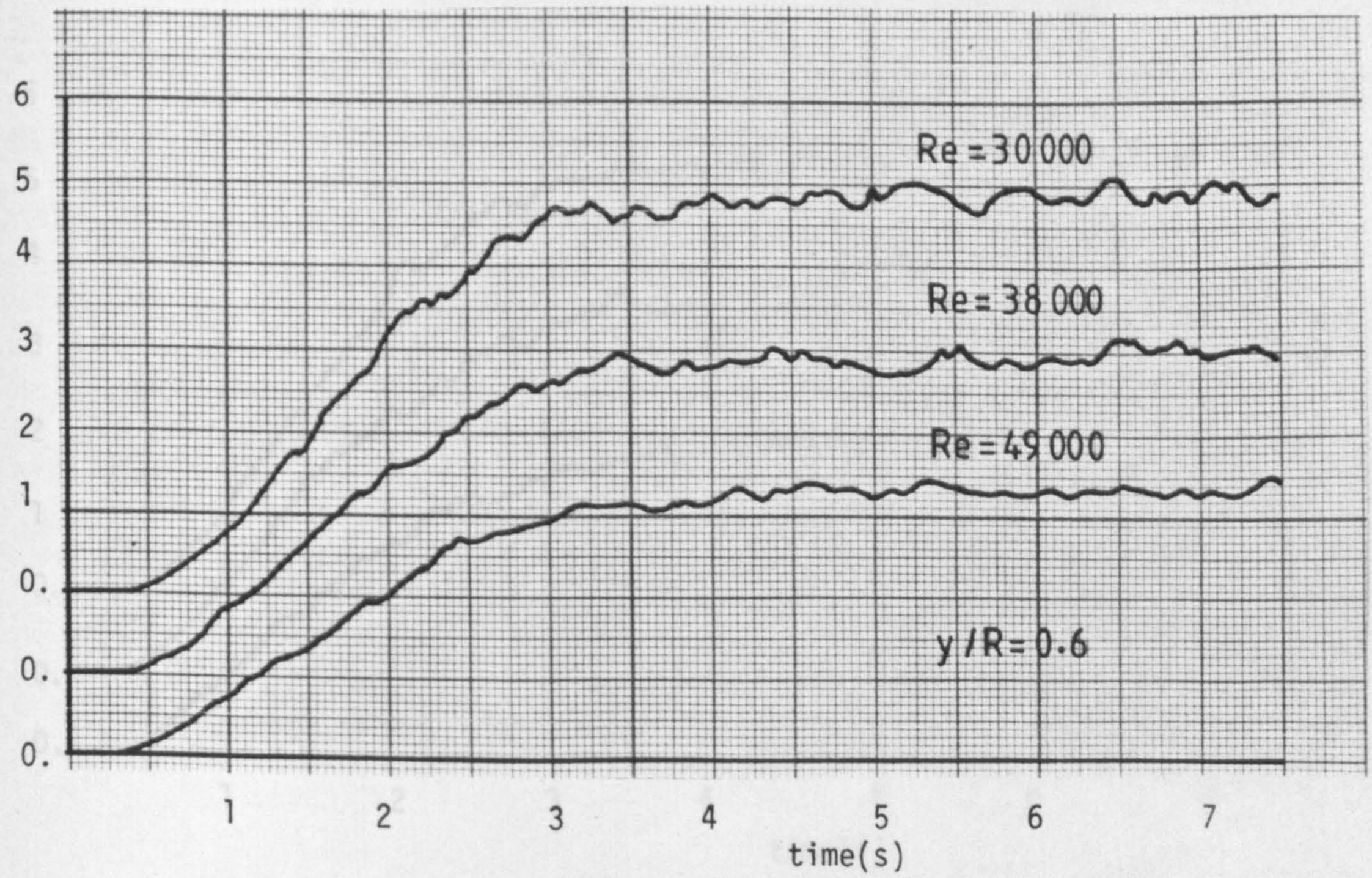


Fig (5.**9**.b) Fluid temperature response at y/R=0.6

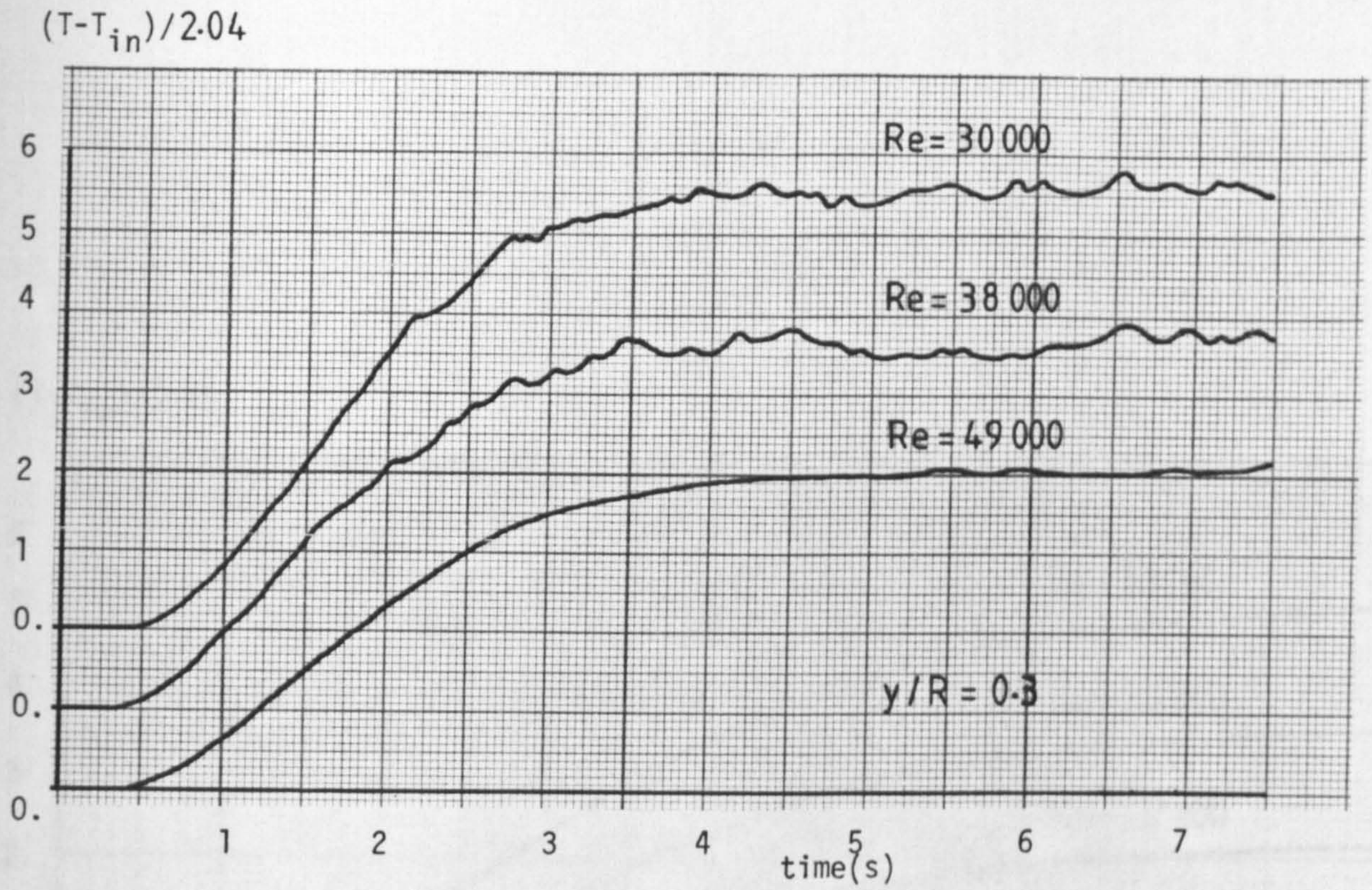


Fig (5.9.c) Fluid temperature response at y/R=0.3

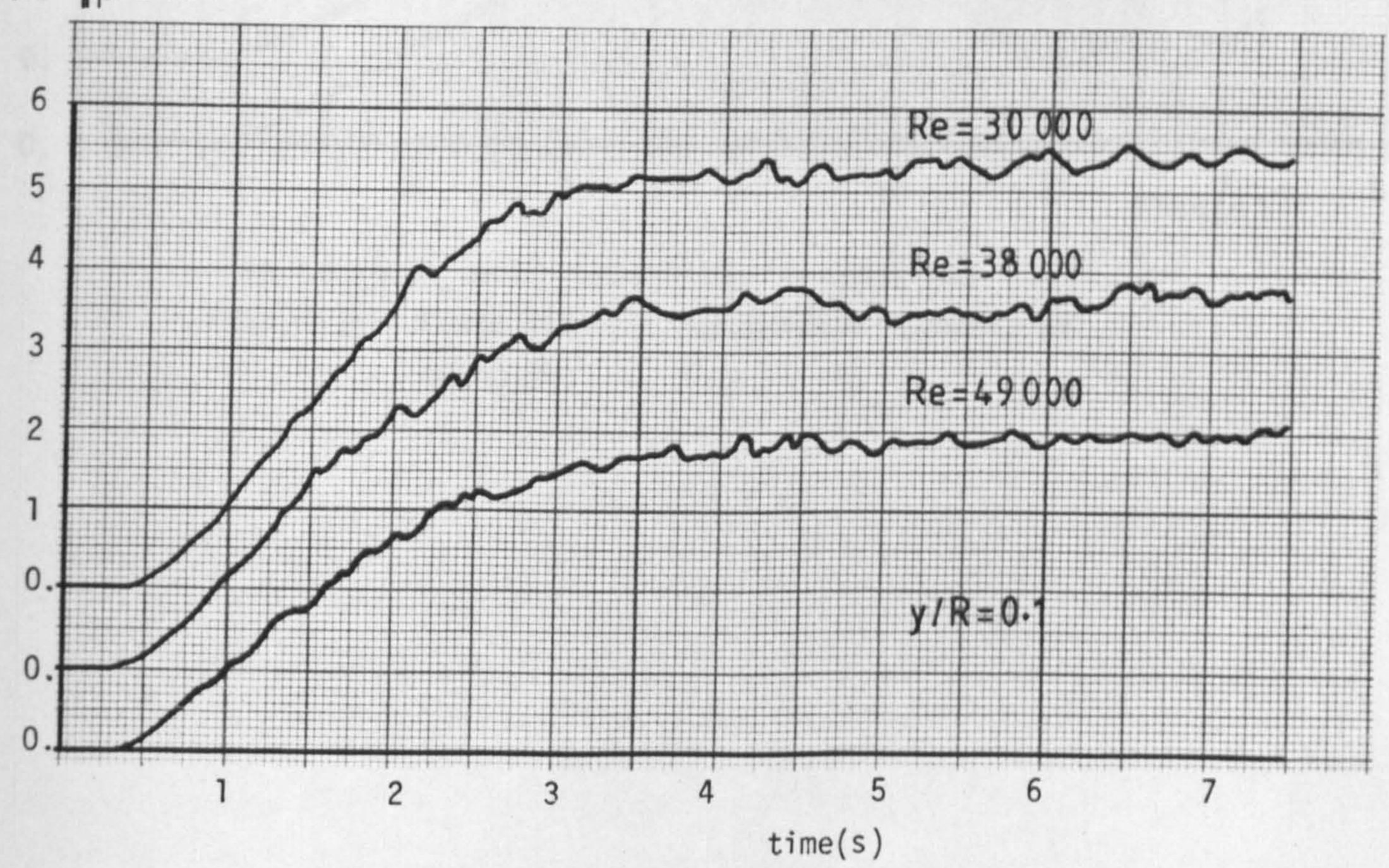


Fig (5.9.d) Fluid temperature response at y/R=0.1

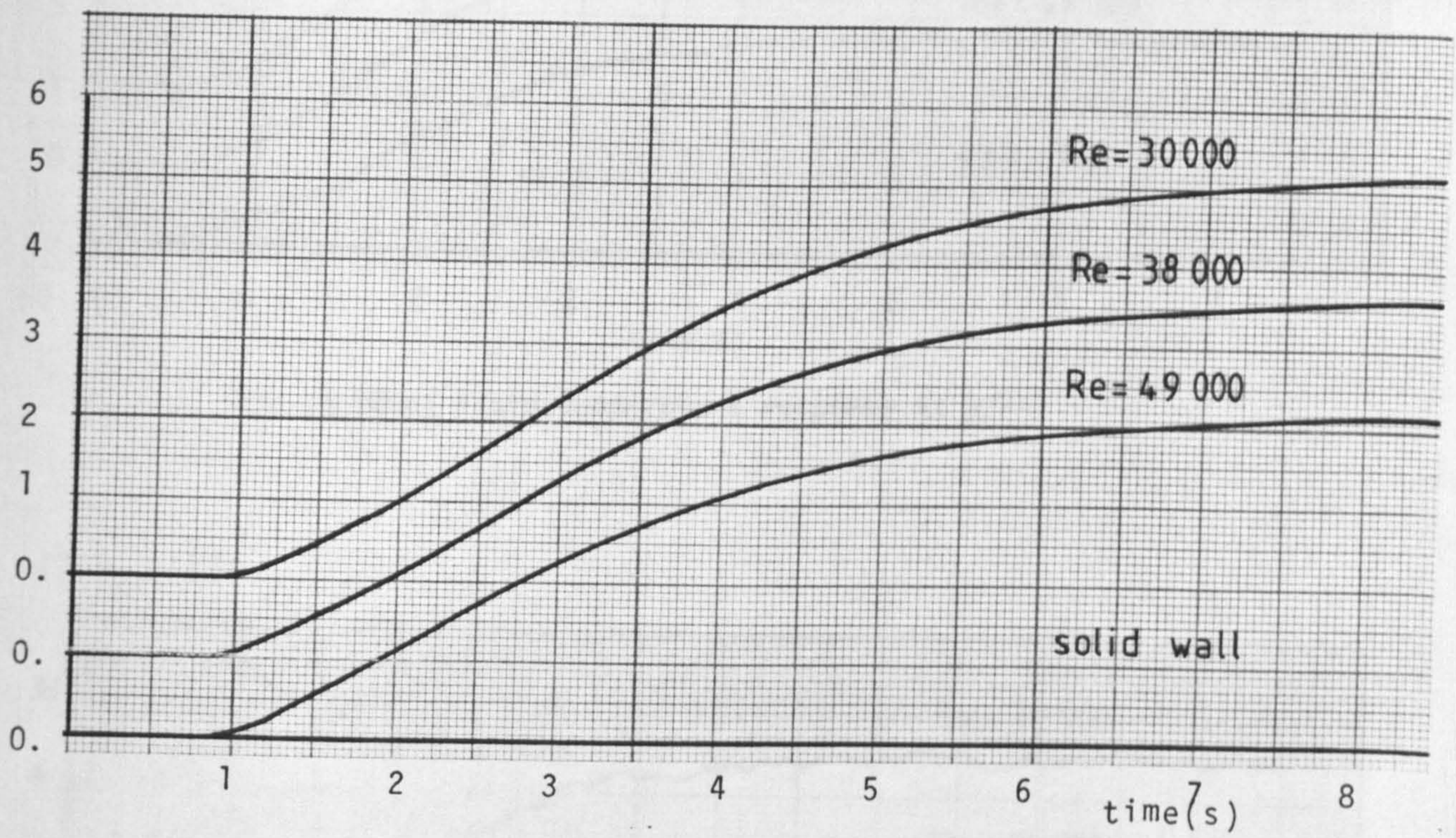


Fig (5.9.e) Wall temperature response

Fig (5.9) Fluid and wall temperature response at x/D=6.25

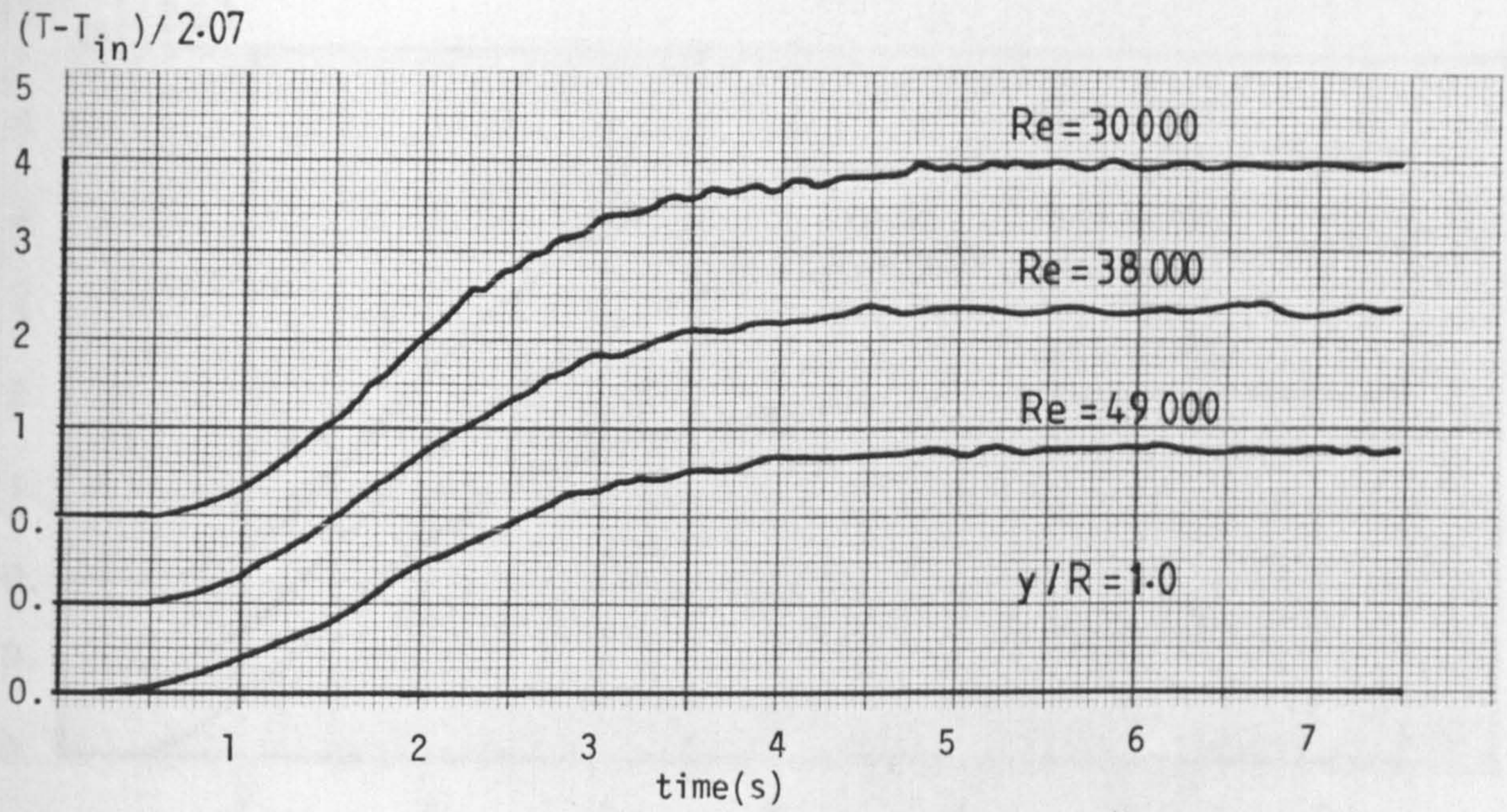


Fig (5.**10**.a) Fluid temperature response at y/R=1

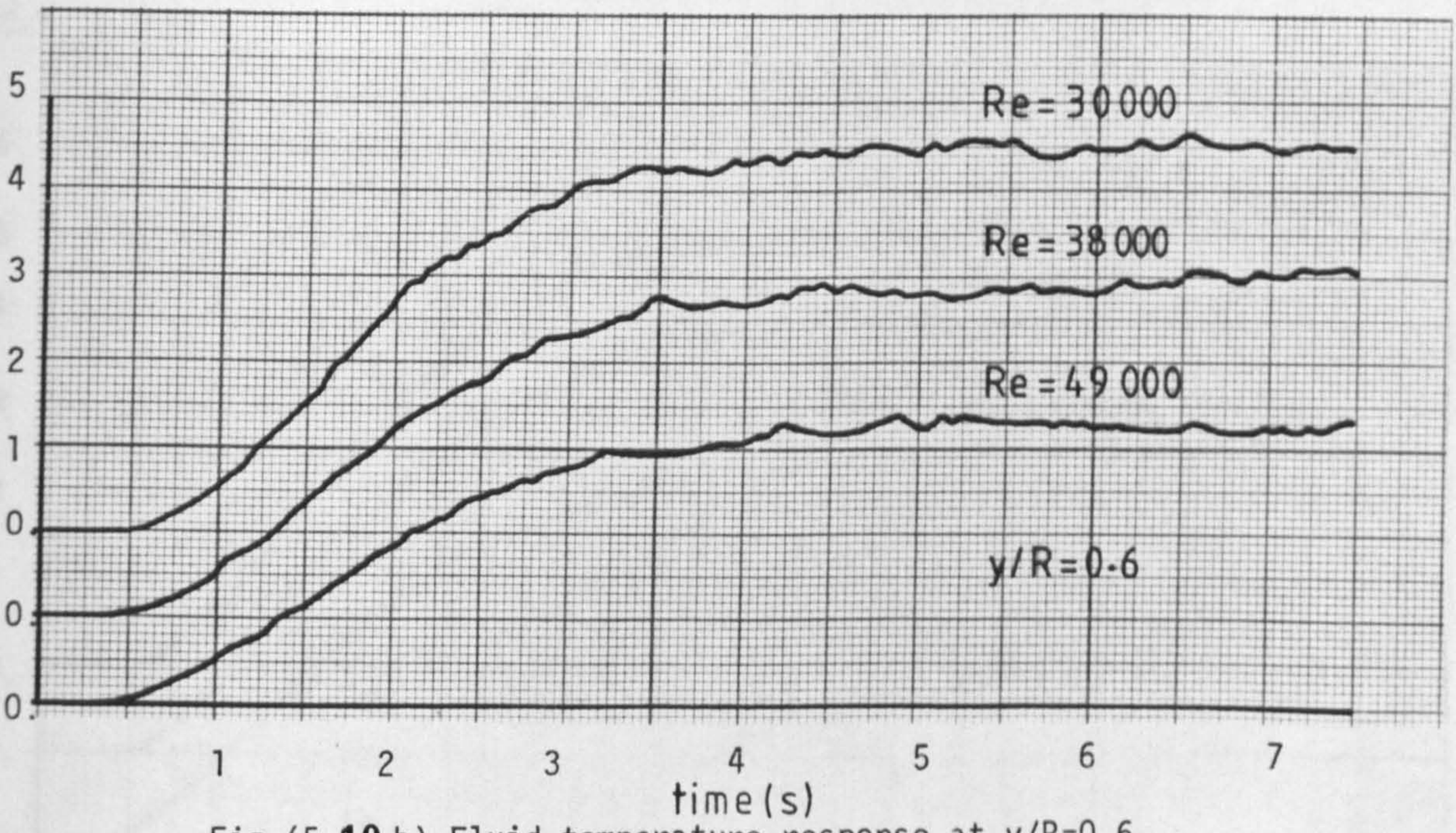


Fig (5.**10**.b) Fluid temperature response at y/R=0.6

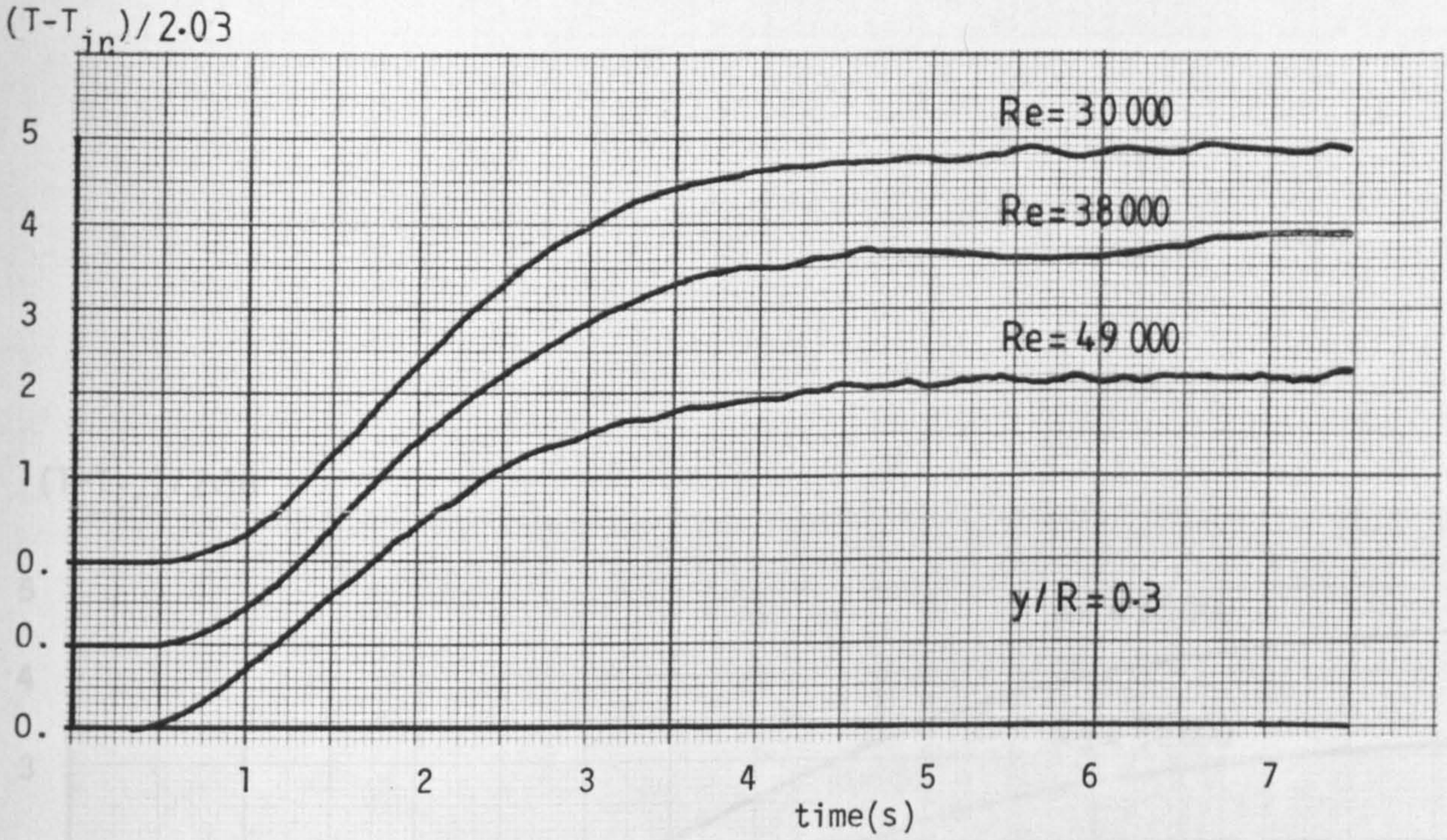


Fig (5.**10**.c) Fluid temperature response at y/R=0.3

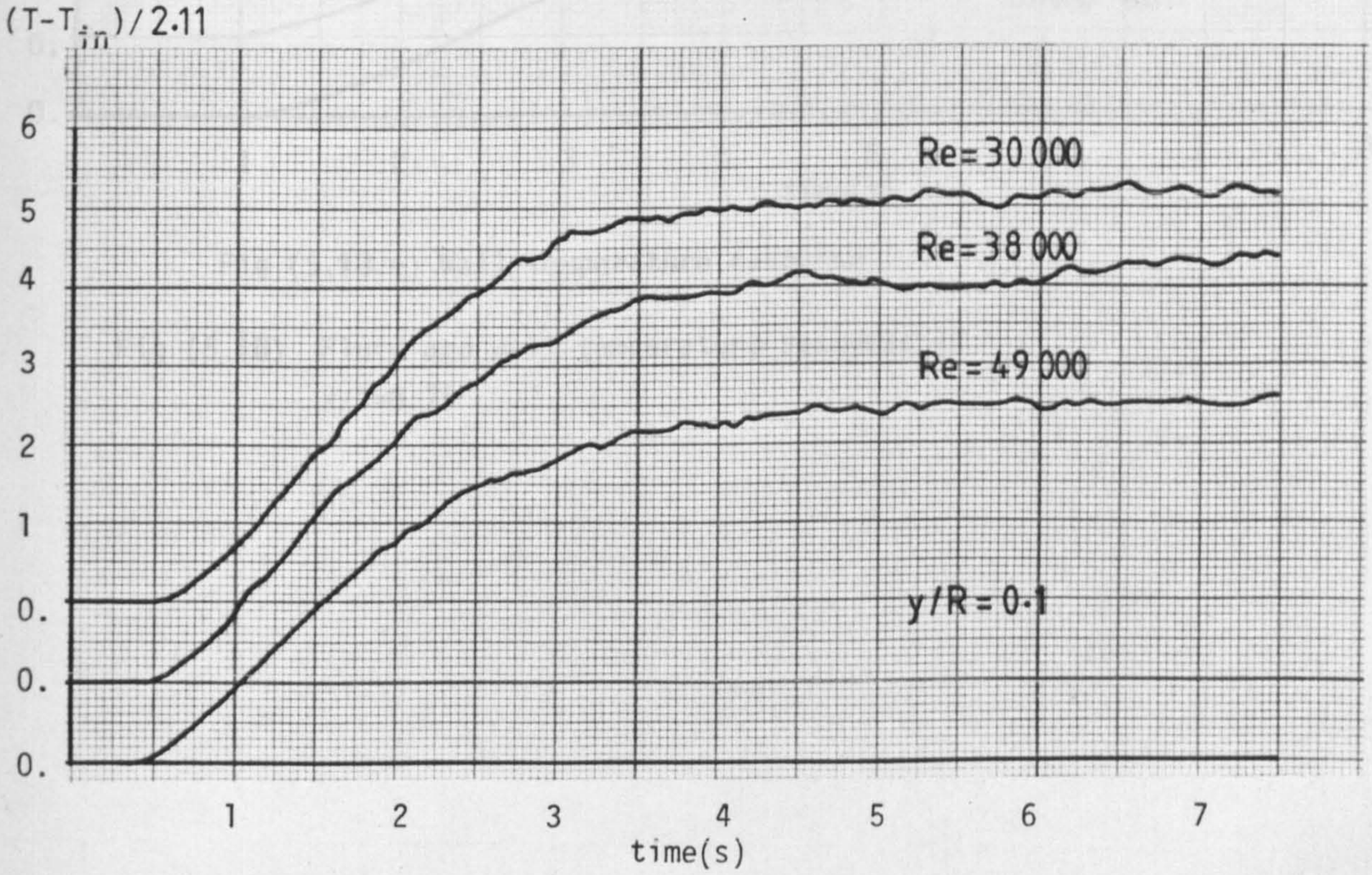


Fig (5.**10**.d) Fluid temperature response at y/R=0.1

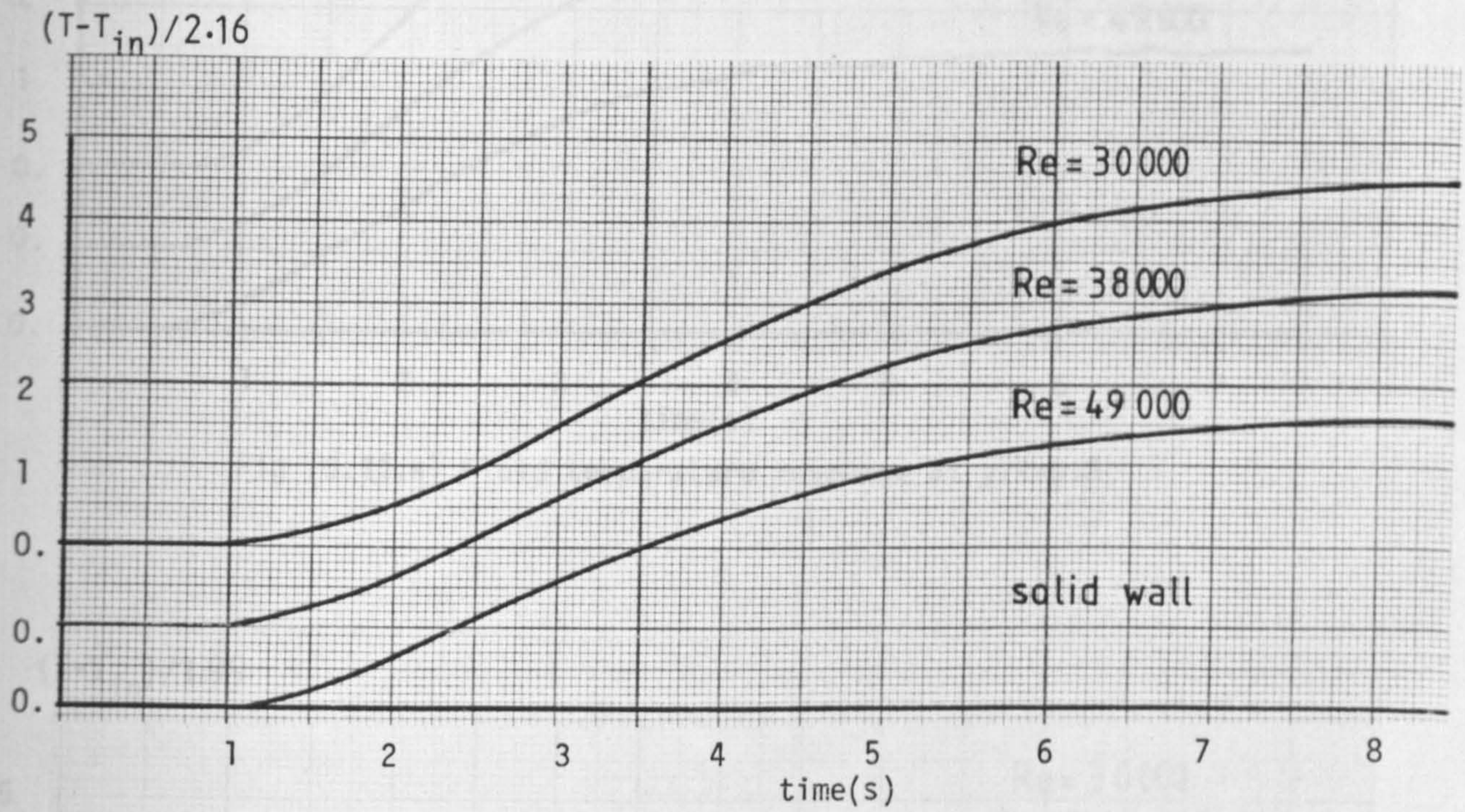


Fig (5.**10**.e) Wall temperature response

Fig (5.**10**) Fluid and wall temperature response at x/D=8.75

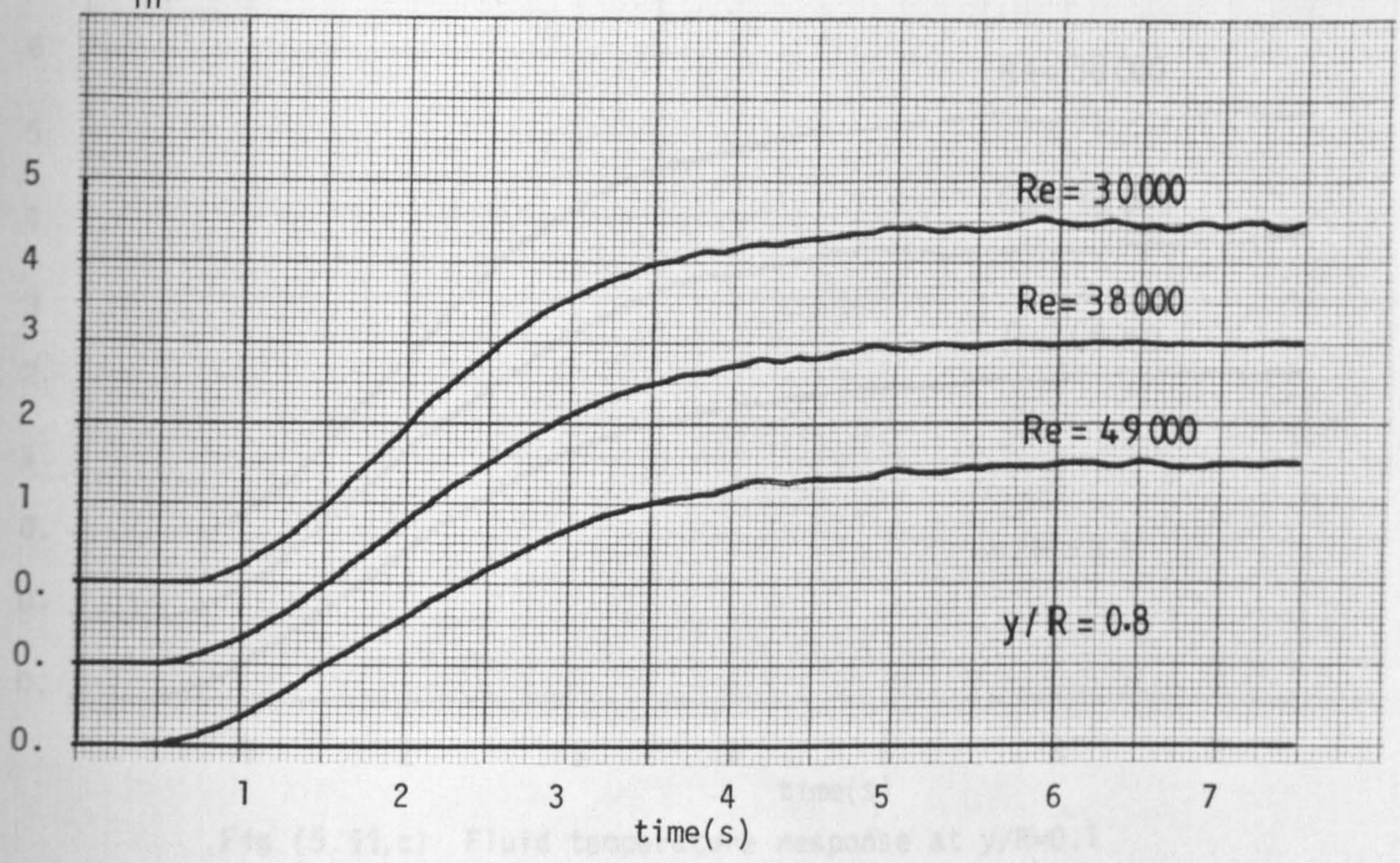


Fig (5.**11**.a) Fluid temperature response at y/R=0.8

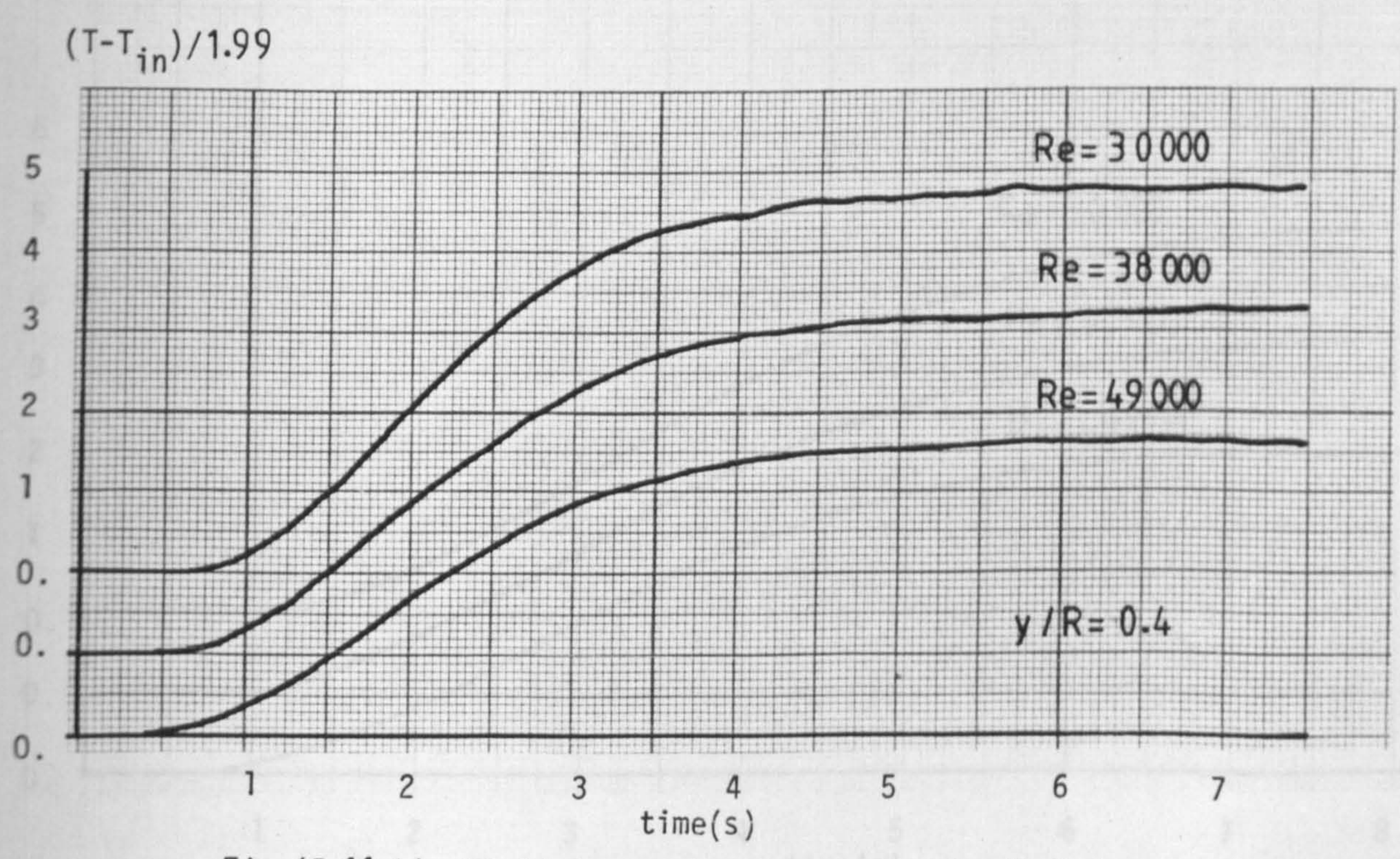


Fig (5.**11**.b) Fluid temperature response at y/R=0.4

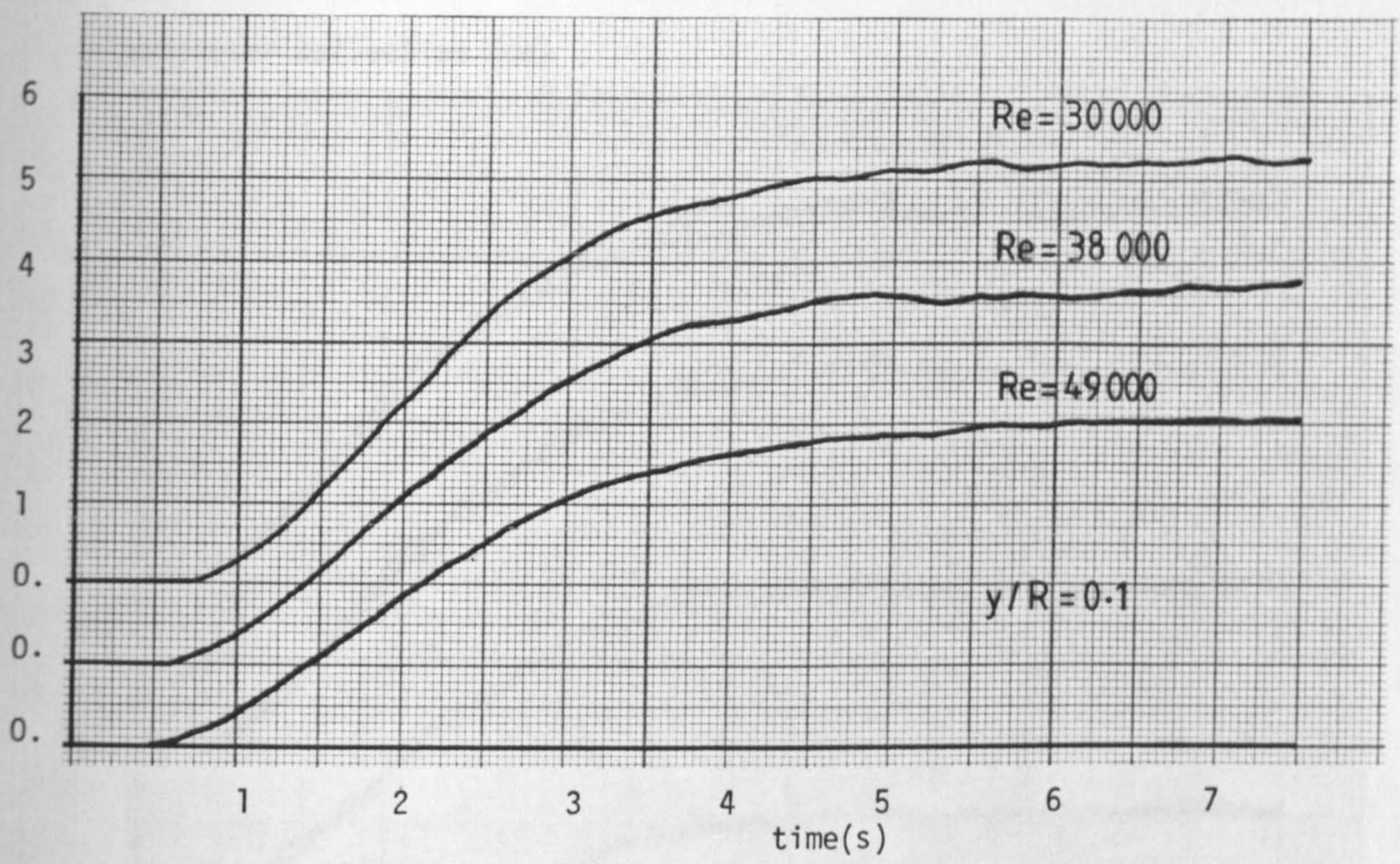


Fig (5.**11**.c) Fluid temperature response at y/R=0.1

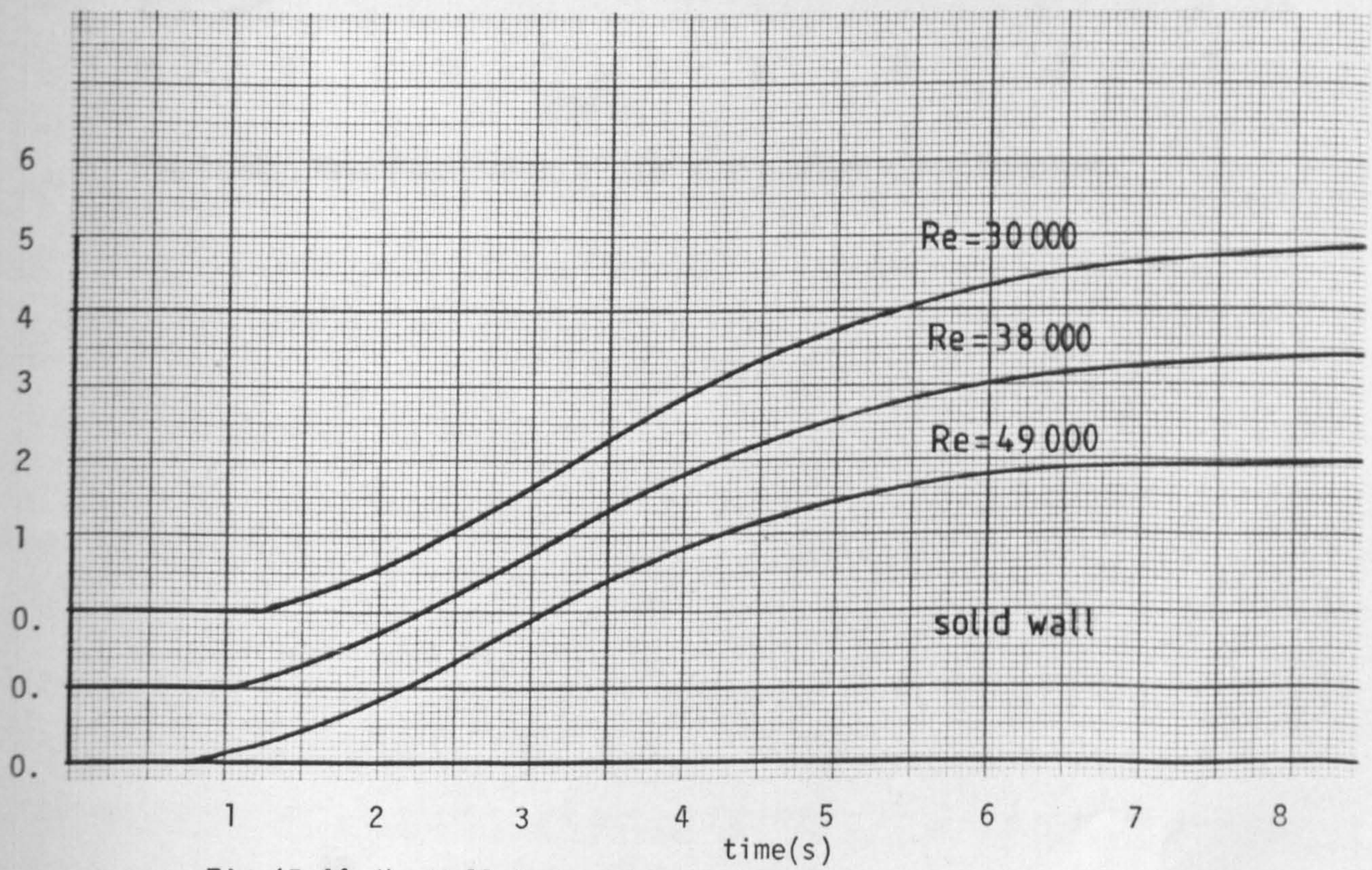


Fig (5.**11**.d) Wall temperature response

Fig (5.**11**) Fluid and wall temperature responses at x/D=13.75

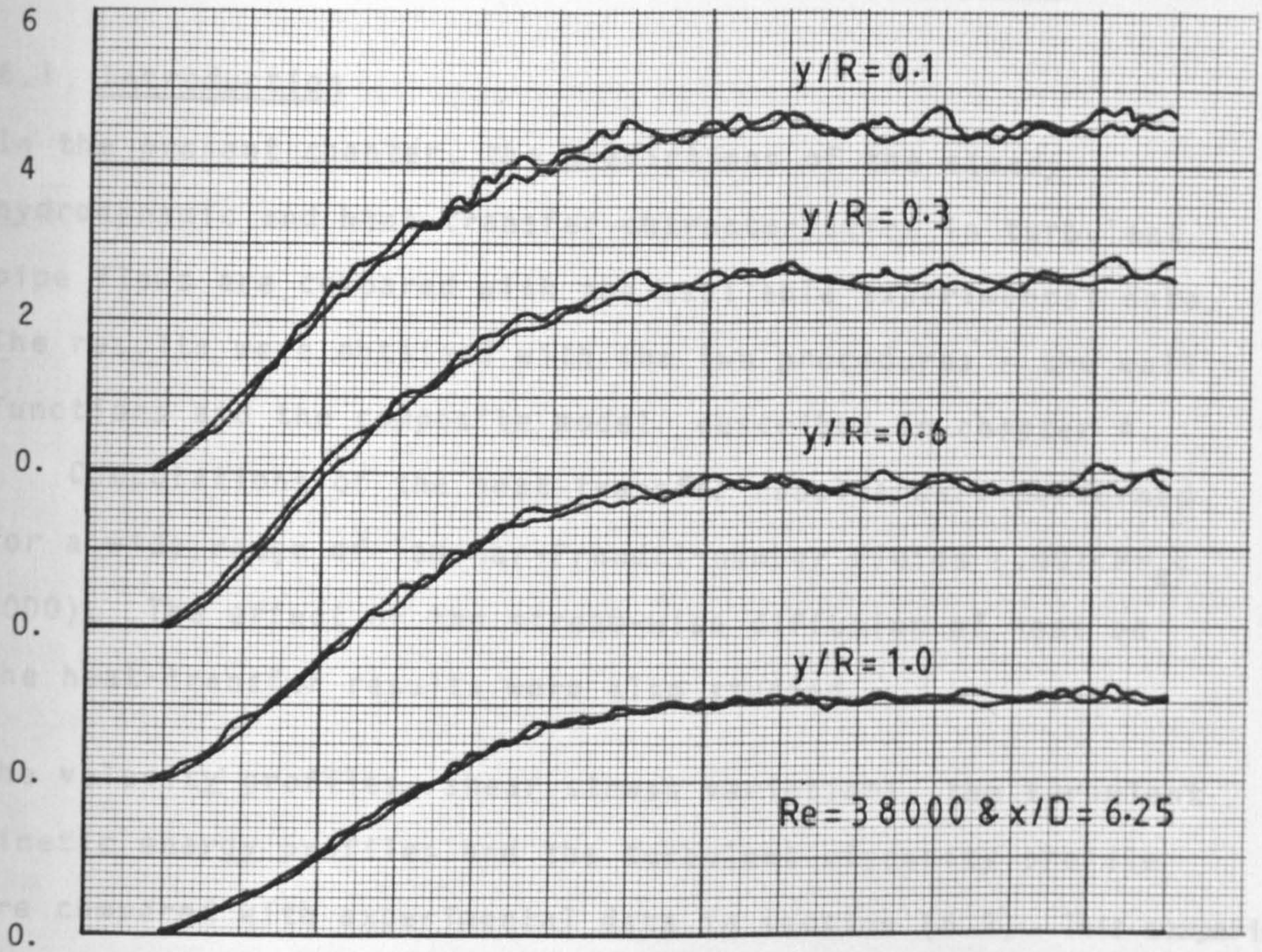


Fig (5.12) Reproducibility of the fluid temperature response

CHAPTER 6

STEADY HYDRODYNAMIC AND HEAT-TRANSFER RESULTS

6.1 Introduction

In the present chapter, the predictions of the steady hydrodynamic and heat-transfer characteristics in turbulent pipe flows are compared with the available experimental data. The results were obtained with the two procedures - the wall functions and the composite model described in chapter 4.

Computations of the heat-transfer results were performed for a wide range of laminar-Prandtl-number fluids ($.001<Pr_{\ell}<1000$). The effect of the stream-wise diffusion of heat on the heat-transfer results were also studied.

The velocity profiles, shear stress variations, the turbulent kinetic energy profiles and the turbulent-viscosity profile are compared with experimental data in section (6.2). This comparison is followed by a comparison of the predicted temperature profiles and the Nusselt number variations against experimental data in section (6.3); while in section (6.4) the heat-transfer results for the conjugate problems are presented. Finally, section (6.5) contains some concluding remarks.

6.2 Hydrodynamic Results

6.2.1 Computational details

The algebraic finite-difference equations presented in chapter (4) were derived from the relevant partial differential equations. In the derivation process, it was necessary to introduce assumptions regarding the variation of the dependent variables (ϕ and $\tilde{\tilde{h}}$) over the control volume. Such assumptions

are accurate only when the grid spacing is sufficiently small; thus the stream-wise and cross-stream grid intervals must be systematically reduced until the errors introduced by these assumptions become insignificant. This will be indicated by insensitivity to further refinement ; the solution is then said to be 'grid independent'.

In order to present the error introduced by the grid spacing on the hydrodynamic results, attention is focussed on the dimensionless centreline velocity (u^+) in the entrance region. The error was calculated as a percentage from the results obtained with the smallest grid spacing for both the composite model and the wall-function methods for an air flow with a Reynolds number of 3.88×10^5.

(i) <u>The composite model</u>

The effect of the number of radial grid points in the near-wall region on the centreline velocity (u^+) is presented in figure (6.1), while the effect of grid points in the central region is shown in figure (6.2). The results were given for 10, 20 and 40 grid points as a percentage deviation from the results obtained with 60 grid points in figure (6.1). This figure indicates that the results become independent of the radial grid spacing in the near-wall region when forty or more grid points are used. Figure (6.2) shows the results for 10, 20 and 30 grid points as percentage deviations from the results obtained with 40 grid points. It is seen that the effect of radial grid spacing in the central region becomes insignificant when 30 or more grid points are used to span the central region.

The effect of the stream-wise grid spacing on the centreline velocity (u^+) is indicated in figure (6.3). The results were presented for a grid spacing (δx) of 2,1 and 0.5 the pipe diameter in the form of percentage deviations from the results obtained with a (δx) of 0.25 the pipe diameter. These results reveal that a stream-wise grid spacing of 0.5 the pipe diameter or smaller was sufficient to yield grid-independent results.

The hydrodynamic results obtained with the composite model and presented in this chapter were all obtained with a grid distribution of 40 nodes in the near-wall region and 30 outside, as shown in table (6.1), and forward steps of 0.25 the pipe diameter. The number of line-iterations required at each forward step in this case are plotted in figure (6.4); a large number of iterations were required at the first few forward steps where the large stream-wise variation in the dependent variables exists. The changes in the shear velocity ($\sqrt{\tau/\rho}$) from one iteration to another is present for the first and second forward steps in figures (6.5 and 6.6) respectively. The execution time for 50 diameters pipe length was 56.5 seconds on the CDC 6600 computer machine.

(ii) <u>The wall-function method</u>

The effect of the number of radial grid points on the centreline velocity (u^+) is presented in figure (6.7), while the effect of the stream-wise grid spacing is shown in figure (6.8). Figure (6.7) showed the results for 20, 30, 40 and 50 radial grid points in the form of percentage deviations from the results obtained with 60 radial grid points. This figure indicates that the results become essentially independent

Table (6.1)

Grid distribution

I	Y	YPLUS
1	0	6.205E+03
2	2.294E-02	6.425E+03
3	3.121E-02	5.693E+03
4	3.830E-02	5.112E+03
5	5.221E-02	3.988E+03
6	6.169E-02	3.223E+03
7	6.870E-02	2.852E+03
8	7.427E-02	2.287E+03
9	7.866E-02	1.852E+03
10	8.222E-02	1.565E+03
11	8.514E-02	1.329E+03
12	8.755E-02	1.135E+03
13	8.955E-02	9.732E+02
14	9.121E-02	8.386E+02
15	9.261E-02	7.260E+02
16	9.376E-02	6.316E+02
17	9.476E-02	5.522E+02
18	9.559E-02	4.854E+02
19	9.628E-02	4.292E+02
20	9.687E-02	3.818E+02
21	9.737E-02	3.418E+02
22	9.778E-02	3.080E+02
23	9.814E-02	2.795E+02
24	9.843E-02	2.555E+02
25	9.868E-02	2.353E+02
26	9.890E-02	2.182E+02
27	9.907E-02	2.039E+02
28	9.922E-02	1.918E+02
29	9.935E-02	1.816E+02
30	9.946E-02	1.730E+02
31	9.955E-02	1.659E+02
32	9.963E-02	1.598E+02
33	9.972E-02	1.519E+02
34	9.980E-02	1.452E+02
35	9.988E-02	1.385E+02
36	9.996E-02	1.321E+02
37	1.000E-01	1.257E+02
38	1.001E-01	1.195E+02
39	1.002E-01	1.135E+02
40	1.003E-01	1.076E+02
41	1.003E-01	1.018E+02
42	1.004E-01	9.621E+01
43	1.005E-01	9.075E+01
44	1.005E-01	8.544E+01
45	1.006E-01	8.028E+01
46	1.007E-01	7.526E+01
47	1.007E-01	7.040E+01
48	1.008E-01	6.569E+01
49	1.008E-01	6.113E+01
50	1.009E-01	5.672E+01
51	1.009E-01	5.247E+01
52	1.010E-01	4.837E+01
53	1.010E-01	4.442E+01
54	1.011E-01	4.064E+01
55	1.011E-01	3.701E+01
56	1.012E-01	3.354E+01
57	1.012E-01	3.022E+01
58	1.013E-01	2.707E+01
59	1.013E-01	2.407E+01
60	1.013E-01	2.123E+01
61	1.014E-01	1.855E+01
62	1.014E-01	1.603E+01
63	1.014E-01	1.366E+01
64	1.015E-01	1.145E+01
65	1.015E-01	9.389E+00
66	1.015E-01	7.518E+00
67	1.015E-01	5.765E+00
68	1.016E-01	3.759E+00
69	1.016E-01	1.253E+00
70	1.016E-01	0

of the radial grid spacing when 50 grid points are used. The results presented in fugure (6.8) were for forward steps of 1, .5, .25 and .125 the pipe diameter, and are given as percentage deviations from the results for (δx) of 0.0625 the pipe diameter. For forward steps of 0.125 the pipe diameter, the results are not affected by the stream-wise grid spacing. These spacings were much smaller than those employed in the composite model to obtain grid-independent results; this is due to the line-by-line iteration procedure introduced with the composite model.

The execution time for 50 diameters pipe length in this case was 30.4 seconds on the CDC 6600 computer machine.

6.2.2 Mean-flow results

The mean-velocity variations in the entrance region obtained with the composite model are compared with the experimental data of Barbin and Jones (1963) and Walklate, Heikal and Hatton (1976) for air flow with Reynolds number of 3.88×10^5 and 2.25×10^5 in figures (6.9) and (6.10) respectively. The results are shown at four radial locations ($2y/D$=1., .5, .25 and .064 in figure (6.9), while figure (6.10) shows the results at $2y/D$=1., .26, .09 and .03. The results obtained with the wall-functions are also given in figure (6.10).

A comparison between the results presented in figure (6.9 and 6.10) shows that the results obtained with the wall functions and the composite model are in an acceptable agreement with the experimental data, the maximum deviation being of the order of 6 percent in the composite model case and 9 percent in the wall-function case.

The normalized, fully-developed dimensionless velocity (u^+) distribition obtained with the composite model is compared with the experimental data of Deissler (1950) in figure (6.11). The experimental data were for air-flow with a Reynolds number range of $8x10^3$ - $2.2x10^5$, while the predictions were made for only the two limiting Reynolds numbers. The present results are found to be in good agreement with the experimental data. The predicted results also show that the Reynolds number variation does not affect the results clost to the wall, while it does influence the results far away from the wall, which is in accord with the experimental finding of Sleicher (1958).

Figure (6.12) compares the wall shear-stress variation in the entrance region predicted by the wall functions and by the composite model against the experimental data of Barbin and Jones (1963) for air flow with a Reynolds number of $3.88x10^5$. This comparison shows that the results obtained with the composite model are in better agreement with experiment than those obtained with the wall functions. The shear stress reached its fully-developed value in 15 diameters in the composite model case and in the experimental data, while it reached its fully-developed value in 11 diameters in the wall function case.

Using the composite model, the variation of the fully developed normalized wall shear stress - $\frac{\tau}{\rho u_m^2}$, where u_m is the mean velocity - with the Reynolds number is compared

with the empirical relations of Blasius and Prandtl in figure (6.13). These relations are given by (Schlichting 1970))

- Blasius relation

$$\frac{\tau_w}{\rho u_m^2} = 0.03955 \quad Re^{-.25} \quad , \quad (6.2.1)$$

- Prandtl relation

$$\left(\frac{\tau_w}{\rho u_m^2}\right)^{-\frac{1}{2}} = 5.657 \log Re \left(\frac{\tau}{\rho u_m^2}\right)^{\frac{1}{2}} + 0.2914 \quad . \quad (6.2.2)$$

This comparison indicates that the present results are in good agreement with Prandtl's relation which are the best 'fit' to the experimental data (Schlichting (1970)).

6.2.3 Turbulence results

As mentioned in section (3.3), the different forms proposed for the low-Reynolds number turbulent kinetic energy equation differ in the formulation of the low-Reynolds number effect on the dissipation term of the high-Reynolds number equation. The turbulent kinetic energy profiles in the near-wall region obtained with these different proposals, namely, with no change*, with the length scale being damped** and with the dissipation term being damped*** are presented in figure (6.14). The following damping factor (DF) was employed.

$$DF = 1. - \exp(-A_D R_k) \quad , \quad (6.2.3)$$

where $A_D = .03$ as proposed by Hassid and Poreh (1975).

The experimental data of Laufer (1954) and Clark (1968) were also presented in this figure. Comparison between these

---

* Norris and Reynolds (1975)
** Wolfshtein (1968)
*** Hassid and Poreh (1975)

results reveals that the best agreement with the experimental data was obtained when the dissipation term was damped as proposed by Hassid and Poreh (1975).

The fully-developed turbulent kinetic energy profile obtained with the composite model is compared with the experimental data of Lauefer (1954) for air flow with a Reynolds number of 50 000 in figure (6.15). The present results show an acceptable agreement with the experimental data. The large disagreement found near the centreline, where the velocity and the temperature gradients are nearly zero, does not affect either the mean velocity or the heat-transfer results. However, better agreement can be obtained by increasing the turbulent-Prandtl-number (σ_k) of the turbulent kinetic energy equation to 1.3 as proposed by Svensson (1977).

The turbulent viscosity in the near-wall region is compared with the experimental data of Sleicher (1958) and Hussain and Reynolds (1975) in figure (6.16). Again this comparison indicates good agreement between the present predictions and the experimental data.

6.3 Heat-Transfer Results

6.3.1 Computational details

The heat-transfer results presented in this section are for a wide range of laminar-Prandtl-number ($.005 < Pr_\ell < 1000$) fluids with a wide range of Peclet numbers ($125 < Pe < 5 \times 10^7$). In this range of Peclet number, the stream-wise diffusion of heat was very small in comparison with the other terms of the stagnation-enthalpy equation and so was neglected, thereby

rendering the equation 'parabolic'. Hence, the heat-transfer results were obtained in one sweep. For the small and moderate-laminar-Prandtl-number fluids ($Pr_\ell < 1.$), the grid-independent tests reveal that the grid spacing employed for the hydrodynamic results was sufficiently fine to produce heat-transfer results which were independent of the grid. For the large-laminar-Prandtl-number fluids, where the temperature profiles change rapidly in the near-wall region, the effect of the grid spacing in the near-wall region is presented in figure (6.17) for a flow of laminar Prandtl number of 14.3. This figure shows the percentage error in the Nusselt number results obtained with 40, 50, 60 grid points from those obtained with 70 grid points. These results indicate that the results become independent of the grid spacing when 60 grid points are employed.

The execution time of 50 diameters with 60 grid points in the near-wall region was 71.3 seconds on the CDC 6600 computer machine.

For the wall-function method, too, the heat-transfer results for small and moderate-laminar-Prandtl-number fluids were obtained with the same grid arrangements employed for the hydrodynamic computations. For the large laminar-Prandtl-number fluids, no further grid refinement was required since the computation in the near-wall region was avoided in the wall-function approach.

6.3.2 Temperature profiles

The developing temperature profiles for air flow with a Reynolds number of 35000 are compared with the experimental

data of Hanratty and Johnk (1961) in figure (6.18). The predicted results were obtained with both the wall-function and the composite model approaches at x/D = 1., 2.5, 4, 6, 10 and 15.5, while the measurements were for x/D = .973, 2.607, 3.891, 5.84, 9.7 and 15.56. In both the experiments and the predictions a constant heat transfer rate of 252 watt/m^2 was introduced to the flow at 65 diameters downstream of the inlet section. This figure indicates that the present results obtained with the composite model approach are in better agreement with the experimental data than those of the wall-function approach. The agreement in the region from $y^+ = 50$ up to the centreline, $y^+ \approx 1000$. between the experimental data and the results obtained with the composite model are very good, while a disagreement of up to ten percent exists in the region close to the wall.

In order to examine the accuracy of the measurements close to the wall, the experimental data for a wide range of Reynolds number (17600 – 71200) were presented in figure (6.19) together with the present predictions. The experimental data show a scatter larger in magnitude than the deviation between the present results and the mean data.

The comparison between the fully-developed temperature profile predicted with the composite model and with the wall function approaches and the experimental data of Gowen and Smith (1967) for fluids with laminar-Prandtl-number of 5.7 and 14.3 are presented in figure (6.20). The results obtained from the composite model with a turbulent-Prandtl-number of 1.4 were also shown in figure (6.20). The

comparison between these results shows that the results obtained with the wall functions are in good agreement with the experimental data; while only the composite model results obtained with turbulent Prandtl number of 1.4 are in good agreement with the experimental data. The necessity for a large turbulent-Prandtl-number with the composite model may be attributed to the fact that for large laminar-Prandtl-numbers the temperature changes are restricted to the region close to the wall. In this region, the experimental data of Sleicher (1958) in air flow and of Gowen and Smith* (1967) for water and aqueous ethylene glycol show that the turbulent-Prandtl-number is larger than that in the bulk of the flow field. It is the turbulent-Prandtl number in this region which controls the temperature values.

The fully-developed temperature profiles (predicted with the composite model) in liquid metal fluids with laminar Prandtl numbers of 0.02 and .007 were compared with the experimental data of Buhr et al (1968) and Fuchs (1973) in figures (6.21) and (6.22) respectively. Buhr's results were for Reynolds number of 9.7×10^4 and 1.528×10^5, while the results of Fuchs were for 29650 and 81700. The predicted results with the wall-function approach are also presented in figure (6.21). Comparison between these figures reveals that the results obtained with the composite model are in good agreement while the results obtained with the wall-function are in

---

* These experiments also show a large turbulent-Prandtl-number for Pr_ℓ=5.7 and 14.3 than that for air flow in the whole flow field.

acceptable agreement with the experimental data.

6.3.3 Nusselt-number results

The prediction of the developing Nusselt-number were compared with the experimental data of Hanratty and Johnk (1961) for air flow with a Reynolds number o f $3.5x10^4$ in figure (6.23). The predicted results were obtained with both the wall-function and the composite model approaches. This comparison reveals that the results obtained with the composite model are in better agreement with the experimental data than the wall-function approach; however, the results from both approaches are identical after the first 6 diameters downstream.

The predictions and the experimental data for the fully-developed Stanton-number (St) variation with the laminar Prandtl number for flows of Reynolds number of $2.5x10^4$ and $5x10^4$ are presented in figure (6.24) and (6.25) respectively. The experimental data shown in these figures are those collected by Deissler (1955) for moderate and large laminar Prandtl number fluids and buhr's et al (1968), Johnson's et al (1953), Brown's et al (1957), Baker's et al (1962) and S icher's et al (1973) for small laminar Prandtl number fluids. The predicted results were obtained with the composite model, the turbulent Prandtl number employed for the small laminar Prandtl number fluids being that of Aoki (1963), while a constant value of 0.95 was employed for large and moderate laminar-Prandtl-number fluids.

The comparison between the experimental data and the computed

results presented in figures (6.24) and (6.25) shows satisfactory agreement except at very large laminar Prandtl numbers. This disagreement can be attributed to the small value of the turbulent Prandtl number employed in this range. A better agreement was obtained with a turbulent Prandtl number of 1.4 employed in this range as explained before in section (6.3.2).

The comparison between the results presented in figures (6.24) and (6.25) reveals that the effect of the Reynolds number on the results at moderate and large laminar-Prandtl-numbers is very small, while at small laminar-Prandtl-number the effect is large. An increase in the Reynolds number from $2.5x10^4$ to $5x10^4$ serves to decrease the Stanton-number from 0.055 to 0.03 at a laminar-Prandtl number of 0.005.

Figures (6.26) and (6.27) show the Nusselt number variations with the Peclet number for liquid metal fluids with laminar-Prandtl-numbers 0.02 and 0.005 respectively. The experimental data of Isakoff and Drew (1951), Brown et al (1957) and Buhr et al (1968) and the predicted results obtained with the composite model are plotted in figure (6.26), while figure (6.27) shows the experimental data of Subbotin et al (1962a) and Baker et al (1962) for a range of laminar-Prandtl-numbers of 0.057 to .0075 and 0.0084 to 0.0091 respectively. The comparison between the results presented in figures (6.26) and (6.27) shows good agreement between the present results and the experimental data.

6.4 Conjugate Problems

6.4.1 Problem specification

The conjugate pipe-flow problem considered in this section is shown in figure (6.28). A length of 40 diameters, over which the development of the flow variables occurred, was studied first. This was followed by a heated section for which heat-transfer studies were made with the pipe wall considered as part of the computation domain. Different ratios of the wall thickness to the pipe diameter and solid to fluid conductivities and different values of Peclet number were considered.

The enthalpy-equations governing the temperature changes, equations (2.2.4 and 2.2.6), in the flow domain and in the solid wall are steady and 'elliptic' (contains the stream-wise diffusion). For this type of equation, the boundary conditions are required at the four boundaries of the computation domain. The boundary conditions employed in the present section can be summarized as follows:

(i) The flow domain boundary conditions.

- At $x = 0$

$$T = T_{in} = \text{Constant} \qquad (6.4.1)$$

- At $x = L_h$, where L_h is the pipe length appropriate to the heat-transfer studies.

$$\frac{\partial T}{\partial x} = 0.0 \qquad (6.4.2)$$

- At $r = 0.0$

$$\frac{\partial T}{\partial y} = 0.0 \qquad (6.4.3)$$

(ii) <u>The solid wall boundary conditions</u>

- At $x = 0.0$

$$\frac{\partial T}{\partial x} = 0.0 \qquad \cdot \quad (6.4.4)$$

- At $x = L_h$

$$\frac{\partial T}{\partial x} = 0.0 \qquad \cdot \quad (6.4.5)$$

- At the outer surface of the pipe wall

$$\lambda_s \frac{\partial T}{\partial y} = \dot{q}'' = \text{Constant} \qquad \cdot \quad (6.4.6)$$

6.4.2 <u>Computational details</u>

The computational algorithm presented in section (4.3.2) was employed and the flow domain was divided by 40 radial grid points in the near-wall region and 30 radial grid points in the core, with forward steps of 0.25 times the pipe diameter in the hydrodynamic entrance length and eighty axial steps in the heat transfer length. The effect of the number of grid points inside the solid wall on the inner and outer wall temperature is presented in figure (6.29). The results are shown for 5, 10 and 15 grid points as a percentage deviation from the results obtained with 20 grid points. This figure indicates that the results become independent of the grid size when 15 grid points are used; consequently, this number of nodes was employed in the solid wall.

With the above grid arrangement, the number of iterations required to obtain convergence (which was said to have been achieved when the change in the mean temperature was less than 0.1 percent) was dependent on the Peclet number and on the ratio of the solid to fluid conductivities. The larger the Peclet number, the smaller the number of iterations required, while the opposite is true for the ratio of the conductivities.

In order to reduce the number of iterations required for the cases of large conductivity ratio and small Peclet number, the axial conductions in the flow field and in the solid wall were neglected in the first iteration and the problem was considered as parabolic. The solution obtained was then used as a first guess for the temperature field. With this procedure 110 iterations were required to obtain convergent solutions in a flow with Peclet number of 1.2 and conductivity ratio of 2, while without it 800 iterations were still insufficient. The execution time of the 110 iterations was 187 seconds on a 6600 computer machine.

6.4.3 Results and discussion

In order to present the axial fluid conduction effect on the heat-transfer characteristics, a pipe length of four diameters was considered. This length was chosen based on the previous investigations of Schneider (1957) and Chu and Bankoff (1965) - for laminar and slug flows respectively - which show that the effect is restricted to the thermal entrance length of approximately two pipe diameters.

The temperature profiles in the flow domain are presented in figures (6.30 and 6.31) at two downstream locations, $x/R = .5$ and 1., respectively. The results are given for a wall thickness of 0.2 times the pipe radius and three Peclet numbers, 1.2, 6 and 30, for flows with and without the axial flow conduction. For the same flow situations, the normalized Nusselt number Nu/Nu_{Lyon}, where Nu_{Lyon} is the Nusselt number calculated from the Lyon-Martinelli

equation recommended for liquid metal flows, are shown in figure (6.32).

The comparison between the results given in figures (6.30 - 6.32) indicate that the larger the downstream distance, where the axial temperature gradient becomes nearly constant, the smaller the effect of the axial conduction whereas the smaller the Peclet number, the larger the effect. The comparison also shows that the axial conduction increases the Nusselt number values while the axial conduction decreases the normalized temperature values. These effects of the axial conduction were similar to those found by Schneider (1957) and Chu and Bankoff (1965).

The effect of the solid to fluid conductivities ratio is presented in figures (6.33, 6.34 and 6.35) for a flow with a Peclet number of 30 and a wall thickness of 0.4 times the pipe radius. The temperature profile at $x/R = 2$ are given in figure (6.33) for two ratios of conductivities (λ_s/λ_f = 1.98 and 19.8) with the results without axial conduction in the solid wall while the wall temperature and the Nusselt number variations in the entrance region are plotted in figures (6.34 and 6.35) respectively. These results indicate that the effect of the wall conduction can be neglected when the conductivity ratio is of the order of unity, or less, and must be accounted for in the cases of large conductivity ratio. The results presented in figure (6.35) also indicate that the larger the conductivity ratio, the smaller is the Nusselt number and the shorter is the thermal developing length; this agreed with the results of Sakakibara and Endoh (1977).

The temperature profiles inside the solid wall at different axial locations (x/R = .2, .5, 1. and 2) for a flow of a Peclet number of 6 and wall thickness of 0.2 times the pipe radius are given in figure (6.3.6). In obtaining these results the axial conduction inside the solid wall was neglected in order to establish the importance of the conjugate problems and two conductivities ratio (λ_s/λ_f = 1.98 and 19.8) were considered. In these results a large temperature variation was observed in the case of small conductivity ratio while the temperature was nearly uniform in the case of large conductivity ratio.

The effects of the wall thickness on the temperature profile at x/R=2 and on the wall temperature variation in the entrance region are given in figures (6.37 and 6.38) respectively for a flow with a Peclet number of 30, solid to fluid conductivity ratio of 1.98 and three well thicknesses (δ/R = .2, .4 and .6). These results show that the larger the wall thickness, the greater is the effect of the axial conduction in the solid wall and an increase in the wall thickness leads to an increase in the wall temperature and a decrease in the fluid temperature.

Finally, the developing temperature profiles in both the flow domain and in the solid wall are given in figure (6.39) for a flow of a Peclet number of 6, wall to fluid conductivity of 1.98 and wall thickness of 0.2 times the pipe radius.

6.5 Concluding Remarks

The computations of the steady hydrodynamic and heat-transfer characteristics have been compared with previous experimental

data in this chapter. The comparisons show that the results obtained with the composite model of turbulence are in good agreement with experimental data over a wide range of Reynolds numbers and laminar Prandtl numbers. The comparison also reveals that the wall-function approach yields results which are not as good as those obtained with the composite model; however they are still in an acceptable agreement with the experimental data.

It is also concluded from the results presented in this chapter that Aoki's formulation for the turbulent-Prandtl number for temperature gives heat transfer results which are in satisfactory agreement with the experimental data of liquid metal fluids. For air flows, a turbulent Prandtl number of 0.95 gives the best agreement with the experimental data, while for larger laminar Prandtl numbers a larger turbulent-Prandtl number (as much as 1.4) is necessary, at least close to the wall, if good agreement with experimental data is to be obtained.

The conjugate heat-transfer problem for low laminar-Prandtl number fluids has also been studied in this chapter. This study leads to the following conclusions:

(i) The axial fluid conduction effect is restricted to the thermal entrance region, where the axial temperature gradient changes considerably, and may be neglected for flows with Peclet numbers greater than 30.

(ii) The effect of the axial conduction inside the solid wall is also restricted to the thermal region, and this effect may be neglected in the cases where the ratio of the solid to

fluid conductivity is less than unity.

(iii) There is a relatively large radial temperature gradient inside the solid wall, and this gradient may be neglected for the cases where the ratio of the solid to fluid conductivity is greater than 2.

(iv) It is necessary to consider the wall heat-transfer problem as a conjugate problem. This is due to the importance of both the radial temperature variation inside the solid wall in the cases of low solid to fluid conductivity ratio, and the axial conduction in the case of large conductivity ratios.

$$\frac{u^+_{60} - u^+}{u^+_{60}} \times 10^{+2}$$

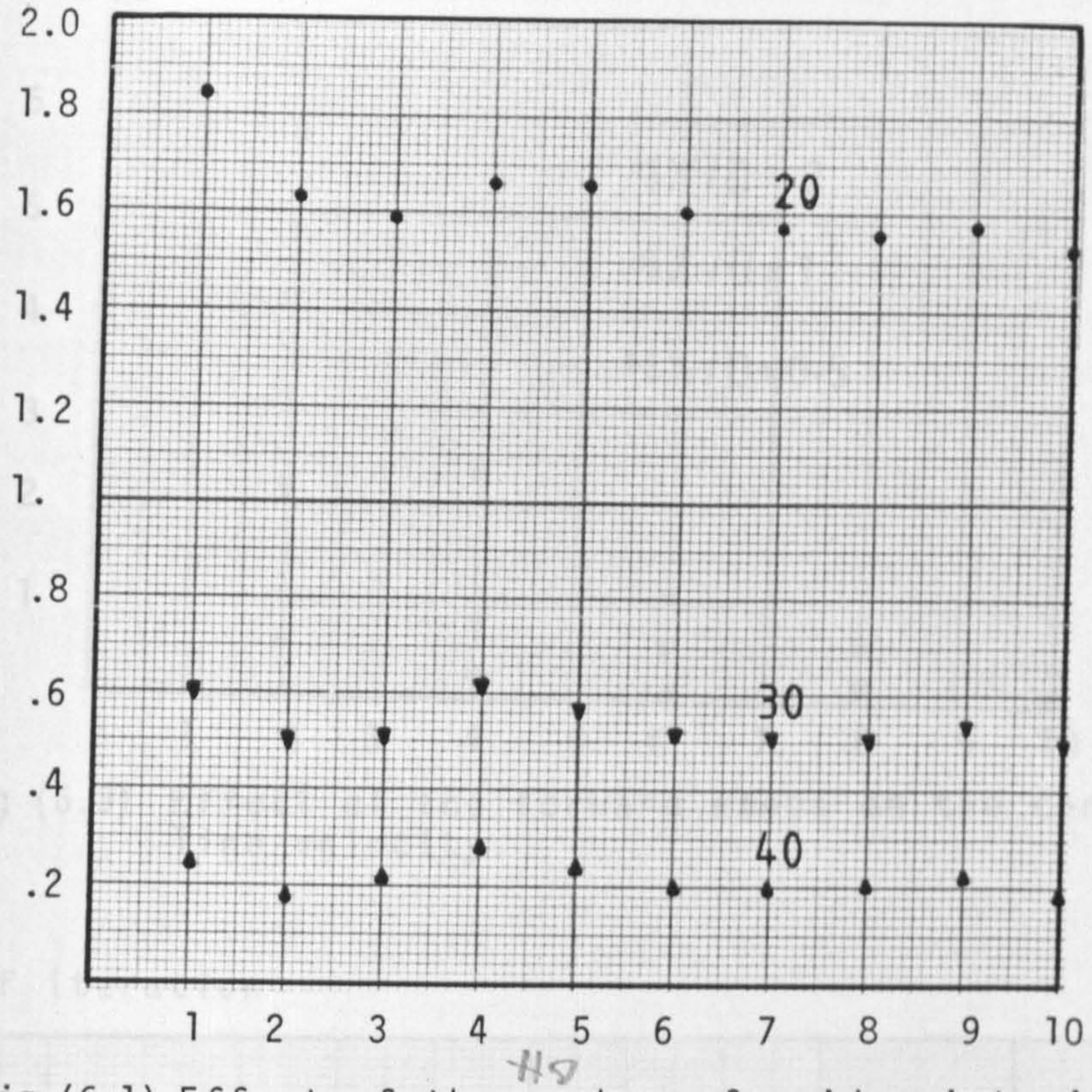


Fig (6.1) Effect of the number of grid points in the near wall region on the centreline velocity.

$$\frac{u^+_{40} - u^+}{u^+_{40}} \times 10^{2}$$

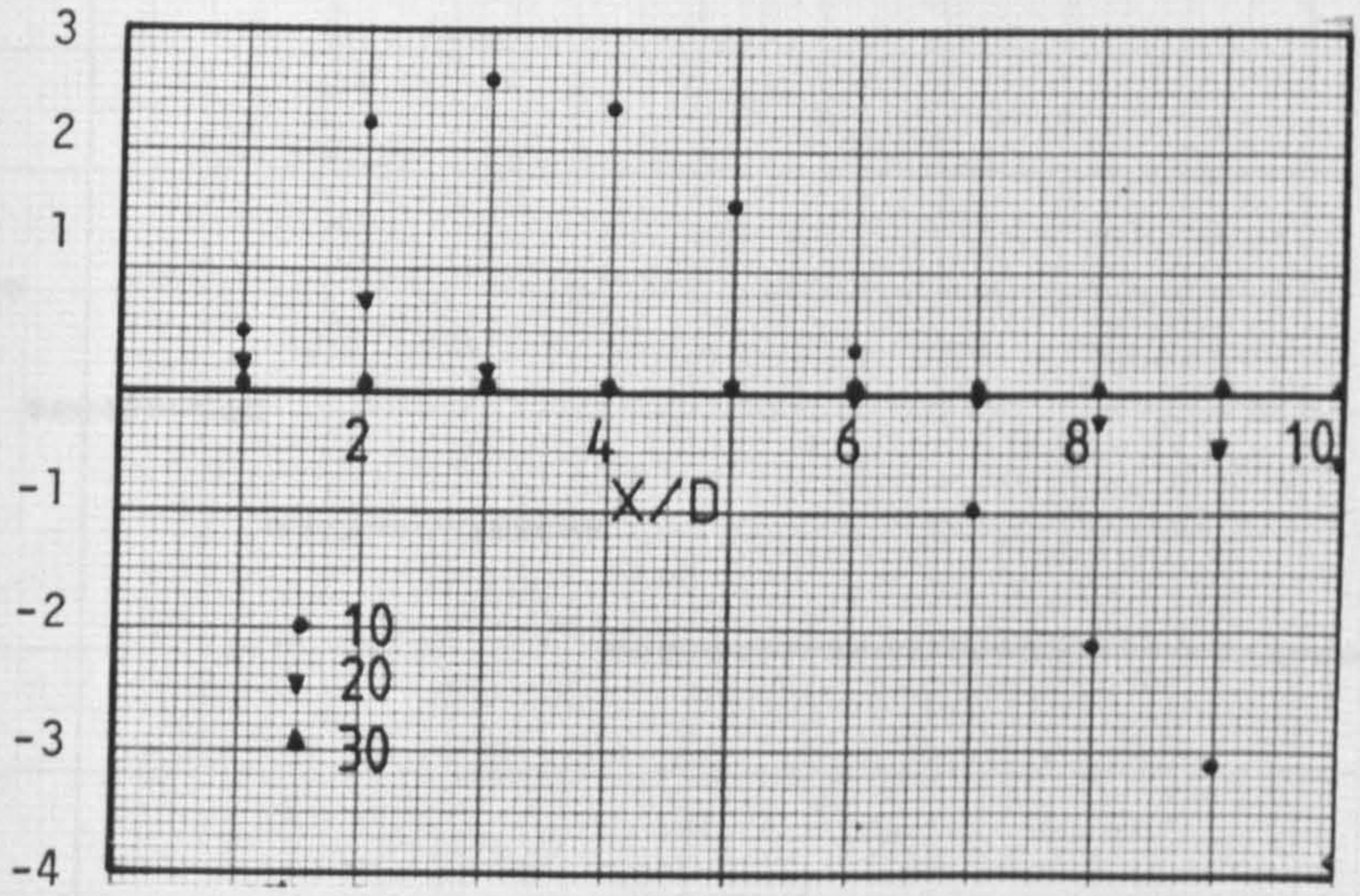


Fig (6.2) Effect of the number of grid points in the central region on the centre line velocity

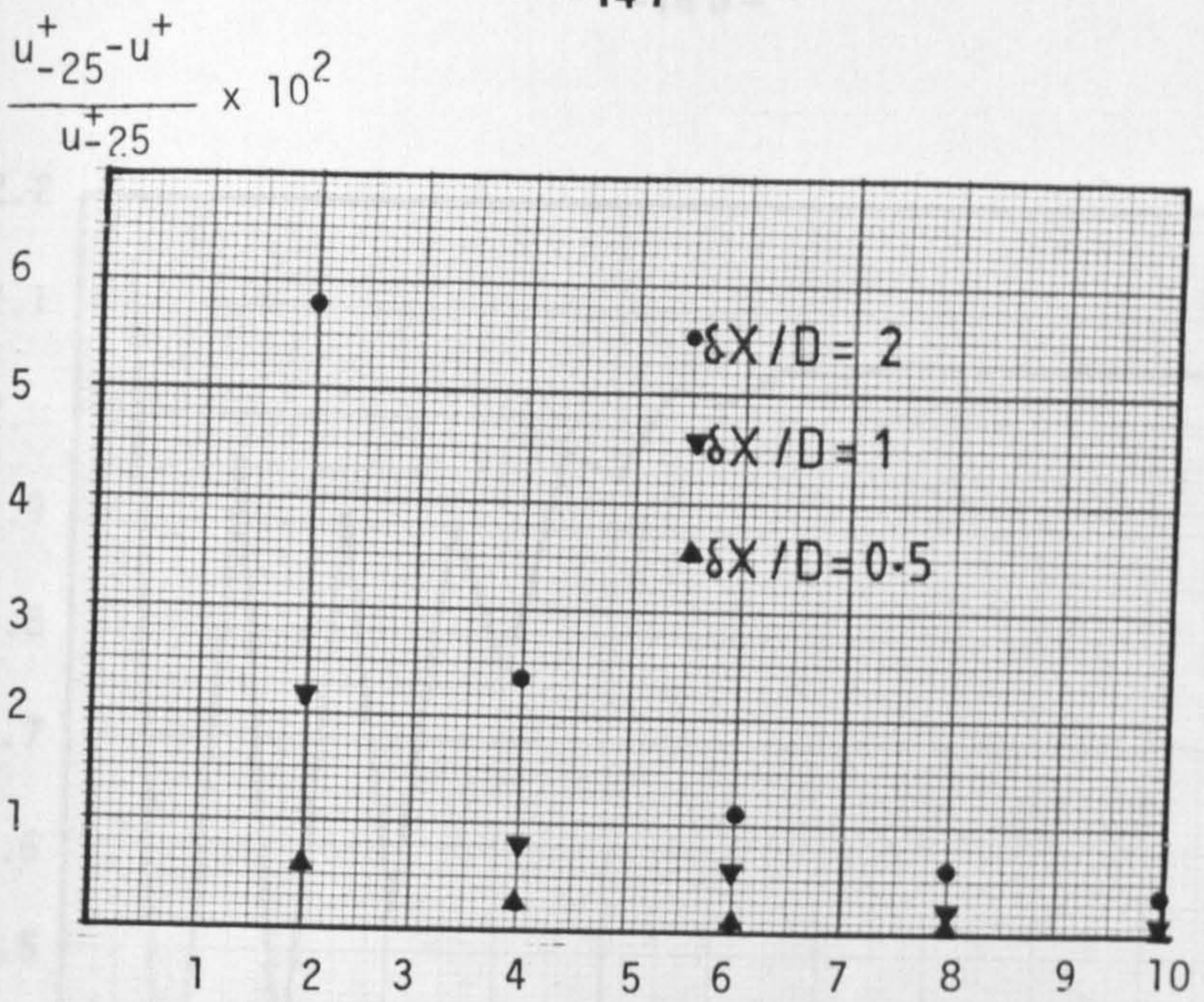
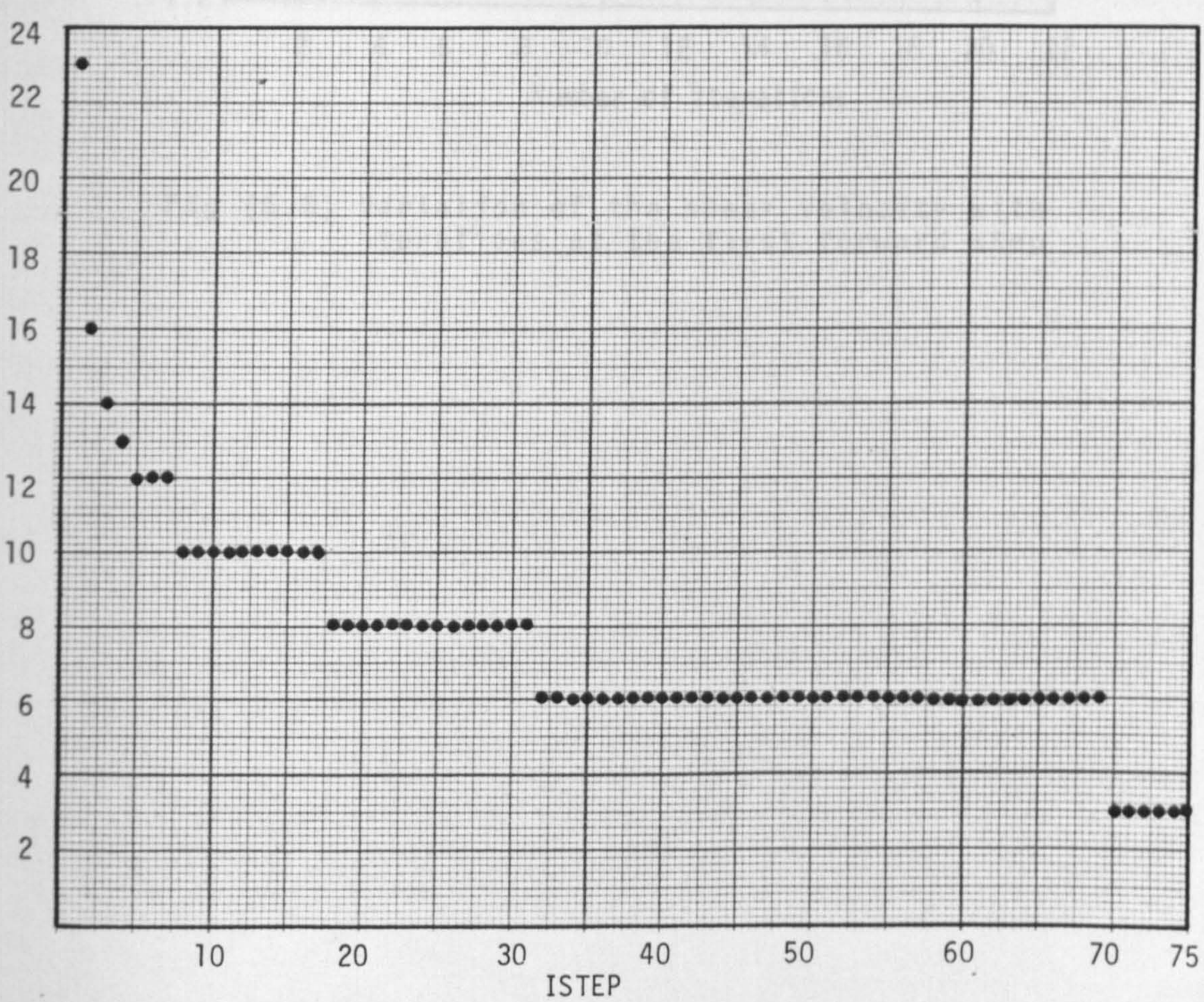


Fig (6.3) Effect of the forward steps on the centre line velocity.



(Fig 6.4) Number of line-by-line iterations required at each forward step

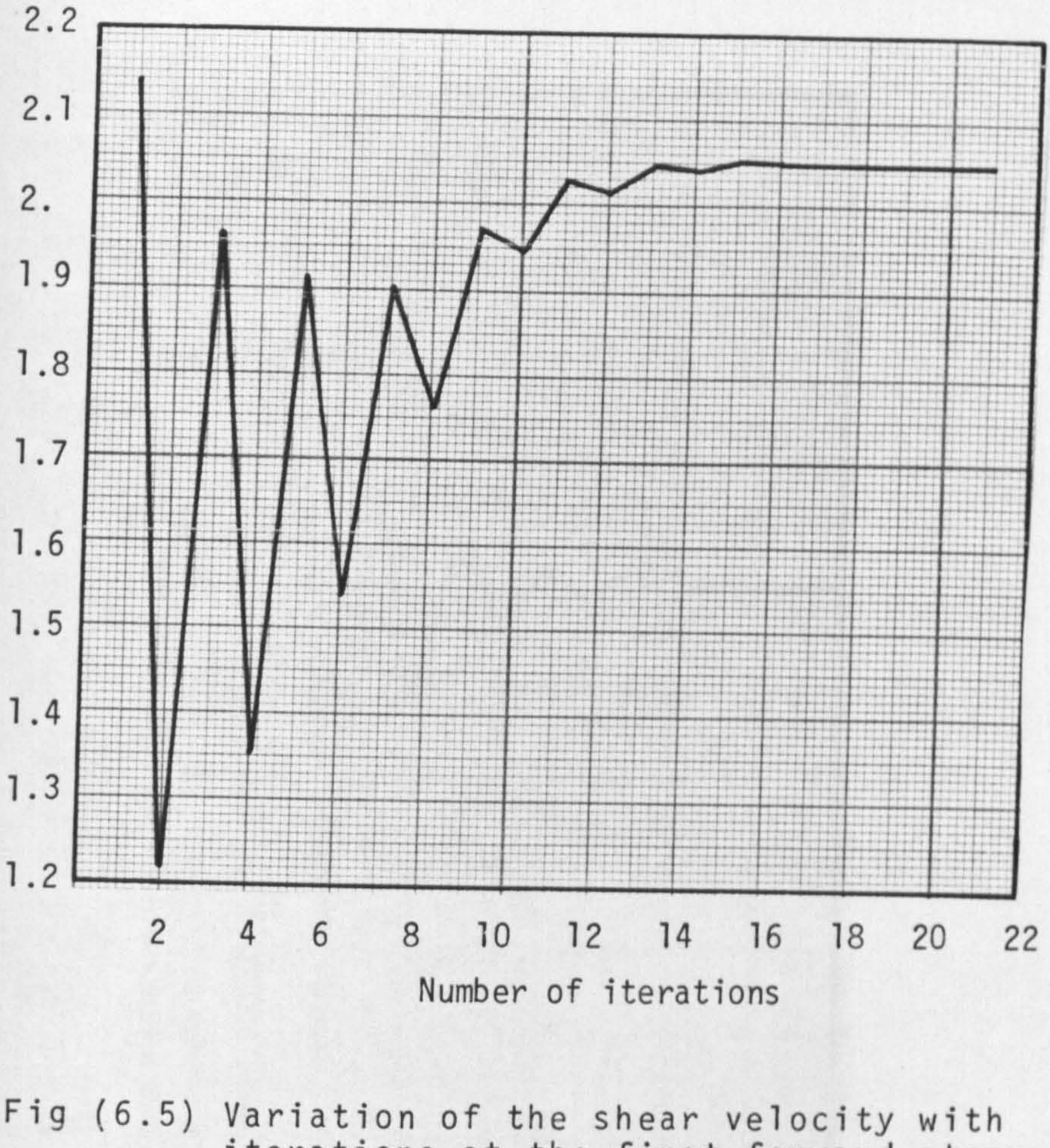


Fig (6.5) Variation of the shear velocity with iterations at the first forward step

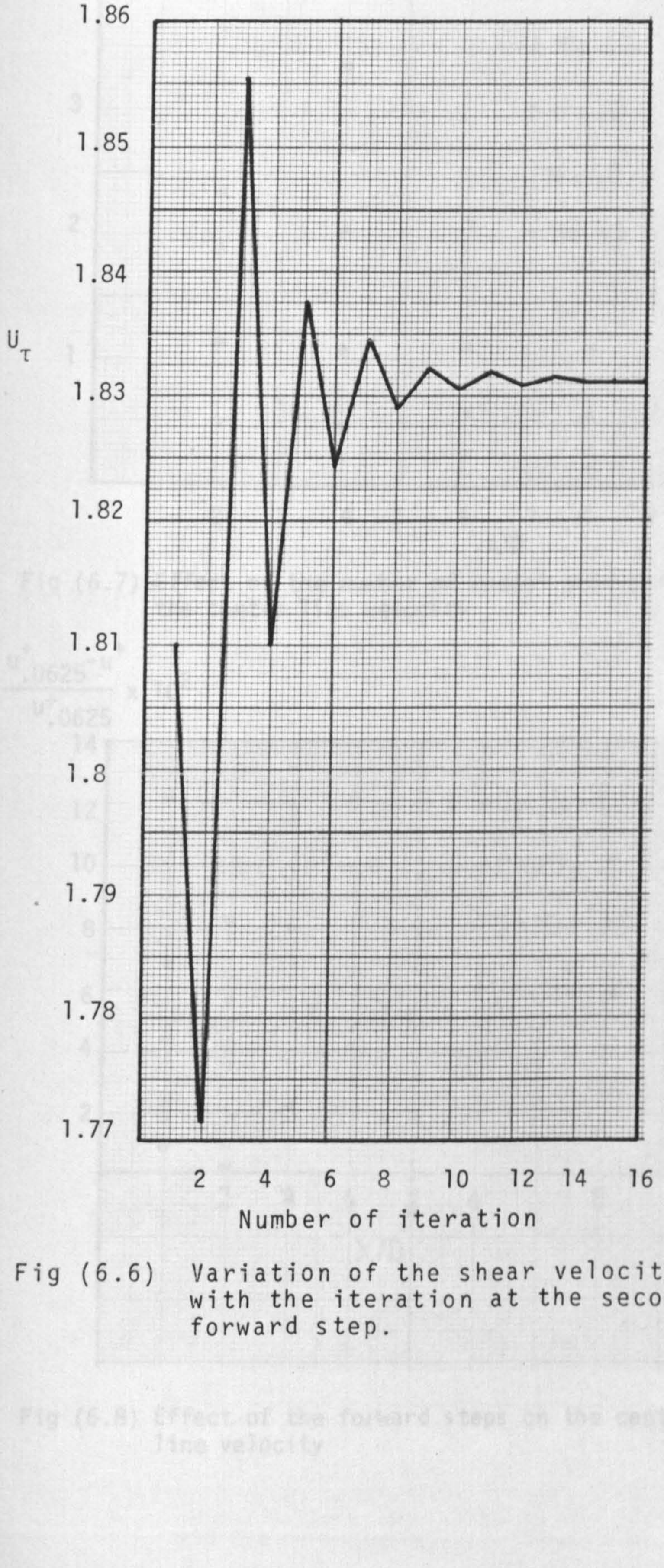


Fig (6.6) Variation of the shear velocity with the iteration at the second forward step.

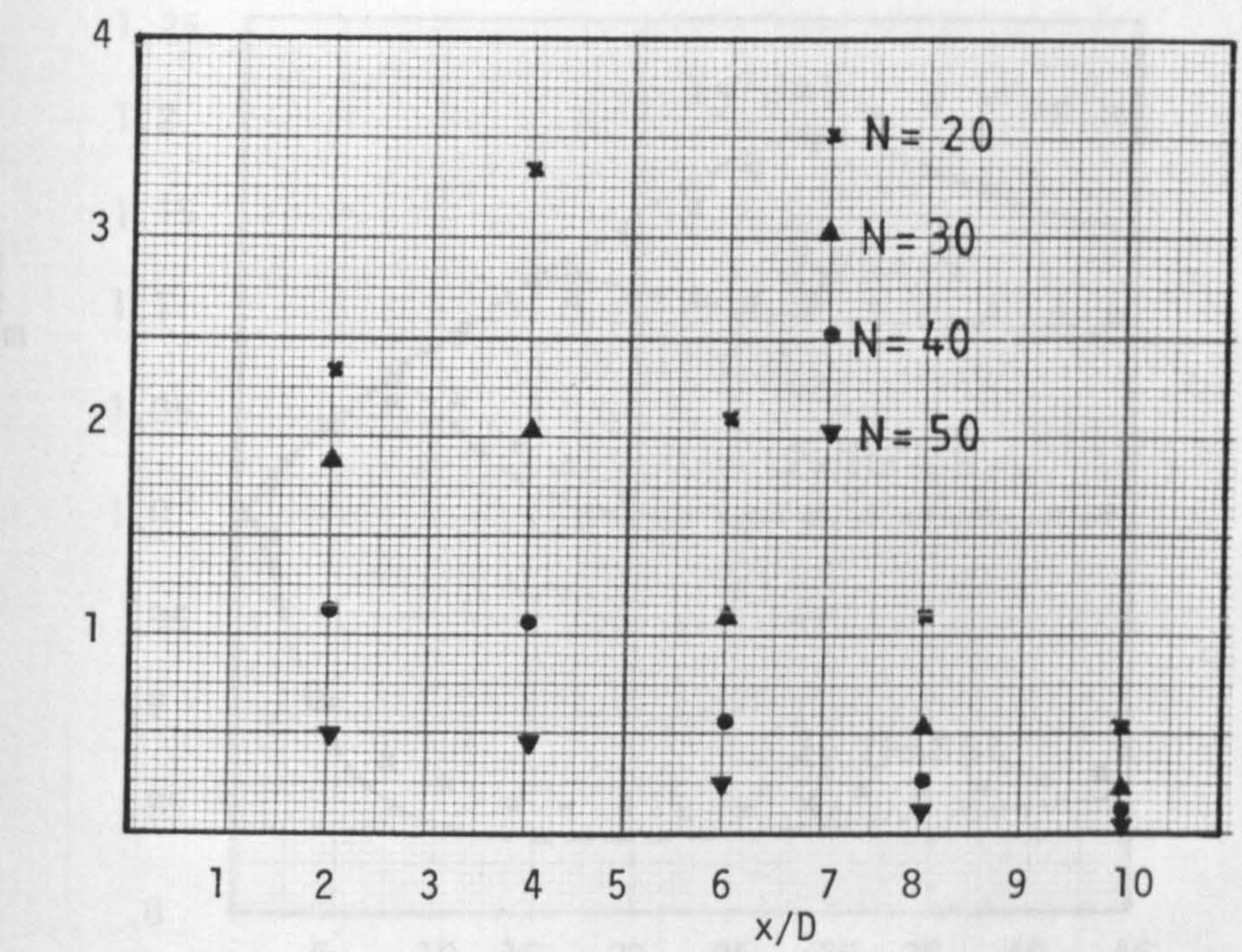


Fig (6.7) Effect of the number of radial grid points on the centre line velocity

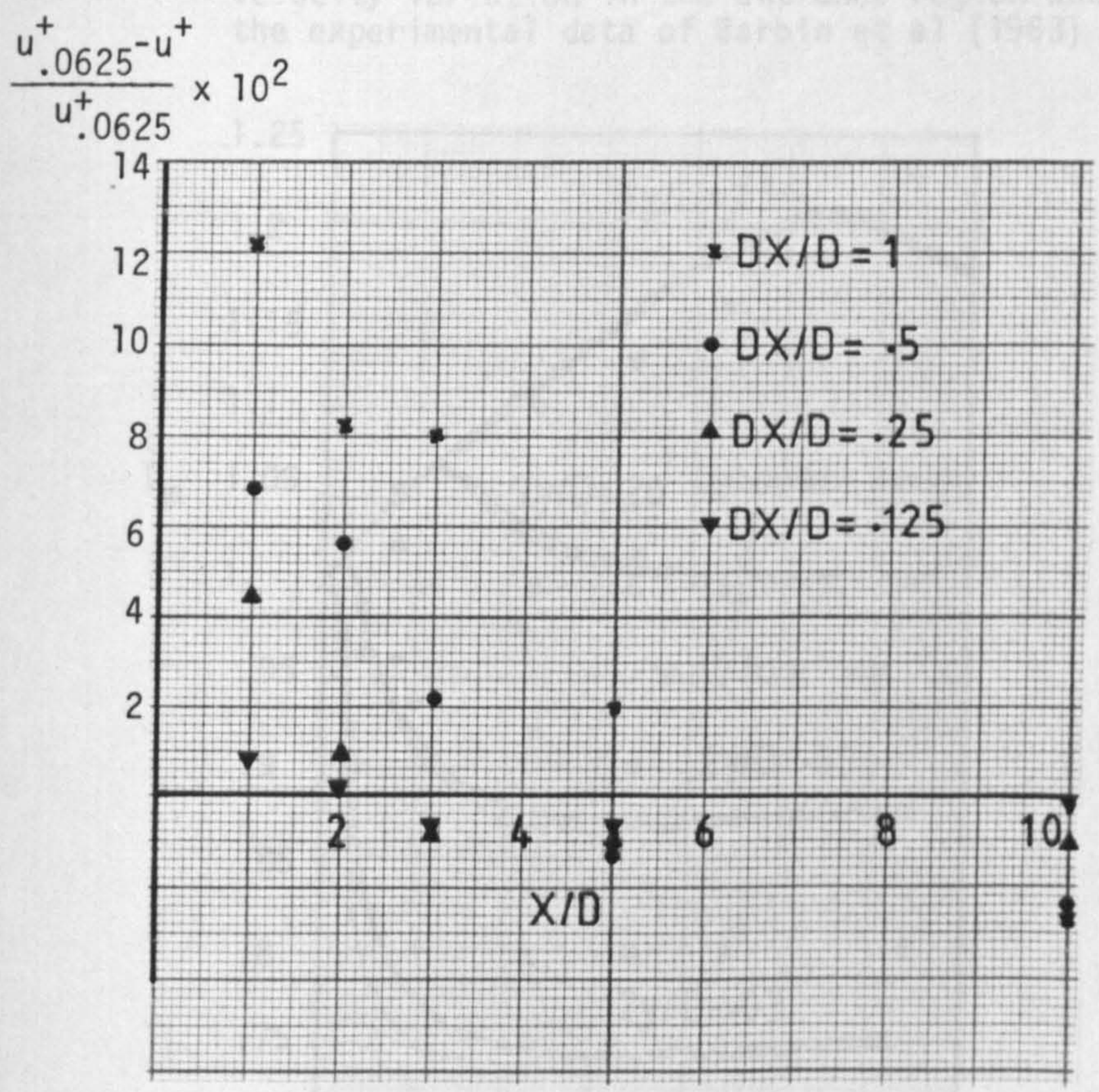


Fig (6.8) Effect of the forward steps on the centre line velocity

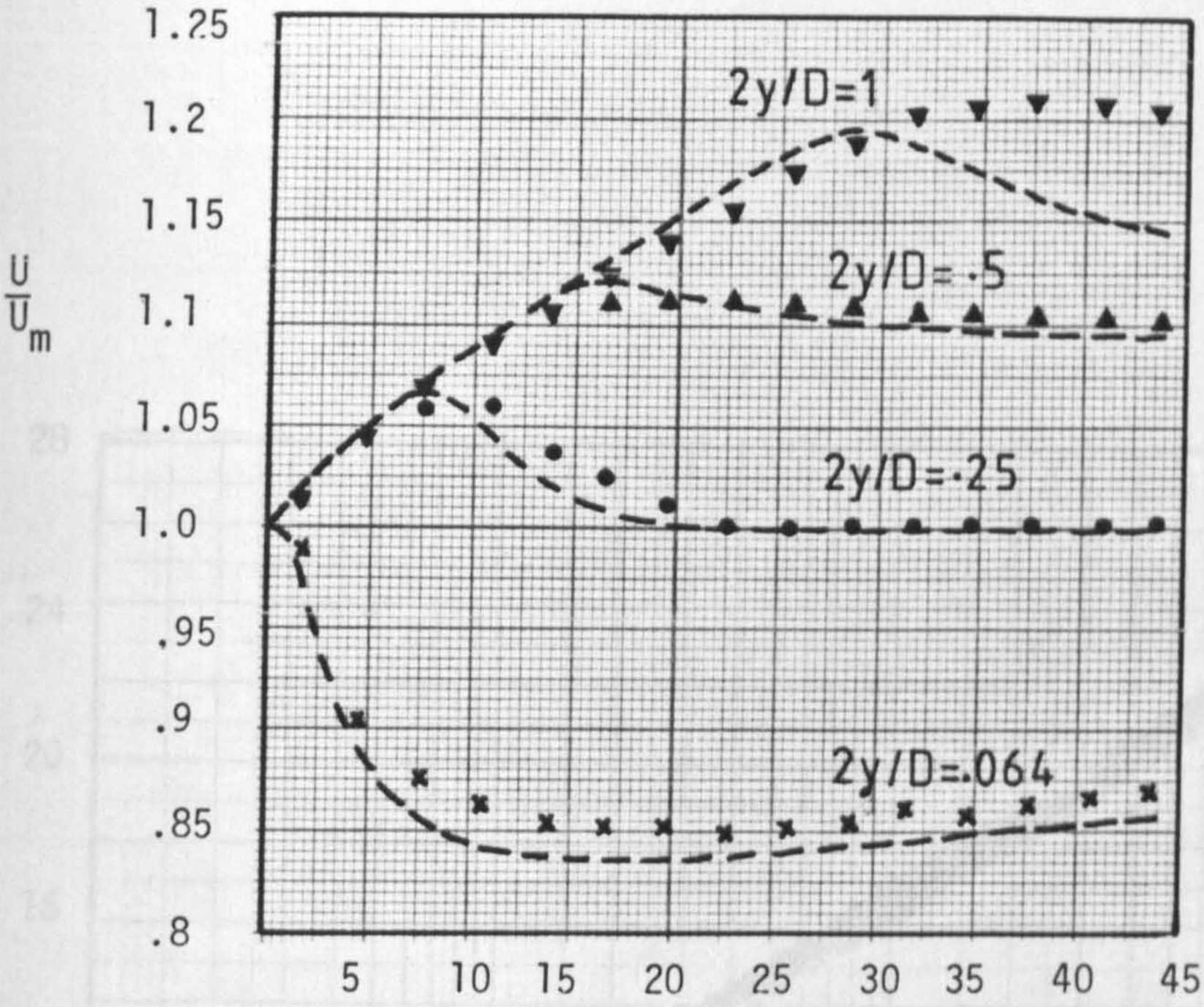


Fig (6.9) Comparison between the present prediction of the velocity variation in the entrance region and the experimental data of Barbin et al (1963)

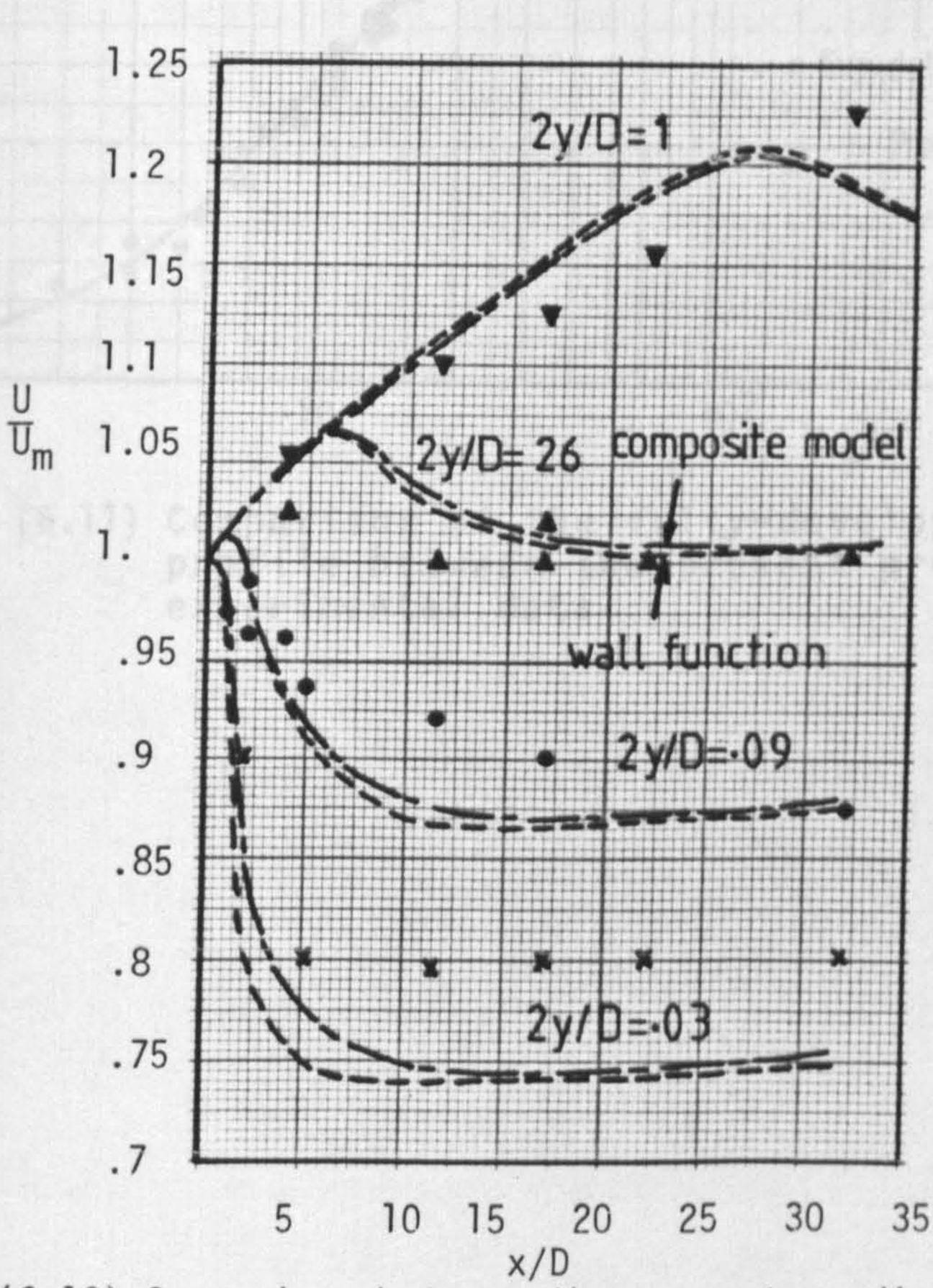


Fig (6.10) Comparison between the present prediction of the velocity variation in the entrance region and the experimental data of Walklate (1976)

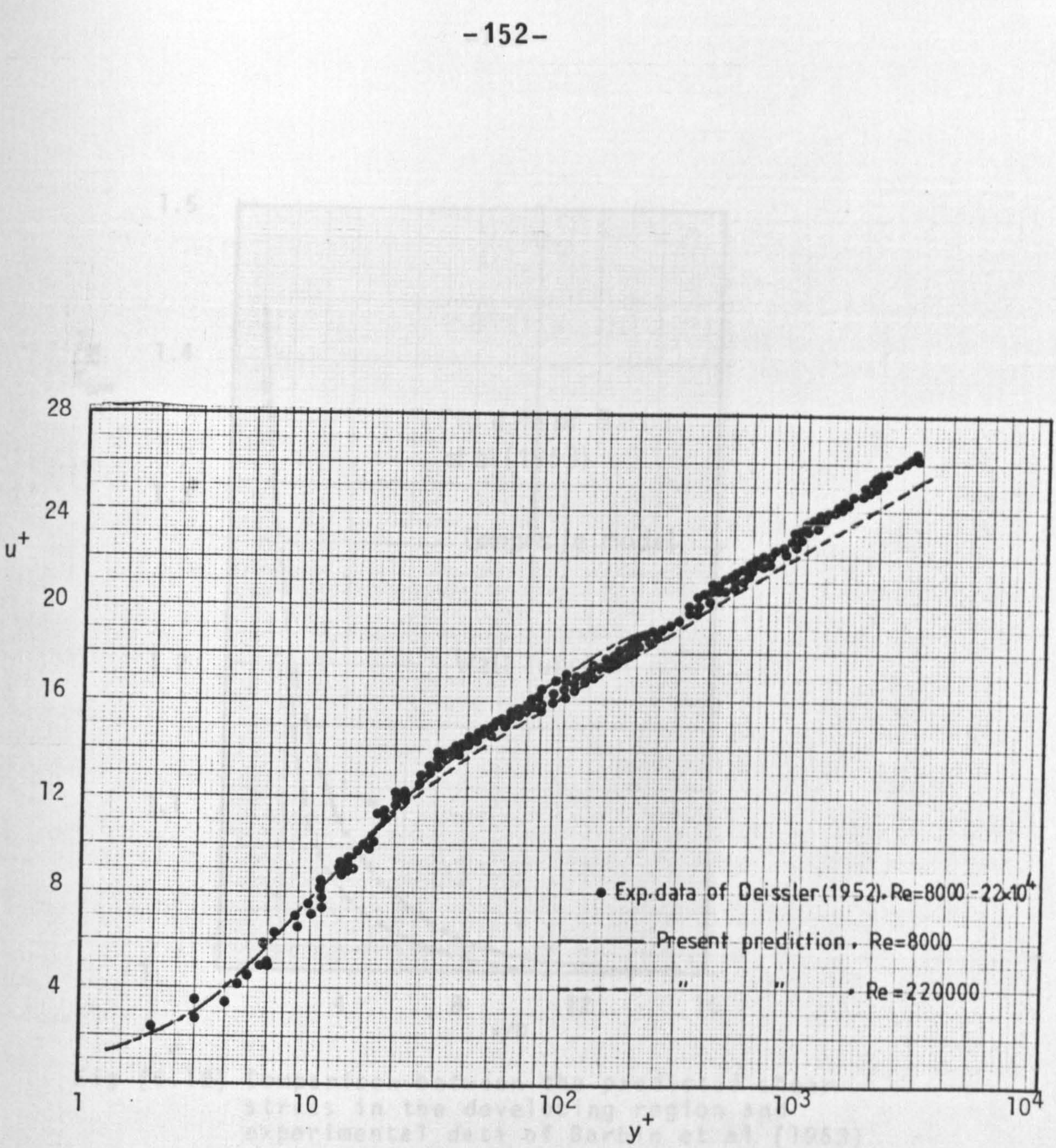


Fig (6.11) Comparison of the fully-developed velocity profile between the present prediction and experimental data

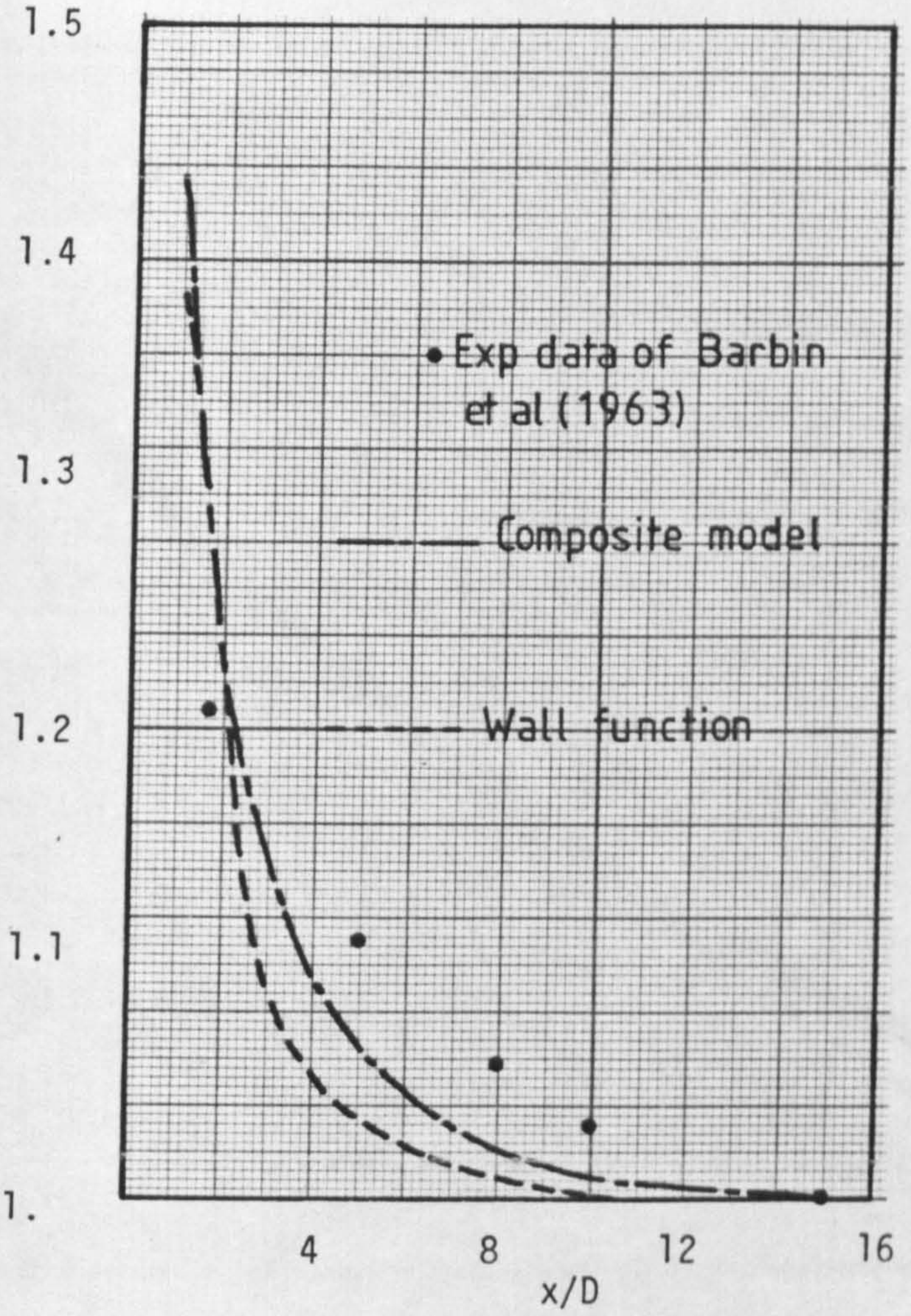


Fig (6.12) Comparison between the predicted shear stress in the developing region and experimental data of Barbin et al (1963)

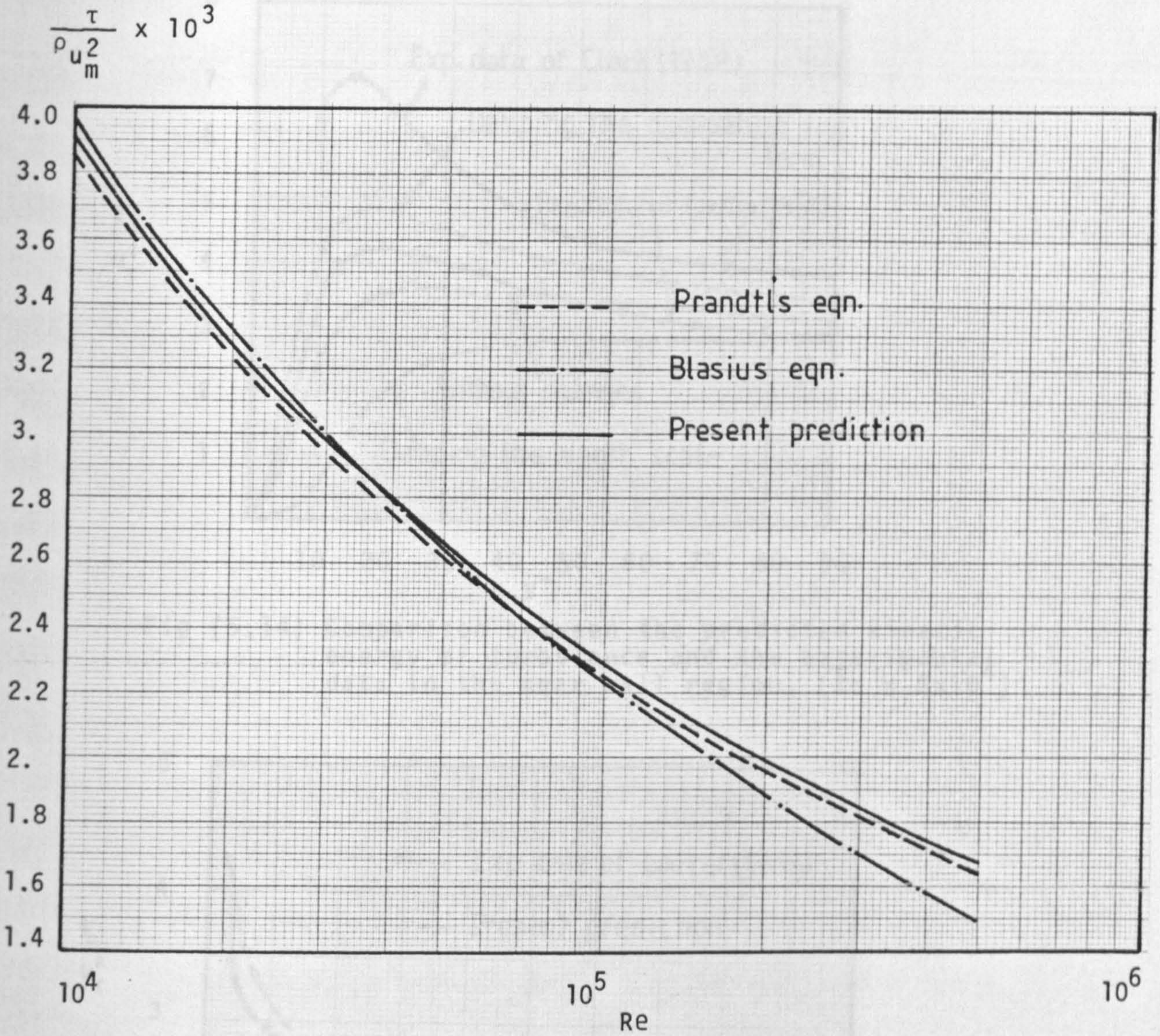


Fig (6.13) Comparison between the predicted fully-developed shear stress variations with the Reynolds number and the recommended equations of Blasius and Prandtl.

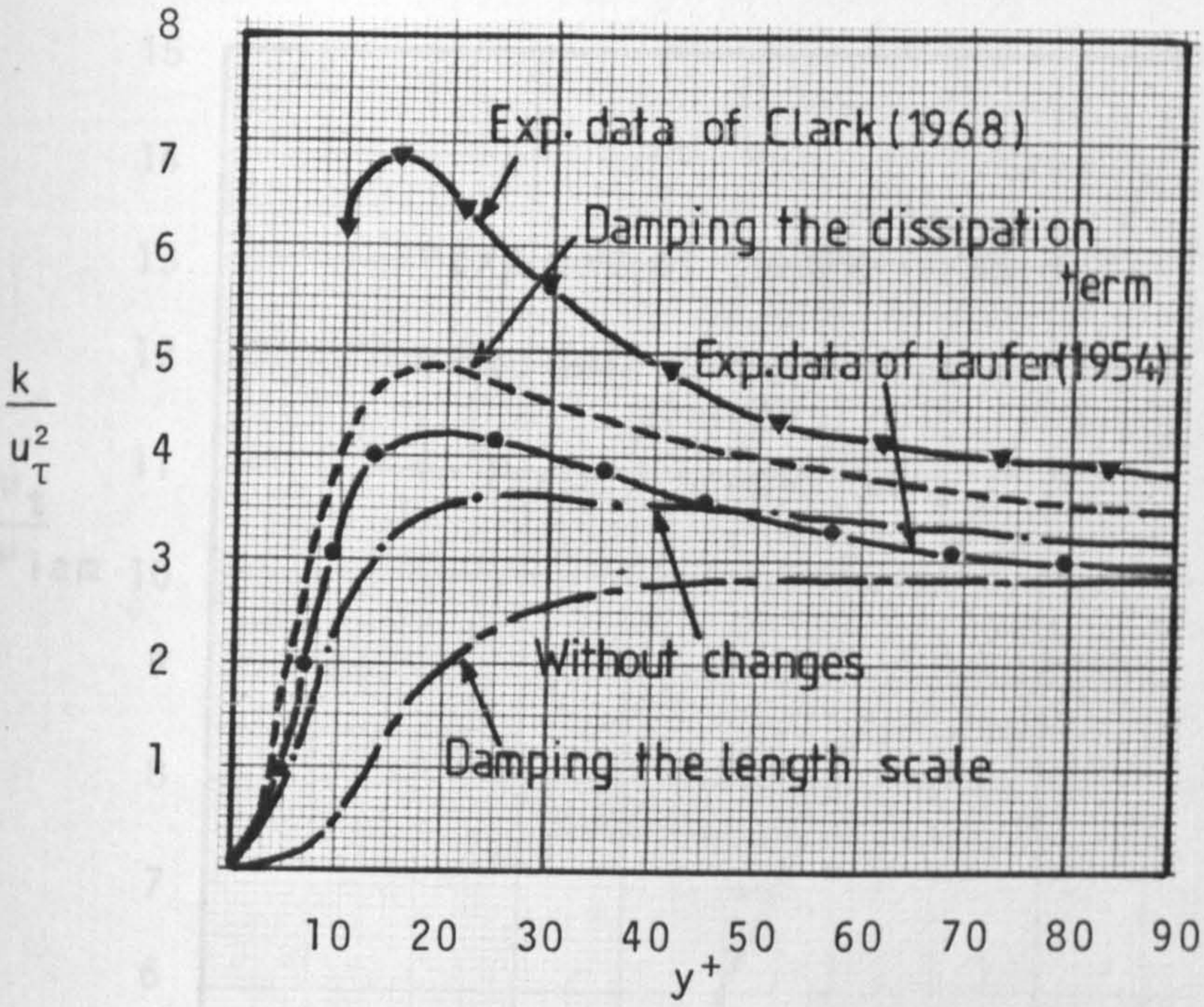


Fig (6.14) Comparison between the predicted kinetic energy of turbulence and the experimental data in the near wall region, ($Re = 5x10^4$)

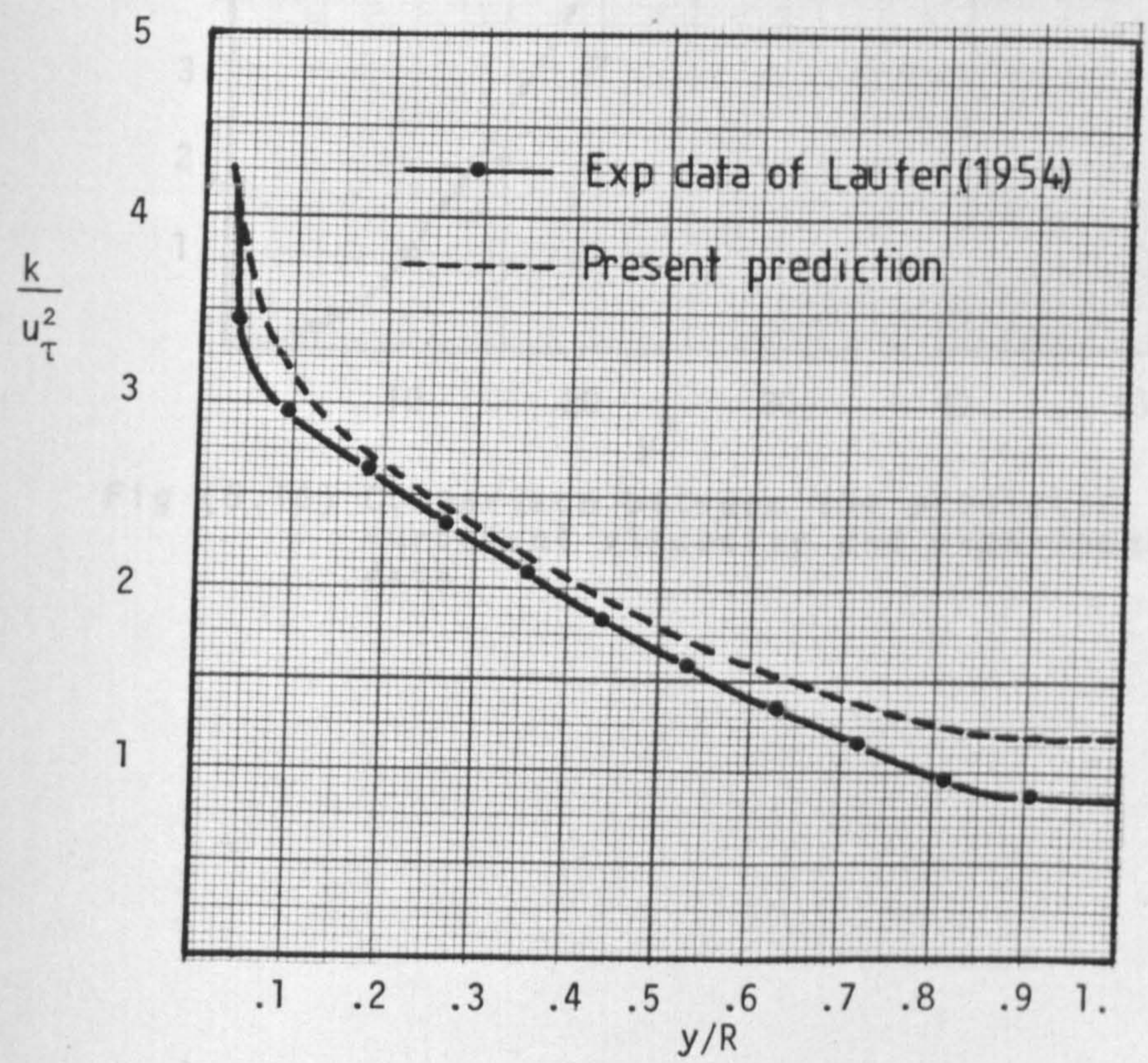


Fig (6.15) Comparison between the predicted turbulence kinetic energy and the experimental data outside the near-wall region, ($Re=5x10^4$)

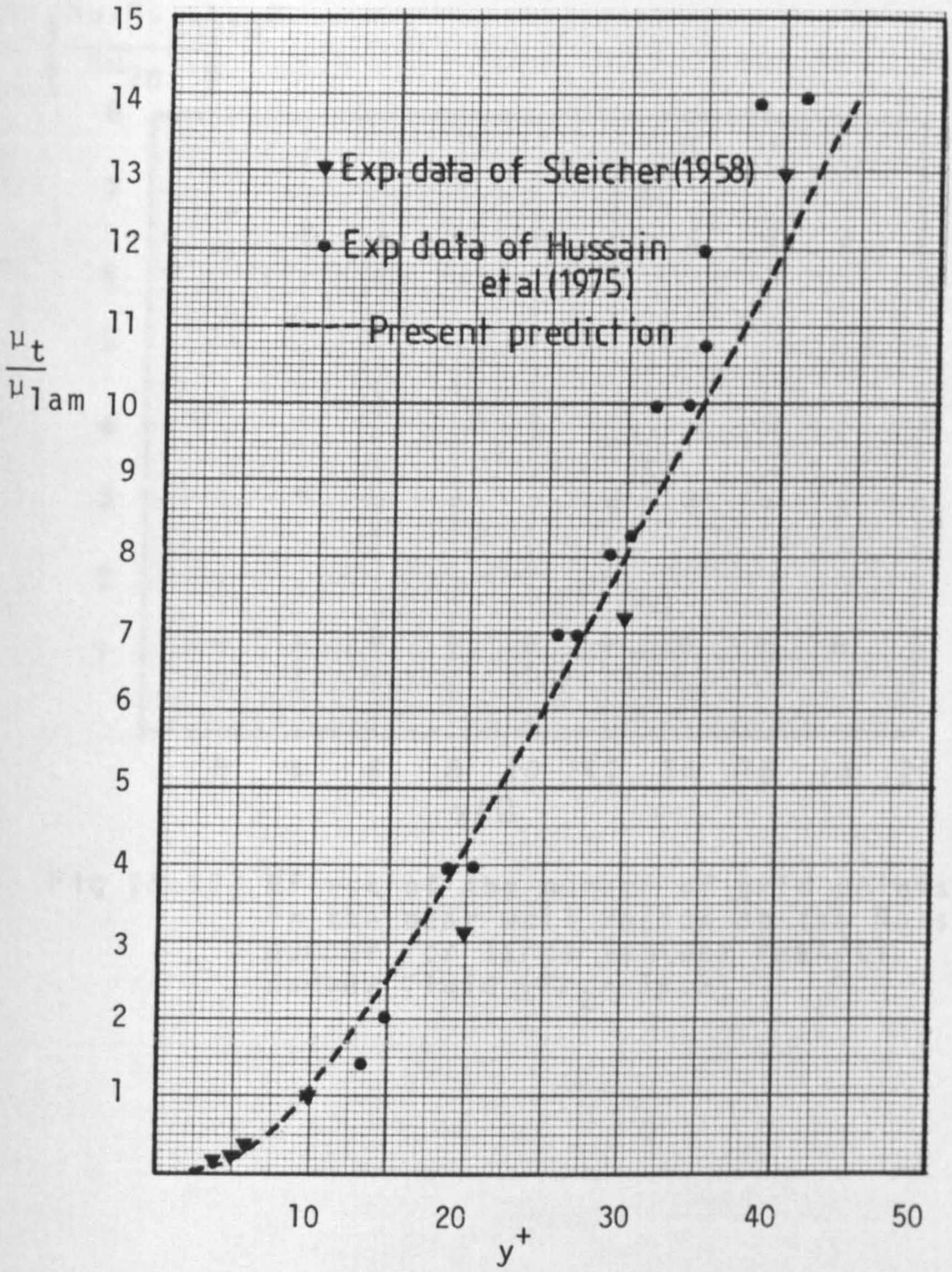


Fig (6.16) Comparison between the predicted turbulent viscosity and experimental data

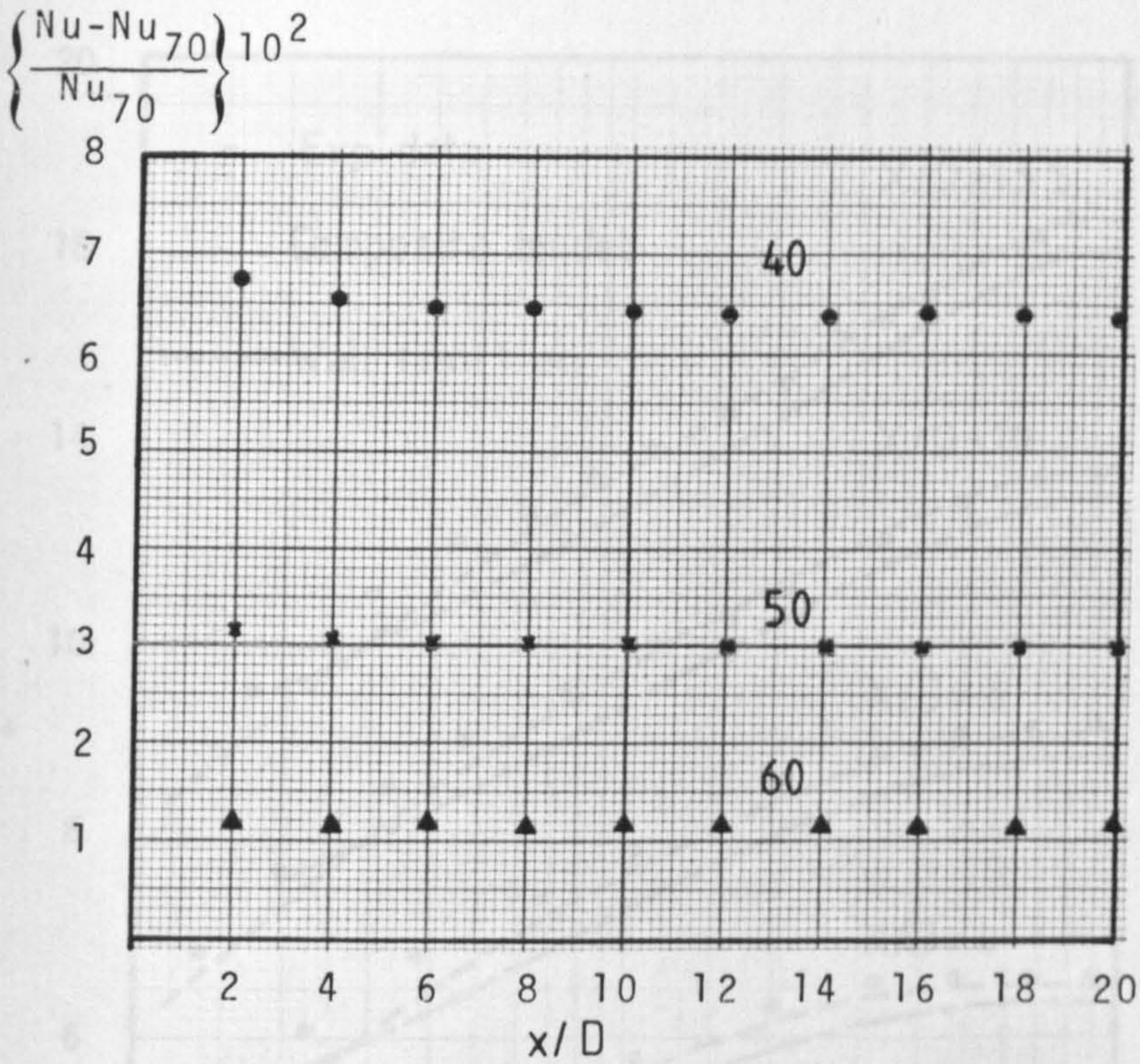


Fig (6.17) Effect of the number of grid points in the near-wall region on the Nusselt number for large laminar Prandtl number fluid (Pr_ℓ = 14.3)

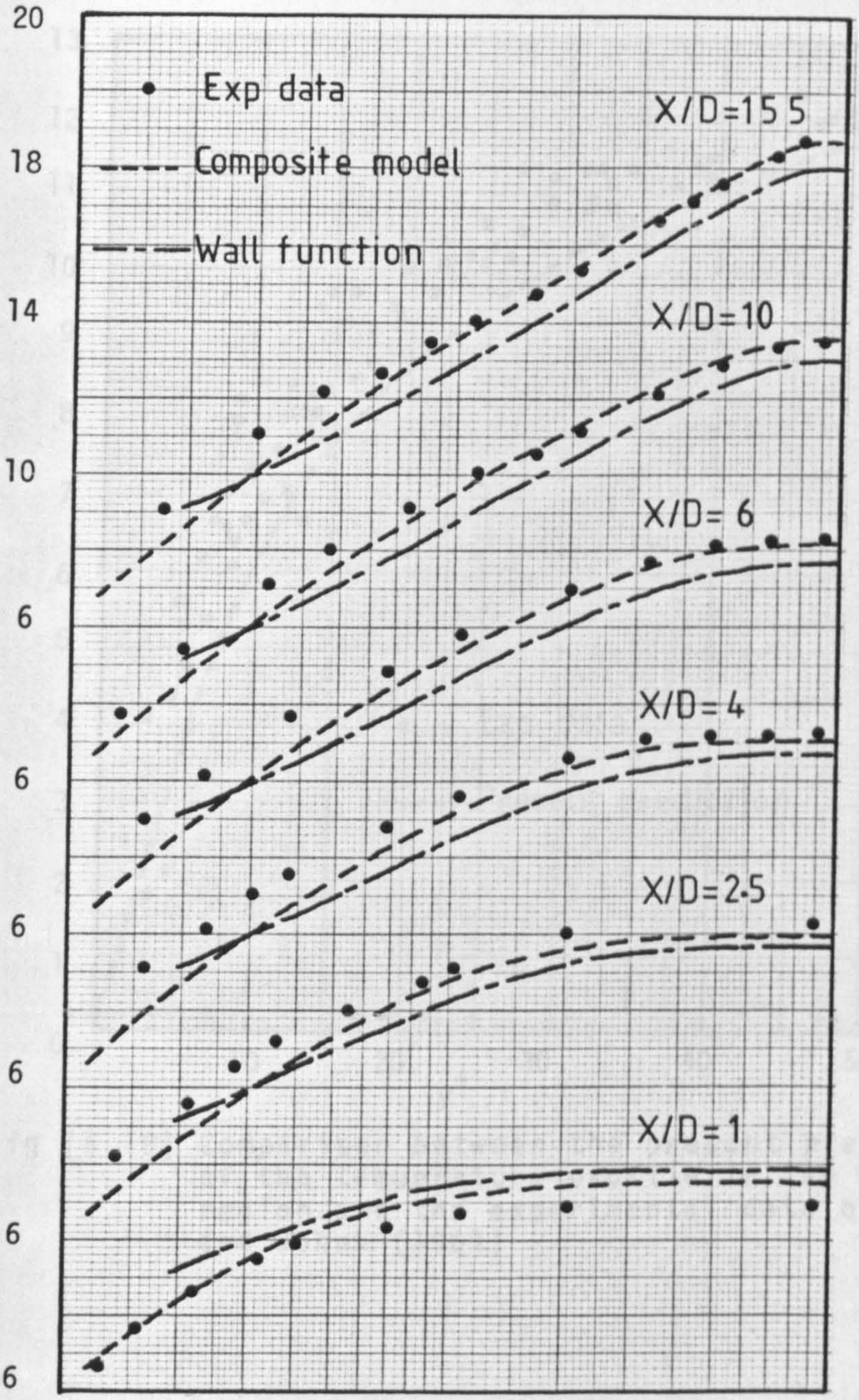


Fig (6.18) Comparison between the predicted temperature profiles and the experimental data of Hanratty and Johnk (1961), Pr_{ℓ}=.7 and R_N=3.5x10^4

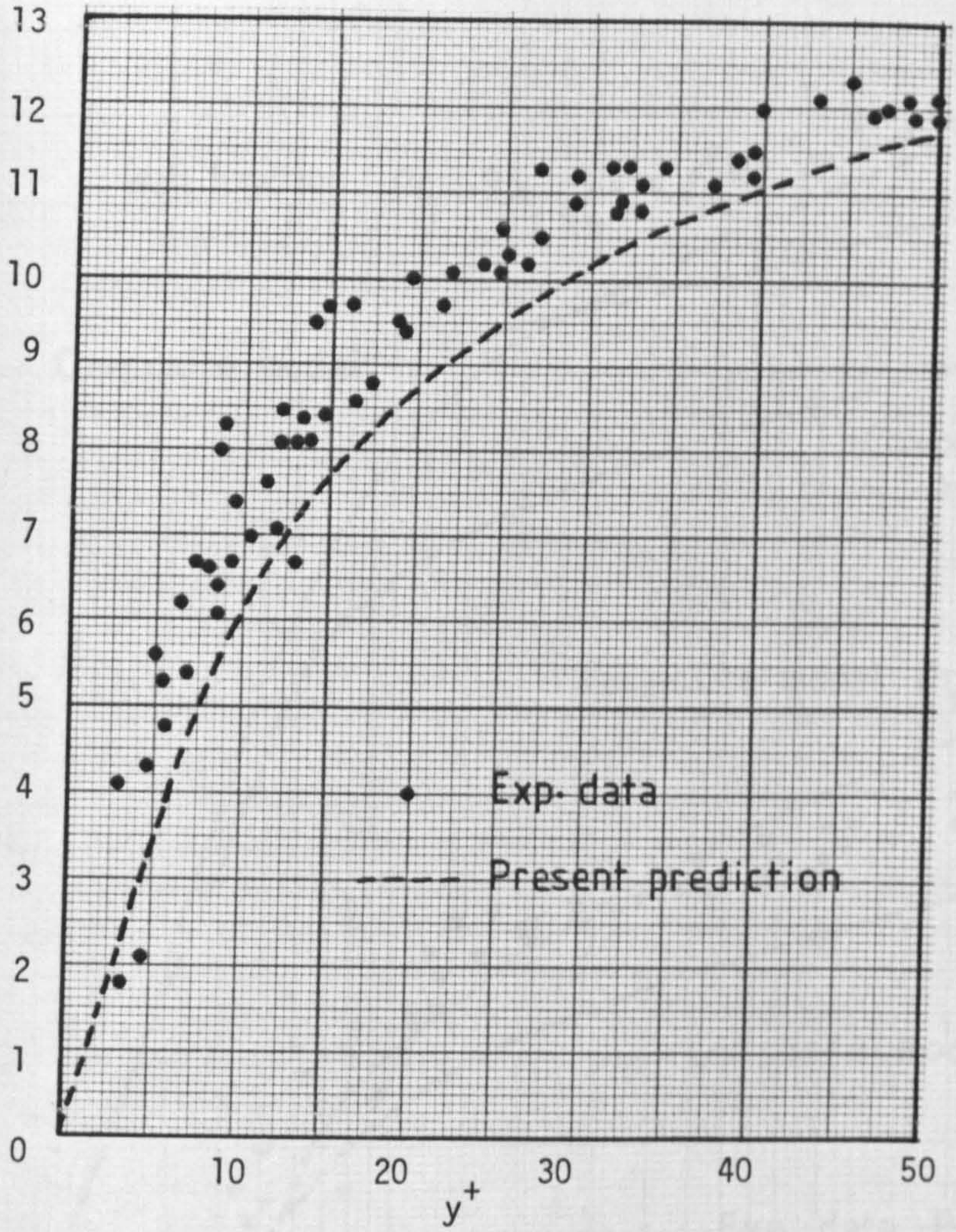


Fig (6.19) Comparison between the present prediction of the temperature profile in the near wall region and the experimental data of Hanratty and Johnk (1961)

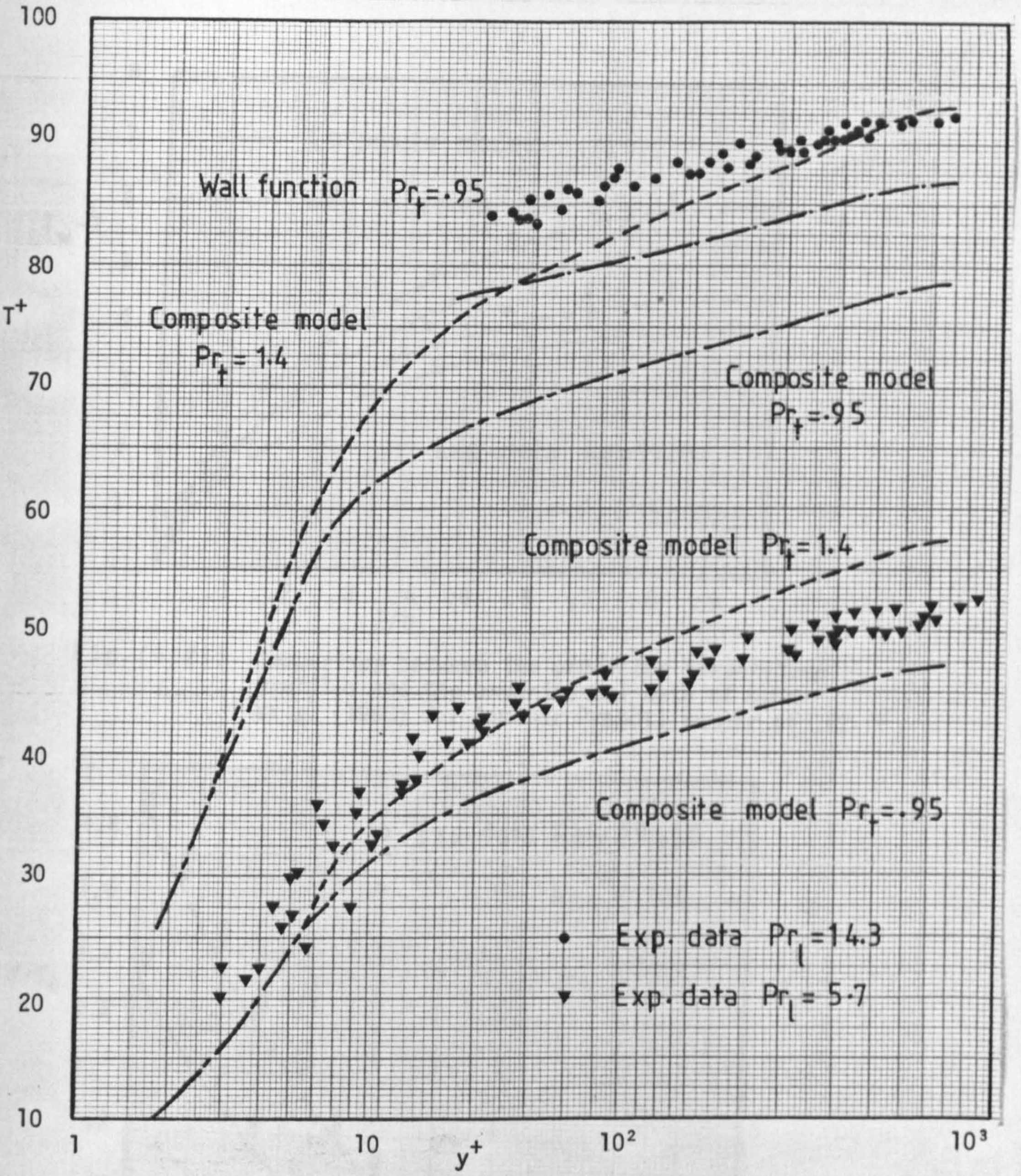


Fig (6.20) Comparison between the present prediction of the fully-developed temperature profiles and the experimental data of Gowen et al (1967) for large laminar Prandtl number fluids (Pr_ℓ=5.7 and 14.3).

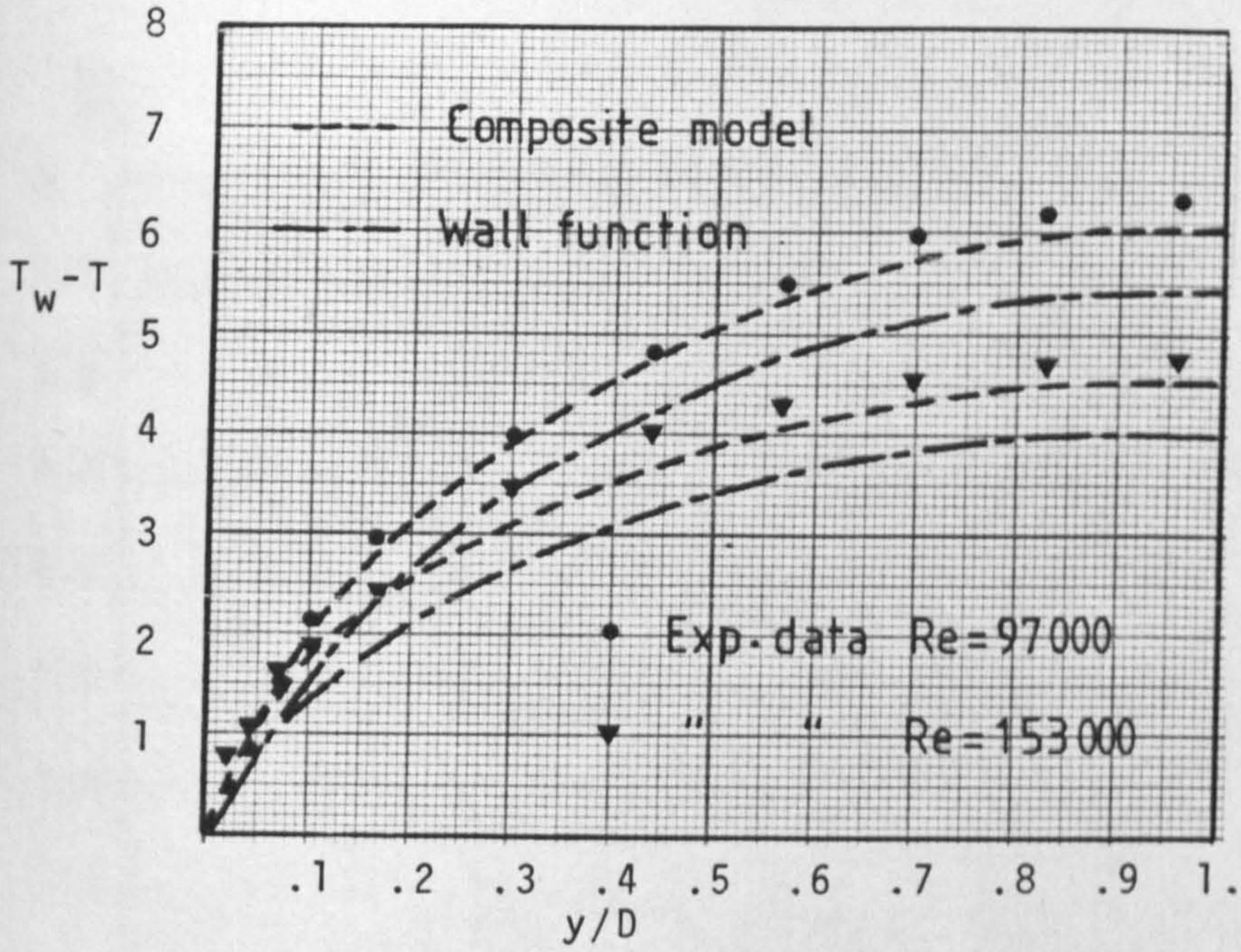


Fig (6.21) Comparison between the predicted temperature profiles and the experimental data of Buhr et al (1968) for laminar Prandtl number of .02

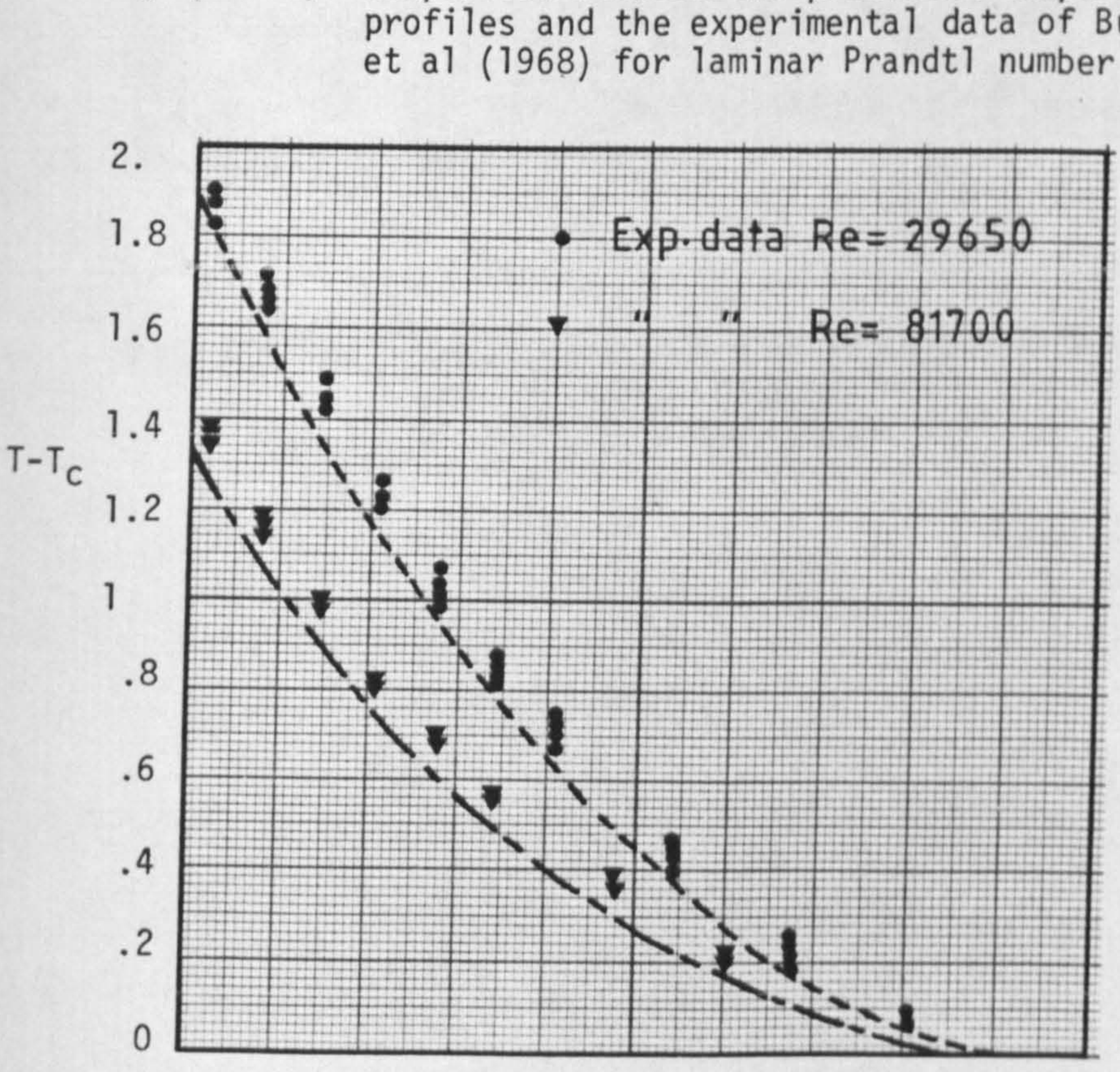


Fig (6.22) Comparison between the predicted temperature profiles and the experimental data of Fuchs et al (1973) for laminar Prandtl number of .007

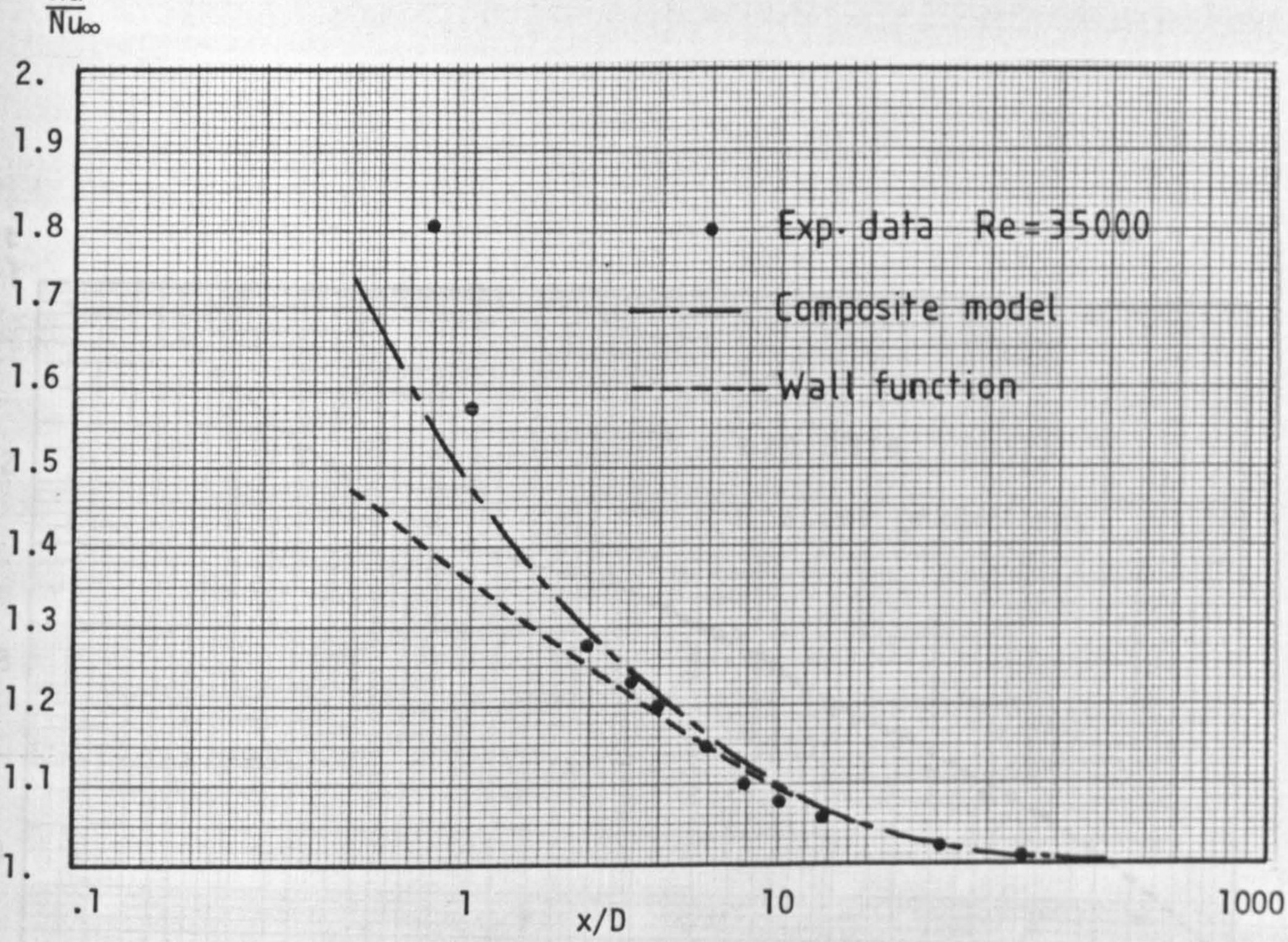


Fig (6.23) Comparison of the predicted Nusselt number in the entrance region with the experimental data of Hanratty and Johnk (1961)

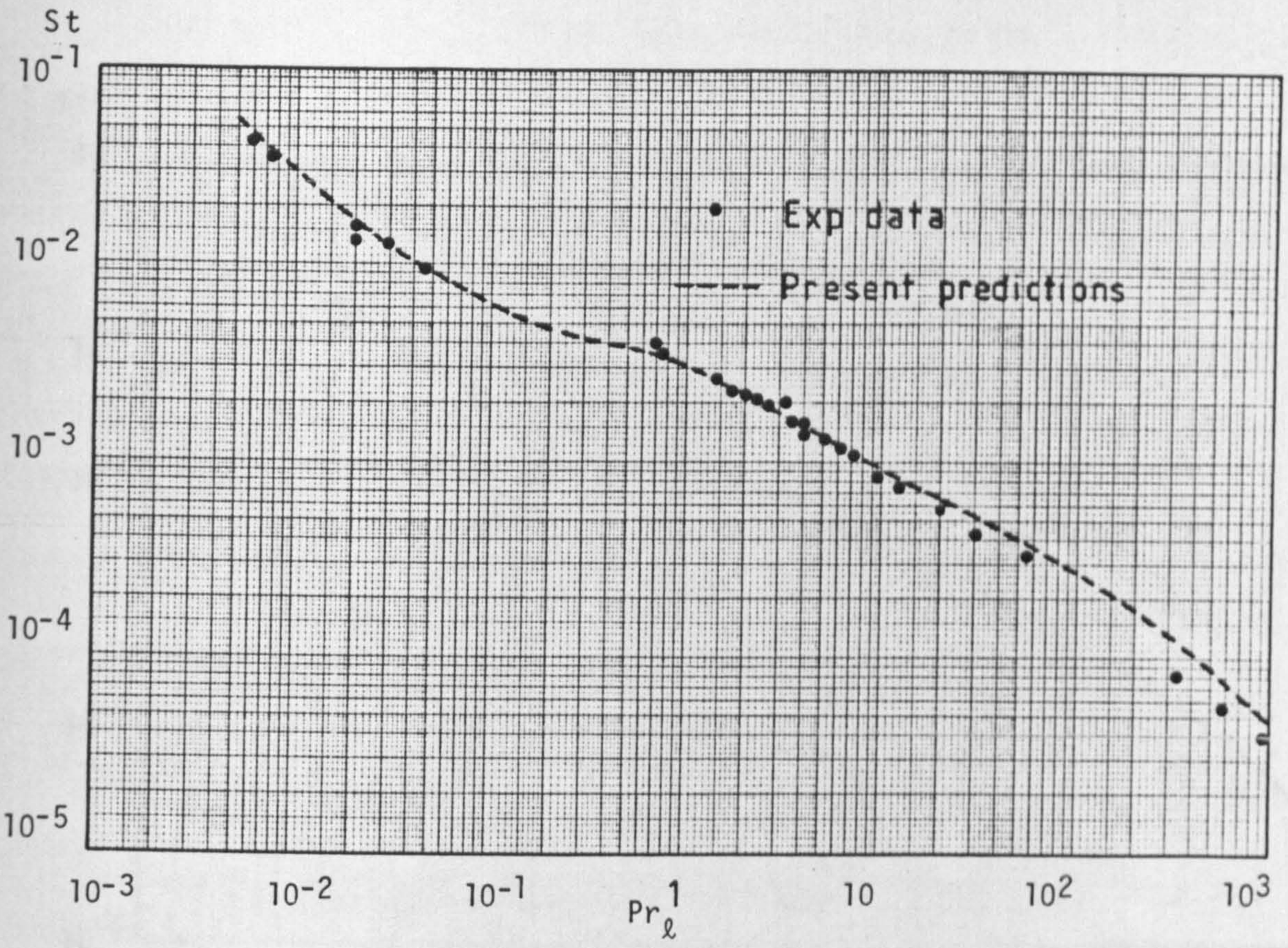


Fig (6.24) Comparison between the predicted Stanton number and the experimental data, $Re=2.5\times10^4$

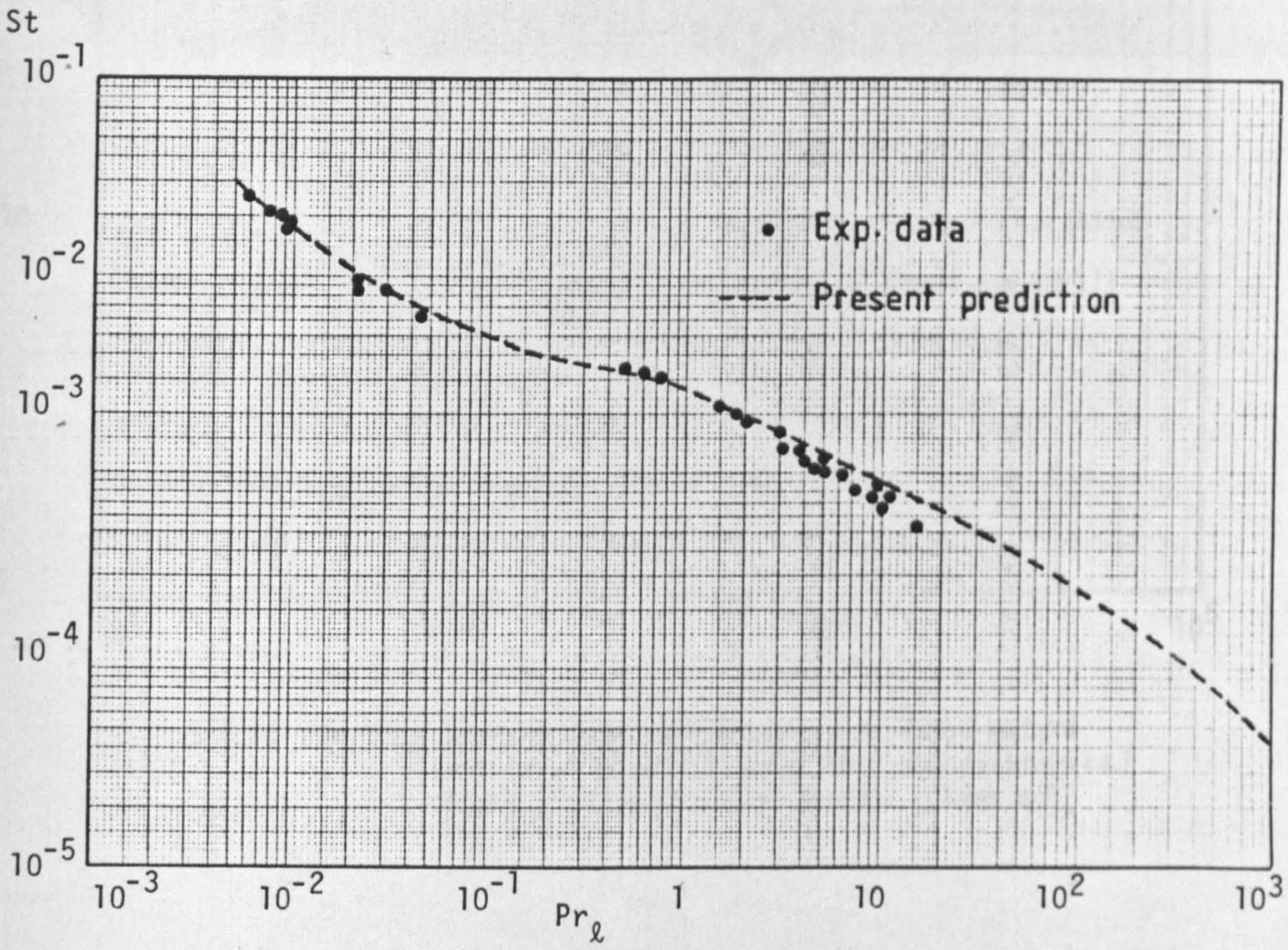


Fig (6.25) Comparison between the predicted Stanton number and the experimental data, $Re=5x10^4$

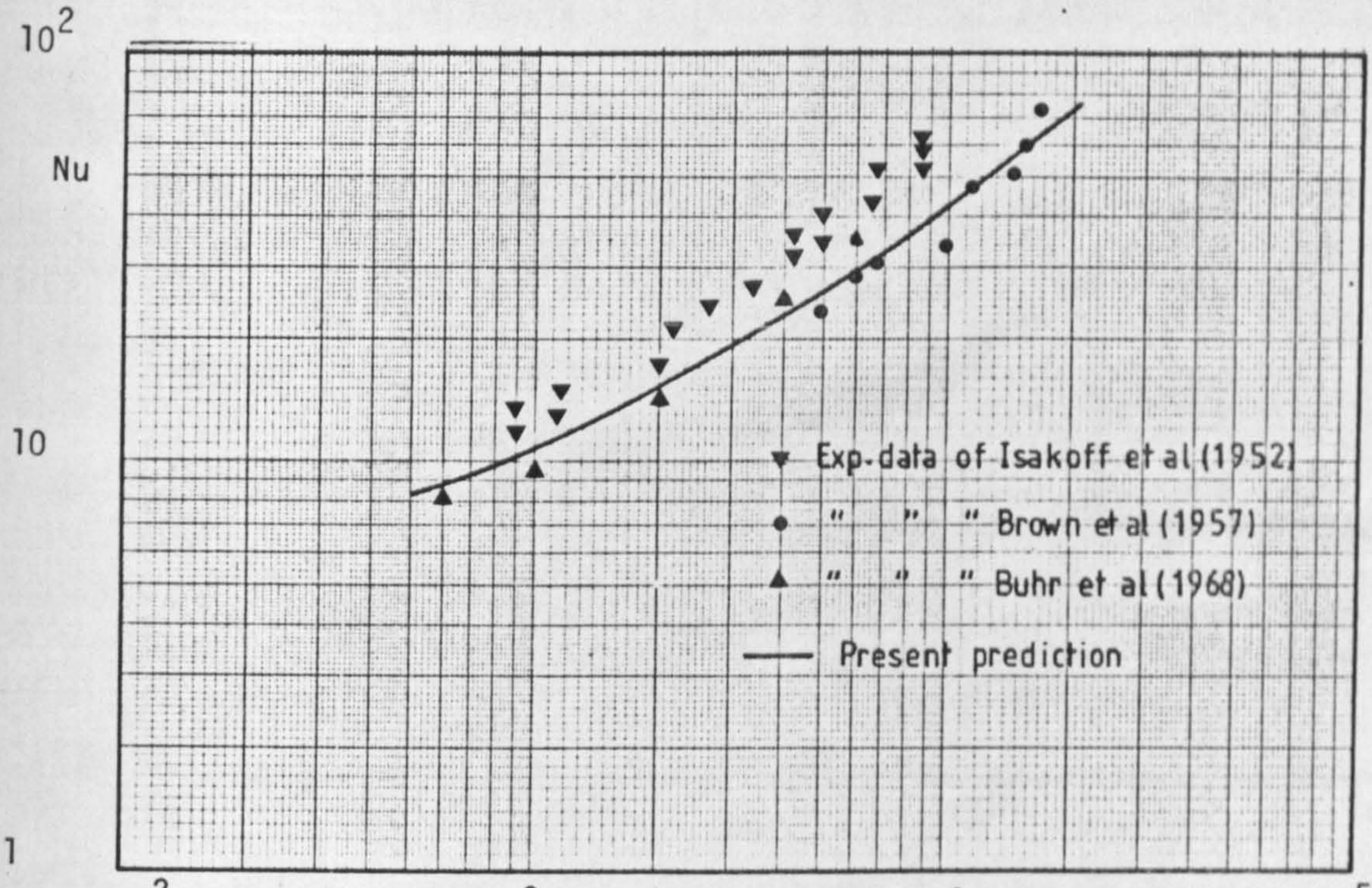


Fig (6.26) Comparison between the Predicted Nusselt number and the experimental data for a liquid metal flow of $Pr_\ell = .02$.

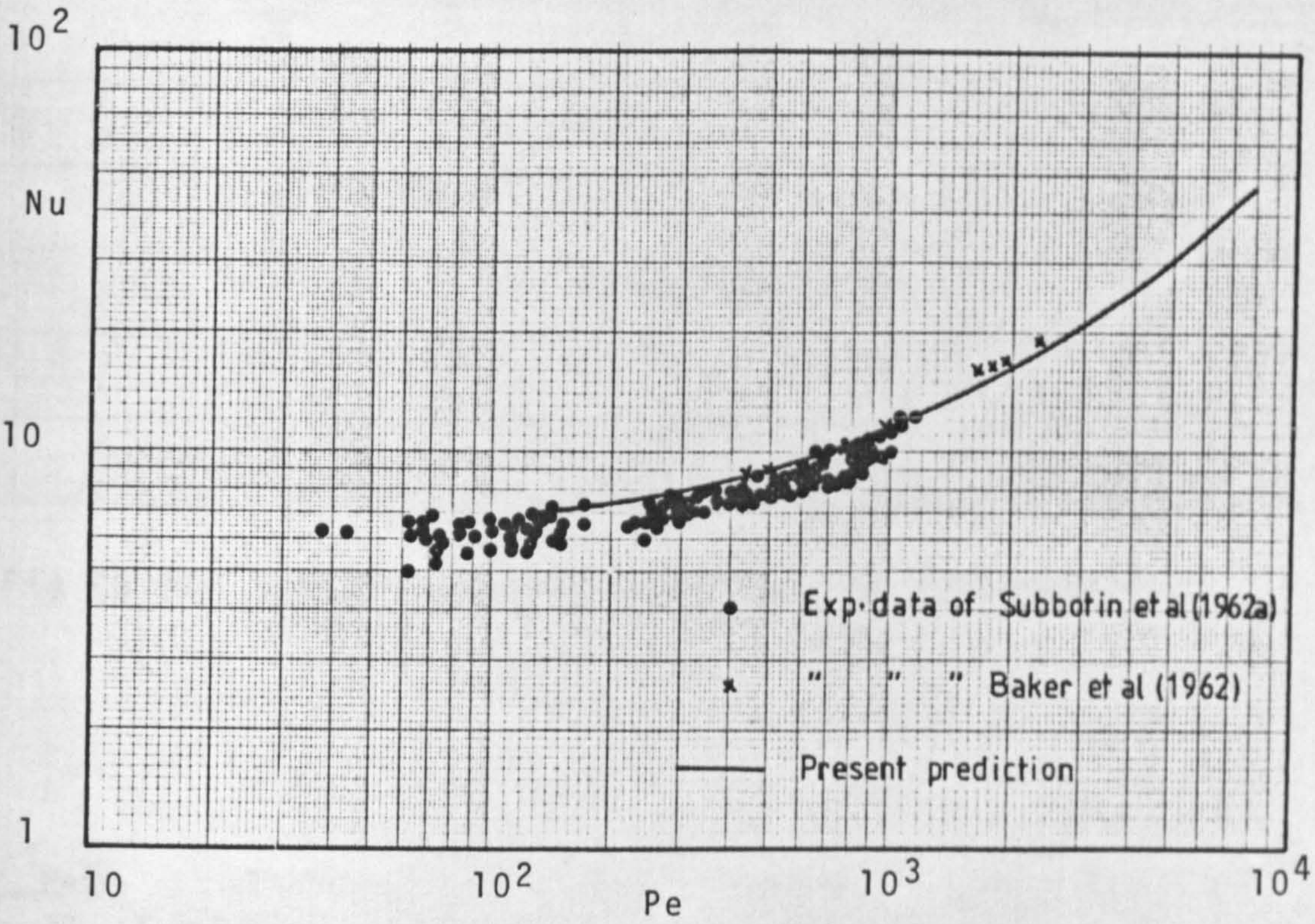


Fig (6.27) Comparison between the present prediction of Nusselt numbers and the experimental data for a liquid metal of Pr_ℓ=.005

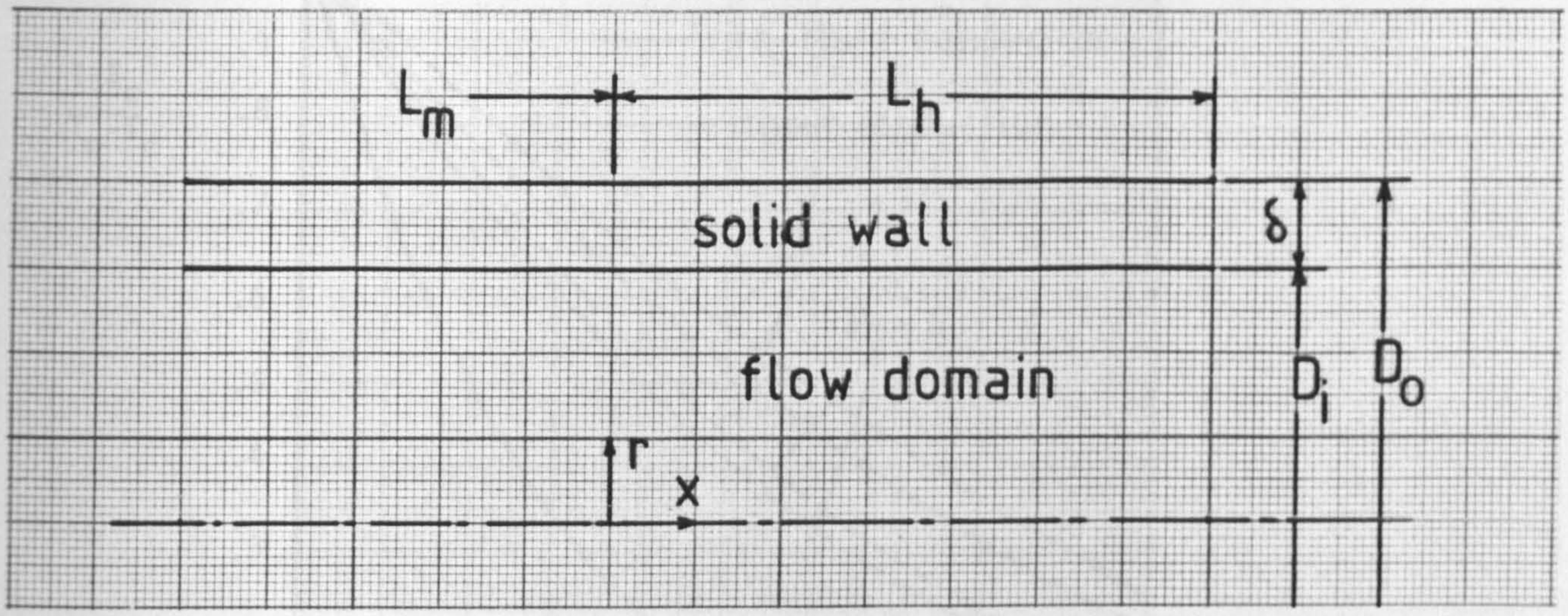


Fig (6.28) The computation domain of the conjugate problem.

$\left(\frac{T_w - T_{w,20}}{T_{w,20}}\right)$ i and 0

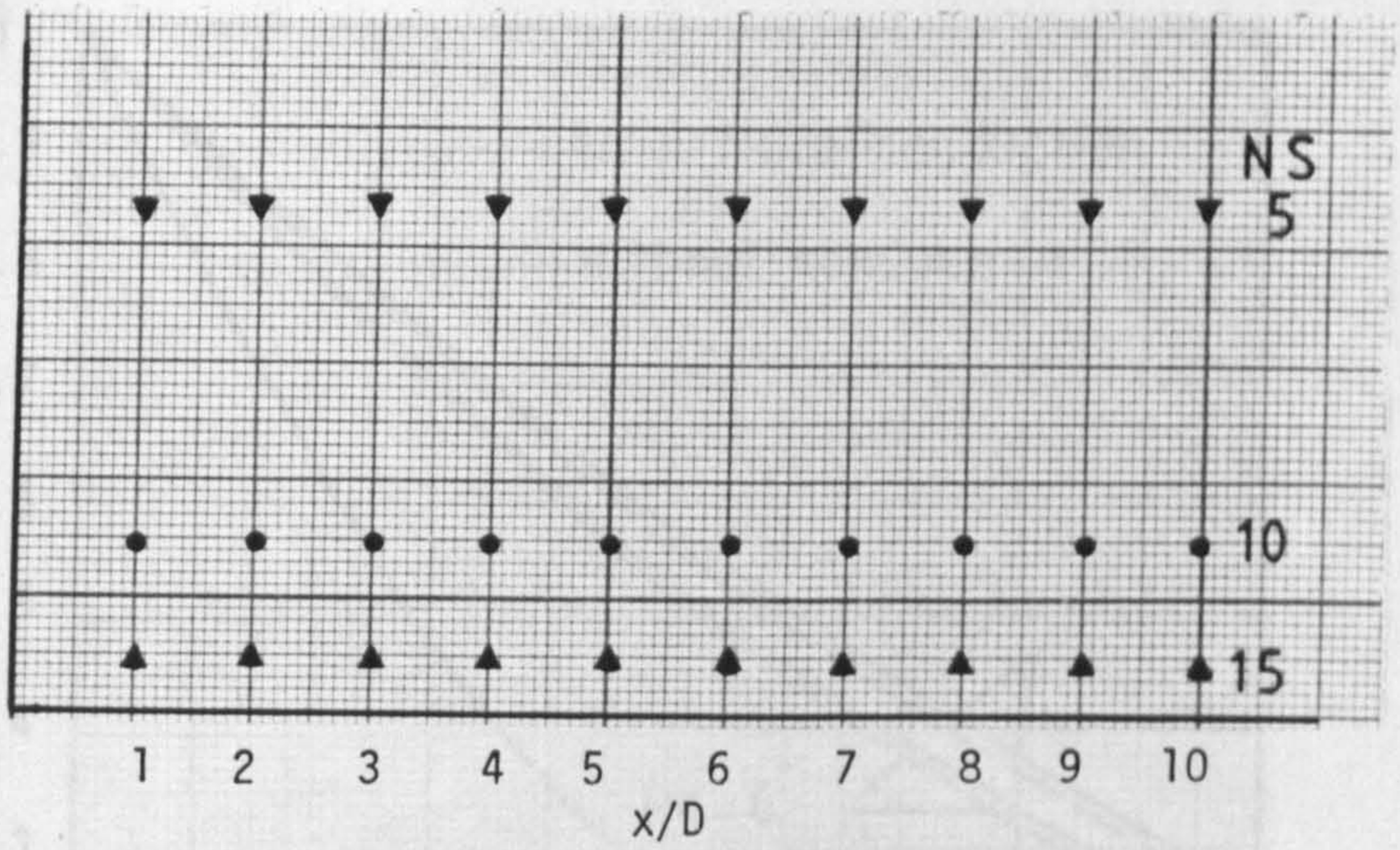


Fig (6.29) Effect of the number of grid points in the solid wall on the inner and outer wall temperatures

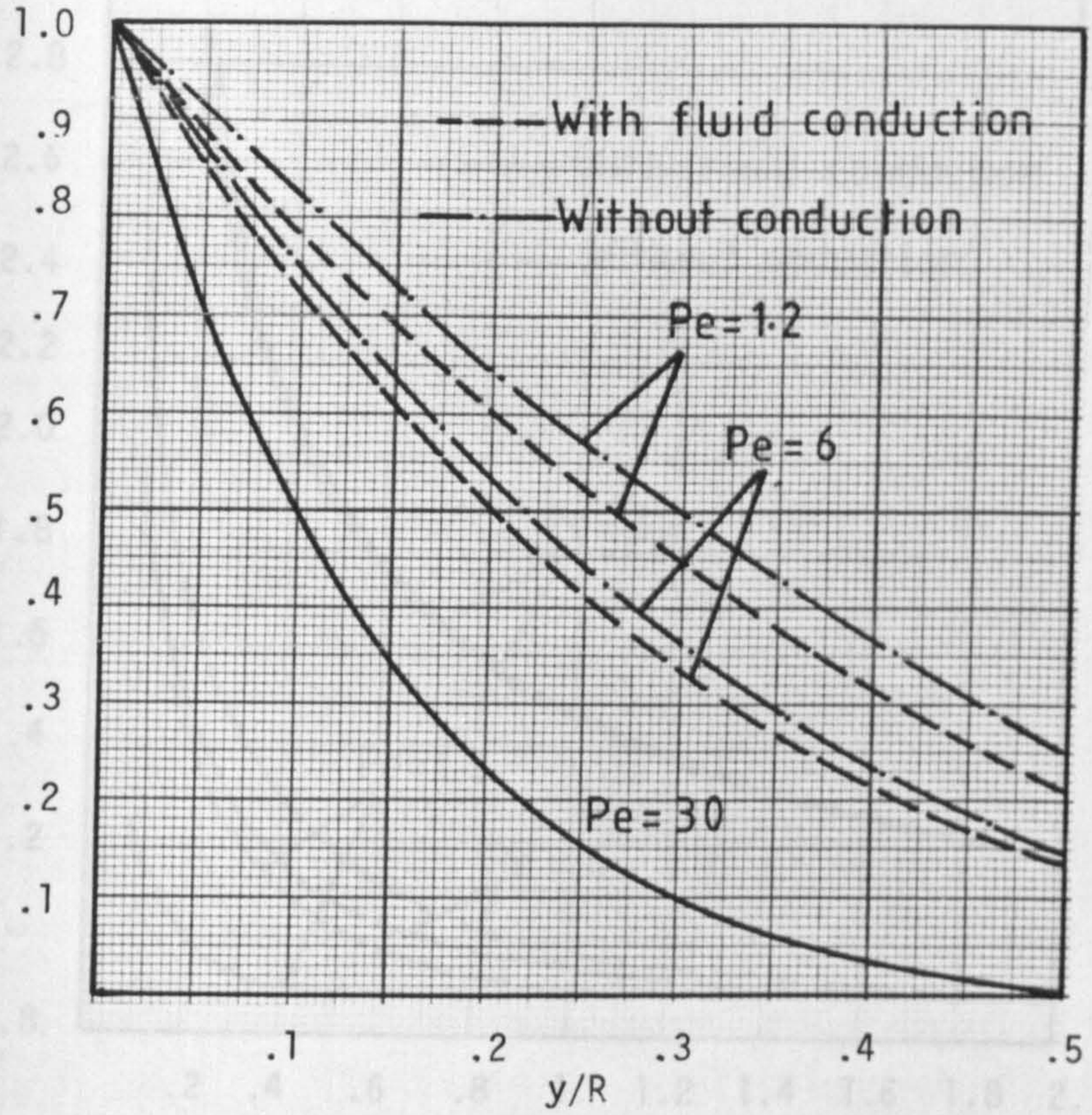


Fig (6.30) Effect of the axial fluid conduction on the temperature profiles at x/R=.5

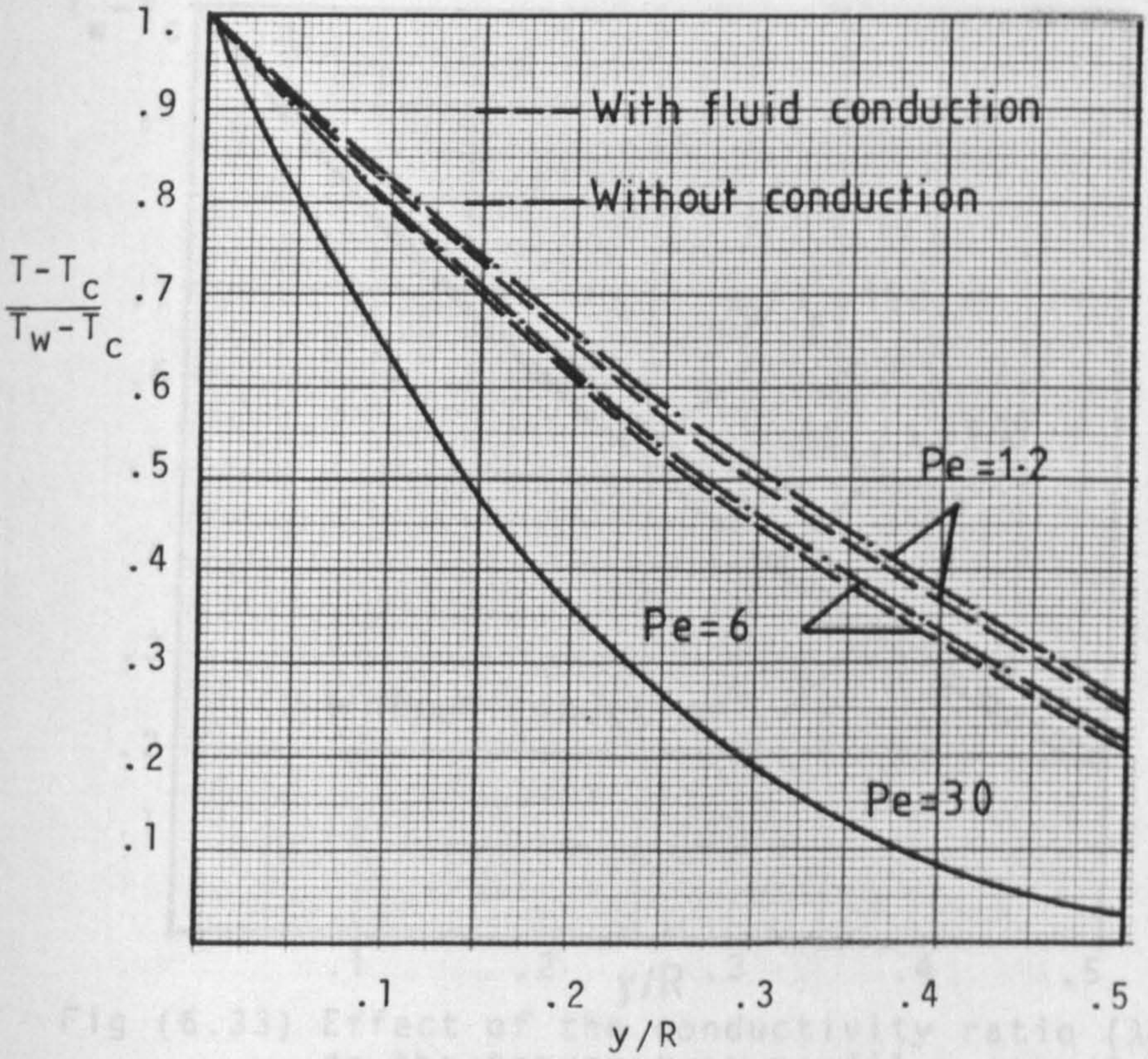


Fig (6.31) Effect of the axial conduction on the temperature profiles at x/R=1.0

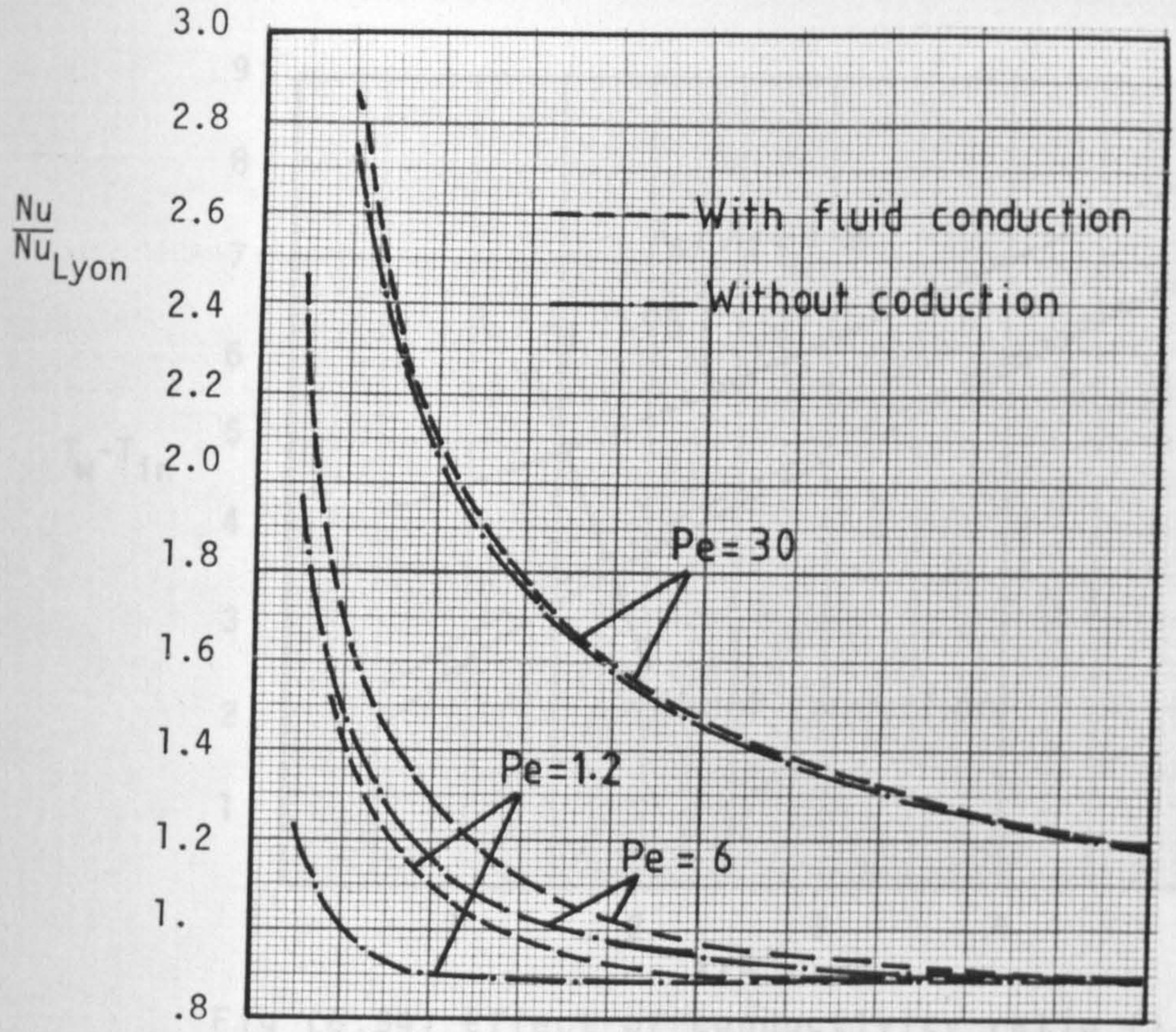


Fig (6.32) Effect of the axial conduction on the Nusselt number

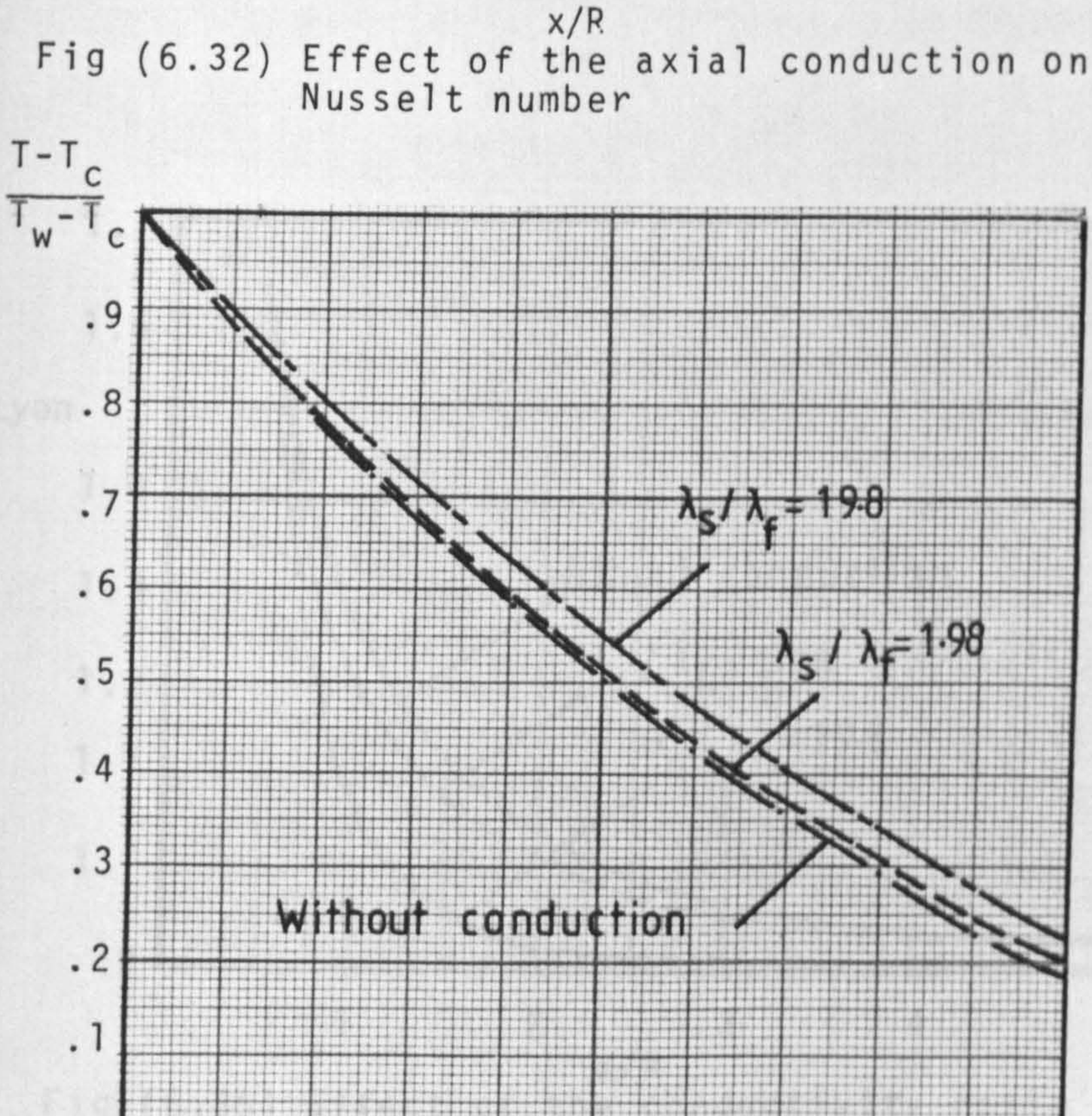


Fig (6.33) Effect of the conductivity ratio (λ_s/λ_f) on the temperature profiles at x/R=2

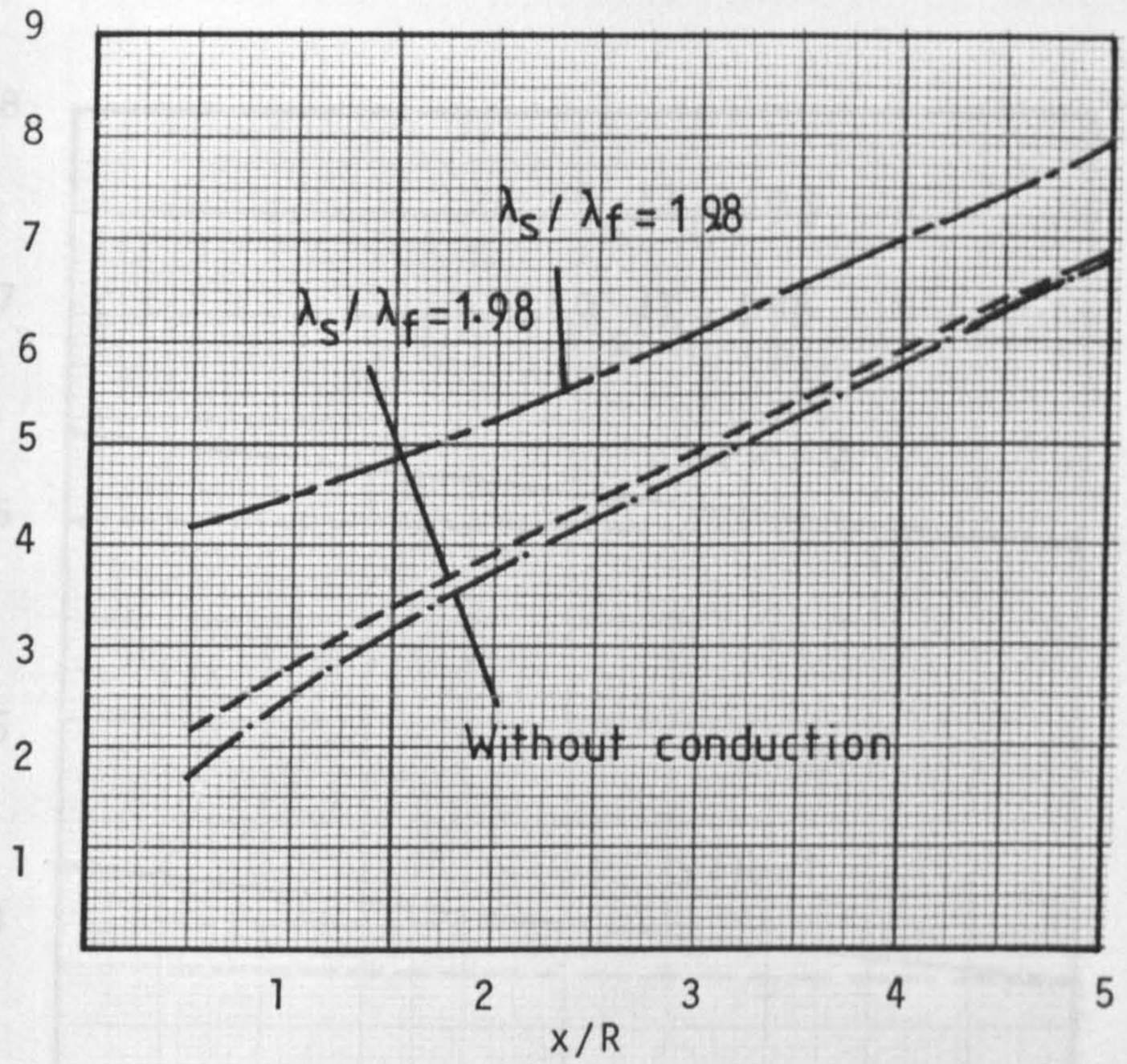


Fig (6.34) Effect of conductivity ratio (λ_s/λ_f) on the inner wall temperature

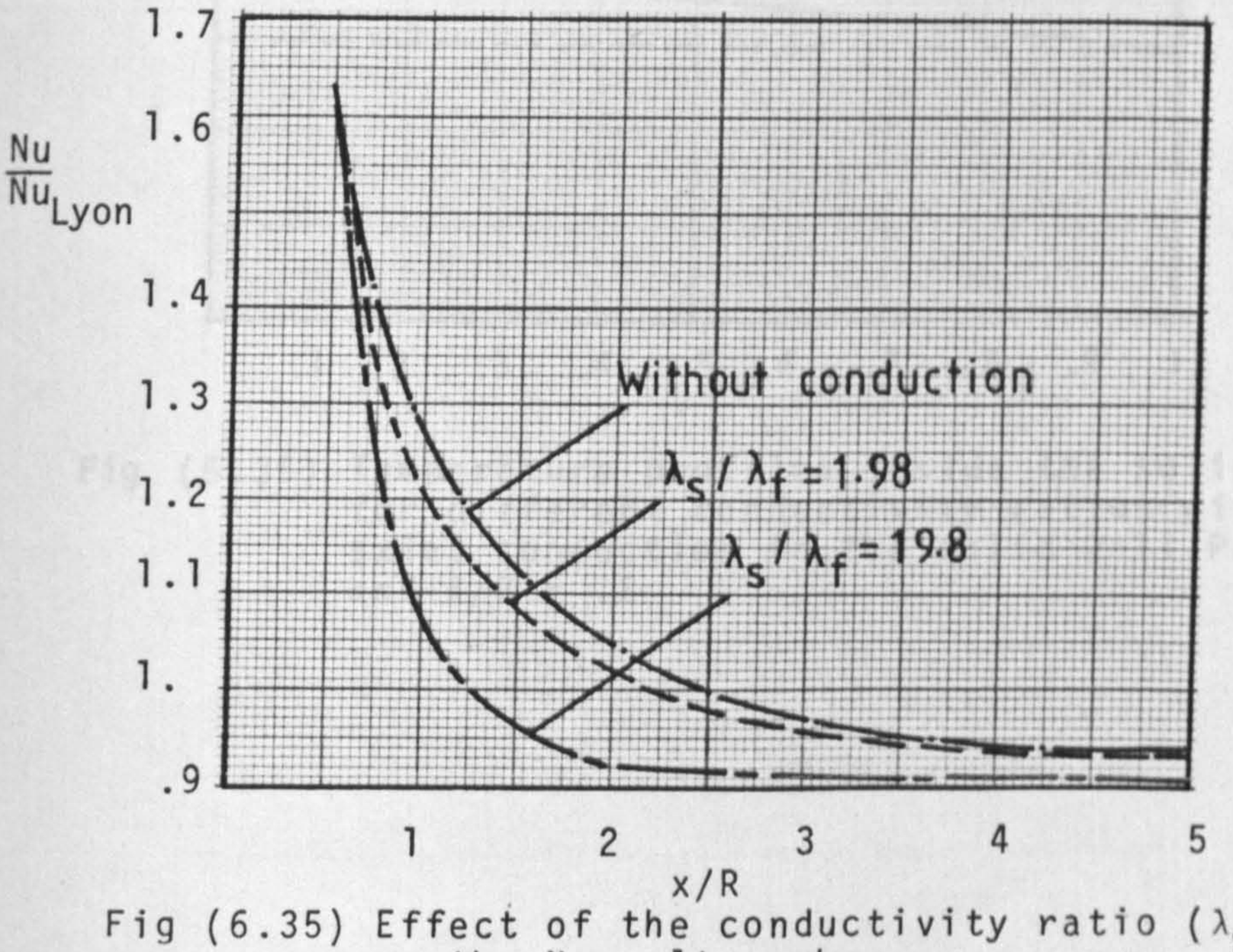


Fig (6.35) Effect of the conductivity ratio (λ_s/λ_f) on the Nusselt number

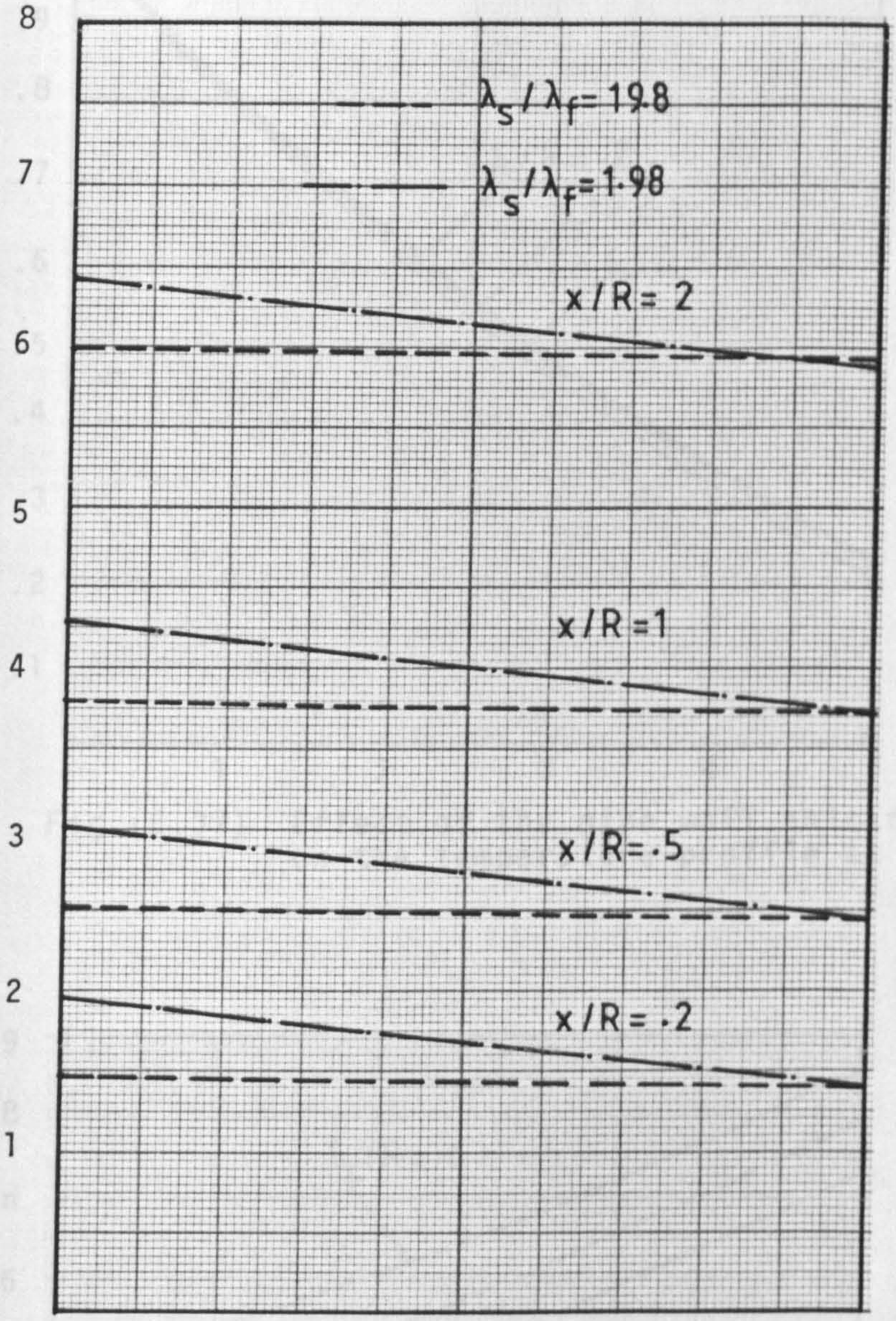


Fig (6.36) Temperature profiles inside the solid wall for different conductivity ratios without axial conduction in the solid wall Pe=6 and δ/R = .2

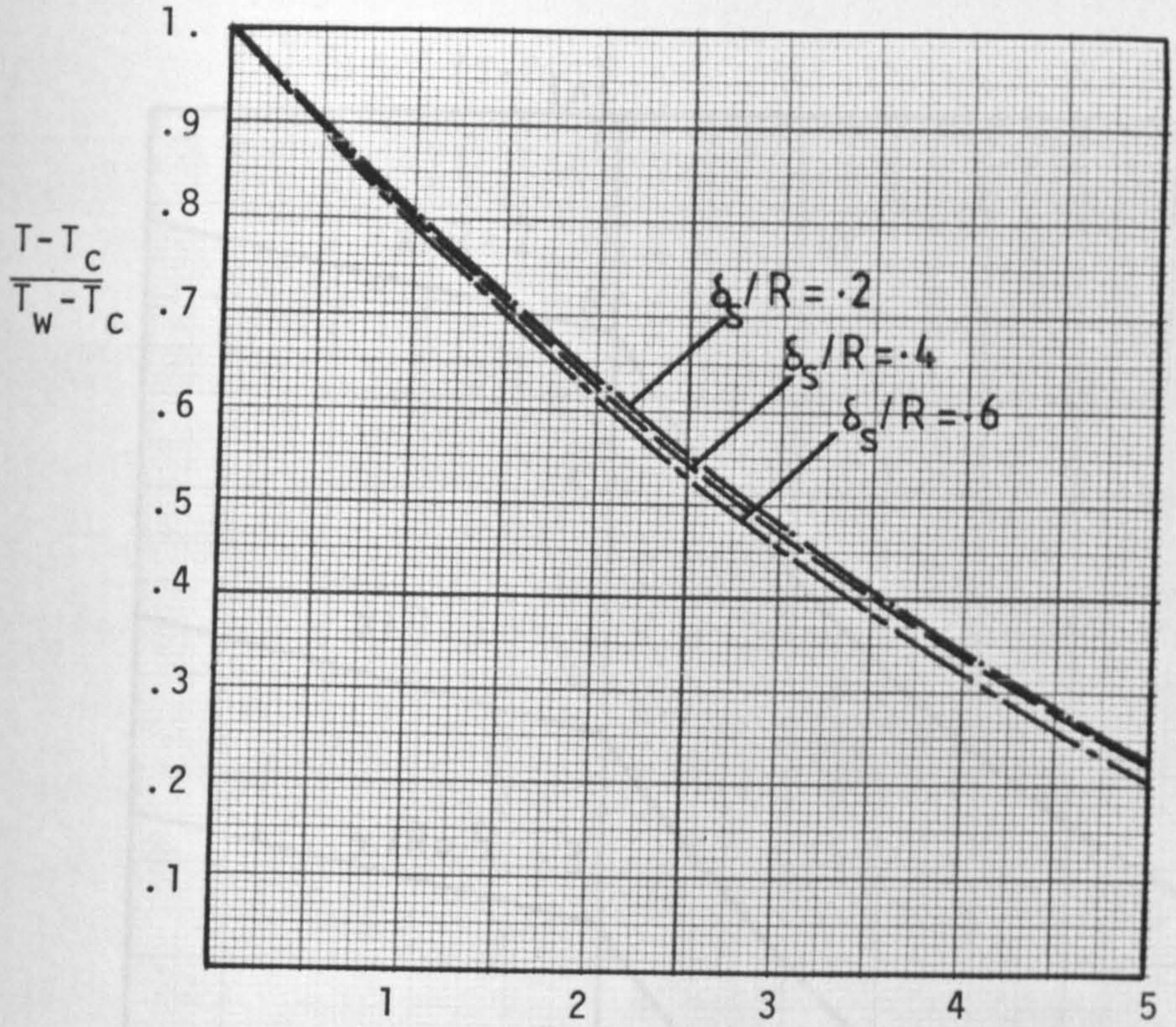


Fig (6.37) Effect of the pipe wall thickness on the temperature profile at x/R=2

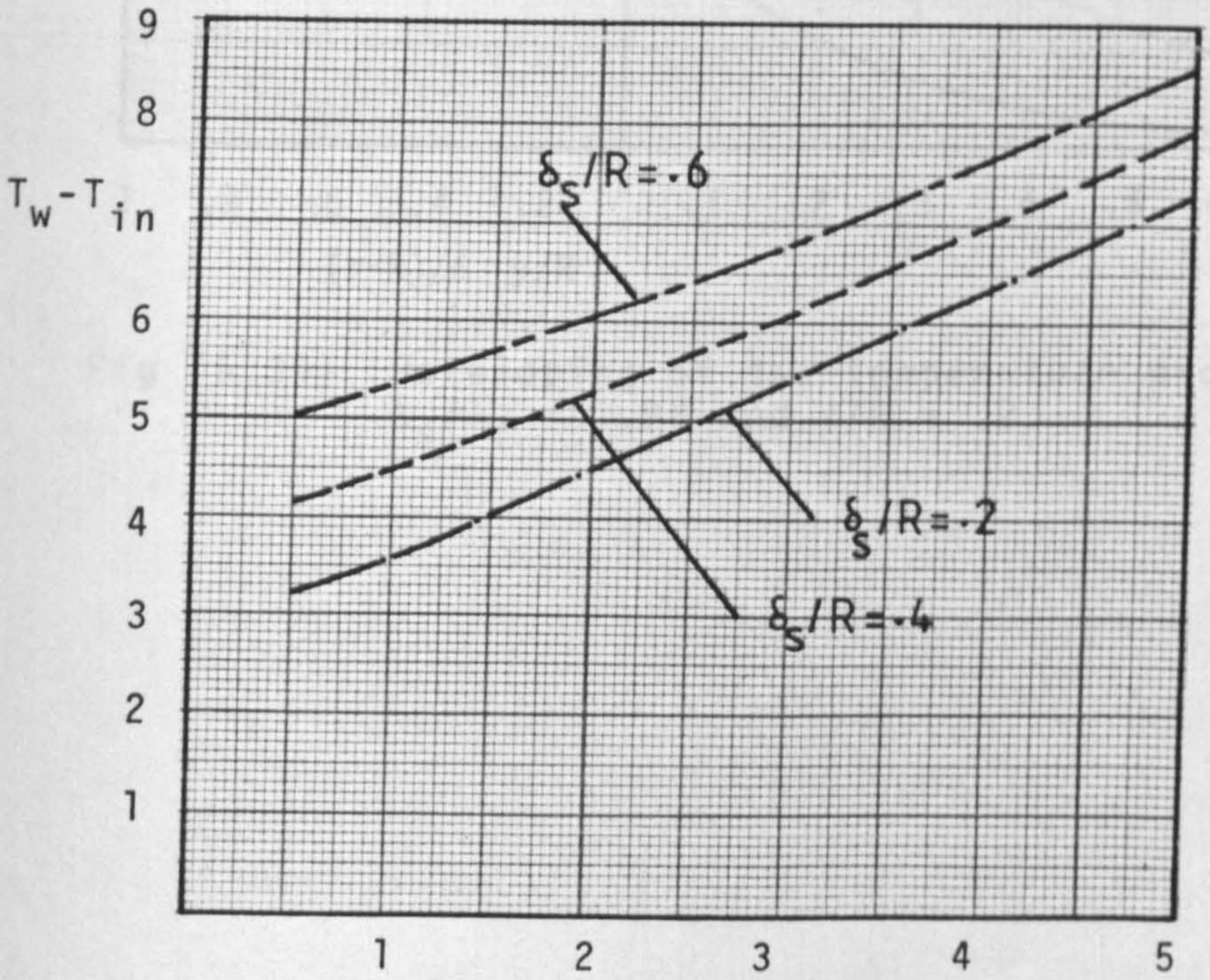


Fig (6.38) Effect of the wall thickness on the inner wall temperature

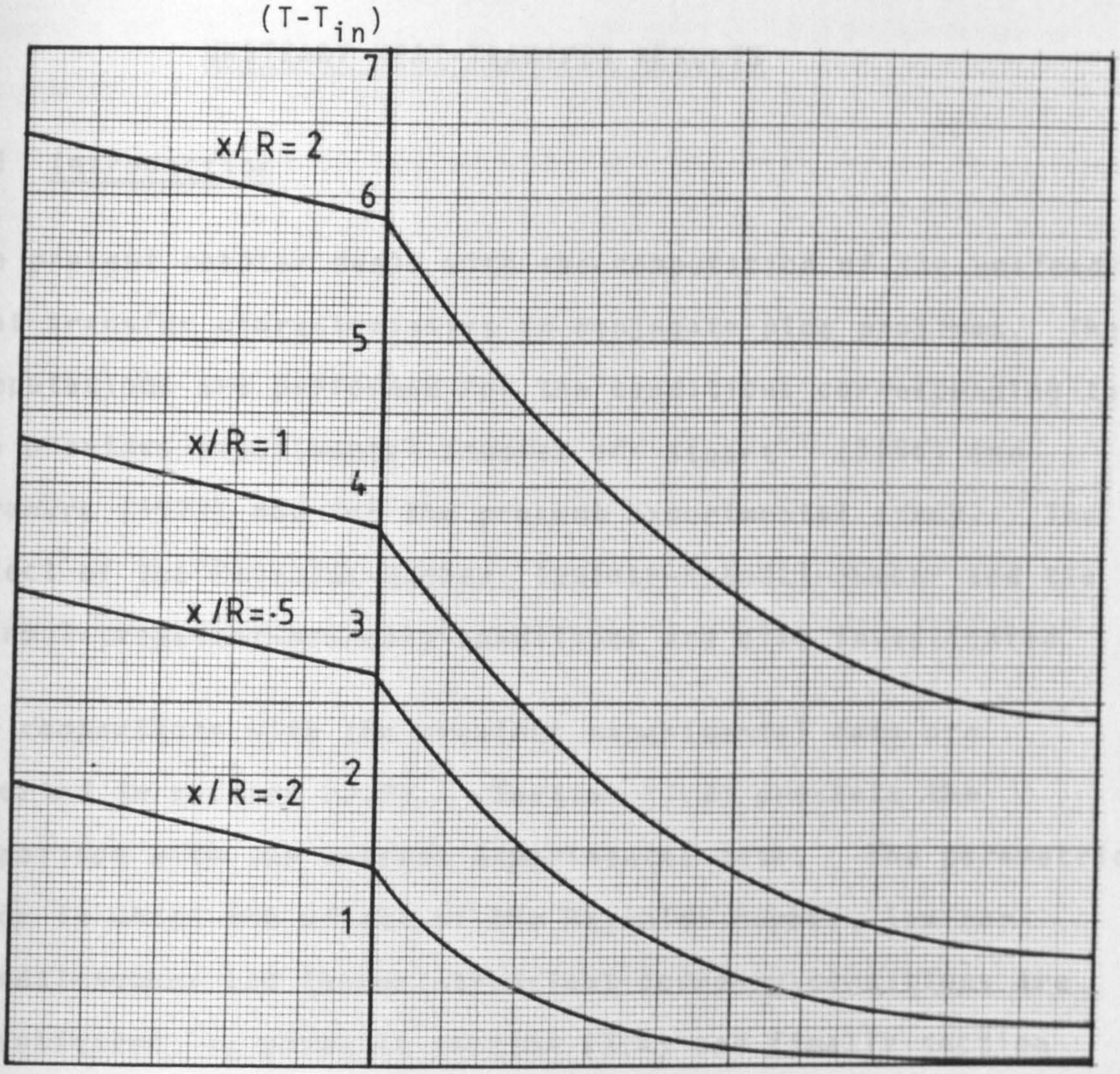


Fig (6.39) Developing of the temperature profiles, Pe=6., λ_s/λ_f = 1.98 and δ/R = .2.

CHAPTER 7

UNSTEADY HEAT-TRANSFER RESULTS

7.1 Introduction

The present chapter deals with the computation of the unsteady heat-transfer characteristics in conjugate-pipe problems. The computations are performed for the conditions corresponding to the previous experimental studies of Stuart (1956) and Kawamura (1977) and for the present experimental study. The effect of the Reynolds-number, laminar-Prandtl-number and the thermal-transient-boundary-conditions are also investigated.

The comparisons with the previous experimental data are reported in section (7.2). Section (7.3) presents the comparison with the present experimental data. The parametric study in which the effect of the Reynolds-number, laminar-Prandtl-number and thermal-transient-boundary-conditions are investigated, is given in section (7.4) and finally section (7.5) presents some concluding remarks.

7.2 Comparison with Previous Experimental Data

7.2.1 Problem specifications

The previous experimental studies of Stuart (1956) and Kawamura (1977) were all performed in water flowing through a stainless-steel tube. Stuart (1956) used a tube of . 0.0127 meters inner diameter and a thickness of 0.0008 meters while Kawamura (1977) used a tube of .03 meters inner diameter and a thickness of 0.000457 meters. In these experimental

studies, the hydrodynamic properties were developed over a length of 50 tube diameters (Stuart (1956)) and over a length of 34 tube diameters (Kawamura (1977)). The hydrodynamic-entrance region was then followed by an insulated-heated length, where the heating took place by electric energy dissipated into the solid wall.

The fluid hydrodynamic properties (u, k and ε) at the inlet section in the experimental situations were kept nearly uniform; while the inlet temperature as well as the fluid and wall temperatures before the heating took place were maintained constant. These conditions were incorporated in the present computations and the heat input was assumed to be uniformally distributed inside the solid wall.

7.2.2 Computational details

The study of the conjugate problem presented in chapter (6) showed that the axial fluid conduction can be neglected for flows with Peclet numbers greater than thirty, while the importance of the axial conduction inside the solid wall depends on the laminar Prandtl number, the ratio of the solid to fluid conductivities and the ratio of the solid wall thickness to the tube diameter. The previous experimental data of Stuart (1956) and Kawamura (1977) were reported for Peclet numbers greater than 60000, conductivity ratios of less than 28 and wall thickness less than 0.125 the pipe diameter. For these conditions the computations indicated that the axial conduction inside the solid wall and in the flow domain could be neglected. Consequently, the enthalpy equations (2.2.4

and 2.2.6) were reduced to their parabolic form and the parabolic computational procedure presented in section (4.3.2) was adopted.

The grid size employed in the present computations was the same as that used in the steady-state problem; while the effect of the time steps on the inner wall and mean-bulk-temperature responses are given in figures (7.1 and 7.2) respectively. These results, which are presented for time steps of 0.1, 0.05, 0.02, 0.005 and 0.001 seconds become independent of the time step when a value of .005 was employed. In this case, the "Courant number" $(\frac{u\delta t}{\delta x})$ is equal to two; however, Roache (1976) recommended a value of one and consequently a Courant number of one was used in the present investigation in order to calculate the time steps.

The execution time for a typical run with Kawamura's conditions was 151 seconds on the CDC 6600 computer.

Table (7.1)

Experimental conditions of Stuart's data

u	T_{inl}	T_{out}	R_N	$\dot{q}_{(kw)}$	$\dot{q}_{cal}$
.701	14.56	45.8	6720	1267	11.55
1.241	15.22	23.5	11980	6.68	5.432
1.241	14.56	32.08	11980	13.08	11.55

7.2.3 Results and discussions

The predicted fully-developed (x/D=70) mean-bulk-temperature responses are compared with the experimental data of Stuart

(1956) in figures (7.3 and 7.4); these experimental data were reported for the conditions given in table (7.1). The heat absorbed by the flow for the three reported cases are also given in table (7.1), where this heat was calculated as follows:

$$\dot{q}_{calculated} = \frac{\pi}{4} D^2 \rho u_m \{(C_p T)_{out} - (C_p T)_{inl}\} \quad , (7.1)$$

the subscripts 'out' and 'inl' stand for the steady state outlet and inlet bulk conditions respectively. These heat inputs, which are calculated from equation (7.1), were smaller than the reported values of Stuart (1956), this indicates that one or more of the measured temperatures, the mass-flow rate and the heat input are in error.

Comparison between the predicted results, which were obtained with the reported heat inputs, and the experimental results shown in figures (7.3 and 7.4) reveals that the predicted results are always higher than the experimental data, but not by a uniform amount. This was expected due to the errors encountered in the experimental data.

The mean-bulk-temperature responses for different downstream locations (x/D = 5, 10, 20, 40 and 50) are plotted in figure (7.5) for a Reynolds number of 6720. These results show that the time required to reach a steady state increases with increasing downstream distance. However the results at initial times reveal that the temperature responses for different downstream values are the same over a time interval which depends on the downstream distance; the smaller the downstream distance the smaller is this interval. This may be explained by consideration of the heat-transfer mechanism in the unsteady problem; the heat transfer is first purely

by radial conduction which does not depend on the axial location, and consequently the same temperature response will be obtained all over the pipe length. This time of pure conduction depends on the downstream distance, the fluid velocity and the laminar Prandtl number; the larger the downstream distance the longer is this time, while the opposite is true for the fluid velocity and the laminar Prandtl number.

The inner and outer wall temperature responses are given in figure (7.6). These results show that the inner and outer temperatures are not the same, thereby emphasising the importance of the conjugate analysis. The results, however, show that the temperature responses at different locations are the same for short times, this time is larger than the corresponding time for the pure radial conduction and does not depend on the axial distance.

The comparison between the present predictions and the experimental data of Kawamura (1977) are presented in figures (7.7, 7.8, 7.9 and 7.10), and the predicted temperature profiles at different downstream locations (x/D=5, 10 and 20) are plotted in figures (7.11, 7.12 and 7.13). These experimental data were reported over an average length of five tube diameters, beginning at x/D=23; while the predictions in figures (7.7, 7.8, 7.9 and 7.10) are reported at x/D=25 for a water flow with an assumed (due to the lack of information about inlet and outlet temperatures) laminar Prandtl number of 7.2 and a Reynolds

number of 8740. The mean-bulk-fluid temperature and wall-temperature responses are shown in figures (7.7 and 7.8) respectively. Figures (7.9 and 7.10) give the time variations of the heat-transfer coefficient and the heat-transfer rate from the solid wall to the fluid respectively.

A comparison of the results given in figure (7.7) reveals that the predicted mean-bulk-temperature response is lower than the measured one; while the comparison, presented previously in figures (7.3 and 7.4), between the present predictions and the experimental data of Stuart (1956) shows the opposite to hold. This indicates that the predicted results lie between the experimental data of Stuart (1956) and Kawamura (1977) (if these results were reported for the same Reynolds number). However, the present results are still in acceptable agreement with Kawamura's data.

Figure (7.8) indicates that the present results for the wall-temperature response are lower than the experimental data, with a maximum difference of 14 percent; while the results given in figures (7.9 and 7.10) show that the present results for the time variations of the heat-transfer coefficient and the heat-transfer rate from the solid wall to the fluid are in good agreement with the corresponding experimental data.

The results presented in figure (7.9) also show that the heat-transfer coefficient behaves in a similar manner to the other variables and cannot be considered as a constant. This indicates that neither the application of the wall

functions (without modification to account for the transient effects) nor the use of quasi-steady assumptions is appropriate in the analysis of unsteady heat-transfer problems.

The results given in figure (7.10) show that although the solid wall was subjected to a sudden heat input the fluid was not, and, moreover, the heat transfer rate to the fluid reaches its steady-state value at almost the same time as do the other properties. This underscores the necessity of considering such unsteady problems as conjugate ones.

The temperature profile results given in figures (7.11, 7.12 and 7.13) at different times (t = 1.5, 3, 4.5, 6 and 7.5 seconds) show that the difference between the temperature profiles at the smallest time (t=1.5) is very small; this is as explained before, due to the heat transfer process being dominated by pure conduction over the whole pipe length at early times.

7.3 Comparison with the present experimental data

The present experiments, which were reported in Chapter 5, were conducted for a steady fully-developed pipe flow of water; the hydrodynamic properties were considered to be fully developed over a length of 47 pipe diameters. This length was followed by the heating section which provided the heating-boundary conditions. There, the outer surface wall-temperature responses were measured at seven locations (x/D = 4, 12.25, 27, 29.25, 31.5, 33.75 and 36; measured

from the end of the hydrodynamic-entrance length). The heating section was followed by the insulated test section in which the fluid-temperature response was measured at 11 locations and the outer surface wall-temperature response at four locations as shown in figure (5.3).

In order to perform the computations for the above conditions, a water flow with uniform properties (u, k, ε and T) was studied without heat-transfer over a length of 47 pipe diameters. Then, the heating boundary conditions were introduced, the heating length was divided into seven parts, every part representing one thermo-couple location, i.e. the dividing line between two consecutive zones lay midway between two successive thermo-couples. Over each zone, the temperature response was assumed to be the same as that obtained from a least-square-curve fit* of the measured temperature response at this location. In the remainder of the studied length a zero heat-transfer boundary condition was imposed on the outer surface of the pipe wall.

The comparisons between the predicted and measured temperature response data for two different Reynolds numbers (38000 and 49000) are shown in figures (7.14, 7.15 and 7.16) at down-stream distances of 6.25, 8.75 and 13.75 times of the pipe respectively. Figure (7.14) shows the results at four radial

---

* A polynomial of a fourth degree was used in this curve fitting.

locations in the flow (2y/D = 1., .6, .3 and .1) and one location at the outer surface of the pipe wall. Both the predicted and measured results at early time indicate that the increase in the Reynolds number serve to increase the temperature. This is due to the large velocities associated with the high Reynolds number which convect the thermal energy faster than the low velocities. However, at large time the high velocities associated with high mass flow rate decrease the temperature which was observed in both the predictions and the measurements. The results presented in figure (7.14) also show that the temperature increases towards the pipe wall, which is an expected trend.

The comparisons presented in figures (7.14a, 7.14b, 7.14c and 7.14d) reveal that the present predictions show acceptable agreement with the present experimental data.

The comparison of the wall-temperature results, given in figure (7.14c), shows a maximum difference of about 25 percent in the response rate. On the other hand, the present predictions of the wall-temperature response (presented previously in section (7.2)) showed that the predictions were in good agreement with the experimental data* of Kawamura (1977). This suggests that the relatively large differences between prediction and measurement in Fig (7.14e) could probably be due to the accuracy of the present measurements of the wall temperature. Errors could arise by the thermo-couple not being in good contact with the solid wall.

---

* These wall temperatures were obtained by measuring the electric resistance of the solid wall, i.e. not using a thermocouple.

The results given in figures (7.15a, 7.15b, 7.15c and 7.15d) at 2y/D = 1., .6, .3 and .1 distances respectively, show the same trends as those observed in figure (7.14). The comparison between the results of figures (7.14 and 7.15) indicate that the centreline temperature increases as the downstream distance increases; while the opposite is true close to the wall. This phenomena could be explained via proper understanding of the heat-transfer mechanism in both the heating and the test sections. In the heating section, since the heat was added through the pipe walls, it is expected that the maximum fluid temperature would be close to the wall. In the insulated test section, thermal energy would diffuse from the near wall region to the fluid core. The comparison between the predicted and measured temperature responses in figure (7.15) show an acceptable overal agreement.

The comparison between the wall-temperature response given in figures (7.14e and 7.15e) shows that the wall temperature at large time decreases as the downstream distance increases which was expected. However, the comparison between predicted and measured wall-temperature response given in figure (7.15e) is unsatisfactory. Furthermore, the comparison between the results of the steady-state-wall temperature given in figures (7.14e, 7.15e and 7.16d) shows that the measured wall - temperature decreases over the distance from x/D = 6.25 to 8.75 and then increases from x/D = 8.75 to 13.75, which is not to be expected. This

suggests that the measured wall temperatures reported in figure (7.15c) are in error.

The results given in figure (7.16) at x/D = 13.75, show the same trends as those observed in figures (7.14 and 7.15). The comparison between the predicted results and the experimental data presented in figure (7.16) shows an acceptable agreement. For this section, the wall-temperature response plotted in figure (7.16d) shows a better agreement with the experimental data than those shown in figures (7.14e and 7.15e).

7.4 Parametric Study

7.4.1 Reynolds-number effect

The time variations of the mean bulk fluid temperature and heat-transfer coefficient for two different Reynolds numbers (Re = 8.74×10^3 and 2×10^4) are given in figures (7.17 and 7.18) respectively. The latter shows the results at x/D=25 while the results are presented for different axial locations (x/D = 5, 10 and 20) in the former.

Comparison between the results given in figure (7.17) indicates that the time required to reach the steady state increases as the Reynolds number decreases and the same is true for the variation of the pure-conduction time with the Reynolds number. This behaviour as explained before in section (7.2), is due to the decrease in the fluid velocity associated with the decrease in the Reynolds number.

7.4.2 Laminar-Prandtl-number effect

The mean-bulk-fluid-temperature response is presented in figures (7.19 and 7.20) for fluids with laminar Prandtl numbers of .026 and .005 respectively. These results are given for a Reynolds number of 2×10^4 at three different downstream distances (x/D = 5, 10 and 20).

Figure (7.21) shows the time variation of the heat-transfer coefficient at a downstream location of x/D = 20 for fluids with a Reynolds number of $2. \times 10^4$ and different laminar Prandtl numbers (Pr_ℓ = .005, .026 and 7.2).

Comparison between the results given in figures (7.19 and 7.20) and those given in figure (7.17) for water with a

laminar Prandtl number of 7.2 and a Reynolds number of $2.x10^4$ shows that the time required to reach the steady state increases considerably with the decrease in the laminar Prandtl number. The comparison also shows a considerable change in the time of pure conduction. The increase in the time required to reach the steady state is mainly due to the changes in the mean-fluid velocity which have resulted from the changes in the physical properties (μ and ρ) from one fluid to another; the mean velocities were 0.14, .4208 and .75 for the laminar Prandtl numbers of 0.005, 0.026 and 7.2 respectively. As explained earlier in section (7.2), the time required to reach the steady state increases as the velocity decreases; while the increase in the pure conduction time observed as the laminar Prandtl number decreases is partially due to the decrease in the velocity and partially to the increase of the conduction.

The results given in figure (7.21) reveal that the heat-transfer coefficient changes smoothly with time for the laminar Prandtl numbers of 7.2 and .026, but this is not so for the laminar Prandtl number of .005. This is because, at the smallest laminar Prandtl number, the time of pure conduction (x/u) is approximately 4.4 seconds, which is relatively large. Consequently, temporary steady state due to conduction has been established before the convection starts to affect the results.

7.4.3 Result of a step jump in the inlet fluid temperature

The mean-bulk fluid, and inner and outer wall temperatures

are given in figures (7.22 and 7.23) respectively for water flow with a Reynolds number of 2. x 10^4 and a laminar-Prandtl-number of 7.2 and subjected to a step jump in the inlet temperature of 120^{o}C, while the outer surface of the pipe is insulated. In each of these figures the results are plotted at four downstream locations (x/D=5, 10, 20 and 30).

The results reported in figure (7.22) indicate that, initially, the mean-bulk-fluid temperature is zero over a time interval which is equivalent to the time of pure conduction when the heating takes place through the solid wall. This time of zero temperature changes depends on the fluid velocity and the downstream distance, and approximately equal to the latter devided by the former. The results also show that the time required to reach the steady state increases as the downstream distance increases while the opposite is true for the slope of the temperature response. The change in the slope is mainly due to the change in the heat-transfer coefficient, the heat-transfer coefficient decreasing with increasing time and also with increasing downstream distance.

The wall-temperatures responses presented in figure (7.23) show that the time of zero temperature response at each downstream location is larger than the corresponding time in the flow. This is because the heat is convected at the centreline faster than that close to the wall, and with the small conduction associated with high-laminar-Prandtl-number fluids one would expect such a delay in the wall response. The results also show a large difference between the inner and outer wall

temperatures at early times and this difference disappears as the steady state is reached. This is mainly due to the zero temperature gradient imposed at the outer pipe wall, this condition implies a zero gradient at the inner wall when the steady state is reached and consequently, the result is a uniform radial temperature profile in the solid wall.

The comparison between the time required to reach the steady state in the solid wall and in the flow at the same downstream distance indicates that the former is greater than the latter and the difference decreases as the downstream distance increases. This is again due to the large convection and the small diffusion in the flow under consideration.

7.5 Concluding Remarks

In this chapter, the predictions of the unsteady conjugate heat-transfer characteristics have been compared with previous and present experimental data. The comparisons show that the results obtained with a composite model of turbulence are generally in good agreement with the experimental data over a wide range of Reynolds numbers for water flows.

Prediction results for a wide range of laminar Prandtl numbers and for a different transient thermal boundary condition are also presented.

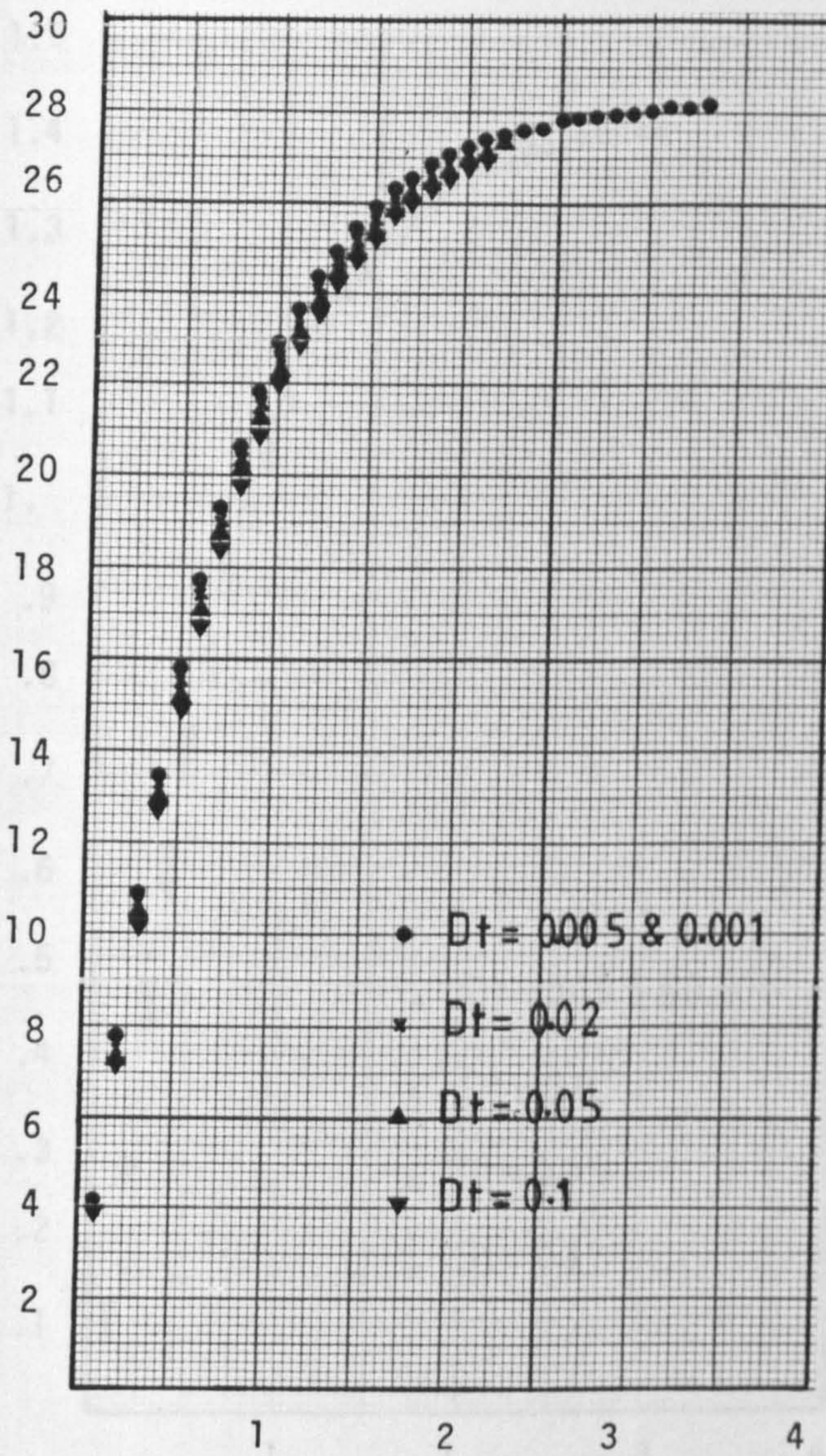


Fig (7.1) Effect of time step on the inner wall temperature.

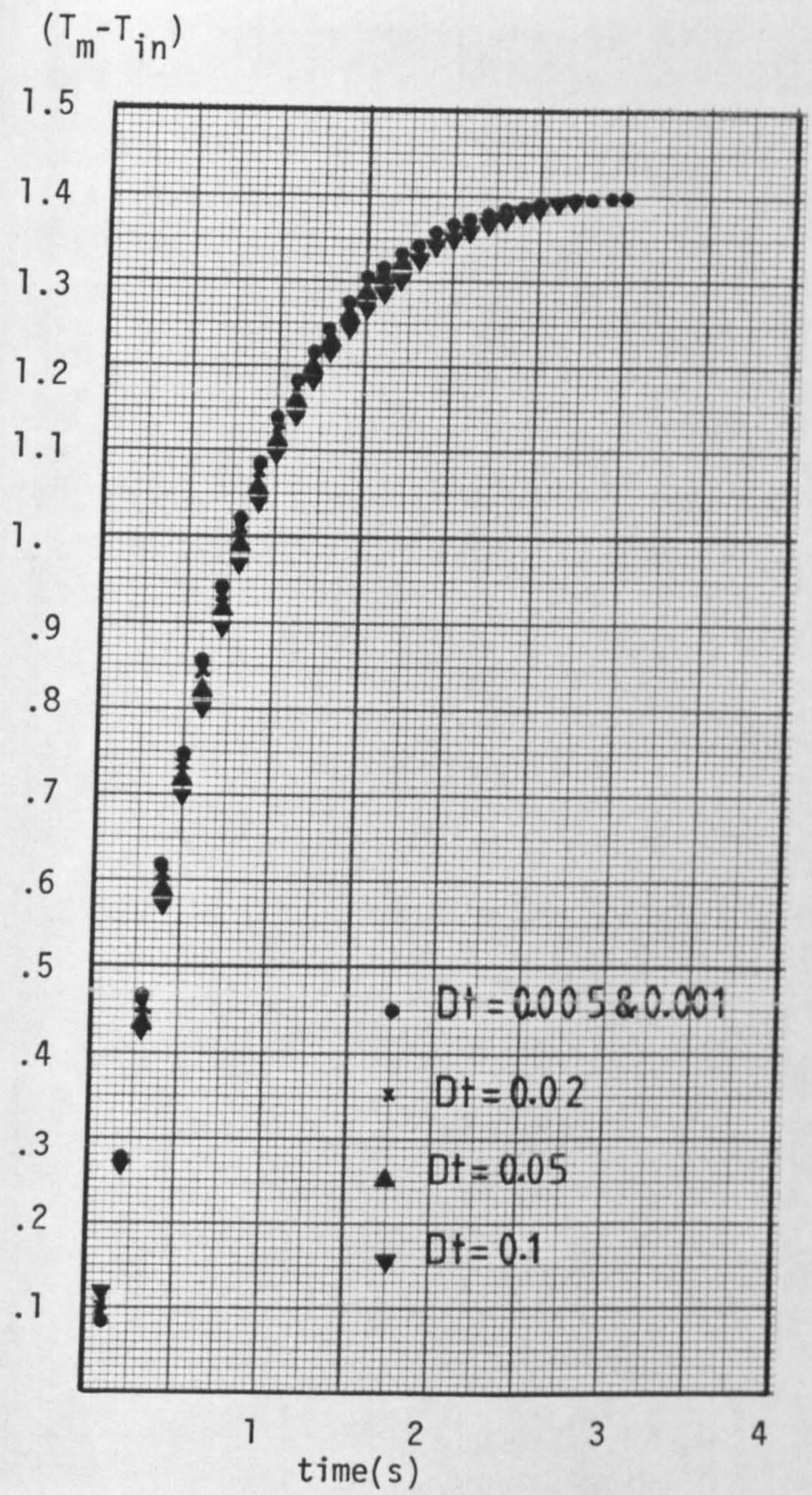


Fig (7.2) Effect of the time steps on the mean bulk temperature

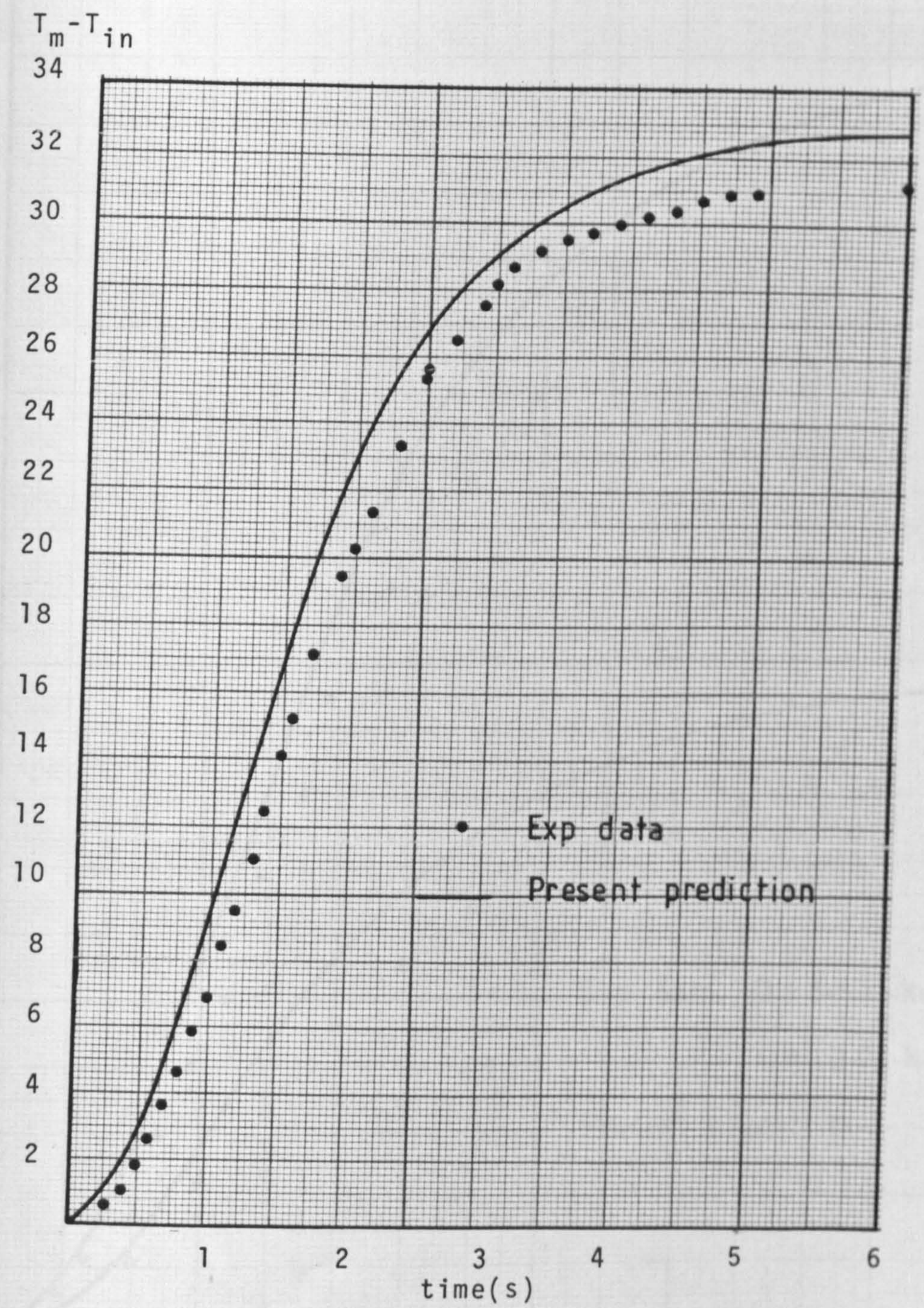


Fig (7.3) Comparison of the fully developed (x/D=70) mean fluid temperature response with the experimental data of Stuart (1956), for water with a Reynolds number of 6720.

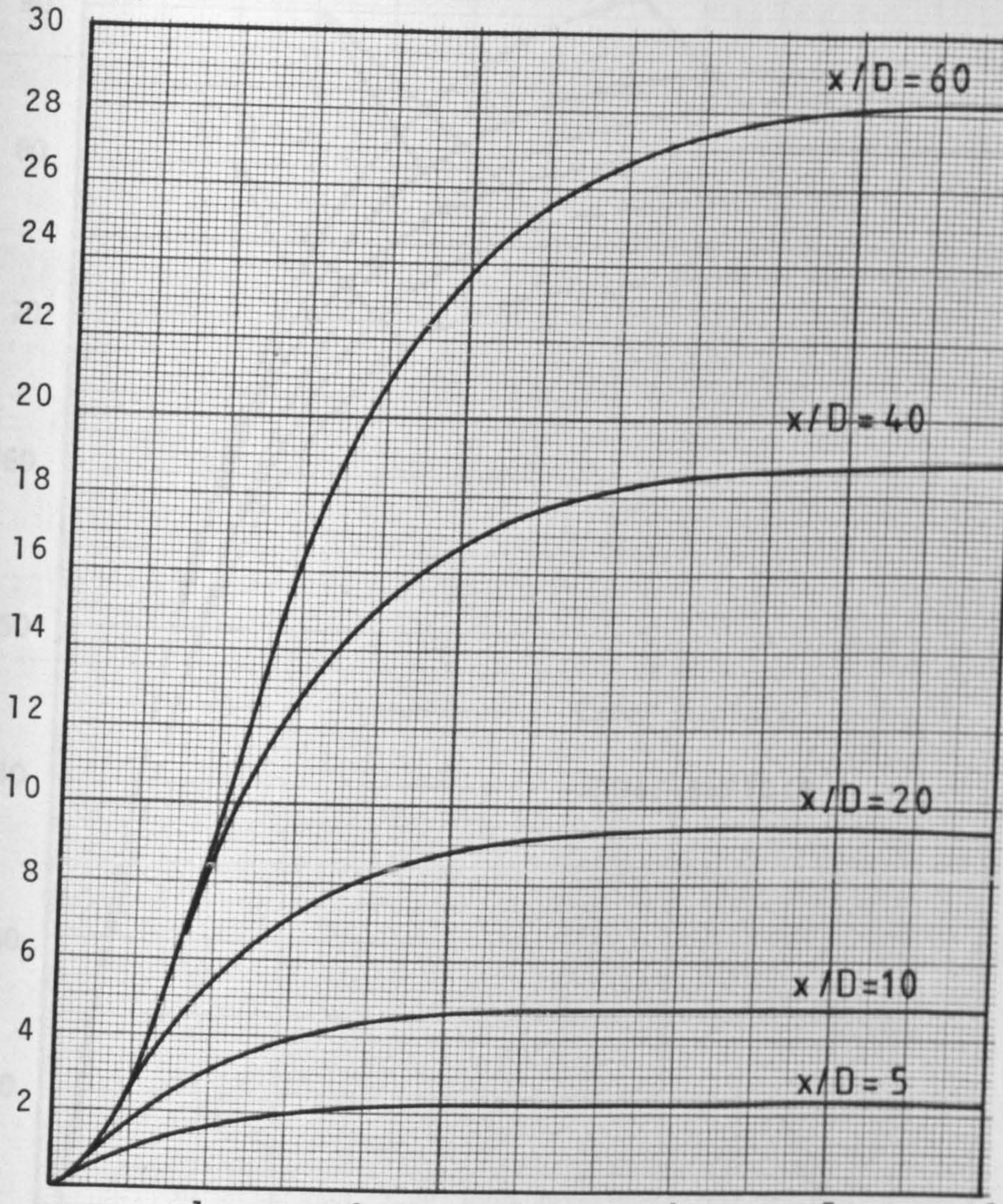


Fig (7.5) Mean fluid temperature responses at differ downstream locations for water fluid with Reynolds number of 6720

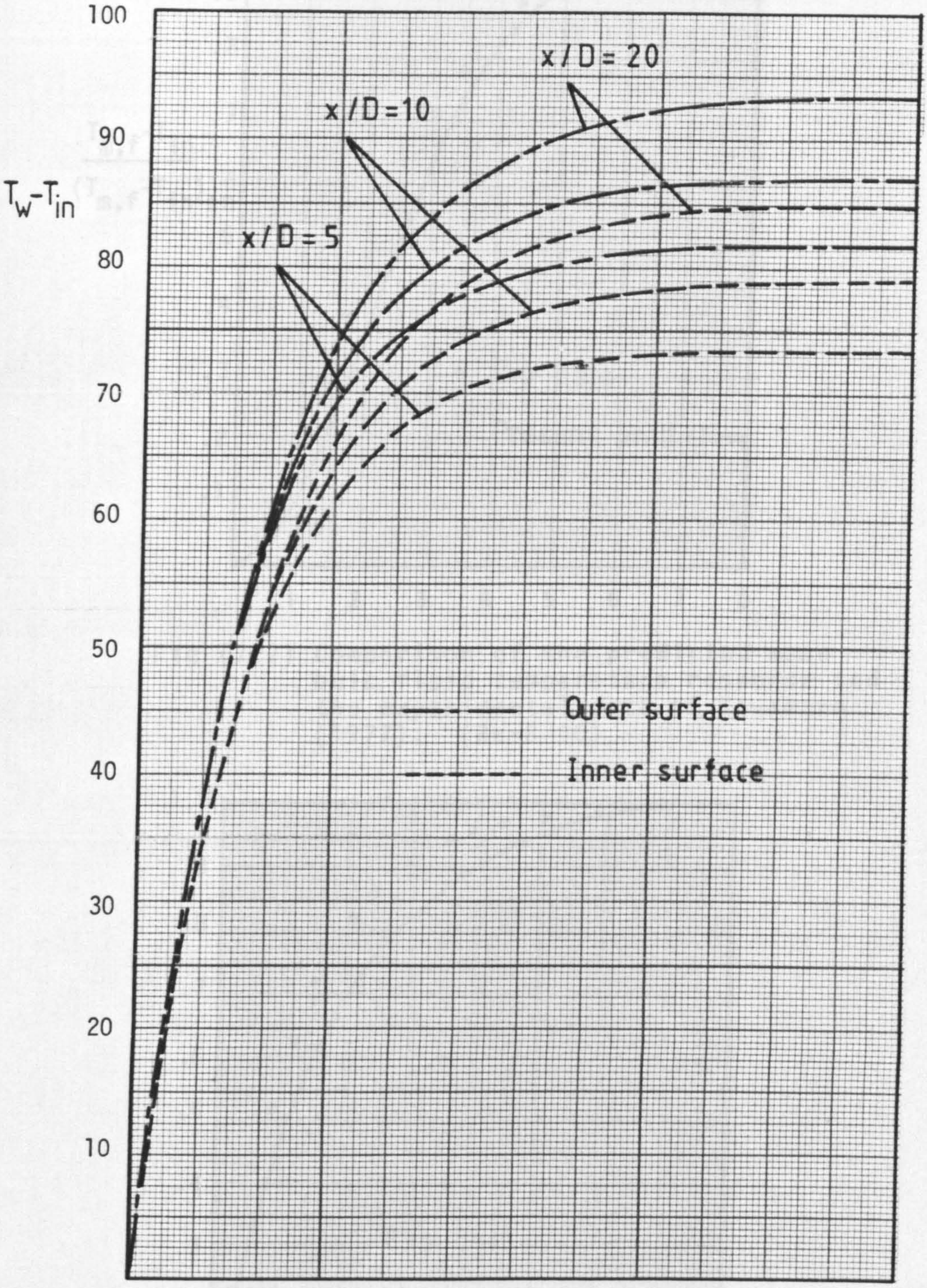


Fig (7.6) Inner and outer wall temperature responses at different downstream locations for water fluid with a Reynolds number of 6720

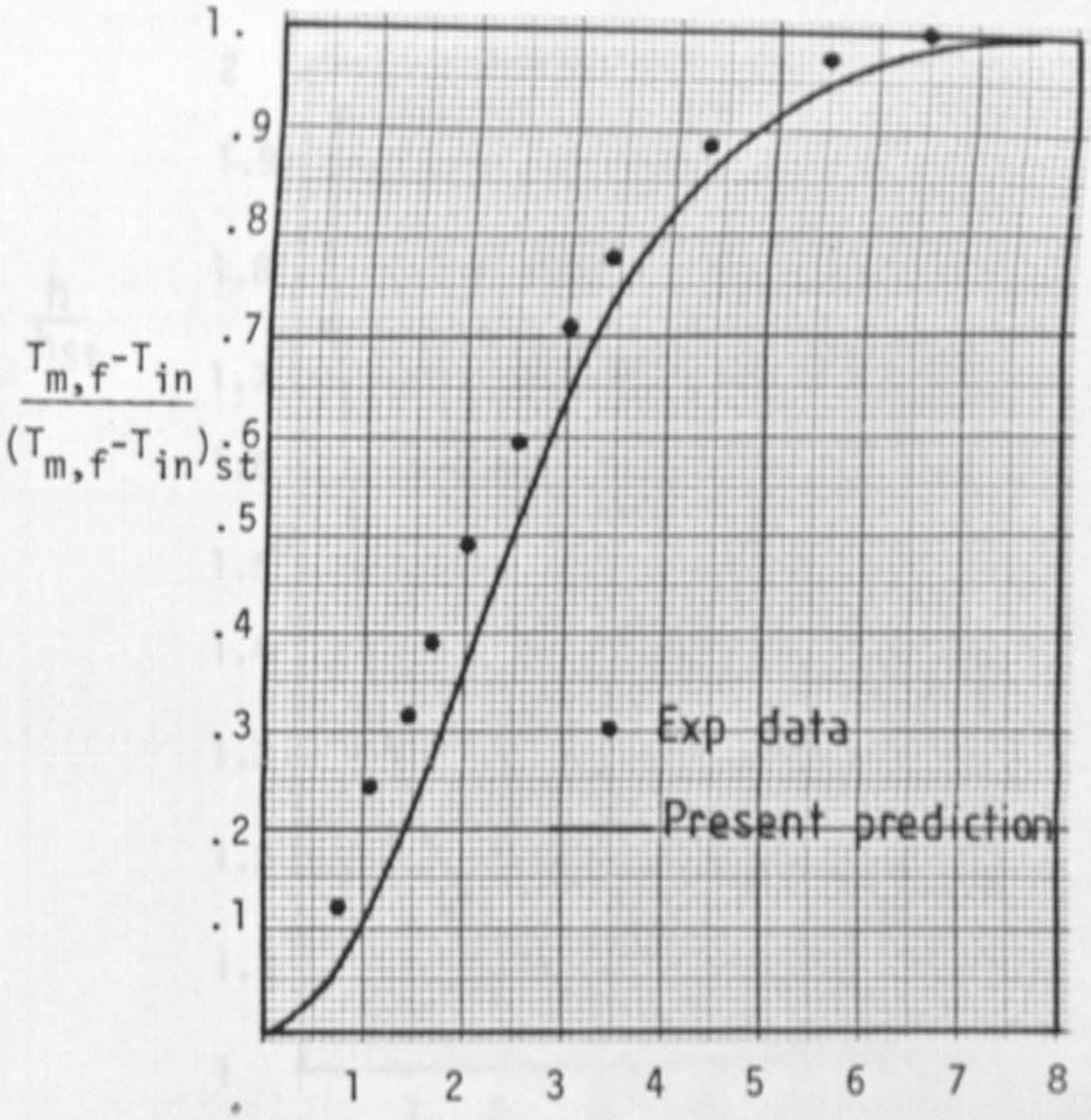


Fig (7.7) Comparison of the predicted mean bulk fluid temperature response and the experimental data of Kawamura (1977); (*Re=8740*)

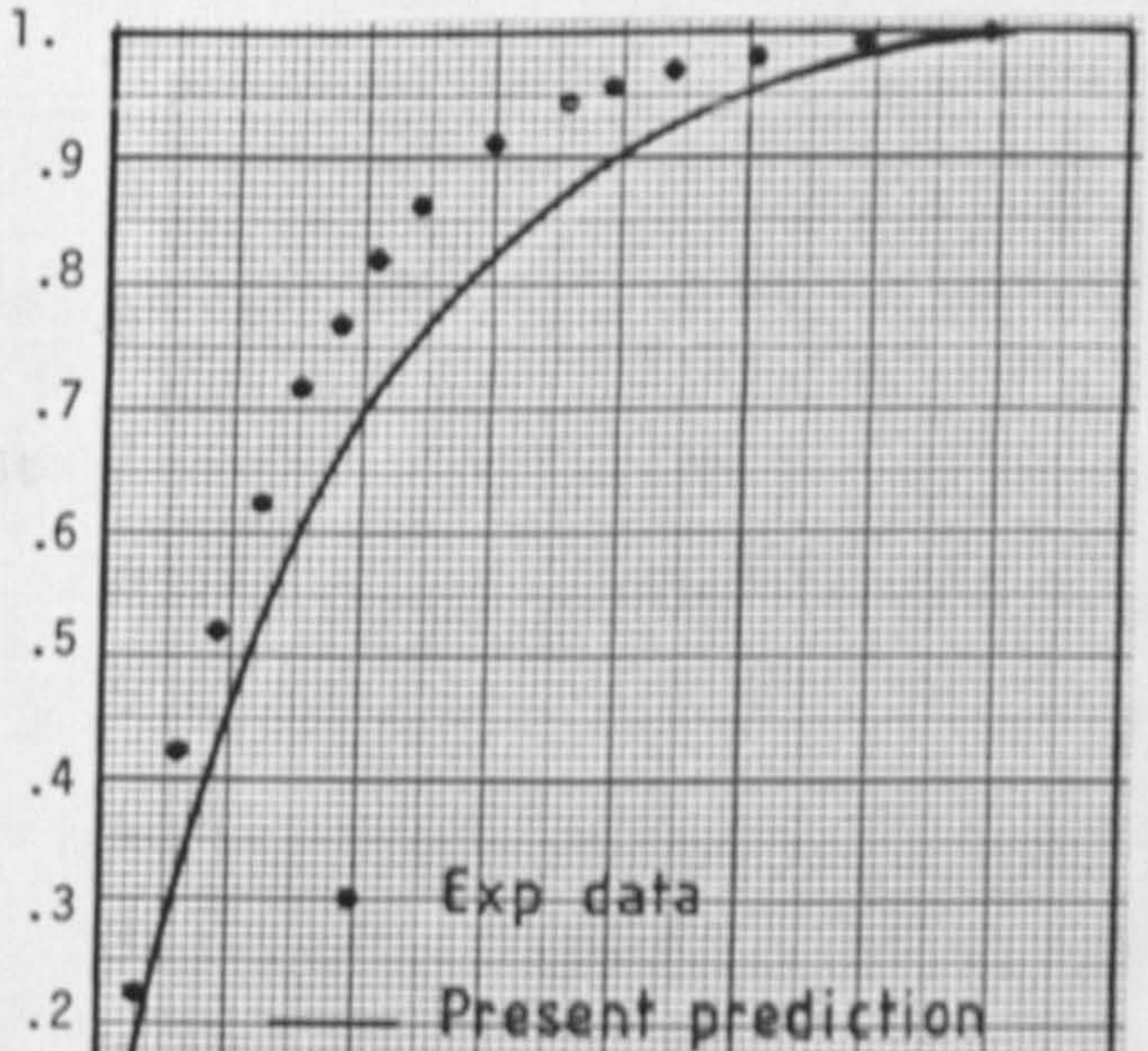


Fig (7.8) Comparison of the predicted wall temperature with the experimental data of Kawamura (1977); (Re=8740)

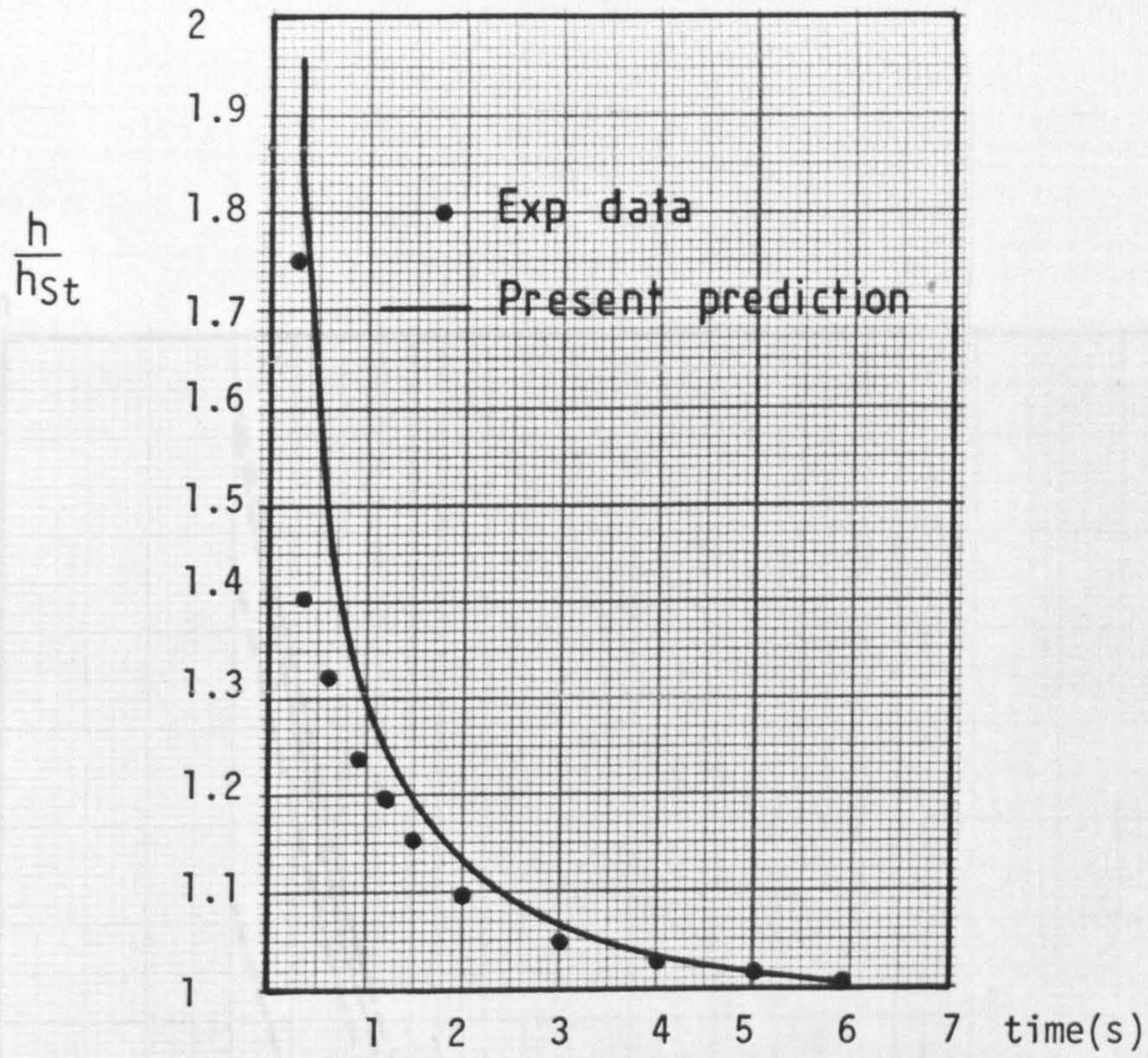


Fig (7.9) Comparison of the predicted heat-transfer coefficient with the experimental data of Kawamura (1977); (Re = 8740)

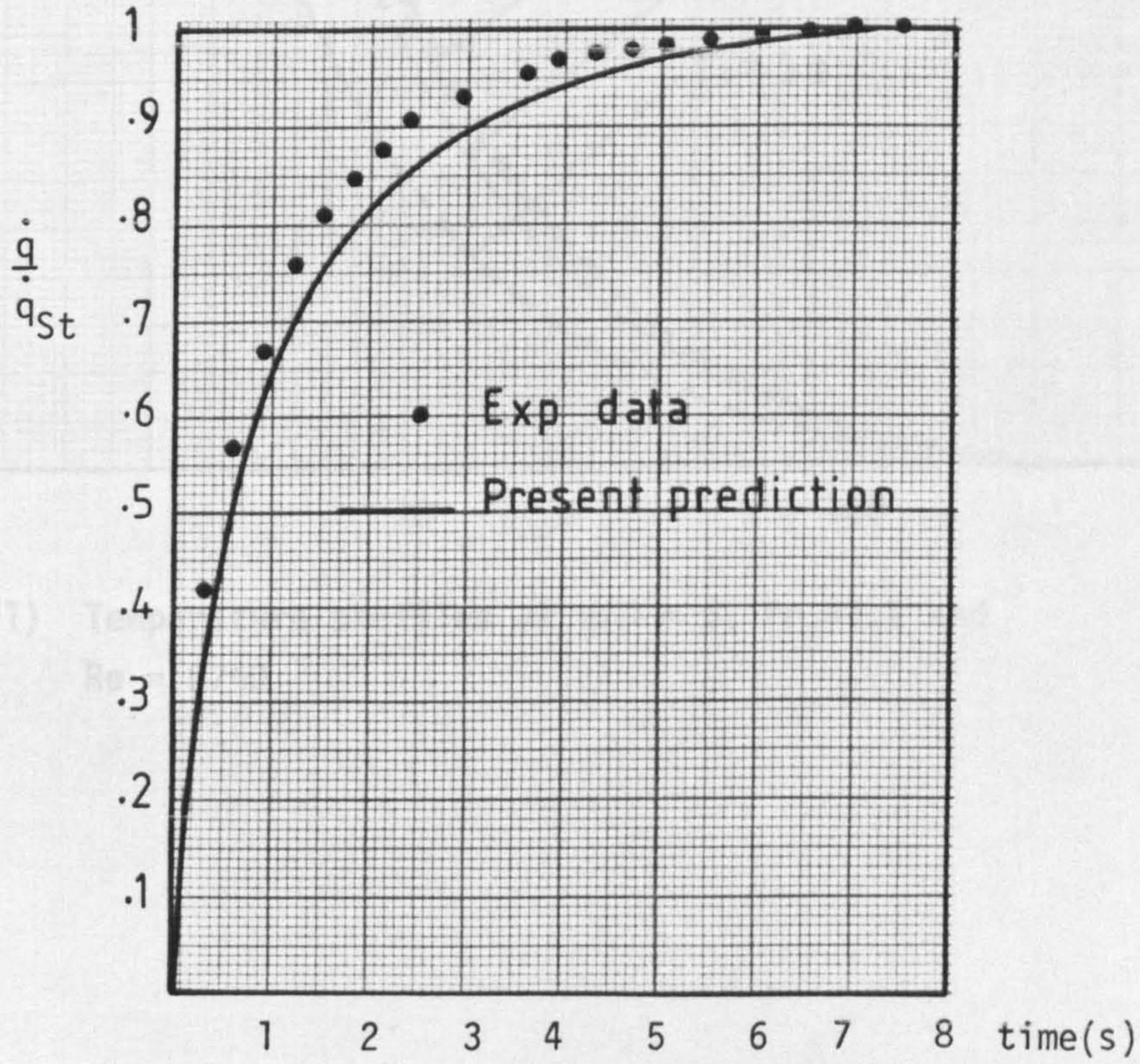


Fig (7.10) Comparison of the predicted heat-transfer response with the experimental data of Kawamura (1977); (Re = 8740)

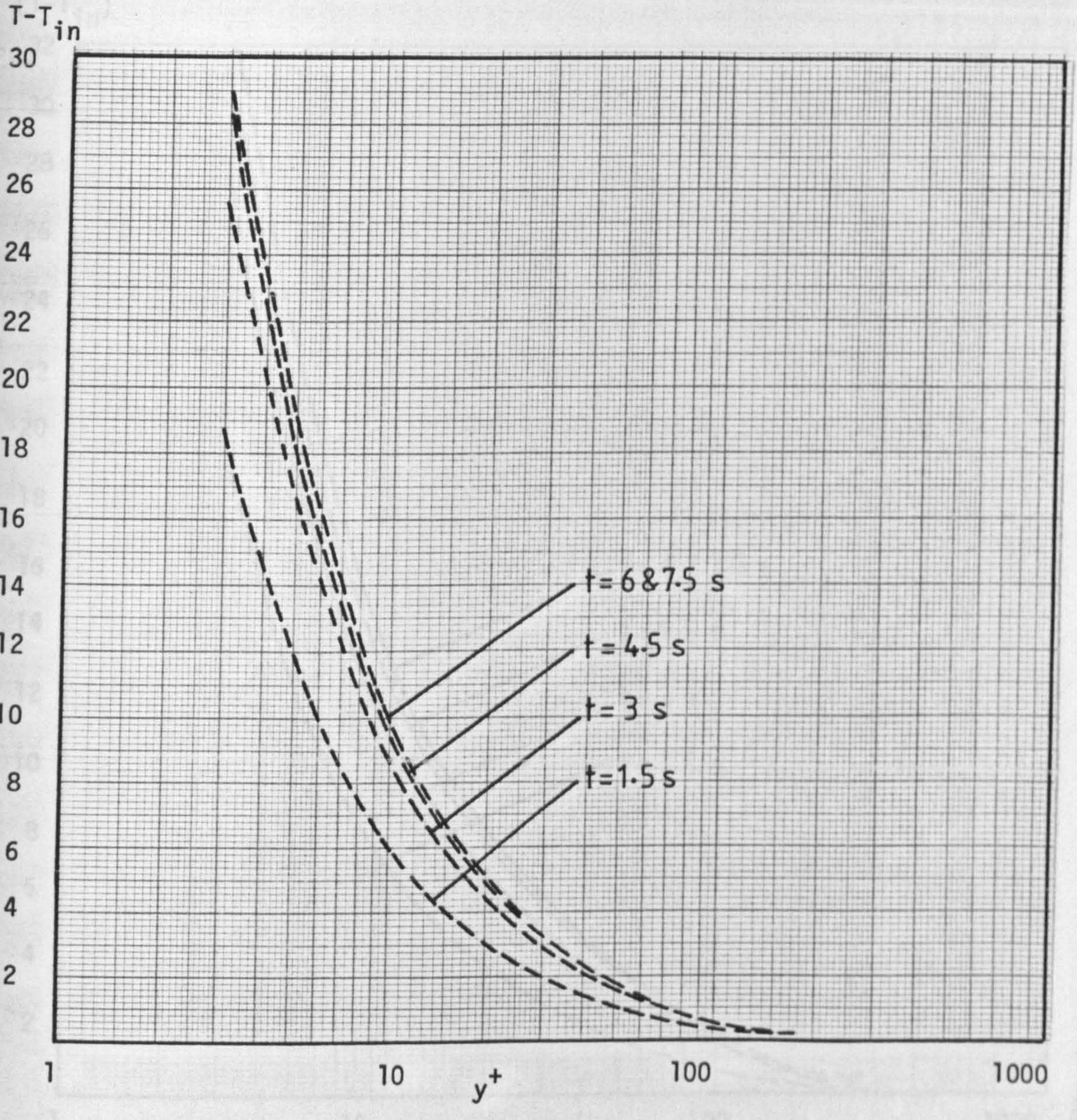


Fig (7.11) Temperature profiles at x/D = 5, Pr_{ℓ}=7.2 and Re = 8740

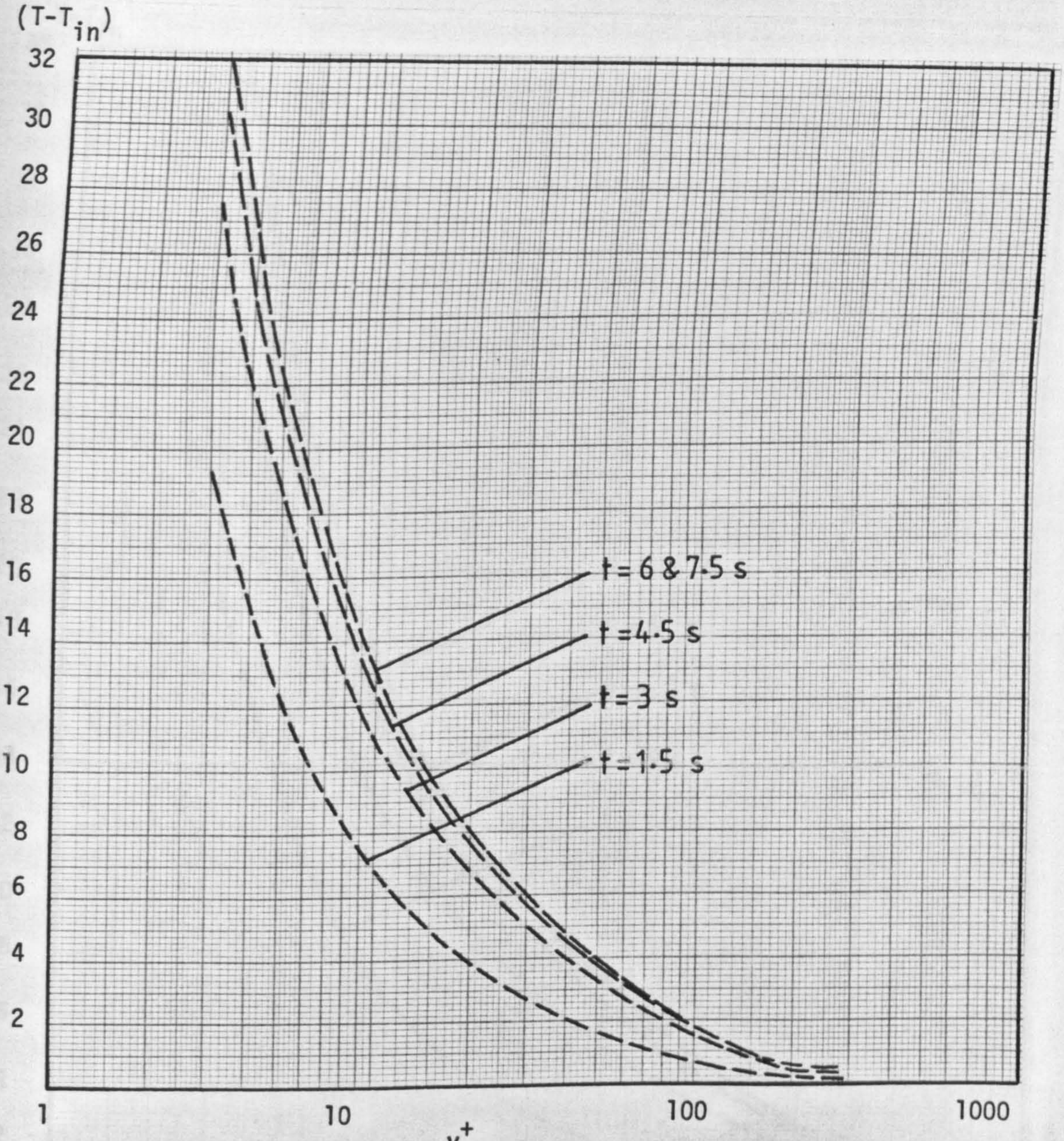


Fig (7.12) Temperature profiles at x/D = 10, Pr_{ℓ}=7.2 and Re=8740

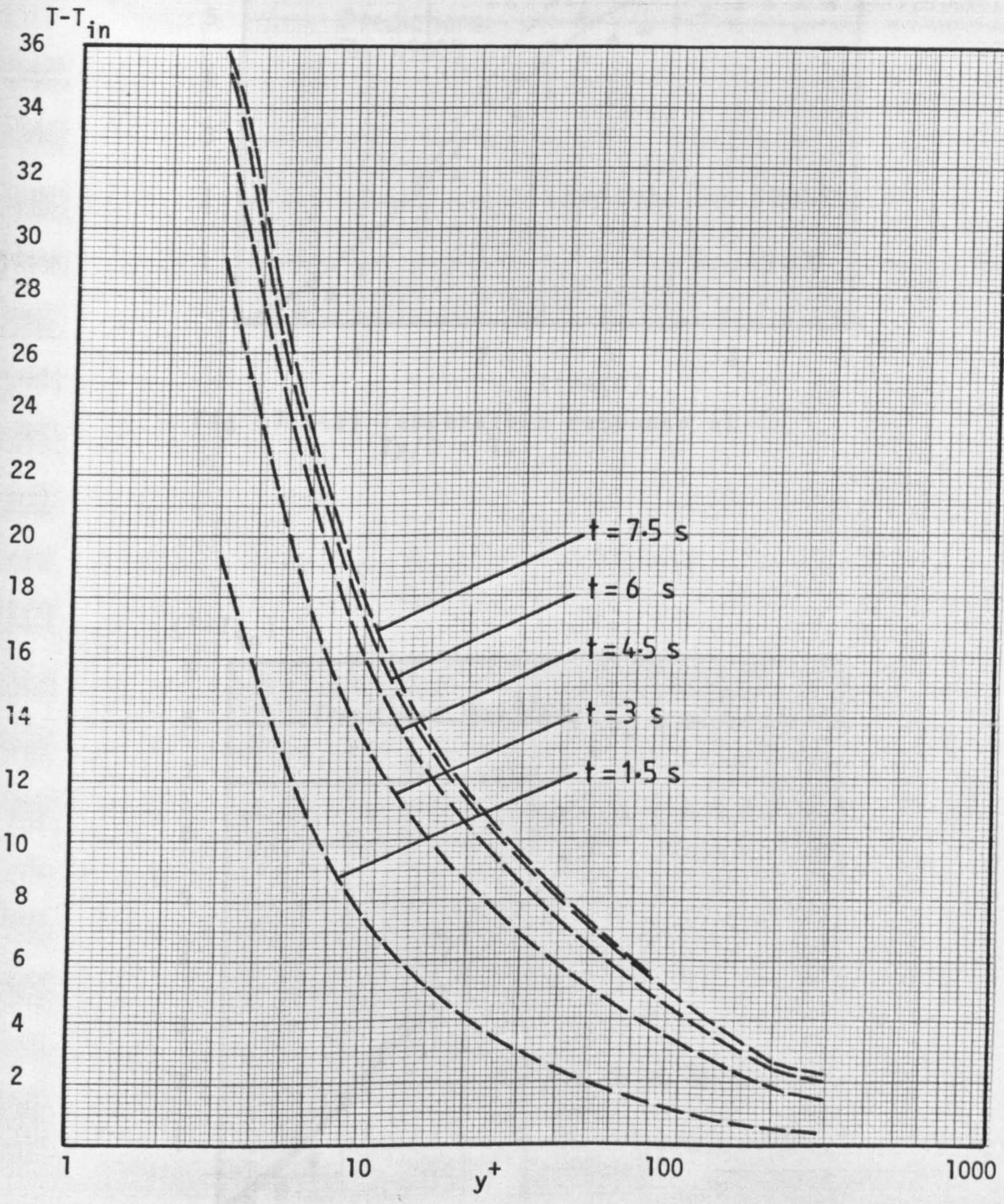


Fig (7.13) Temperature profiles at x/D=20, Pr_ℓ=7.2 and Re=8740

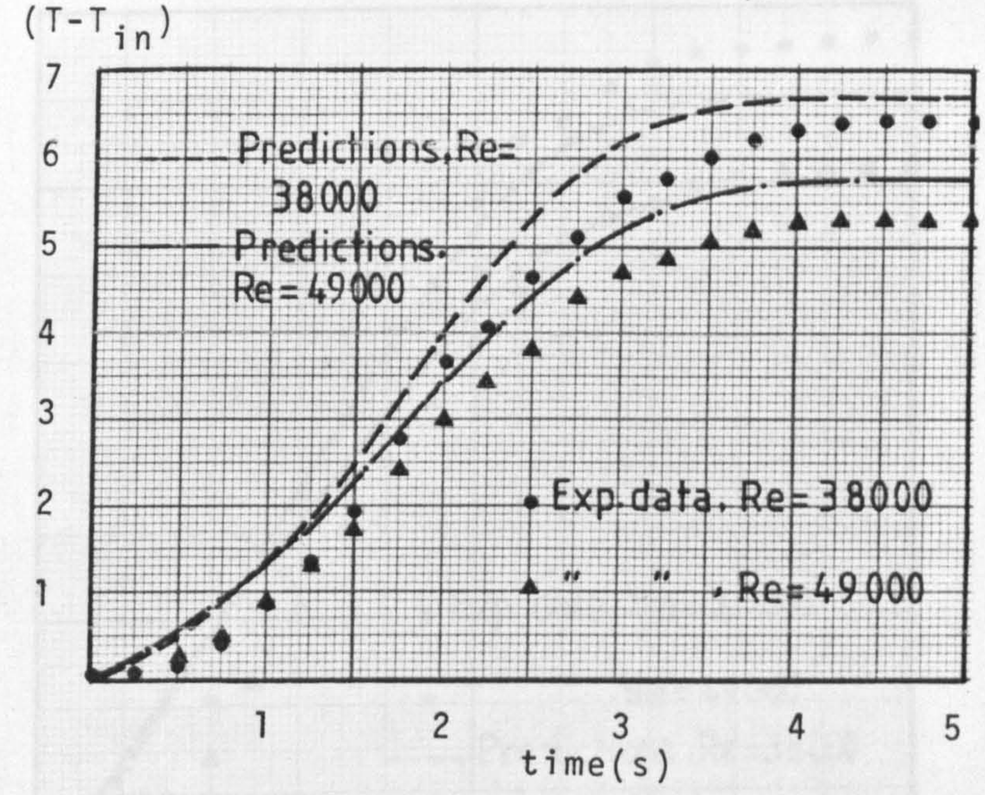


Fig (7.14a) Temperature response at 2y/D = 1.

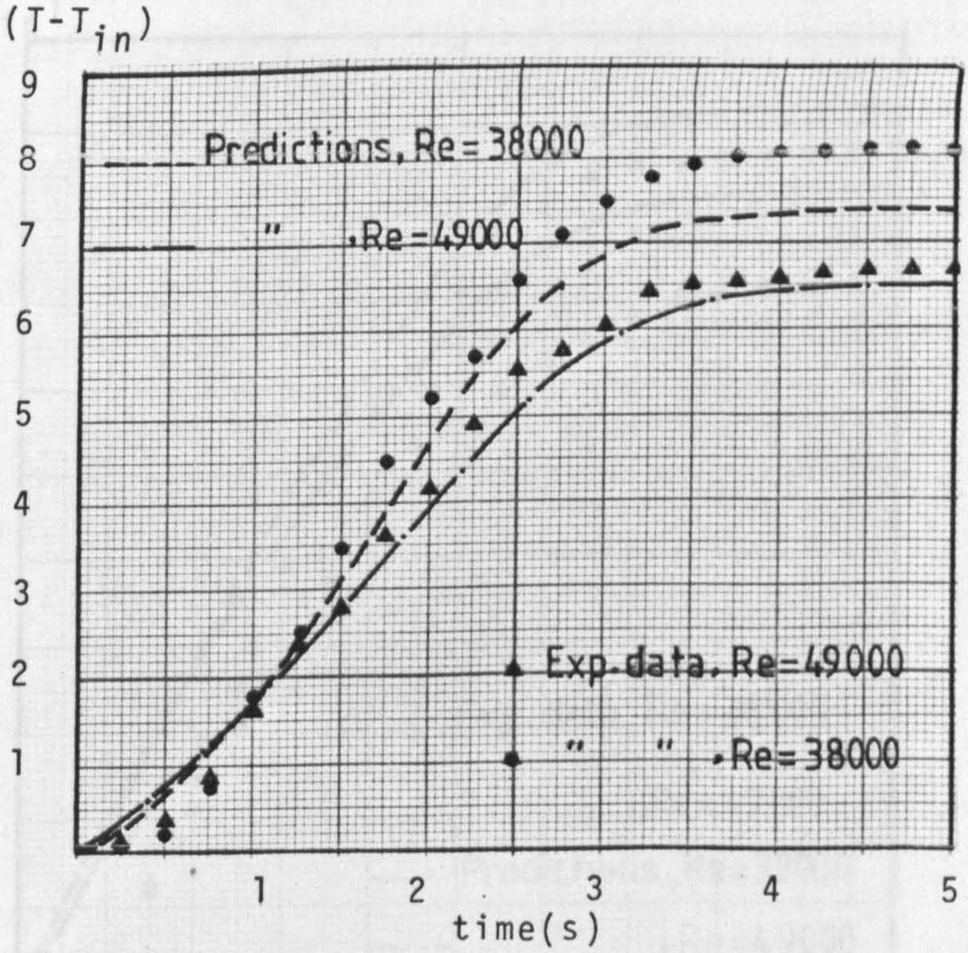


Fig (7.14b) Temperature response at 2y/D = 0.6

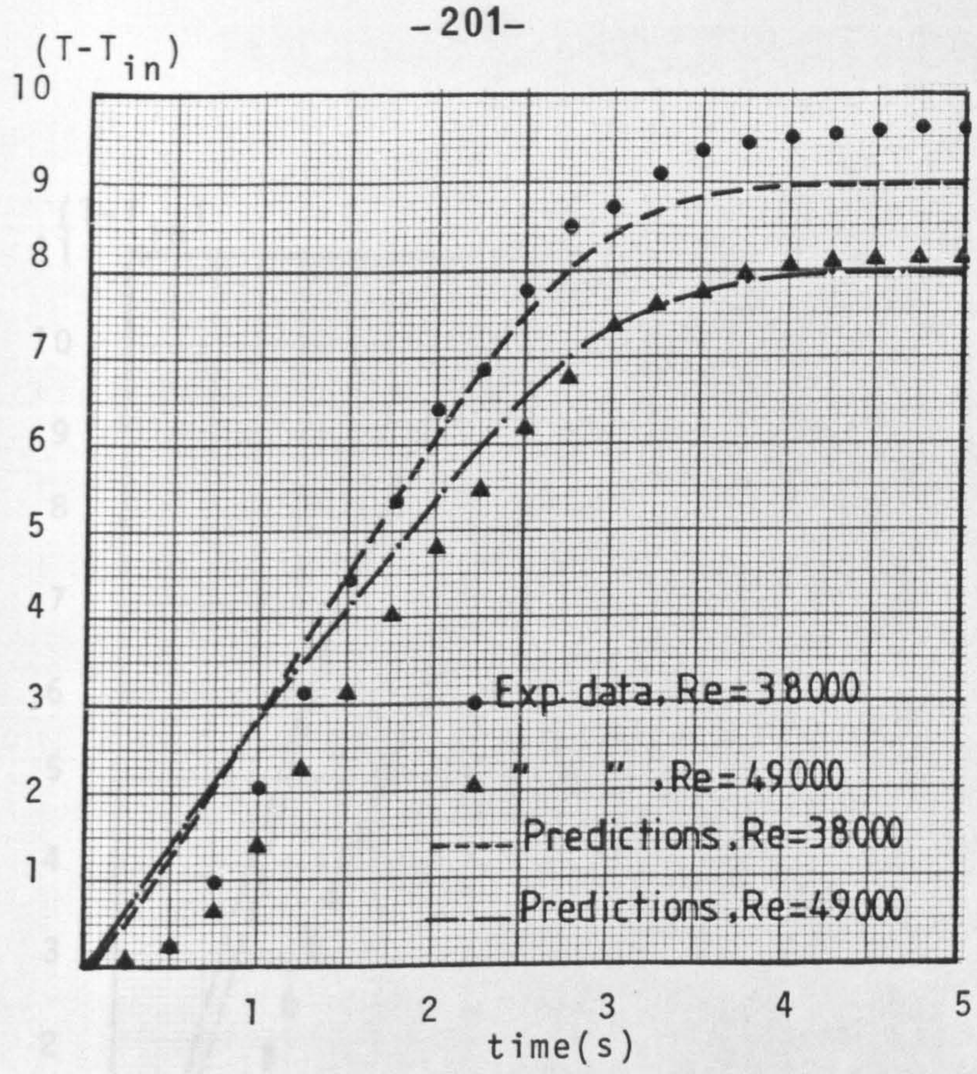


Fig (7.14c) Temperature response at 2y/D = .3

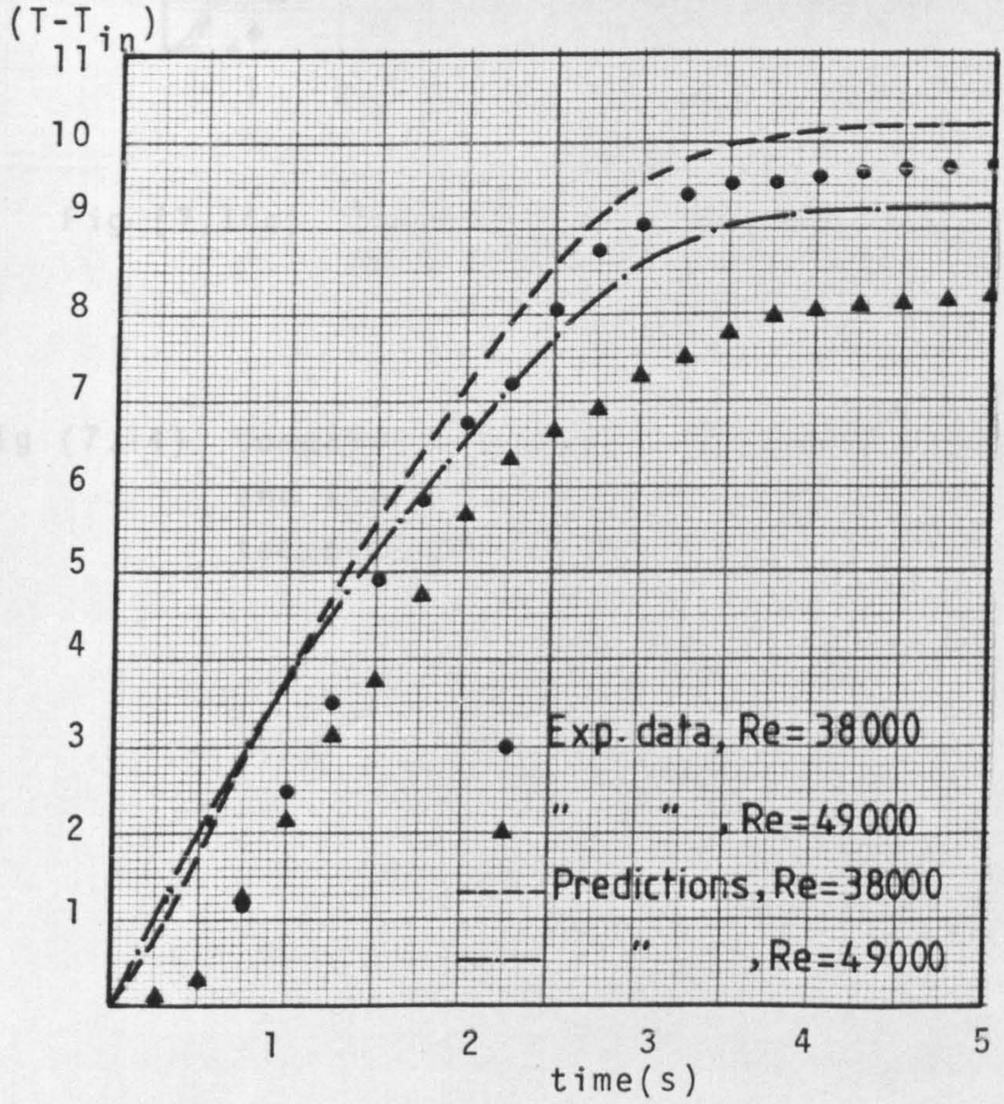


Fig (7.14d) Temperature response at 2y/D = .1

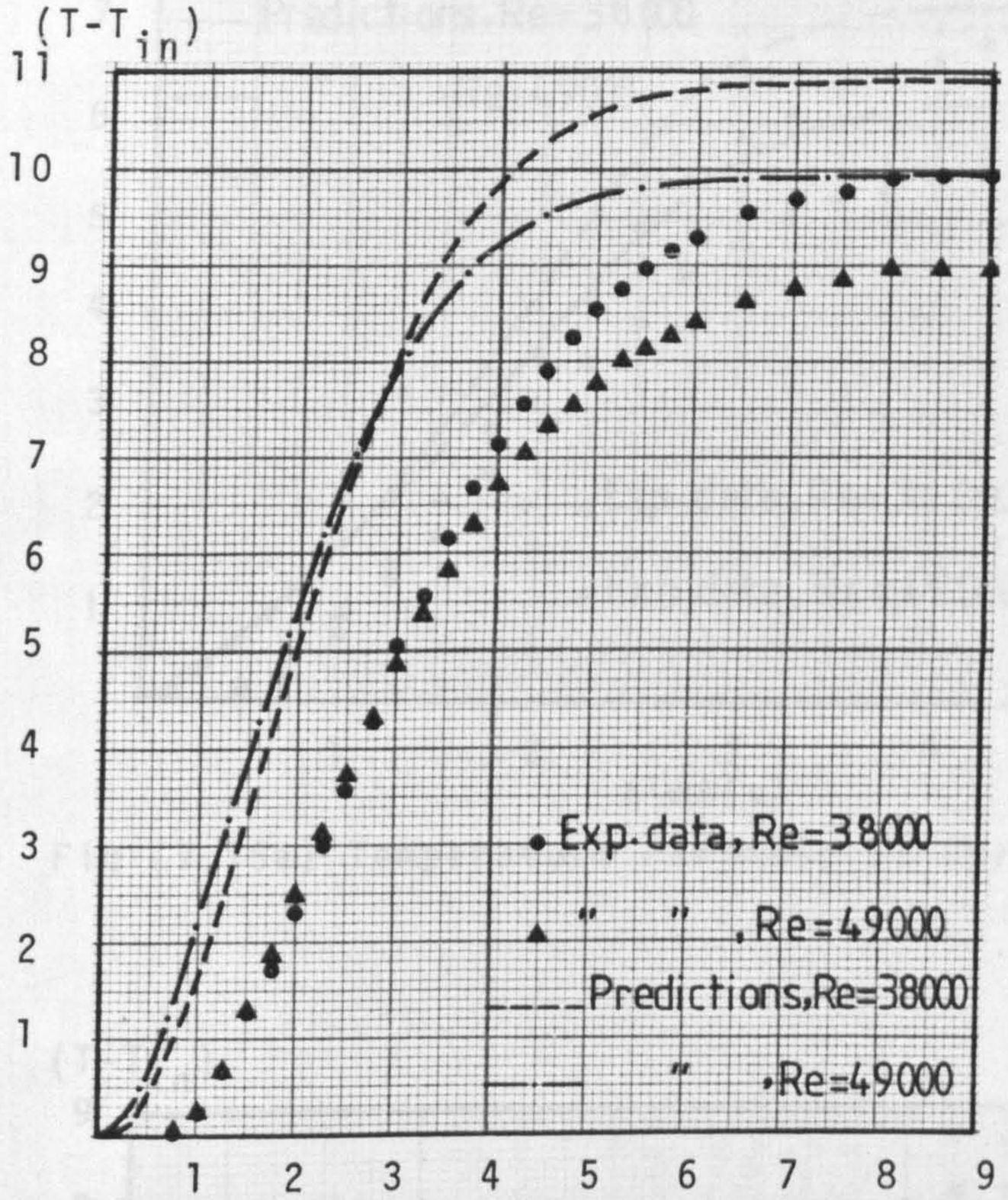


Fig (7.14e) Temperature response on the outer surface of the tube wall

Fig (7.14) Comparison between the present predictions and the present measurements of the temperature responses at x/D = 6.25

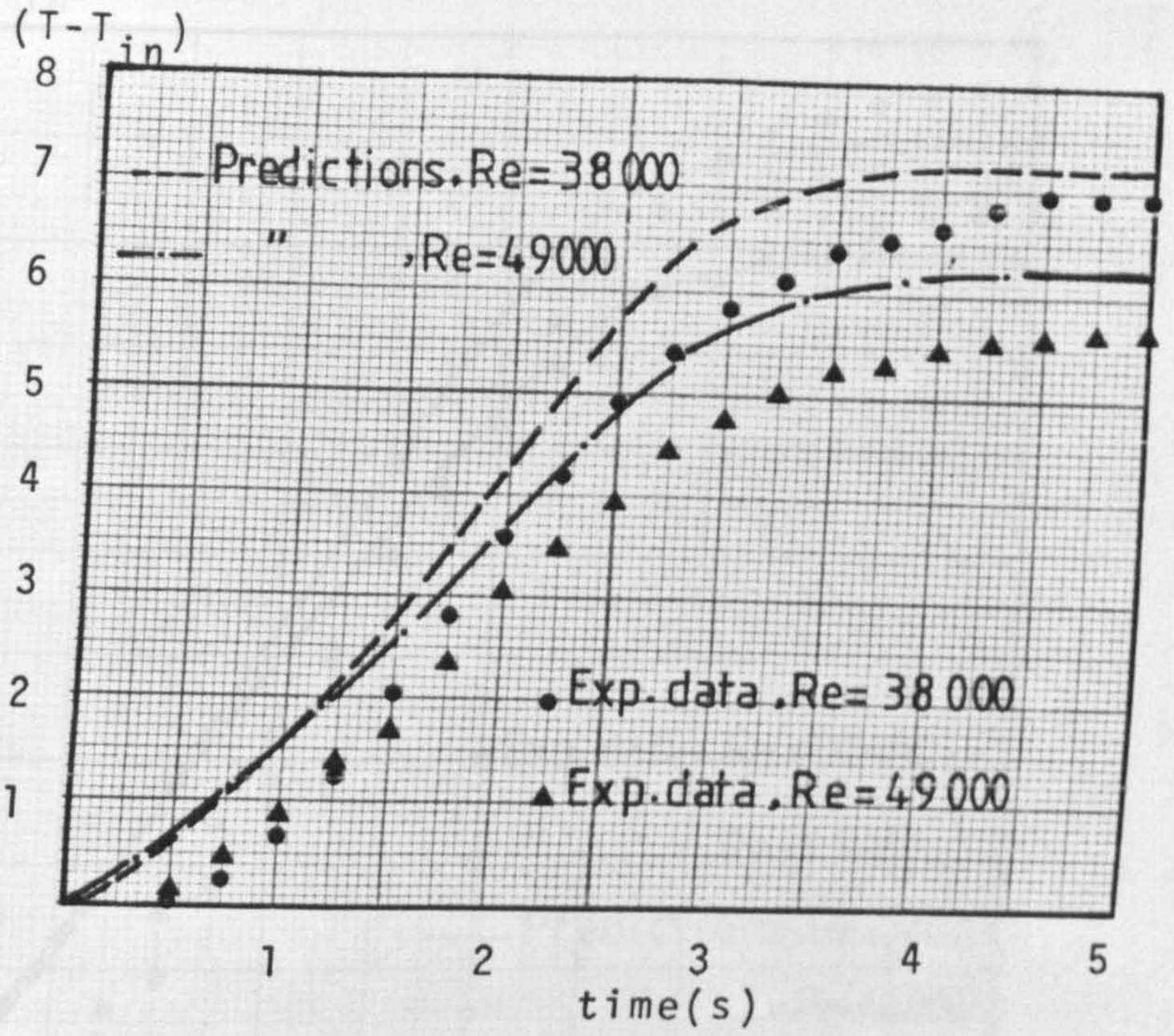


Fig (7.15a) Temperature response at $2y/D = 1$.

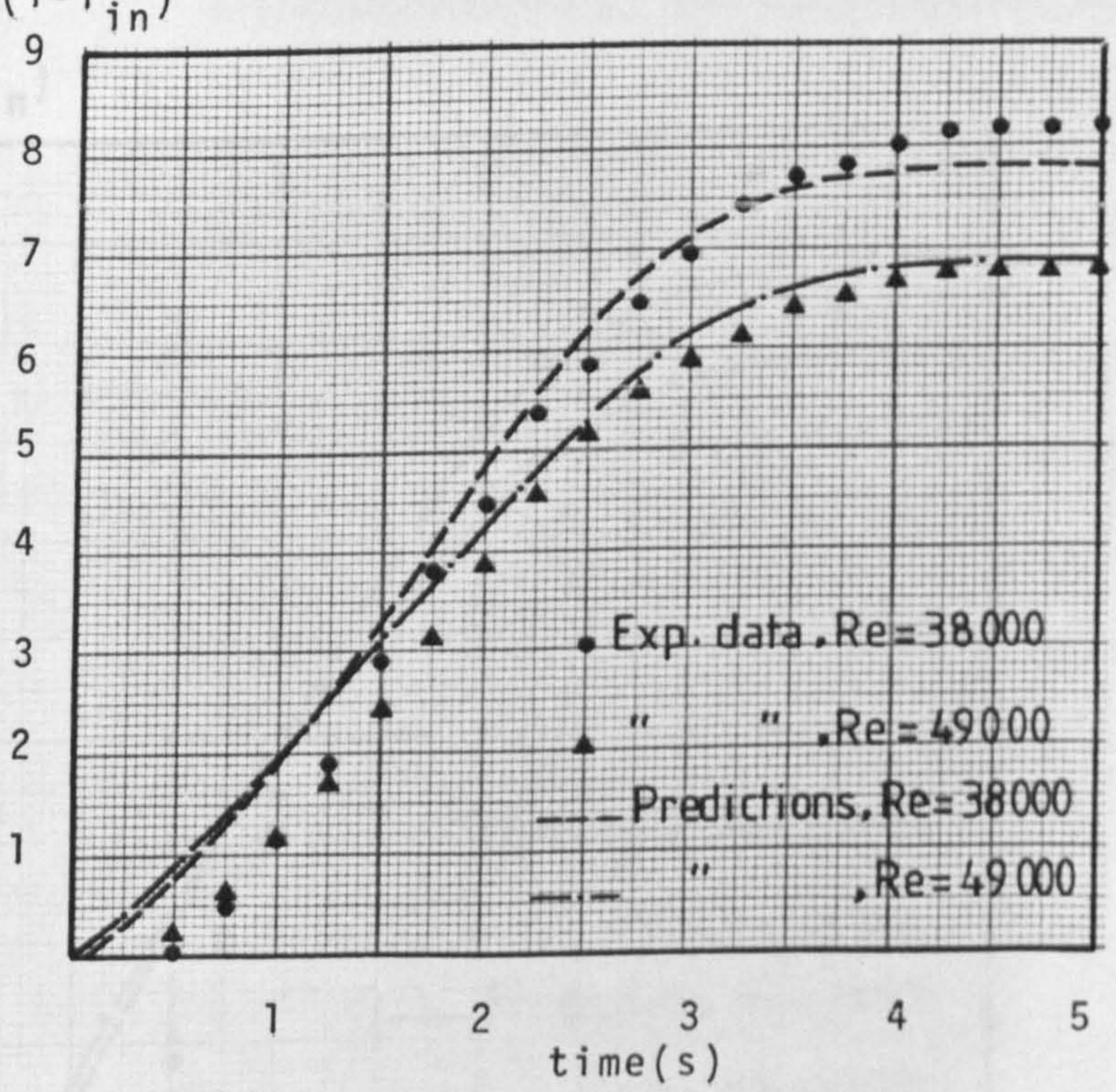


Fig (7.15b) Temperature response at $2y/D = 0.6$

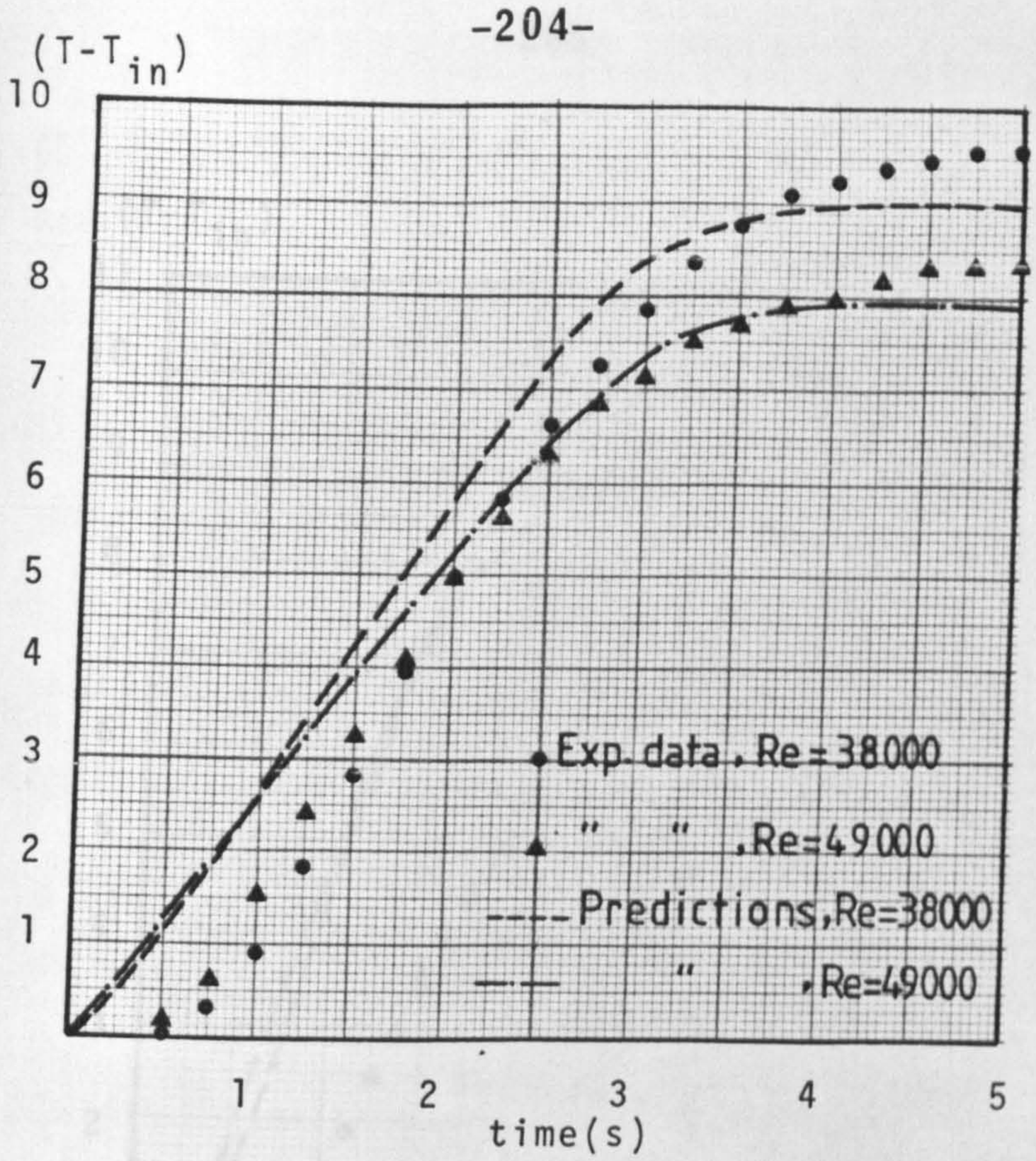


Fig (7.15c) Temperature response at 2y/D = .3

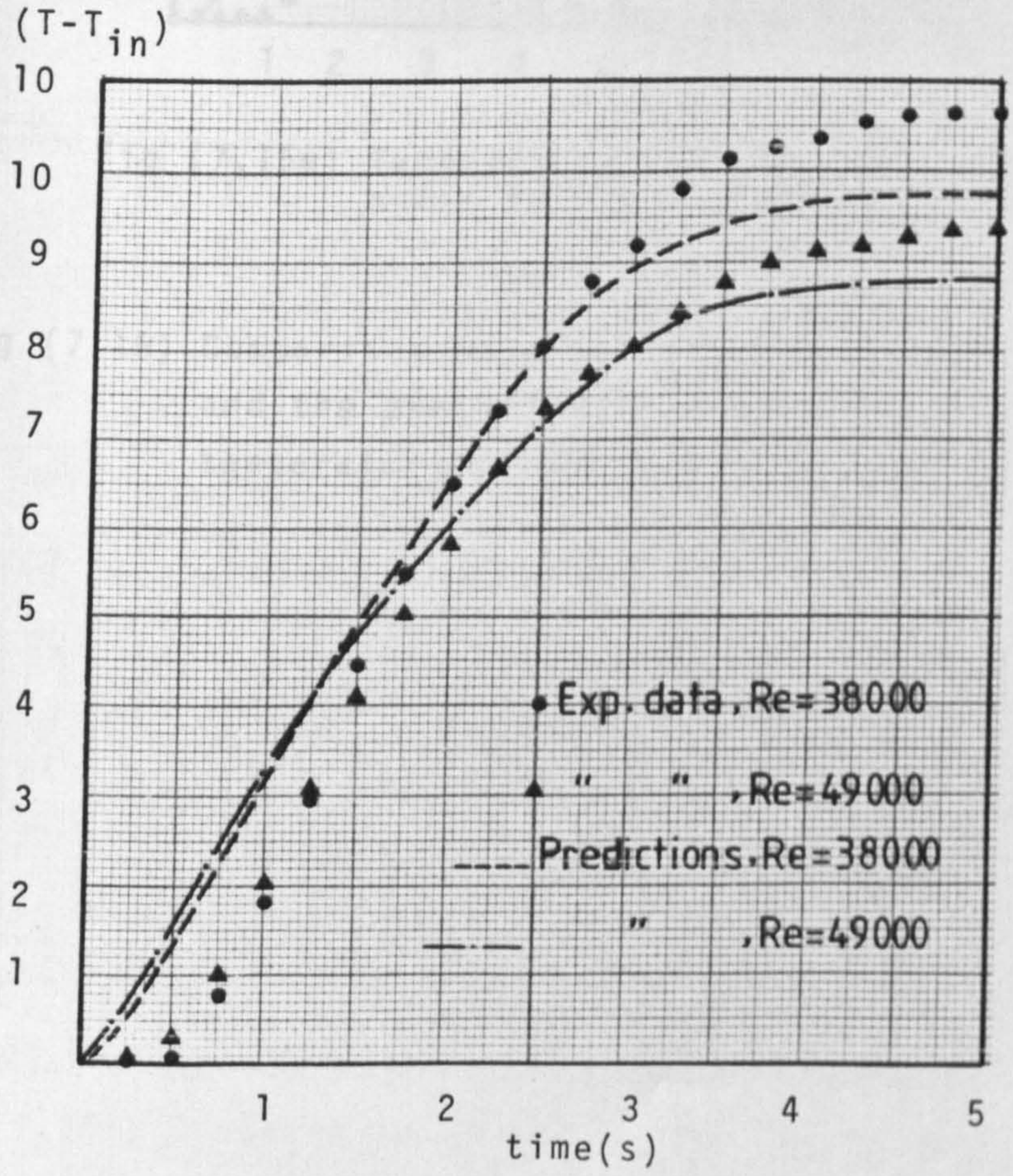


Fig (7.15d) Temperature response at 2y/D = 0.1

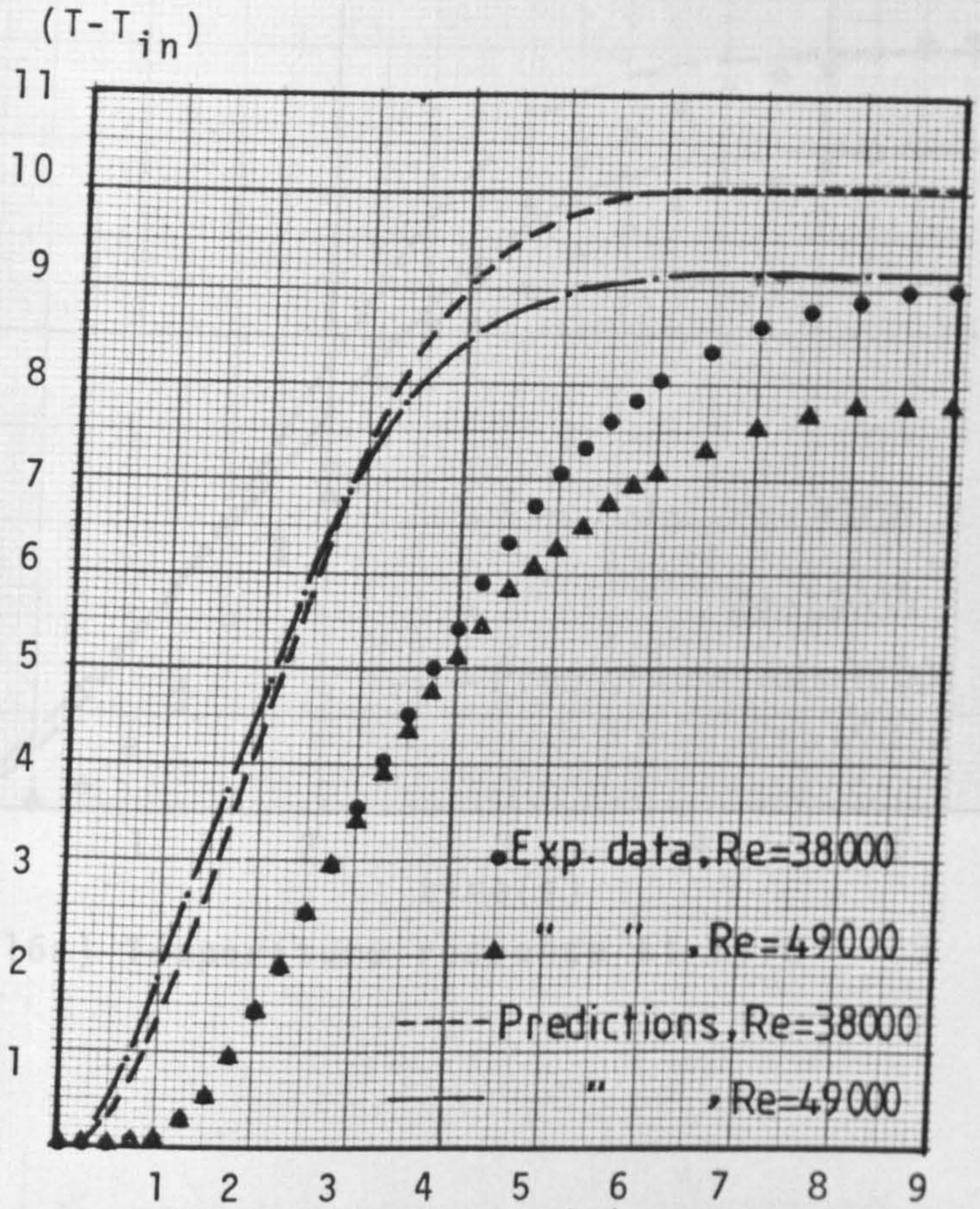


Fig (7.15e) Temperature response on the outer surface of the pipe wall

Fig (7.15) Comparison between the present predictions and the present measurements of the temperature response at x/D = 8.75

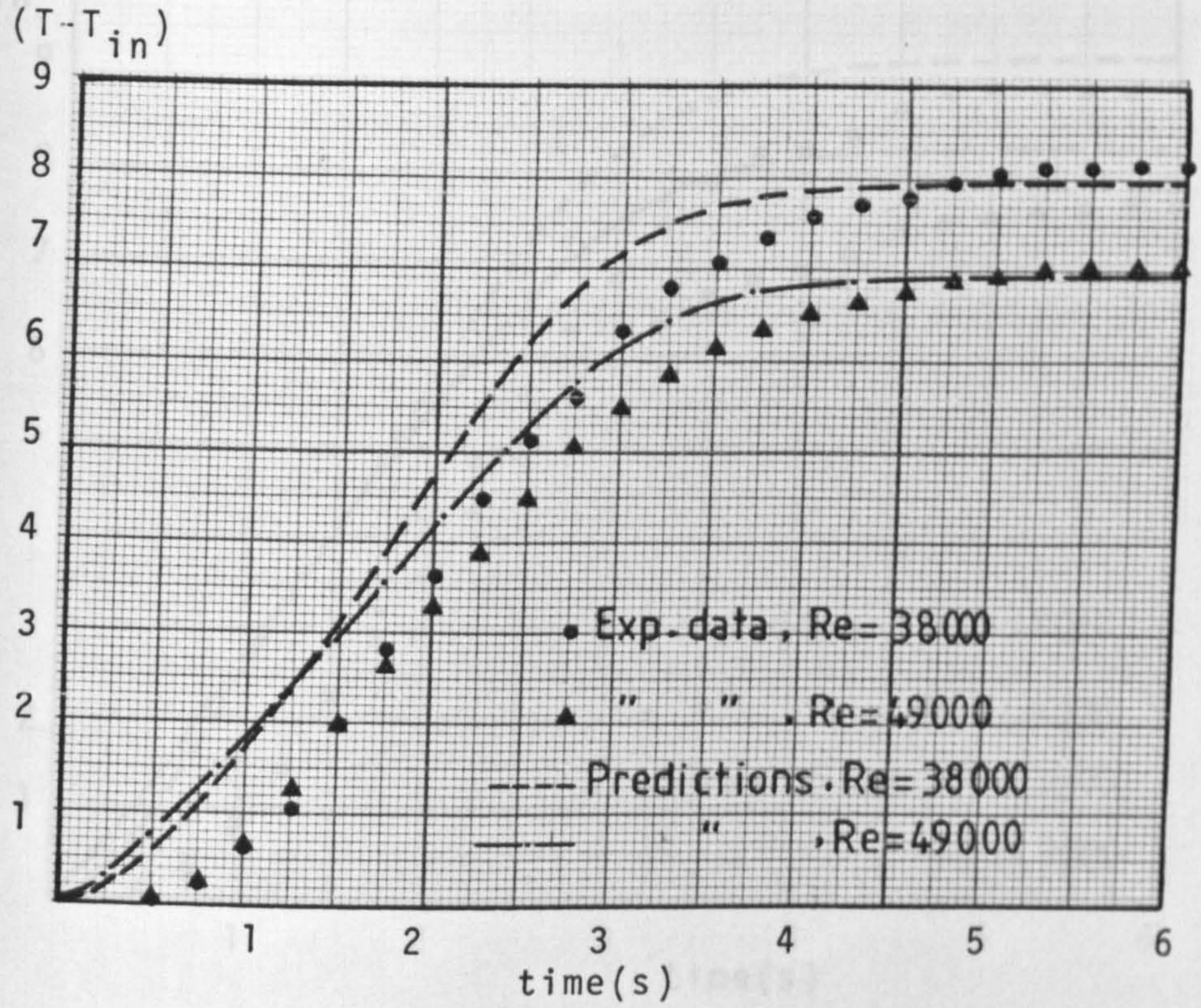


Fig (7.16a) Temperature response at 2y/D = .8

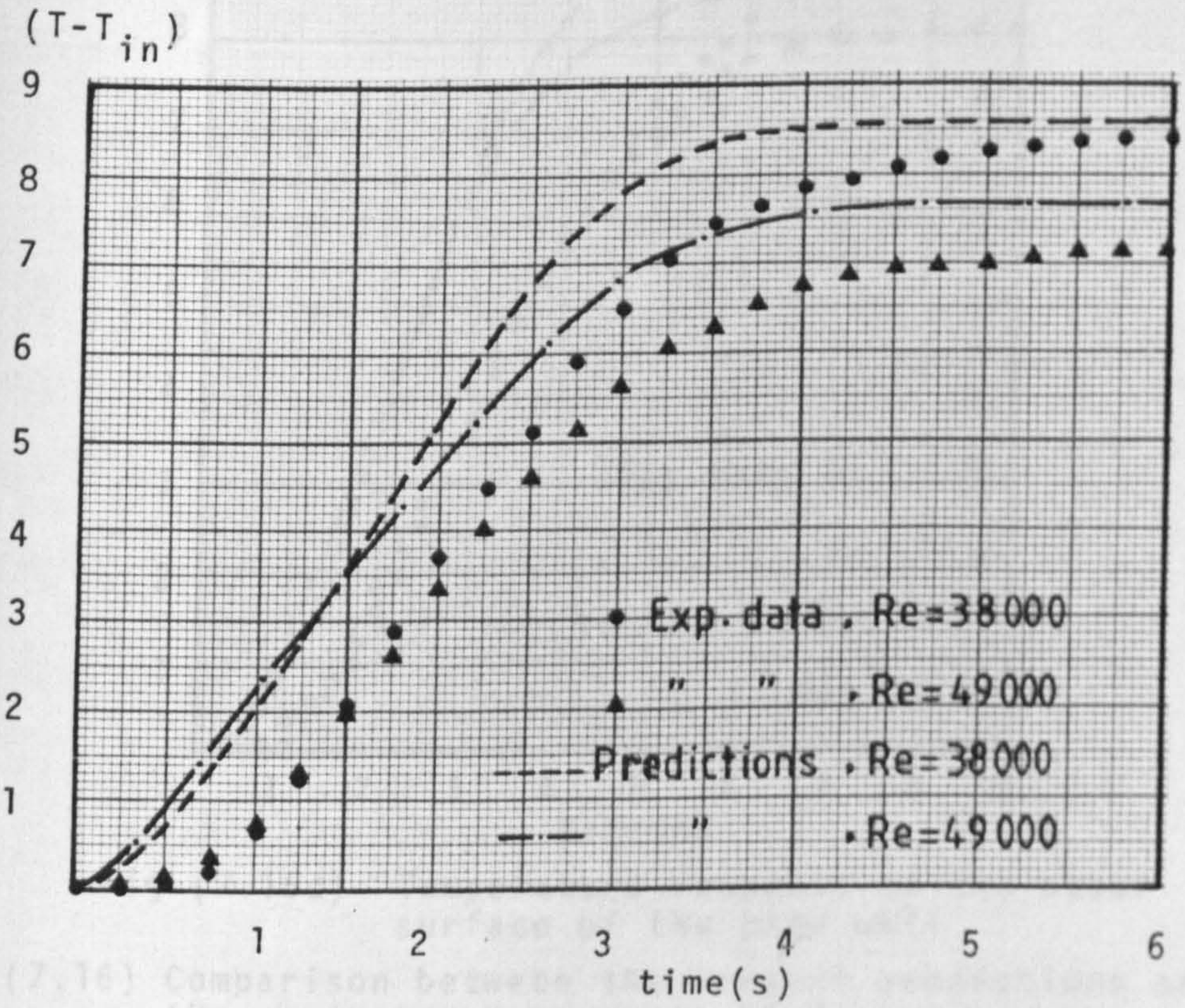


Fig (7.16b) Temperature response at 2y/D = .4

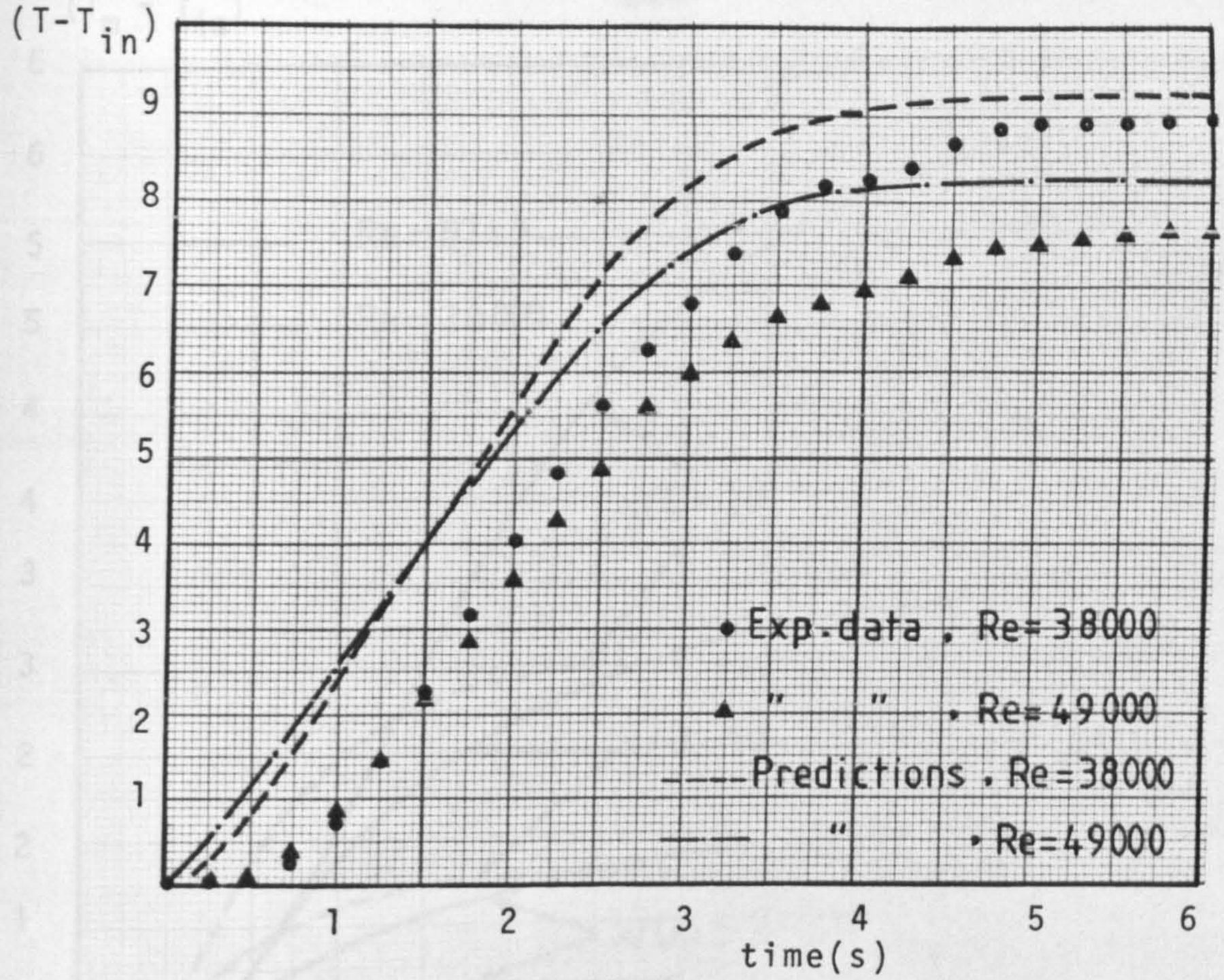


Fig (7.16c) Temperature response at 2y/D = .1

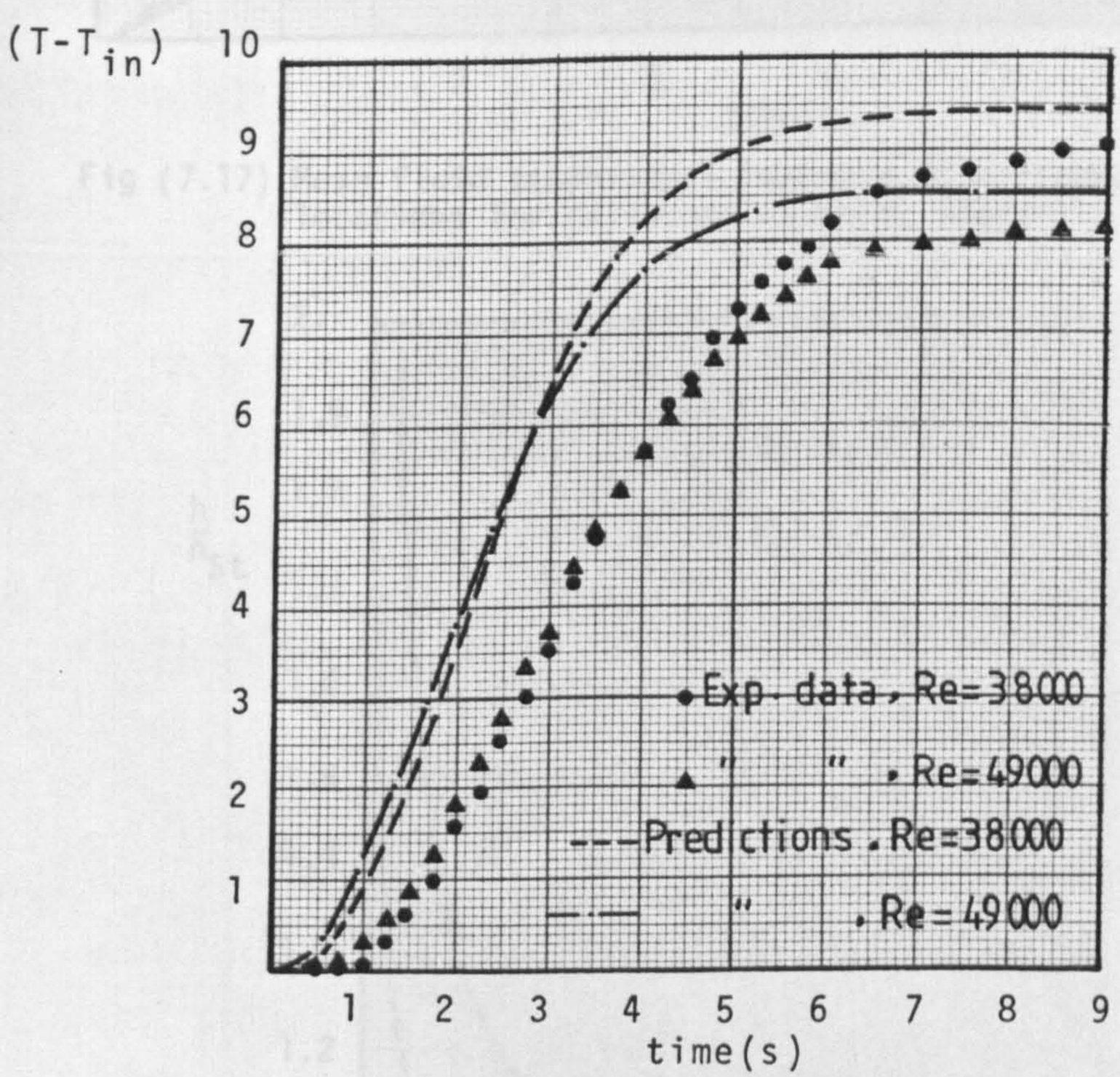


Fig (7.16d) Temperature response on the outer surface of the pipe wall

Fig (7.16) Comparison between the present predictions and the present measurements of the temperature response at x/D = 13.75

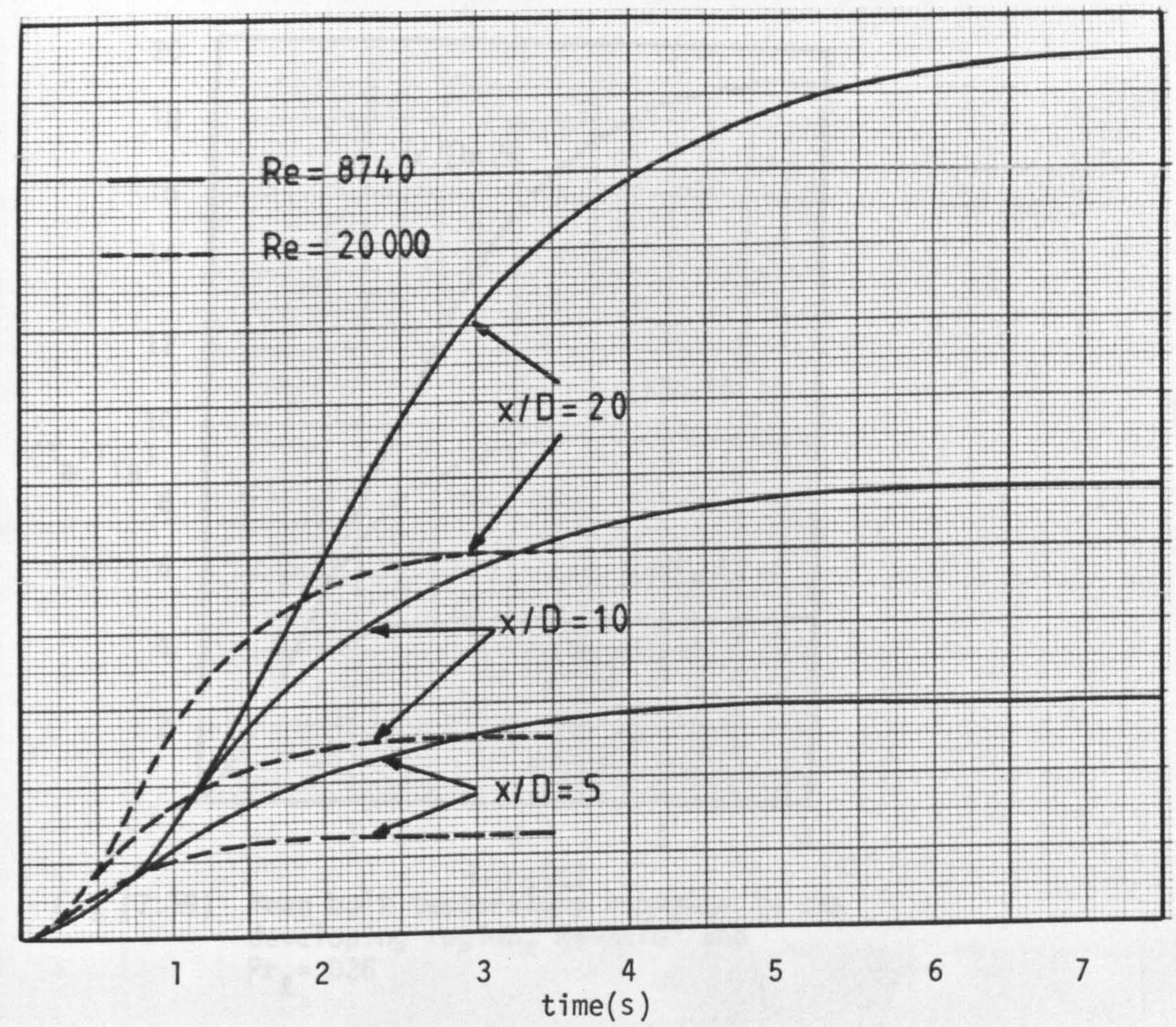


Fig (7.17) Mean fluid temperature response at different downstream locations for different Reynolds numbers

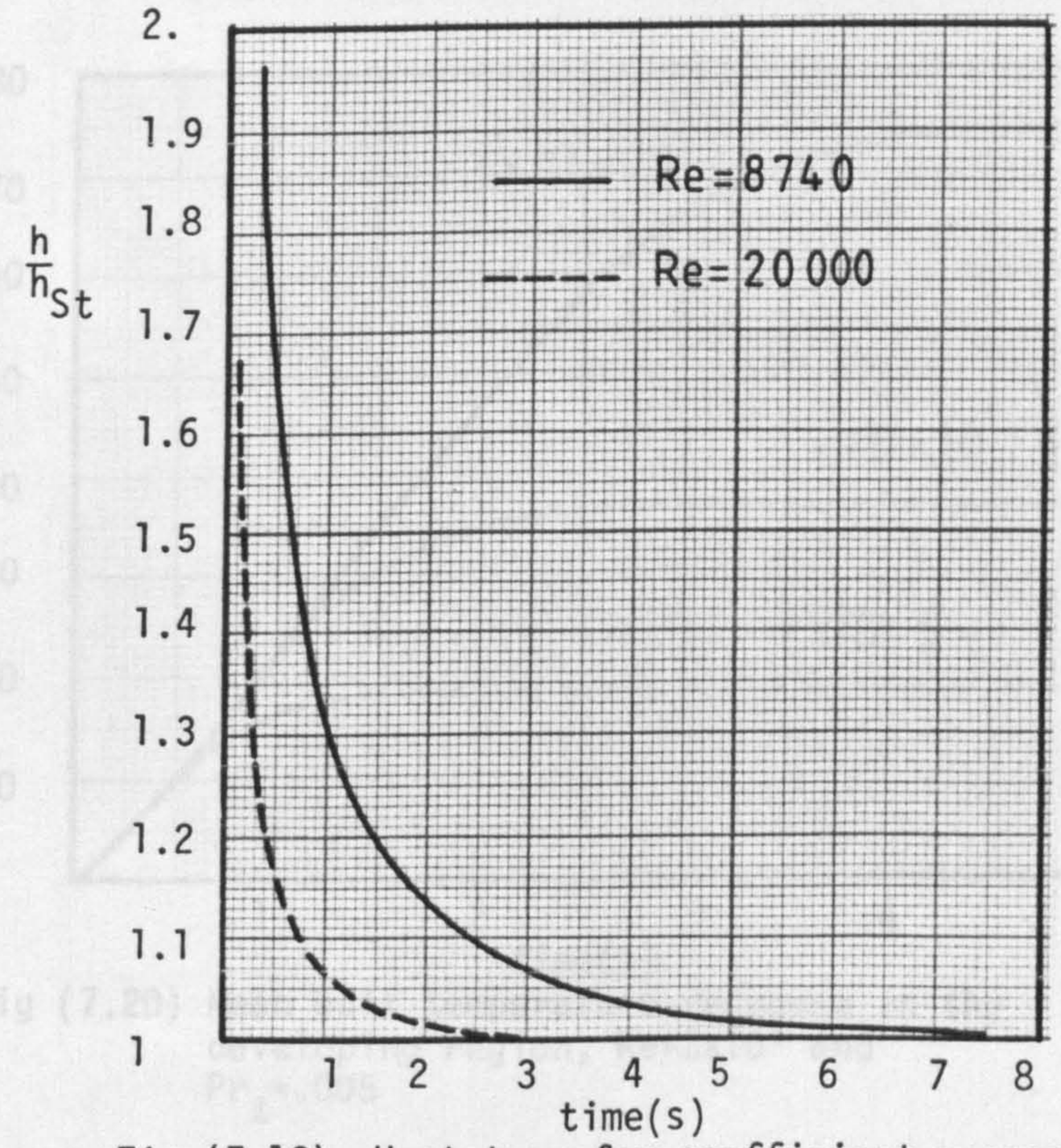


Fig (7.18) Heat-transfer coefficient response at x/D=25 for different Reynolds numbers

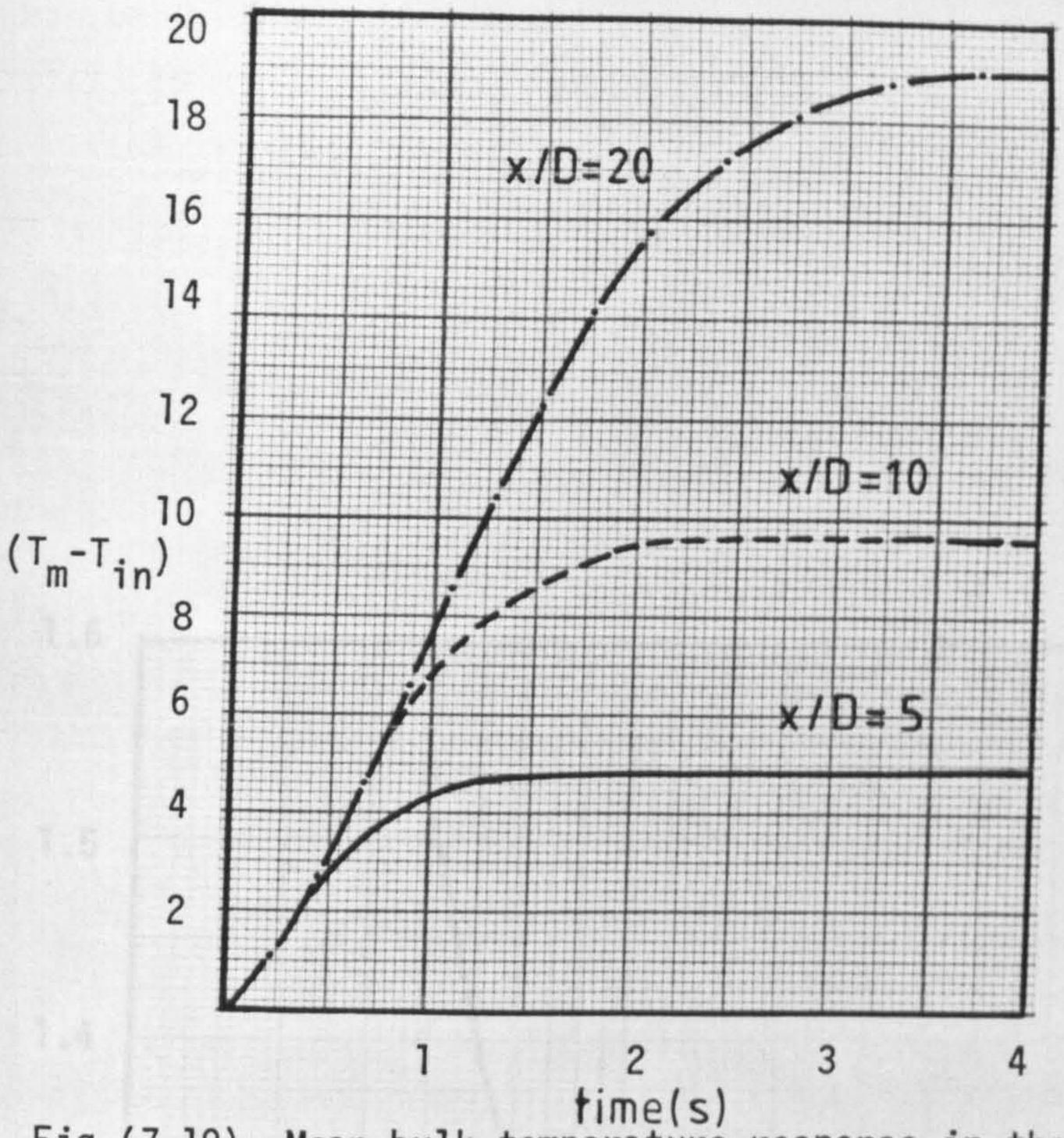


Fig (7.19) Mean bulk temperature response in the developing region, $Re=2x10^4$ and $Pr_\ell=.026$

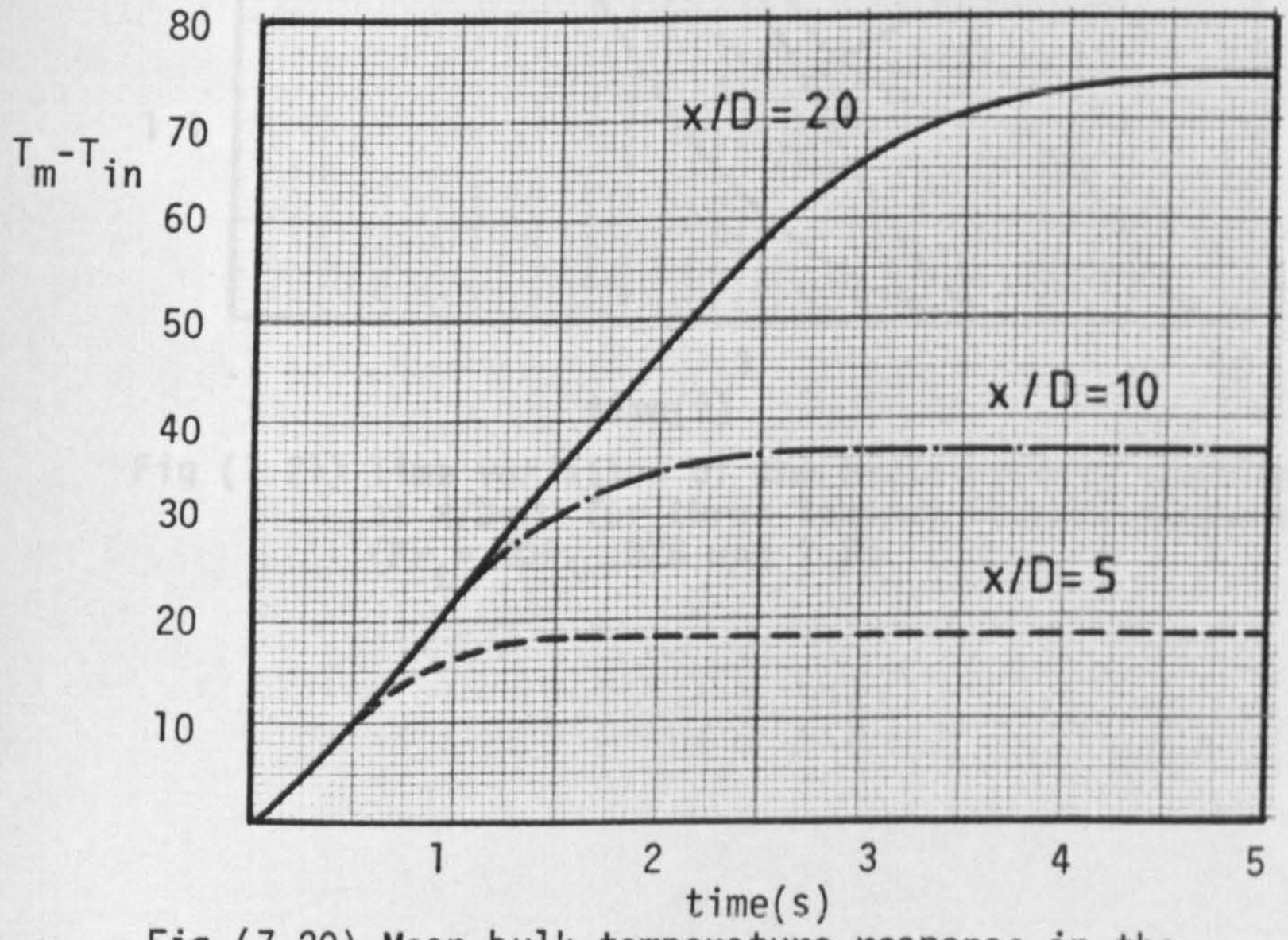


Fig (7.20) Mean bulk temperature response in the developing region, $Re=2x10^4$ and $Pr_\ell=.005$

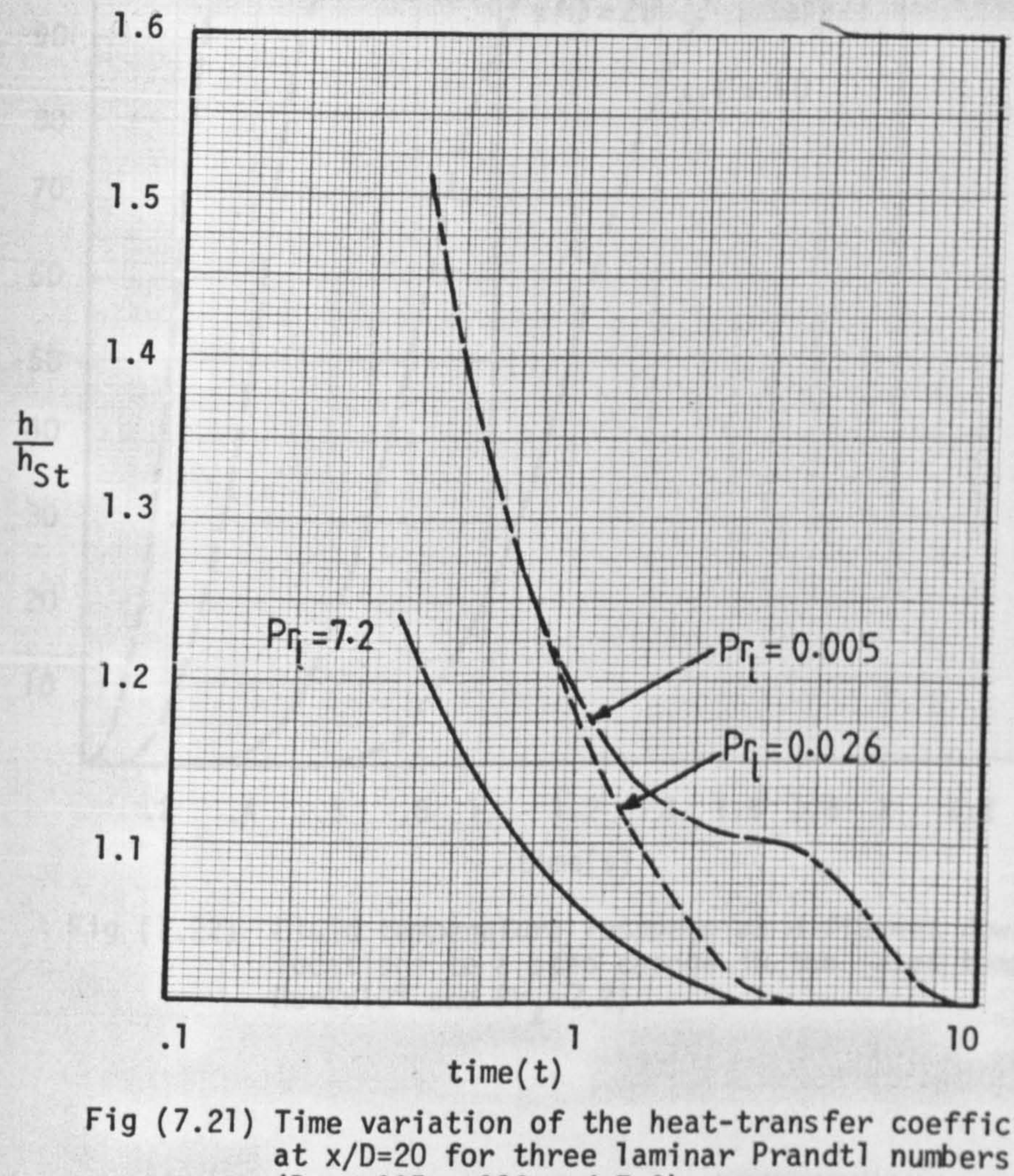


Fig (7.21) Time variation of the heat-transfer coefficient at x/D=20 for three laminar Prandtl numbers (Pr_ℓ=.005, .026 and 7.2)

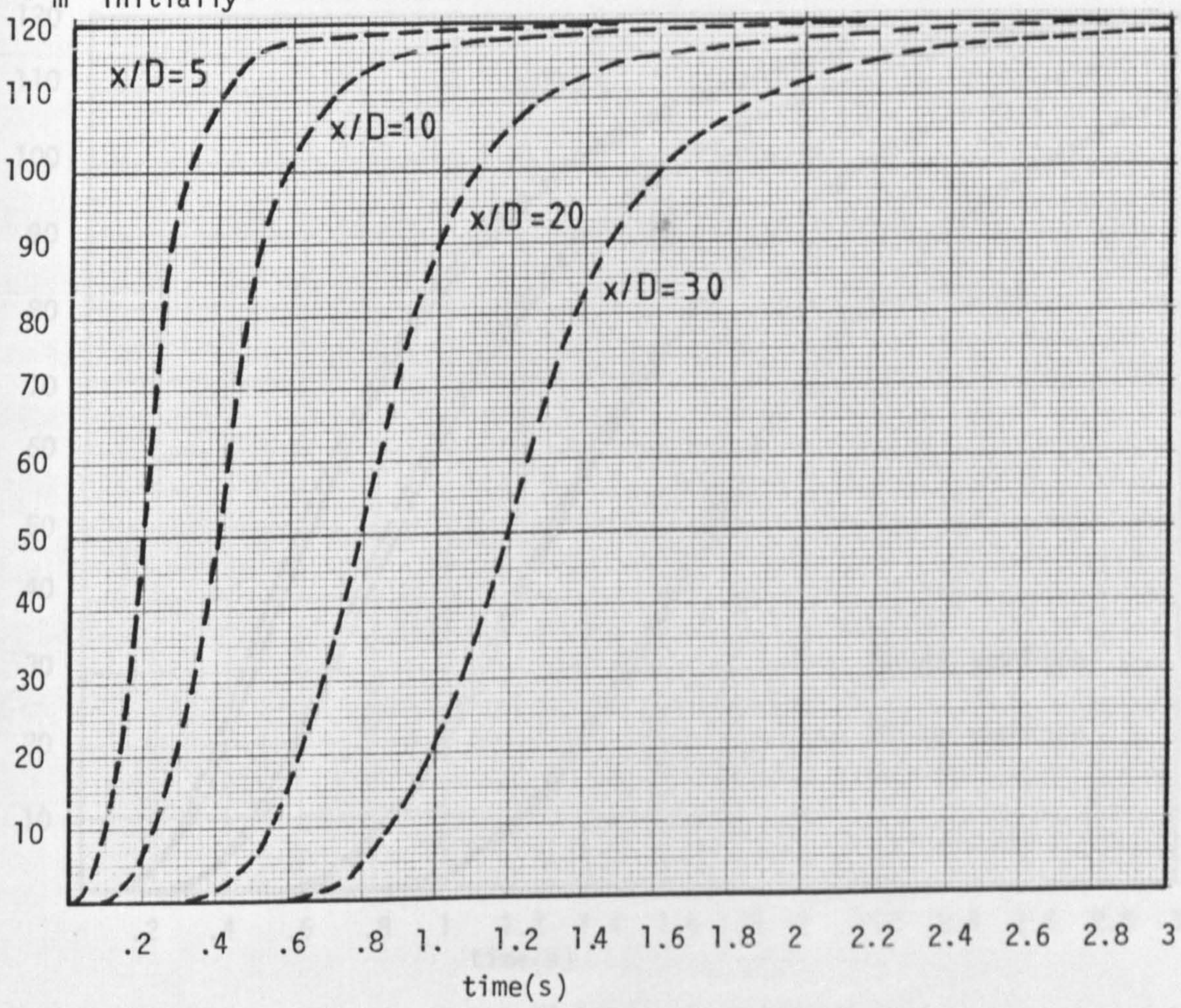


Fig (7.22) Fluid temperature response at different downstream locations to a step change in the inlet temperature($Re=2x10^4$ and $Pr_\ell=7.2$)

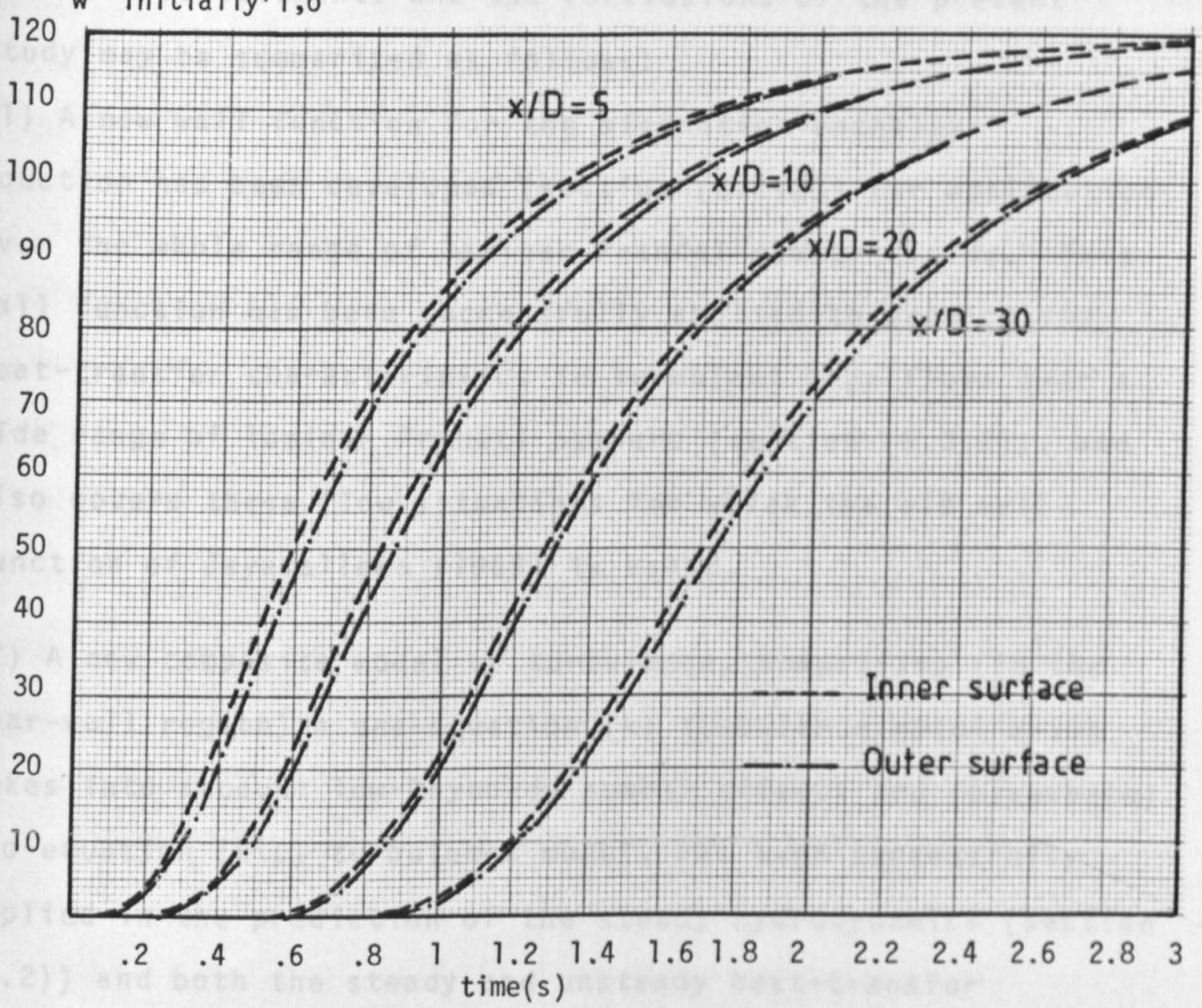


Fig (7.23) Inner and outer wall temperature responses at different downstream locations to a step change in the inlet temperature ($Re=2\times10^4$ and $Pr_\ell=7.2$)

CHAPTER 8

CONCLUDING REMARKS

8.1 Main Results of the Present Study

The main achievements and the conclusions of the present study may be summarized as follows:

(1) A new wall function for the stagnation-enthalpy equation has been developed (section (3.2.2)) for application over the whole range of laminar Prandtl number fluids. This wall function has been successfully applied to predict the heat-transfer characteristics in turbulent pipe flows over a wide range of laminar Prandtl numbers (section (6.3.2)), and also covers these flow situations for which the old wall function of Jayatallaka (1969) is valid.

(2) A new composite model of turbulence, comprising (in the near-wall region) a one-equation (k) turbulence model which takes into account low-Reynolds number effects and (elsewhere) two-equation ($k\sim\varepsilon$) turbulence model, has been successfully applied in the prediction of the steady hydrodynamics (section (6.2)) and both the steady and unsteady heat-transfer characteristics of turbulent pipe flows (sections (6.3) and chapter 7 respectively) over a wide range of laminar Prandtl numbers and Reynolds numbers.

(3) Improvements have been introduced to a basic two-dimensional parabolic solution procedure, in order to make it more efficient in the computation of the fast developing regions of turbulent wall flows (section (4.3)). The improvement consists of the introduction of a line-by-line iteration technique, which resulted in substantial reductions in the computational

time and storage. The solution procedure for the elliptic equations of heat transfer was also improved by the employment of a special starting procedure for the iteration; this resulted in a substantial improvement in the solution convergence rate (section (6.4)).

(4) The turbulent-Prandtl-number equation developed by Aoki (1963) has been recommended for application with liquid-metal fluids (section (1.3.2)). This equation has yielded good heat-transfer results (section (6.3)). For large laminar-Prandtl-number fluids, the turbulent Prandtl number should be larger than the value employed for air flows, viz. 0.95, specially close to the wall (section (6.3.2)).

(5) The steady and unsteady heat-transfer characteristics of the conjugate pipe problem have been investigated (section (6.4) and chapter (7) respectively. For the steady state case, the axial conductions in the flow domain and inside the solid wall were considered and the effect of the laminar Prandtl number, the solid to fluid conductivities ratio and the ratio of the solid wall to the pipe diameter were investigated. These studies have confirmed that the heat-transfer problems of wall flows should be analysed as conjugate problems.

(6) An experimental programme has been successfully completed; measurements of the unsteady fluid and wall temperature responses were pergormed in the flow of water through a straight pipe (chapter 5). The data obtained from this investigation have been useful in the validation of the composite model of turbulence for unsteady, conjugate heat-transfer problems.

8.2 Suggestions for Future Work

The present investigation suggests some areas where further research is needed to improve the capabilities of the composite model; these areas are as follows:

(1) The turbulent Prandtl/Schmidt number of the kinetic energy equation requires refinement if improved agreement with experimental data is to be obtained. This in turn requires accurate turbulence measurements in the developing region of a pipe flow over a wide range of Reynolds numbers.

(2) The turbulent Prandtl number for large laminar-Prandtl-number fluids requires further investigation.

(3) More accurate experimental data for the heat-transfer characteristics are required, especially in the regions close to the wall for very large and very small laminar-Prandtl number fluids.

(4) The composite model of turbulence needs to be tested in flows where regions of recirculation occur.

LIST OF REFERENCES

ABBRECHT, P H & CHURCHILL, S W (1960)

"The thermal entrance region in fully-developed turbulent flow."

AICHE Journal, vol. 6, no. 2, pp 268-273.

AOKI, S (1963)

"A consideration on the heat transfer in liquid metal."

Bulletin of the Tokyo Institute of Technology, vol. 54, pp 63-73.

AZER, N A & CHAO, B T (1960)

"A mechanism of turbulent heat transfer in liquid metal."

Int. J. Heat and Mass Transfer, vol. 1, pp 121-138.

BAKER, R A & SESONSKE, A (1962)

"Heat transfer in sodium-potassium allow."

Nuclear Science and Engineering, vol. 13, pp 283-288.

BARBIN, A B & JONES, J B (1963)

"Turbulent flow in the inlet region of a smooth pipe."

Trans. of the ASME, J. of Basic Engineering, vol. 85 pp 29-34.

BROWN, H E, AMSTEAD, B H, & SHORT, B E (1957)

"Temperature and velocity distribution and transfer of heat in a liquid metal."

Trans. of the ASME, vol. 79, pp 279-285.

BUHR, H O, CARR, A D & BALZHISER, R . (1968)

"Temperature profiles in liquid metals and the effect of superimposed free convection in turbulent flow."

Int. J. Heat and Mass Transfer, vol. 11, pp 641-654.

CARR, A D & BALZHISER, R E (1967)

"Temperature profiles and eddy diffusivities in liquid metals."

British Chemical Engineering, vol. 12, No. 1, pp 53-57.

CHOU, P Y (1945)

"On the velocity correlations and the solution of the equations of turbulent fluctuation."

Quart. Appl. Math., vol. 3, pp 38-54.

CHU, S C & BANKOFF, S G (1965)

"Unsteady heat transfer to slug flows: effect of axial conduction."

AICHE Journal, vol. 11, No 4, pp 607-612.

CLARK, J A, ARPACI, V S & TREADWELL, K M (1958a)

"Dynamic response of heat exchangers having internal heat source - Part I."

Trans of the ASME, vol. 80, pp 612-624.

CLARK, J A, & ARPACI, V S (1958b)

"Dynamic response of heat exchangers having internal heat source - Part II."

Trans. of the ASME, vol. 80, pp 625-634.

CLARK, J A, & ARPACI, V S (1959)

"Dynamic response of heat exchangers having internal heat source - Part III."

Trans. of the ASME, vol. 81c, pp 253-266.

CLARK, J A (1968)

"A study of incompressible turbulent boundary layers in channel flow."

Trans. of the ASME, J. of Basic Engineering, vol. 90, pp 455-468.

DALY, B T & HARLOW, F H (1970)

"Transport equations in turbulence."

The Physics of Fluids, vol. 13, part 11, pp 80-95.

DAVIDOV, B I (1961)

"On the statistical dynamics of an incompressible flow."

Dokl. AN SSSR, 136, 47.

DAVIS, E J & GILL, W N (1970)

"The effect of axial conduction in the wall on heat transfer with laminar flow."

Int. J. Heat and Mass Transfer, vol. 13, pp 459-470.

DAVIES, J T (1972)

"Turbulence phenomena."

Academic Press.

DIESSLER, R G (1952)

"Analysis of fully-developed turbulent heat transfer at low Peclet number in smooth tubes with application to liquid metal."

NACA, RME 52 F05.

DEISSLER, R G & EIAN, C S (1952)

"Analytical and experimental investigation of fully-developed turbulent flow of air in a smooth tube with heat transfer with variable fluid properties."

NACA, TN 2629.

DEISSLER, R G (1953)

"Analysis of turbulent heat transfer and flow in the entrance regions of smooth passages."

NACA, TN 3016.

DEISSLER, R G (1955)

"Analysis of turbulent heat transfer, mass transfer and friction in smooth tubes at high Prandtl and Schmidt number."

NACA, TN3145, Report no 1210

ECKERT, E R G & DRAKE, R M Jr (1972)

"Analysis of heat and mass transfer."

McGraw Hill.

ELHADIDY, M A (1976)

"Temperature, Nusselt number and amplitude of temperature fluctuations in air and liquid metal flows."

CHAM, TR/26.

ELHADIDY, M A (1977a)

"Turbulent flow of mercury in annuli."

CHAM, 478/1.

ELHADIDY, M A (1977b)

"Prediction of the unsteady temperature distribution in a free turbulent jet flow of sodium impinging on cylindrical body."

CHAM, 478/3.

ELHADIDY, M A & HUIMES, G (1977c)

"Prediction of the unsteady temperature distribution inside a solid body and the flow of a turbulent free jet of sodium impinging on that body."

CHAM, 478/4

ELHADIDY, M A & SPALDING, D B (1979a)

"New approach to calculating turbulent flows in the near-wall region."

Imperial College, Mech. Eng. Dept., Heat Transfer Section Report No HTS 79/9.

ELHADIDY, M A, GORI, F & SPALDING, D B (1979b)

"Numerical predictions of the heat transfer to low-Prandtl number fluids."

To be published in the Numerical Heat Transfer Journal.

EL-TAHRY, S H (1979)

"Turbulent plume dispersal"

Ph.D. thesis, Imperial College, Mech. Eng. Dept., Fluid Section.

FLAHERTY, T (1974)

"An investigation of non-isothermal turbulent flow of mercury."

Ph.D. thesis, Purdue University.

FUCHS, H (1973)

"Warmenbergang an stromendes natrium."

E.I.R. Wurenlingen, Switzerland, Rep. No. 241.

FUCHS, H & FAESCH (1973)

"Measurements of eddy conductivity in sodium."

Progress of Heat and Mass Transfer, vol. 7, pp 39-43.

GLUSHKO, G (1965)

"Turbulent boundary layer on a flat plate in an incompressible fluid."

IZV. Acad. Nauk SSSR Mekh no. 4, 13.

GOWEN, R A & SMITH, J W (1967)

"The effect of the Prandtl number on temperature profiles for heat transfer in turbulent pipe flow."

Chem. Eng. Science, vol. 22, pp 1701-1711.

HARLOW, F H & NAKAYAMA, P I (1967)

"Turbulence transport equations."

The Physics of Fluid, vol. 10, No 11, pp 2323-2332

HARLOW, F H & NAKAYAMA, P I (1968)

"Transport of turbulence energy decay rate."

Los Alamos, Sci. Lab., University California, Rep No LA-3854.

HASSID, S & POREH, M (1975)

"A turbulent energy model for flow with drag reduction."

Trans. of the ASME, J. Fluids Eng., vol. 97, pp 234-241.

HASSID, S & POREH, M (1975b)

"A turbulent energy dissipation model for flows with drag reduction."

Israel Institute of Technology, Faculty of Civil Engineering, Publication No. 215.

HINZE, J O (1975)

"Turbulence."

McGraw-Hill Book Co.

HOCHREITER, L (1971)

"Turbulent structure of isothermal and non-isothermal liquid metal pipe flow."

Ph.D. thesis, Purdue University.

HUSSAIN, A K M F & REYNOLDS, W C (1975)

"Measurements in fully-developed turbulent channel flow."
Trans of the ASME, J. of Basic Engineering, December 1975, pp 568-580.

ISAKOFF, S E & DREW, T B (1951)

"Heat and momentum transfer in turbulent flow of mercury."
General Discussion on Heat Transfer, Inst. Mech. Eng and ASME, pp. 405-409.

JAYATILLAKA, C L V (1969)

"The influence of Prandtl number and surface roughness on the resistance of the laminar sublayer to momentum and heat transfer."
Progress in Heat and Mass Transfer, vol. 1, pp 193-329.

JENKINS, R (1951)

"Variation of the eddy conductivity with Prandtl number modulus and its use in prediction of turbulent heat transfer."
Heat Transfer and Fluid Mech. Institute, Stanford Univ., pp 147-158.

JOHNK, R E & HANRATTY, T J (1961)

"Development of temperature profile for turbulent heat exchange in a pipe."
Eng. Experimental Section, University of Illinois, Technical Report No 10.

JOHNK, R E & HANRATTY T J (1962)

"Temperature profiles for turbulent flow of air in a pipe - I the fully-developed heat transfer region."
Chemical Engineering Science, vol. 17, pp 867-879.

JOHNK, R E & HANRATTY, T J (1962b)

"Temperature profiles for turbulent flow of air in a pipe - II. The thermal entrance region."

Chemical Engineering Science, vol. 17, pp 881-892.

JOHNSON, H A, HARTNETT, J P & CLABAUGH, W J (1953)

"Heat transfer to molten lead-bismuth entectic in turbulent pipe flow."

Trans. of the ASME, vol. 75, pp 1191-1198.

JONES, W P & LAUNDER, B E (1972)

"The prediction of laminarization with a two-equation model of turbulence."

Int. J. Heat and Mass Transfer, vol. 15, pp 301-314.

JONES, W P & LAUNDER, B E (1973)

"The calculation of low-Reynolds-number phenomena with a two-equation model of turbulence."

Int. J. Heat and Mass Transfer, vol. 16, pp 1119-1130.

KAKAC, S & YENER, Y (1973)

"Exact solution of the transient forced convection energy equation for timewise variation of inlet temperature."

Int. J. Heat and Mass Transfer, vol. 16, pp 2205-2214.

KAKAC, S (1975)

"A general analytical solution to the equation of transient forced convection with fully developed flow."

Int. J. Heat and Mass Transfer, vol. 18, pp 1449-1453.

KAKAC, S (1978)

"Transient heat transfer by forced convection in channels."
In "Turbulent force convection in channels and bundles".

Ed. S. Kakac & D B Spalding (1979)

KAWAMURA, H (1977)

"Experimental and analytical study of transient heat-transfer for turbulent flow in a circular tube."

Int. J. Heat and Mass Transfer, vol. 20, pp 443-450.

KHALIL, E E, SPALDING, D B & WHITELAW, J H (1975)

"The calculation of local flow properties in two-dimensional furnaces."

Int. J. Heat and Mass Transfer, vol. 18, pp 775-791.

KIRILLOV, P L (1962)

"Generalization of experimental data on heat transfer in molten metals."

Translated from Atomnaya Energiya, vol. 13, No 5, pp 481-484.

KOSHKIN, V K, KALININ, E K, DREITSER, G A, GALILSEISKY, B M and IZASIMOV, V G (1970)

"Experimental study of non-steady convective heat transfer in tubes."

Int. J. Heat and Mass Transfer, vol. 13, pp 1271-1281.

KROPHOLLER, H W & CARR, A D (1962)

"The prediction of heat and mass transfer coefficient for turbulent flow in pipes at all values of the Prandtl or Schmidt number."

Int. J. Heat and Mass Transfer, vol. 5, pp 1191-1205.

KUNZ, H R & YERAZUNIS, S (1969)

"An analysis of film condensation, film evaporation and single-phase heat transfer for liquid Prandtl number from 10^{-3} to 10^{4}."

Trans of the ASME, J. of Heat Transfer vol. 91c, pp 413-420.

KUZNETZOV, Yu N (1970)

"Investigation of unsteady convective heat transfer in tubes."

4th Int. Heat Transfer Conference.

LAUFER, J (1954)

"The structure of turbulence in fully-developed pipe flow."

NACA, TN 1174

LAUNDER, B E, MORSE, A, RODI, W & SPALDING, D B (1972)

"The prediction of free shear flows. A comparison of the performance of six turbulence models."

Proc. of NASA Conference on Free Shear Flows, Langly.

LAUNDER, B E & SPALDING, D B (1972)

"Mathematical models of turbulence."

Academic Press

LAUNDER, B E & SPALDING, D B (1973)

"The numerical computation of turbulence flows."

Imperial College, Mech. Eng. Dept. Report ref. HTS/73/2.

LAWN, C J (1977)

"Turbulent temperature fluctuation in liquid metals."

Int. J. Heat and Mass Transfer, vol. 20, pp 1035-1044.

LESLIE, D C (1977)

"A recalculation of turbulent heat transfer to liquid metal."

Letters in Heat and Mass Transfer, vol. 4., pp 25-34.

LEVICH, V G (1962)

"Physiochemical hydrodynamics."

English translation published by Prentice-Hall, New Jersey.

LUBARSKY, B & KAUFMAN, S (1955)

"Review of experimental investigations of liquid metal heat transfer."

NACA, TN 3336

LUIKOV, A V, ALEKSASHENKO, V A & ALEKSASHENKO, A A (1971)

"Analytical methods of solution of CONJUGATED problems in convective heat transfer."

Int. J. Heat and Mass Transfer, vol. 14, pp 1047-1056.

LUIKOV, A V (1974)

"CONJUGATE convective heat transfer problems."

Int. J. Heat and Mass Transfer, vol. 17, pp 257-265.

LYON, R N (1951)

"Liquid metal heat-transfer coefficients."

Chemical Eng. Progress, vol. 47, No 2, pp 75-79.

MALHOTRA, A (1977)

"An analytical investigation of forced convective heat-transfer to supercritical."

Ph.D. thesis, Dept of Mech. Eng. The University of British Columbia.

MARTINELLI, R C (1947)

"Heat transfer to molten metals."

Trans. of the ASME, vol. 69, pp 947-959

MIZUSHINA, T, OGINO, F, OKA, Y and FUKUDA, H (1971)

"Turbulent heat and mass transfer between wall and fluid stream at large Prandtl and Schmidt number."

Int. J. Heat and Mass Transfer, vol. 14, pp 1705-1716.

MOFFAT, R J (1958)

"Designing thermocouples for response rate."

Trans. of the ASME, vol. 80, pp 257-262.

MOFFAT, R J (1962)

"Gas temperature measurements."

Temperature Measurement and Control in Science and Industry, vol. III, Ed. C.M. Herzfeld, pp 553-572.

NORRIS, L H & REYNOLDS, W C (1975)

"Turbulent channel flow with a moving wavy boundary."

Stanford Univ., Dept. Mech. Eng., Rep. F.M.10.

PATANKAR, S V & SPALDING D B (1970)

"Heat and mass transfer in boundary layers."

2nd Edition, Inter text Books, London.

PERELMAN, T L (1961)

"On CONJUGATED problems of heat transfer."

Int. J. Heat and Mass Transfer, vol. 3, pp 293-303.

PUN, W M & SPALDING, D B (1977)

"A general computer program for two-dimensional elliptic flows."

Imperial College, Mech. Eng. Dept. Report ref. HTS/76/2.

RAMACHANDRA, V (1979)

"The numerical prediction of flow and heat transfer in rod-bundle geometrics."

Ph.D. thesis, Imperial College, Mechanical Engineering Department, Heat Transfer Section.

ROACHE, P J (1976)

"Computational fluid dynamics."

Hermosa Publisher

SAKAKIBARA, M & ENDOH, K (1977)

"Effect of conduction in wall on heat transfer with turbulent flow between parallel plates."

Int. J. Heat and Mass Transfer, vol. 20, pp 507-516.

SAMARAWEERA, D S A (1978)

"Turbulent heat transport in two- and three-dimensional fields."

Ph.D thesis, Lawrence Berkely Laboratory, University of California, Berkely.

SCHLICHTING, H (1968)

"Boundary-layer theory"

Sixth Edition, McGraw-Hill Book Company

SCHNEIDER, P J (1957)

"Effect of axial fluid conduction on heat transfer in the entrance regions of parallel plates and tubes."

Trans. of the ASME, vol. 79, pp 765-773.

SELL, M G Jr, & HUDSON, J L (1966)

"The effect of wall conduction on heat transfer to a slug flow."

Int. J. Heat and Mass Transfer, vol. 9, pp 11-16.

SHERIFF, N, O'KANE, D J & MATHER, B (1972)

"Sodium eddy diffusivity of heat measurements in a circular duct."

United Kingdom Atomic Energy Authority, TRG Report 2191 (R).

SHERIFF, N & O'KANE, D J (1973)

"Sodium eddy diffusivity of heat measurements in a circular duct."

Progress in Heat and Mass Transfer, vol. 7, pp 25-38.

SIEGEL, R (1959a)

"Transient heat transfer for laminar slug flow in ducts."

Trans. of the ASME, J. of Applied Mechanics, vol. 81, pp 140-142.

SIEGEL, R & SPARROW, E M (1959b)

"Transient heat transfer for laminar forced convection in the thermal entrance region of flat ducts."

Trans. of the ASME, J. of Heat Transfer vol. 81c, pp 29-36.

SIEGEL, R & PERLMUTTER, M (1961)

"Unsteady laminar flow in a duct with unsteady heat addition."

Trans of the ASME, J. of Heat Transfer, vol. 83, pp 432-440.

SIEGEL, R & PERLMUTTER, M (1963)

"Laminar heat transfer in a channel with unsteady flow and wall heating varying with position and time."

Trans. of the ASME, J. of Heat Transfer, vol. 85, pp 358-365.

SLEICHER, C A Jr (1958)

"Experimental velocity and temperature profiles for air in turbulent pipe flow."

Trans of the ASME, vol. 80, pp 693-704.

SLEICHER, C A, AWAD, A S & NOTTER, R H (1973)

"Temperature and eddy diffusivity profiles in Nak"

Int. J. of Heat and Mass Transfer, vol. 16, pp 1565-1575.

SMITH, J W, GOWEN, R A & WASMUND, B O (1967)

"Eddy diffusivities and temperature profiles for turbulent heat transfer to water in pipes."

Chemical Engineering, Progress Symposium series, No 77, vol. 63, pp 92-101.

SPALDING, D B (1961)

"A single formula for the 'low of the wall'"

J. of Applied Mech. vol. 28E, pp 455-458.

SPALDING, D B (1967)

"Heat transfer from turbulent separated flows."

J. of Fluid Mechanics. vol. 27, pp 97-109.

SPALDING, D B (1972)

"A novel finite-difference formulation for differential expressions involving both first and second derivatives."

Int J. Numerical Method in Engineering, vol. 4, pp 551-559.

SPALDING, D B (1977)

"A note on the proper way to linearise the sources of k and ϵ."

Unpublished work.

SPALDING, D B (1978)

"GENMIX: A general computer program for two-dimensional parabolic phenomena."

Heat Mass Transfer, vol. 1. Pergamon Press.

SPARROW, E M, HALLMON, T M & SIEGEL, R (1957)

"Turbulent heat transfer in the thermal entrance region of a pipe with uniform heat flux."

Appl. Sci. Res., Section A, vol. 7, pp 37-52.

SPARROW, E M & SIEGEL, R (1960)

"Unsteady turbulent heat transfer in tubes."

Trans. of the ASME, J. of Heat Transfer, vol. 82, pp 170-180.

SPARROW, E M & FARIAS, F N (1968)

"Unsteady heat transfer in ducts with time-varying inlet temperature and participating walls."

Int. J. Heat and Mass Transfer, vol. 11, pp 837-853.

SPARROW, E M (1968)

"Error estimates in temperature measurement."

Measurements in Heat Transfer, Ed by E R G Eckert and R I Goldstein, McGraw-Hill.

STEPHENSON, P L, MASSEY, T H & OLIVER, A T (1974)

"Developing turbulent flow and heat transfer in a circular tube. A finite difference solution using the mixing length hypothesis."

Central Electricity Research Laboratories, RD/L/N8/74.

STUART, W M (1956)

"Thermal response of nuclear reactor coolants to power transients."

B.Sc thesis, Massachusetts Institute of Technology.

SVENSSON, U (1977)

"A note on the value of the Prandtl/Schmidt number for turbulent kinetic energy, as used in the k∿ε turbulence model."

Lund Institute of Technology, Dept. of Water Resources Engineering Rep. No 7001.

SUBBOTIN, V I, IBRAGIMOV, M K, IVANOVSKY, M N, AROL'DOV, M N and NOMOFILOV, E V (1961)

"Turbulent heat transfer in a flow of liquid metals."

Int. J. Heat and Mass Transfer, vol. 4, pp 79-87.

SUBBOTIN, V I, PAPOVYANTS, A K, KIRILLOV, P L & IVANOVSKII, N N (1962a)

"A study of heat transfer to molten sodium in tubes."

Atomnaya Energiya, vol. 13, No 4, pp 380-382.

SUBBOTIN, V I, IBRAGIMOV, M. Kh, & NOMOFILOV, E V (1962b)

"Heat transfer in a region of thermal stabilization in the turbulent flow of liquid metals in a tube."

Atomnaya Energiya, vol. 13, No 2, pp 155-161.

SUBBOTIN, V I, IBRAGIMOV M Kh, & NOMOFILOV, E V (1963)

"Determination of the relationship between the coefficient of the turbulent transfer of heat and momentum."

Atomnaya Energiya, vol. 14, pp 414-416.

TOWNSEND, A A (1954)

"The structure of turbulent shear flow."

Cambridge Univ. Press, Cambridge.

TREADWELL, K M (1955)

"Theoretical and experimental investigation of fluid temperature response in flowing incompressible fluid systems with internal heat generation."

M.Sc thesis, Massachusetts Institute of Technology.

VAN DRIEST, E R (1956)

"On turbulent flow near a wall."

J. Aero. Sci. vol. 23, No 11, pp 1007-1011

VILENSKY, V D (1970)

"Unsteady heat transfer with laminar flow fluid in cylindrical tube."

4th Int. Heat Transfer Conference.

WALKLATE, P, HEIKAL, M.R F & HATTON, A P (1976)

"Measurements and prediction of turbulence and heat transfer in the entrance region of a pipe."

Proc Inst. Mech. Engrs. vol. 90, pp 401-407.

WATSON, G G (1956)

"A survey of work on heat transfer with liquid metal."

Mech. Eng. Research Laboratory, Heat Division, Heat

WOLFSHTEIN, M (1969)

"The velocity and temperature distribution in one-dimensional flow with turbulence augmentation and pressure gradient."

Int. J. Heat and Mass Transfer, vol. 12, pp 301-318

APPENDIX A

Transformation of the stagnation-enthalpy equation from (ψ-x) to (ω-x) coordinate system

The unsteady-elliptic stagnation-enthalpy equation (2.4.8) may be re-written as follows:

$$\frac{1}{u}\frac{\partial \tilde{h}}{\partial t} + \frac{\partial \tilde{h}}{\partial x} = \frac{\partial}{\partial \psi}\{(b_1)\frac{\partial \tilde{h}}{\partial \psi}\} + \frac{1}{\rho u r}\frac{\partial}{\partial x}\{(b_2)\frac{\partial \tilde{h}}{\partial x}\} + \frac{\partial}{\partial \psi}\{(b_3)\frac{\partial u^2/2}{\partial \psi}\} \quad , (A.1)$$

where

$$b_1 \equiv r^2 \rho u \Gamma_{h,eff}$$

$$b_2 \equiv r\, \Gamma_{h,eff} \quad . (A.2)$$

$$b_3 \equiv r^2 \rho u (\mu_{eff} - \Gamma_{h,eff})$$

The dimensionless stream function coordinate (ω) was related to the stream function coordinate (ψ) as follows:

$$\omega = \frac{\psi - \psi_I}{\psi_E - \psi_I} \quad . (A.3)$$

while the streamwise coordinate (x) was approximately the same in both systems.

In order to transform equation (A-1) to the (ω-x) coordinate system it was necessary to express:

(i) $(\frac{\partial}{\partial x})_\psi$ in terms of $(\frac{\partial}{\partial x})_\omega$ and $(\frac{\partial}{\partial \omega})_x$

(ii) $(\frac{\partial}{\partial \psi})_x$ in terms of $(\frac{\partial}{\partial x})_\omega$ and $(\frac{\partial}{\partial \omega})_x$

(iii) $(\frac{\partial}{\partial \psi}(b_1\frac{\partial}{\partial \psi})_x)_x$ in terms of $(\frac{\partial}{\partial x}(b_1\frac{\partial}{\partial x})_\omega)_\omega$, $(\frac{\partial}{\partial x}(b_1\frac{\partial}{\partial \omega})_x)_\omega$, $(\frac{\partial}{\partial \omega}(b_1\frac{\partial}{\partial x})_\omega)_x$ and $(\frac{\partial}{\partial \omega}(b_1\frac{\partial}{\partial \omega})_x)_x$

(iv) $(\frac{\partial}{\partial x}(b_2\frac{\partial}{\partial x})_\psi)_\psi$ in terms of $(\frac{\partial}{\partial x}(b_2\frac{\partial}{\partial x})_\omega)_\omega$, $(\frac{\partial}{\partial x}(b_2\frac{\partial}{\partial \omega})_x)_\omega$, $(\frac{\partial}{\partial \omega}(b_2\frac{\partial}{\partial \omega})_\omega)_x$ and $(\frac{\partial}{\partial \omega}(b_2\frac{\partial}{\partial \omega})_x)_x$

where the subscript outside the bracket indicates the variable kept constant during the differentiation.

A.I Transformation of $(\frac{\partial}{\partial x})_\psi$

The partial differentiation with respect to x, $(\frac{\partial}{\partial x})_\psi$, in the ($\psi$-x) coordinates can be expressed as follows:

$$(\frac{\partial}{\partial x})_\psi = (\frac{\partial}{\partial x})_\omega + (\frac{\partial}{\partial \omega})_x \, (\frac{\partial \omega}{\partial x})_\psi \quad , \quad (A.4)$$

where $(\frac{\partial \omega}{\partial x})_\psi$ can be obtained from the differentiation of equation (A.3); as follows:

$$(\frac{\partial \omega}{\partial x})_\psi = \frac{-1}{(\psi_E - \psi_I)} \left\{ \frac{d\psi_I}{dx} + \omega \frac{d(\psi_E - \psi_I)}{dx} \right\} \quad . \quad (A.5)$$

Substitution from (A.5) into (A.4) yields

$$(\frac{\partial}{\partial x})_\psi = (\frac{\partial}{\partial x})_\omega - \frac{1}{(\psi_E - \psi_I)} \left[\frac{d\psi_I}{dx} + \omega \frac{d(\psi_E - \psi_I)}{dx} \right] (\frac{\partial}{\partial \omega})_x \quad , \quad (A.6)$$

which may be written more compactly as:

$$(\frac{\partial}{\partial x})_\psi = (\frac{\partial}{\partial x})_\omega + (a + b\omega) \, (\frac{\partial}{\partial \omega})_x \quad . \quad (A.7)$$

Here a and b are defined by

$$a \equiv \frac{-1}{(\psi_E - \psi_I)} \frac{d\psi_I}{dx} \quad , \quad (A.8)$$

$$b \equiv \frac{-1}{(\psi_E - \psi_I)} \frac{d(\psi_E - \psi_I)}{dx} \quad . \quad (A.9)$$

A.II Transformation of $(\frac{\partial}{\partial \psi})_x$ and $(\frac{\partial}{\partial \psi}(b_1 \frac{\partial}{\partial \psi})_x)_x$

The partial differentiation with respect to the stream function can be expressed as follows:

$$(\frac{\partial}{\partial \psi})_x = (\frac{\partial}{\partial \omega})_x (\frac{\partial \omega}{\partial \psi})_x + (\frac{\partial}{\partial x})_\omega (\frac{\partial x}{\partial \psi})_\omega \quad . \quad (A.10)$$

The last term in equation (A.10) is zero, x and ψ are independent

variables, while $(\frac{\partial\omega}{\partial\psi})_x$ can be obtained from the differentiation of (A.3) as follows:

$$(\frac{\partial\omega}{\partial\psi})_x = \frac{1}{(\psi_E-\psi_I)} \quad \cdot \text{(A.11)}$$

Substitution from (A.11) into (A.10) yields:

$$(\frac{\partial}{\partial\psi})_x = \frac{1}{(\psi_E-\psi_I)} \quad (\frac{\partial}{\partial\omega})_x \quad \cdot \text{(A.12)}$$

Multiplying equation (A.12) by b_1, and the differential, similarly to that performed in (A.10), gives:

$$(\frac{\partial}{\partial\psi}(b_1\frac{\partial}{\partial\psi})_x)_x = (\frac{\partial\omega}{\partial x})_x(\frac{\partial}{\partial\omega}(b_1\frac{\partial}{\partial\omega})_x)_x \quad \cdot \text{(A.13)}$$

Substitution from (A.11) and (A.12) into (A.13) gives:

$$\{\frac{\partial}{\partial\psi}\ (b_1\frac{\partial}{\partial\psi})_x\}_x = \left[\frac{\partial}{\partial\omega}\ (\frac{b_1}{(\psi_E-\psi_I)^2}\ \frac{\partial}{\partial\omega})_x\right]_x \quad \cdot \text{(A.14)}$$

A.III <u>Transformation of</u> $\{\frac{\partial}{\partial x}\ (b_2\frac{\partial}{\partial x})_\psi\}_\psi$

Multiplying equation (A.7) by b_2 and using the expression for the derivative given by (A.4) yields:

$$\{\frac{\partial}{\partial x}\ (b_2\ \frac{\partial}{\partial x})_\psi\}_\psi =$$

$$\{\frac{\partial}{\partial x}\left[\ b_2(\frac{\partial}{\partial x})_\omega + (a+b\omega)\ b_2(\frac{\partial}{\partial\omega})_x\right]\}_\psi =$$

$$\{\frac{\partial}{\partial x}\left[b_2(\frac{\partial}{\partial x})_\omega + (a+b\omega)\ b_2(\frac{\partial}{\partial\omega})_x\right]\}_\omega +$$

$$(\frac{\partial\omega}{\partial x})_\psi\left[\frac{\partial}{\partial\omega}\ \{b_2(\frac{\partial}{\partial x})_\omega + (a+b\omega)\ b_2\ (\frac{\partial}{\partial\omega})_x\}\right]_x \quad \cdot \text{(A.15)}$$

Substitution from (A.5) into (A.15) gives:

$$\{\frac{\partial}{\partial x}\ \ b_2\ (\frac{\partial}{\partial x})_\psi\}_\psi = \{\frac{\partial}{\partial x}\ b_2(\frac{\partial}{\partial x})_\omega\}_\omega + \{\frac{\partial}{\partial x}\left[(a+b\omega)\ b_2\ (\frac{\partial}{\partial\omega})_x\right]\}_\omega +$$

$$(a+b\omega)\left[\frac{\partial}{\partial\omega}\{b_2(\frac{\partial}{\partial x})_\omega\}\right]_x + (a+b\omega)\left[\frac{\partial}{\partial\omega}\{(a+b\omega)\ b_2\ (\frac{\partial}{\partial\omega})_x\}\right]_x \quad \cdot \text{(A.16)}$$

Rearrangement of equation (A.16) yields:

$$\{\frac{\partial}{\partial x}\ b_2\ (\frac{\partial}{\partial x})_\psi\}_\psi = \{\frac{\partial}{\partial x}\ b_2\ (\frac{\partial}{\partial x})_\omega\}_\omega +$$

$$(a+b\omega)\{\left[\frac{\partial}{\partial\omega}\ b_2\ (\frac{\partial}{\partial x})_\omega\right]_x + \left[\frac{\partial}{\partial x}\ b_2\ (\frac{\partial}{\partial\omega})_x\right]_\omega\}+$$

$$\left[\frac{\partial}{\partial\omega}\ (a+b\omega)^2\ b_2\ (\frac{\partial}{\partial\omega})_x\right]_x \qquad \cdot (A.17)$$

A. IV <u>The resulting transformed differential equation</u>

Applying the transformation formulae (A.7), (A.12), (A.14) and (A.17) to (A.1), leads to the following final form of the stagnation-enthalpy equation in the ω-x coordinate system.

$$\frac{1}{u}\frac{\partial\tilde{h}}{\partial t} + \frac{\partial h}{\partial x} + (a+b\omega)\frac{\partial\tilde{h}}{\partial\omega} = \frac{\partial}{\partial\omega}\left[\frac{r^2\rho u\ \Gamma_{h,eff}}{(\psi_E-\psi_I)^2}\frac{\partial\tilde{h}}{\partial\omega}\right]+\frac{1}{\rho ur}\frac{\partial}{\partial x}\left[r\ \Gamma_{h,eff}\frac{\partial\tilde{h}}{\partial x}\right]$$

$$+\frac{(a+b\omega)}{\rho ur}\{\frac{\partial}{\partial\omega}\left[r\ \Gamma_{h,eff}\frac{\partial\tilde{h}}{\partial x}\right]+\frac{\partial}{\partial x}\left[r\ \Gamma_{h,eff}\frac{\partial\tilde{h}}{\partial\omega}\right]\}$$

$$+\frac{1}{\rho ur}\frac{\partial}{\partial\omega}\left[(a+b\omega)^2\ r\ \Gamma_{h,eff}\frac{\partial\tilde{h}}{\partial\omega}\right]+\frac{\partial}{\partial\omega}\left[\frac{\mu_{eff}-\Gamma_{h,eff}}{(\psi_E-\psi_I)^2}\ r^2\rho u\frac{\partial u^2/2}{\partial\omega}\right]\cdot(A.18)$$

APPENDIX B

Finite-difference form of the stagnation-enthalpy equation

The stagnation-enthalpy equation (2.4.14) in the (ω-x) coordinate system may be re-written as follows:

$$\frac{1}{u}\frac{\partial \tilde{h}}{\partial t} + \frac{\partial \tilde{h}}{\partial x} = \frac{\partial}{\partial \omega}\left[\frac{r\ \Gamma_{h,eff}}{(\psi_E-\psi_I)}\frac{\partial \tilde{h}}{\partial y}\right] + \frac{1}{\rho u r}\frac{\partial}{\partial x}\left[r\Gamma_{h,eff}\frac{\partial \tilde{h}}{\partial x}\right]$$

I II III IV

$$\pm \frac{\partial}{\partial \omega}\left[\frac{\mu_{eff}-\Gamma_{h,eff}}{(\psi_E-\psi_I)}\, r\, \frac{\partial u^2/2}{\partial y}\right] \qquad \text{(B1)}$$

V

The integration of the above equation over the control volume presented in figure (4.1) leads to the following:

$$\int_t^{t+\delta t}\int_{J-\frac{1}{2}}^{J+\frac{1}{2}}\int_{I-\frac{1}{2}}^{I+\frac{1}{2}} \frac{1}{u}\frac{\partial \tilde{h}}{\partial t}\, d\omega dx dt \qquad \text{,term (I),}$$

$$+ \int_t^{t+\delta t}\int_{J-\frac{1}{2}}^{J+\frac{1}{2}}\int_{I-\frac{1}{2}}^{I+\frac{1}{2}} \frac{\partial \tilde{h}}{\partial x}\, d\omega dx dt \qquad \text{,term (II),}$$

$$= \int_t^{t+\delta t}\int_{J-\frac{1}{2}}^{J+\frac{1}{2}}\int_{I-\frac{1}{2}}^{I+\frac{1}{2}} \frac{\partial}{\partial \omega}\left[\frac{r\ \Gamma_{h,eff}}{(\psi_E-\psi_I)}\frac{\partial \tilde{h}}{\partial y}\right] d\omega dx dt \qquad \text{,term (III),}$$

$$+ \int_t^{t+\delta t}\int_{J-\frac{1}{2}}^{J+\frac{1}{2}}\int_{I-\frac{1}{2}}^{I+\frac{1}{2}} \frac{1}{\rho r u}\frac{\partial}{\partial x}\left[(r\ \Gamma_{h,eff}\frac{\partial \tilde{h}}{\partial x})\right] d\omega dx dt \qquad \text{,term (IV),}$$

$$+ \int_t^{t+\delta t}\int_{J-\frac{1}{2}}^{J+\frac{1}{2}}\int_{I-\frac{1}{2}}^{I+\frac{1}{2}} \frac{\partial}{\partial \omega}\left[\frac{\mu_{eff}-\Gamma_{h,eff}}{(\psi_E-\psi_I)}\, r\, \frac{\partial u^2/2}{\partial y}\right] d\omega dx dt \qquad \text{,term (V), (B.2)}$$

where each term in equation (B.2) can be written as follows:

$$(I) \equiv \frac{1}{u_{I,J}}\left[\tilde{h}_{I,J} - \tilde{h}_{I,J,t}\right]\delta\omega\delta x \qquad \text{, (B.3)}$$

$\tilde{h}_{I,J,t}$ is the stagnation enthalpy at time (t) while the absence of a time subscript indicates the value at time (t + δt)

$$(II) \equiv (\tilde{h}_{I,J+\frac{1}{2}} - \tilde{h}_{I,J-\frac{1}{2}})\delta\omega\delta t \qquad \text{, (B.4)}$$

$$(III) \equiv \left[\left(\frac{r\,\Gamma_{h,eff}}{\psi_E - \psi_I}\right)_{I+\frac{1}{2},J} \frac{\tilde{h}_{I+1,J} - \tilde{h}_{I,J}}{y_{I+1,J} - y_{I,J}} - \left(\frac{r\,\Gamma_{h,eff}}{\psi_E - \psi_I}\right) \frac{\tilde{h}_{I,J} - \tilde{h}_{I-1,J}}{y_{I,j} - y_{I+1,J}}\right]\delta x \delta t \,, \quad (B.5)$$

$$(IV) \equiv \left[(r\,\Gamma_{h,eff})_{I,J+\frac{1}{2}} \frac{\tilde{h}_{I,J+1} - \tilde{h}_{I,J}}{x_{I,J+1} - x_{I,J}} - (r\,\Gamma_{h,eff})_{i,J-\frac{1}{2}} \frac{\tilde{h}_{I,J} - \tilde{h}_{I,J-1}}{x_{I,J} - x_{I,J-1}}\right]\delta\omega\delta t, \quad (B.6)$$

$$(V) \equiv \left[\left\{\frac{(\mu_{eff} - \Gamma_{h,eff})r}{(\psi_E - \psi_I)}\right\}_{I+\frac{1}{2},J} \frac{(u^2/2)_{I+1,J} - (u^2/2)_{I,J}}{y_{I+1,J} - y_{I,J}}\right.$$

$$\left. - \left\{\frac{(\mu_{eff} - \Gamma_{h,eff})r}{(\psi_E - \psi_I)}\right\}_{I-\frac{1}{2},J} \frac{(u^2/2)_{I,J} - (u^2/2)_{I-1,J}}{y_{I,J} - y_{I-1,J}}\right] \delta x \delta t \quad . \quad (B.7)$$

It is now necessary to employ a stagnation-enthalpy profile between two concecutive grid nodes.

The upwind-differencing scheme was employed in relating $\tilde{h}_{I,J+\frac{1}{2}}$ to $\tilde{h}_{I,J}$ and $\tilde{h}_{I,J+1}$ and $\tilde{h}_{I,J-\frac{1}{2}}$ to $\tilde{h}_{I,J}$ and $h_{I,J+1}$. This scheme was chosen in order to maintain similarity between the h-equation and the parabolic equations u, k, ε. However, when the grid Peclet number (Pe_g) was less than two, the central differencing scheme was employed in the computer code. With an upwind-differencing scheme, the term (II) reduces to

$$II \equiv (\tilde{h}_{i,J} - \tilde{h}_{I,J-1})\ \delta\omega\delta t \quad . \quad (B.8)$$

Substitution from (B.3), (B.5), (B.6), (B.7) and (B.8) into (B.2), yields:

$$A_{I,J}\,\tilde{h}_{I,J} = A_{I+1,J}\,\tilde{h}_{I+1,J} + A_{I-1,J}\,\tilde{h}_{I-1,J} + A_{I,J+1}\,\tilde{h}_{I,J+1} + A_{I,J-1}\,\tilde{h}_{I,J-1} + C_{I,J} \quad , \quad (B.9)$$

where,

$$A_{I+1,J} = \left\{\frac{r\,\Gamma_{h,eff}}{(\psi_E - \psi_I)}\right\}_{I+\frac{1}{2},J} \frac{\delta x}{y_{I+1,J} - y_{I,J}} \quad , \quad (B.10)$$

$$A_{I-1,J} = \left\{\frac{r\,\Gamma_{h,eff}}{\psi_E - \psi_I}\right\}_{I-\frac{1}{2},J} \frac{\delta x}{y_{I,J} - y_{I-1,J}} \quad , \quad (B.11)$$

CORRIGENDA

Page No	Line	Text Reads	Correction
1	5	-u'v'	$-\overline{u'v'}$
4	5 and -5	Combustion	Concentration
5	-5	in -x	in ω-x
10	6	5454	54
10	10	5555	55
10	13	7777	77
10	18	7878	78
10	21	7979	79
10	22 and 24	9393	93
10	25	drowning	drawing
11	2	centre line	centreline
13	4	adial	axial
19	-4	Therman	Thermal
26	4	$k^{2/3}$	$k^{3/2}$
29	-6	P_ℓ	Pr_ℓ
30	5	Johank	Johnk
31	13	Claybaugh	Clabaugh
36	7	Siegal	Siegel
36	7	Orino	Ogino
44	-11	Re	Re^n
57	9	Spalding (1978)	$\underline{\text{(Spalding (1978))}}$
57	-4	u'v'	$\underline{u'v'}$
59	-7	$\overline{v'T}$	$\overline{v'T'}$
69	2	Pr	Pr_ℓ
70	11	Jayatillek	Jayatillaka
72	4 and 6	Jayatilleka	Jayatillaka
72	11	Jayatillek	Jayatillaka
73	4	ky	Ky
74	-7	equal	equal to
83	-5	$h_{I+1,J}-y_{I,J}$	$y_{I+I,J}-y_{I,J}$
83	-3	δ	$\delta\omega$
85	-6	$P_{I,J}-P_{I,J-1}$	$(P_{I,J}-P_{I,J-1})$
86	1	-1, and	-1, 0.5, and
88	5	nodel	nodal
97	3	10^o	10^oC
99	13	seperator	separator
100	7	galvanometer	galvanometers
102	2	rate.	rates.
103	-3	whown	shown
103	7	affecte	affected
131	10	clost	close
131	-2	τ	τ_w
133	6	Lauefer	Laufer
133	-9	buhr	Buhr
143	-11	well	wall
146 and 147	horizontal axis	-	x/D
151	"	-	x/D
154	vertical axis	τ	τ_w
165	horizontal axis	-	Pe
171	"	-	$\frac{r_o-r}{r_o-r_i}$
172	"	-	y/R
177	"	-	x/R
176	-6	1267	12.67
195	horizontal axis	-	Time(s)
195	Fig (7.8)	-	$\frac{T_w-T_{in}}{(T_w-T_{in})_{st}}$ Vs Time(s)
214	-4	pergormed	performed
218	-14	DIESSLER	DEISSLER
219	-5	HUIMES	HUIME
229	4	Uni ed	United
233	-5	, Heat	, Heat, DSIR

Note: "-" denotes line counting from end of page upward
"+" denotes line counting from top of page downwards